NEW-TO-NATURE PROCESSES IN BIOCATALYSIS

Laura Kqiku

UNIVERSITAT ROVIRA i VIRGILI

New-to-Nature Processes in Biocatalysis

Laura Kqiku

DOCTORAL THESIS
2024

Laura Kqiku

New-to-Nature Processes in Biocatalysis

Doctoral Thesis

Supervised by Prof. Paolo Melchiorre

ICIQ – Institut Català d'Investigació Química

Tarragona

2024

Prof. Paolo Melchiorre, Professor at the University of Bologna, previously ICIQ Group Leader

I STATE that the present study, entitled "New-to-Nature Processes in Biocatalysis", presented by LAURA KQIKU for the award of the degree of Doctor, has been carried out under my supervision at the Institut Català d'Investigació Química (ICIQ).

Tarragona, May the 30th 2024

Doctoral Thesis Supervisor

Prof. Paolo Melchiorre

Acknowledgments

First, I would like to express my deepest gratitude to my supervisor, Prof. Paolo Melchiorre. This thesis would not have been possible without his support. Thank you for allowing me to join this group and for your guidance and support throughout my PhD.

I also want to thank all the current and past members of the Melchiorre group for the good times we shared both inside and outside the lab. I am especially grateful to the remaining members at ICIQ: Shuo, Florian, Igor, and Thomas, for being there for each other in rather lonely times. A particularly big thank you to Thomas for proofreading this entire thesis. Thanks to Edu and Emilien, the first and for a while only faces I saw in the lab during the pandemic. To Jan and Vasilis, who taught me and somehow managed to make a proper biochemist out of me. To Adriana, Martin, Florian, and the bio guys, with whom I had the pleasure of working. I am deeply thankful for the knowledge and support I gained from you all over this time. I am especially grateful for the friendship I built with Adri; our conversations and activities outside the lab made my time in Tarragona quite memorable. Thanks to Miguel, our Meme-Master, to Wei, the best singer, to Matteo, who taught me that pasta and noodles are not the same, and to Will. Yes, we are the same age, but I still look younger. Thanks to my Erasmus students, Gianluca and Malte, who I had the opportunity to supervise during my PhD.

I also want to express my gratitude to Nuría for the help and administrative support. To Laia and Miguel for their help with the equipment in the lab. I also would like to thank all the research support units, the chromatographic unit, the NMR, the spectroscopic, mass and X-ray units and the HTE lab.

Many thanks also to my family and friends. Danke Mama, Papa und Adrian für eure Unterstützung und den Glauben an mich, egal welche Entscheidung ich treffe. Ich kann mich glücklich schätzen eine solche Familie zu haben.

Danke auch an meine Freunde, insbesondere Vanda und Tanya, für die tollen Zeiten und Gespräche die wir miteinander hatten. Danke, dass ihr für mich da seid.

Also I want to thank Anand, the far most important person I met in Tarragona. Thanks for being my biggest cheerleader and for always believing in me, even when sometimes I didn't do it by myself.

Finally, I am thankful for the financial support from the Minestery of Science for the FPI predoctoral fellowship (PRE2020-095712), the Agencia Estatal de Investigación (PID2019-106278GB-I00) and the MCIN/AEI/10.13039/501100011033.

List of Publications

- Tseliou, V., Faraone, A., **Kqiku, L.**, Vilím, J., Simionato, G., Melchiorre, P. "Enantioselective Biocascade Catalysis With a Single Multifunctional Enzyme" *Angew. Chem. Int. Ed.* **2022**, *61*, e202212176.

Für Andreas

Table of Contents

Chapter 1

General Overview

1.1 Introduction

Chiral molecules are found in all forms of life.[1] The increasing demand for enantiopure chiral compounds in pharmaceuticals, fragrances, and material industries have driven the development of asymmetric catalysis. This approach leverages the principles of catalysis to selectively synthesize chiral compounds, favouring the formation of a single stereoisomer. Notably, the reusability of these valuable and often expensive chiral catalysts in sub-stoichiometric amounts contributes to both cost-effectiveness and improved atom economy in reaction processes.[2,3]

Historically, asymmetric catalysis relied on organometallic reagents and enzymes. In the late 1990s, Sorensen and Nicolaou defined asymmetric catalysis in their book "Classics in Total Synthesis" as: "*In a catalytic asymmetric reaction, a small amount of enantiomerically pure catalyst, either an enzyme or a synthetic, soluble transition metal complex, is used to produce large quantities of optically active compound from a precursor that may be chiral or achiral*."[4] Both strategies induce stereoselectivity in a different ways. In chiral transition metal catalysis, the metal center provides strong chemical activation through its interaction with substrates, and the overall chirality of the metal complex ensures the desired stereoselectivity.[5,6] These catalysts play a central role in a wide range of transformations, with chiral ligands enabling precise stereocontrol. In contrast, in biocatalysis the enzyme induces stereoselectivity through its unique three-dimensional structure, which creates a specific active site that binds substrates in a particular orientation.[7,8] This precise binding ensures that the reaction preferentially forms one enantiomer over the other. The spatial arrangement of amino acids within the enzyme's active site is crucial in guiding the substrate to the correct position, thereby determining the

[1] Yamamonto, H.; Carreira, E. M. (eds.) "Comprehensive Chirality." Elsevier, 2012.

[2] Noyori, R. (eds.) "Asymmetric Catalysis in Organic Synthesis." Wiley, 1994.

[3] The Nobel Prize in Chemistry 2001. NobelPrize.org: 'https://www.nobelprize.org/prizes/chemistry/2001/summary'.

[4] Nicolaou, K. C., Sorensen, E. J. "Classics in Total Synthesis: Targets, Strategies, Methods", Wiley-VCH, 1996, p 344.

[5] Steinlandt, P. S., Zhang, L., Meggers, E. "Metal Stereogenicity in Asymmetric Transition Metal Catalysis." *Chem. Rev.* **2023**, *123*, 4764–4794.

[6] Fanourakis, A., Docherty, P. J., Chuentragool, P., Phipps, R. J. "Recent Developments in Enantioselective Transition Metal Catalysis Featuring Attractive Noncovalent Interactions between Ligand and Substrate." *ACS Catal.* **2020**, *10*, 10672–10714.

[7] Palmer, T. (eds.) "Understanding Enzymes." E. Horwood, 1991.

[8] Bommarius, A. S., Riebel-Bommarius, B. R. (eds.), Biocatalysis: Fundamentals and Applications." Wiley-VCH, 2004.

product's stereochemistry. The binding within the active site enables the enzyme to accelerate reactions and yield products with high specificity and selectivity.

In 2000, organocatalysis emerged as a new strategy for asymmetric catalysis.[9,10] The power of this methodology lies in its ability to interact with substrates and precisely control their activation through various strategies, forming chiral reactive intermediates that trigger mechanistically similar yet diverse reactions with precise control over stereoselectivity.[11] While the use of small chiral organic molecules as catalysts has a long history, dating back to the early example of quinine-promoted benzaldehyde hydrocyanation (Figure 1.1a) in the 19th century, its full potential remained largely untapped. Similarly, the *L*-proline-catalyzed Hajos-Parrish reaction (Figure 1.1b) from the 1970s showcased another early example.[12–14] However, the broader synthetic power of organocatalysis gained significant recognition within the chemical community only around the year 2000, following two groundbreaking publications by MacMillan and List, Lerner, and Barbas III, which established the field of asymmetric aminocatalysis (Figure 1.2).[9,10]

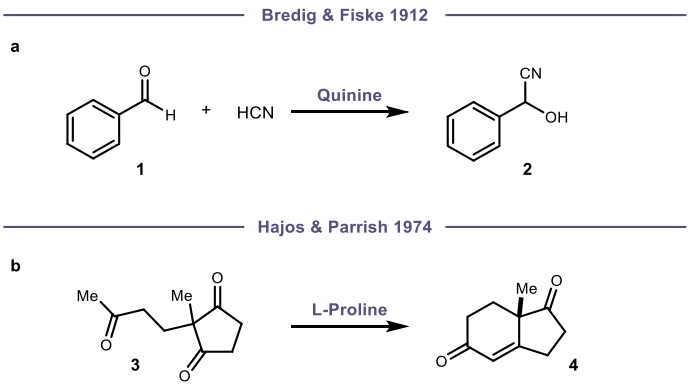

Figure 1.1. Early examples of asymmetric organocatalysis by a) Bredig and Fiske (*1912*) b) Hajosh and Parrish (*1974*).

Aminocatalysis is the most prominent and exploited activation strategy in organocatalysis (Figure 1.2).[15] It relies on the formation of an active intermediate through the condensation of

[9] List, B., Lerner, R. A., Barbas, III, C. F. "Proline-Catalyzed Direct Asymmetric Aldol Reactions" *J. Am. Chem. Soc.* **2000**, *122*, 2395-2396.

[10] Ahrendt, K. A., Borths, C. J., MacMillan, D. W. C. "New Strategies for Organic Catalysis: The First Highly Enantioselective Organocatalytic Diels-Alder Reaction" *J. Am. Chem. Soc.* **2000**, *122*, 4243-4244.

[11] Melchiorre, P.; Marigo, M.; Carlone, A.; Bartoli, G. "Asymmetric Aminocatalysis—Gold Rush in Organic Chemistry" *Angew. Chem. Int. Ed.*, **2008**, *47*, 6138-6171.

[12] Hajos, Z. G; Parrish, D. R. "Asymmetric Synthesis of Bicyclic Intermediates of Natural Product Chemistry" *J. Org. Chem*. **1974**, *39*, 1615-1621.

[13] List, B. "Emil Knoevenagel and the Roots of Aminocatalysis" *Angew. Chem. Int. Ed.* **2010**, *49*, 1730-1734.

[14] Berkessel, A.; Gröger, H. (eds.) "Asymmetric Organocatalysis." Wiley-VCH, 2005.

[15] MacMillan, D. W. C. "The advent and development of asymmetric organocatalysis" *Nature* **2008**, *455*, 304-308.

chiral amines with carbonyl compounds, i.e. enamine or iminium ion intermediates. In enamine-mediated catalysis, the initial step involves the condensation of an aldehyde or ketone substrate with a secondary amine catalyst,[16] followed by a subsequent tautomerization and resulting in the formation of a nucleophilic enamine **I**. This intermediate possesses a significantly enhanced nucleophilic character at the α-carbon position, facilitating reaction with a diverse range of electrophiles (E^+). Iminium-ion-mediated catalysis on the other hand relies on the condensation of a chiral amine with α,β-unsaturated carbonyl compounds generating iminium ions **II**.[17] These iminium ions possess a crucial feature: the β-carbon atom becomes significantly more susceptible to nucleophilic attack then the parent unsaturated carbonyl substrate. This enhanced reactivity allows the β-carbon to readily couple with various nucleophiles.

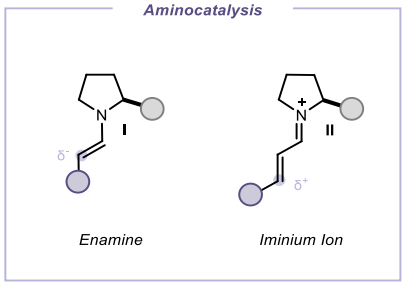

Figure 1.2. Aminocatalysis: enamine and iminium ion activation.

Enders' work of 2006 exemplifies the complexity-generating power of organocatalysis.[18] His groundbreaking triple cascade reaction leverages both enamine and iminium ion activation modes within a single reaction sequence, efficiently transforming simple starting materials into complex chiral products in one-step and using a single chiral amine catalyst **A**. This approach constructed four stereocenters in a single operation, utilizing an enamine-iminium ion-enamine activation sequence (Figure 1.3). The reaction sequence begins with linear aldehydes like butanal **5** undergoing enamine-catalyzed Michael additions with β-nitrostyrenes **6**. This is followed by an iminium ion-catalyzed addition of the resulting nitro aldehyde **9**. Finally, the formed enamine **V** undergoes cyclization and aldol condensation, leading to the cyclic carbaldehyde product **8** as a mixture of only two diastereomers (epimers at C5) and a single enantiomer.

[16] Mukherjee, S., Yang, J. W., Hoffmann, S., List, B. "Asymmetric enamine catalysis." *Chem. Rev.* **2007**, *107*, 5471–5569.

[17] Erkkila, A., Majander, I., Pihko, P.M. "Iminium Catalysis" *Chem. Rev.* **2007**, *107*, 5416−5470.

[18] Enders, D., Hüttl, M. R. M., Grondal, C., Raabe, G. "Control of Four Stereocentres in a Triple Cascade Organocatalytic Reaction" *Nature* **2006**, *441*, 861-863.

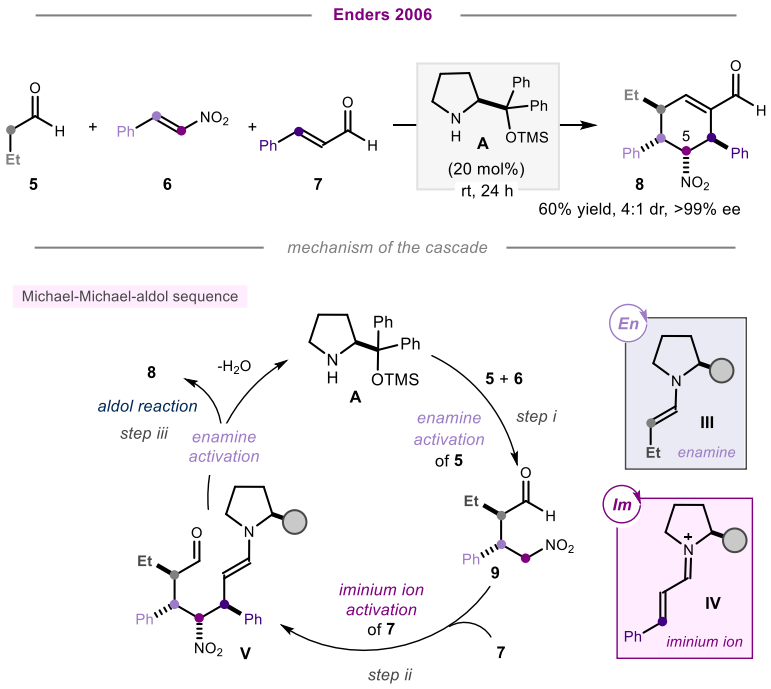

Figure 1.3. Asymmetric three-component cascade reaction operating through a Michael-Michael-aldol sequence reported by Enders in 2006.

The ongoing quest to expand the toolbox of asymmetric catalysis has identified exciting possibilities at the interface of distinct catalytic methods. One such avenue involves the synergistic combination of photocatalysis and organocatalysis. Studies have shown that combining photochemistry with asymmetric aminocatalysis can enable reactions not achievable with traditional ground-state organocatalysis.[19] Visible light irradiation has been demonstrated to activate established chiral catalytic intermediates. These intermediates can then reach a higher energy state and facilitate entirely new reaction pathways.[20] This photochemical approach offers access to energetically demanding transformations, frequently involving unconventional radical mechanisms, which are inaccessible through ionic pathways. In this vein, our research group investigated the light-induced behavior of enamines and iminium ions, classic chiral organocatalytic intermediates with an established reactivity in thermal reactions.[21] During the research on the asymmetric α-functionalization of aldehydes **10** with electron-deficient alkyl bromides **11**, we realized that upon condensation of chiral amine **B** with aldehyde **10**, a photoactive electron donor-acceptor (EDA) complex was formed

[19] Meggers, E. "Asymmetric catalysis activated by visible light" *Chem. Commun* **2015**, *51*, 3290-3301.
[20] Mondal, S., Dumur, F., Gigmes, D., Sibi, M. P., Bertrand, M. P., Nechab, M. "Enantioselective Radical Reactions Using Chiral Catalysts" *Chem. Rev.* **2022**, *122*, 5842-5976.
[21] Silvi, M., Melchiorre, P. "Enhancing the Potential of Enantioselective Organocatalysis with Light", *Nature* **2018**, *554*, 41-49.

between the enamine and the electron-poor benzyl bromide **11** (Figure 1.4). We then found that direct light irradiation, without the need for an external photoredox catalyst, could promote the asymmetric α-functionalization of aldehydes via a photo-induced radical manifold.[22] This finding opened new avenues for the mild generation of open-shell intermediates through single-electron transfer (SET) mechanisms, enabling their participation in asymmetric transformations using a single chiral organocatalyst.

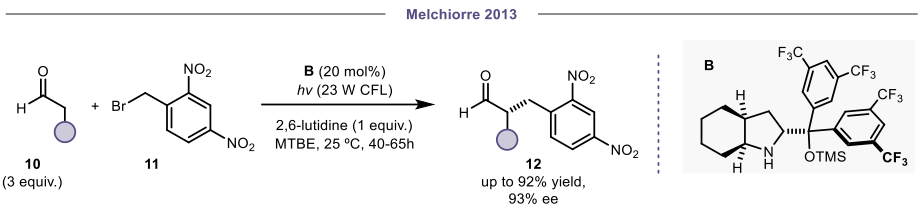

Figure 1.4. α-Functionalization of aldehydes via excitation of an electron donor acceptor (EDA). CFL = compact fluorescent light; MTBE = methyl tertbutyl ether; TMS = trimethyl silyl.

Expanding upon the idea of eliciting new reactivity via direct excitation of organocatalytic intermediates, our group hypothesized that electrophilic iminium ion intermediates could serve as SET oxidant in the excited state. This idea was confirmed in 2017 through the development of an enantioselective β-functionalization of enals **7** (Figure 1.5).[23] This method hinges on directly exciting chiral iminium ions **VI** with visible light. Upon excitation, the iminium ion reaches the excited state **VI***, acting as a potent oxidant. This facilitates the SET activation of organosilanes **13** and subsequent solvent-assisted fragmentation to obtain radical **VII**. A subsequent radical recombination step yields the enamine intermediate **IX**. Ultimately, hydrolysis releases the desired chiral product **14** while regenerating the aminocatalyst, thus completing the catalytic cycle. This research underscores the efficacy of photoexcitation in enabling novel radical-based transformations, particularly with substrates that would typically remain inert in traditional ground-state organocatalytic chemistry.

[22] Arceo, E., Jurberg, I. D., Álvarez-Fernández, A., Melchiorre, P. "Photochemical activity of a key donor-acceptor complex can drive stereoselective catalytic α-alkylation of aldehydes." *Nat. Chem.* **2013**, *5*, 750–756.

[23] Silvi, M., Verrier, C., Rey, Y. P., Buzzetti, L, Melchiorre, P. "Visible-light Excitation of Iminium Ions Enables the Enantioselective Catalytic β-Alkylation of Enals" *Nat. Chem.* **2017**, *9*, 868-873.

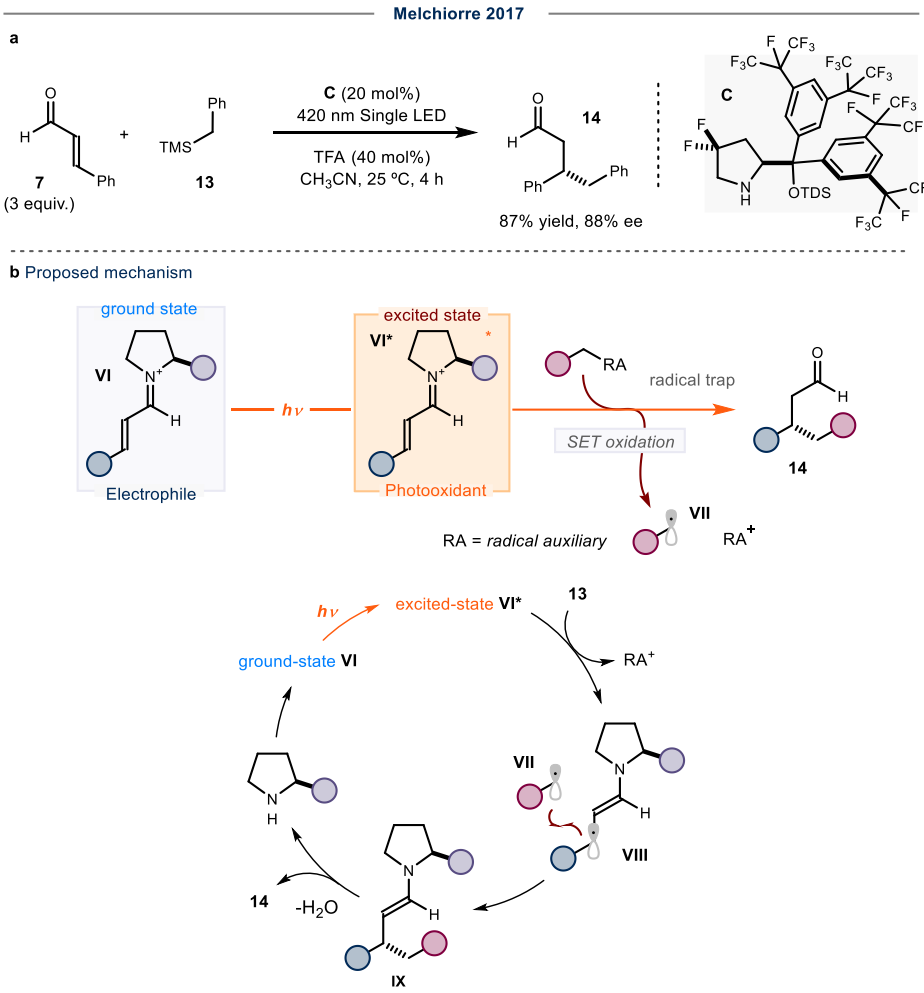

Figure 1.5. a) Direct photoexcitation of chiral iminium ions enables the asymmetric β-functionalization of enals **7** using non-nucleophilic silanes **13** as radical precursors; b) proposed mechanism. TMS = trimethyl silyl; LED = light emitting diode; TFA = trifluoroacetic acid; TDS = thexyl dimethyl silyl; SET = single electron transfer.

One key advantage of organocatalysts lies in their ability to induce enantioselectivity across a wide range of substrates. This flexibility surpasses the natural limitations of enzymes, which are highly specialized for specific reactions and substrates.[24] However, organocatalysts often fall short when compared to enzymes in terms of efficiency and selectivity. Additionally, organocatalytic reactions require a higher catalyst loading. By merging organocatalytic strategies with the enzymatic machinery, the goal is to engineer enzymes capable of activating substrates through new-to-nature mechanisms within their active sites.[25] This emerging

[24] Drauz, K., Gröger, H., May, O. (Eds.) "Enzyme Catalysis in Organic Synthesis" Wiley-VCH, Weinheim, 2012.

strategy holds promise for generating novel enzymes with great synthetic utility, while retaining the remarkable rate acceleration and selectivity inherent to enzymes.

The growing interest in *engineering non-natural enzyme activity* is fueled by the development of powerful protein engineering techniques.[26–28] Optimizing protein structure is crucial for crafting synthetically valuable catalysts. This can be achieved through directed evolution, an iterative process of mutagenesis and activity screening. By introducing targeted mutations and selecting for desired outcomes, scientists can unlock novel reactivities and fine-tune key features like selectivity, activity, and stability.[29,30] This is showcasing the vast potential of directed evolution for creating biocatalysts with entirely new functionalities.

This progress in biocatalysis is exemplified by the creation of amine-containing enzymes capable of both enamine and iminium ion catalysis to enable unique novel transformations. 4-Oxalocrotonate tautomerase (4-OT) contains a terminal, catalytically active proline situated within its active site.[31] In its natural function, 4-OT serves as a catalyst to facilitate the conversion of 2-hydroxy-2,4-hexadienedioate **15** into 2-oxo-3-hexendioate 1**6** (Figure1.6). Inspired by the structure and activities of proline-based organocatalysis, Poelarends speculated that this residue might possess the capability to act as a nucleophilic catalyst for conducting enamine and iminium ion-mediated transformations.

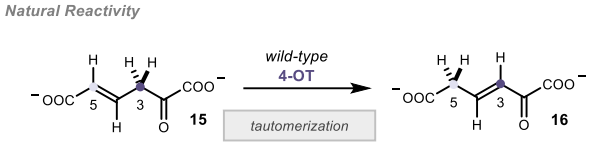

Figure 1.6. Natural reactivity of 4-oxalocrotonate tautomerase.

A recent study demonstrated the feasibility if this idea.[32] By modifying the active site of 4-OT, the researchers enabled the enzyme to catalyze reactions via iminium ion formation (Figure 1.7). This modification allowed 4-OT to promote the enantioselective Michael

[25] Prier, C. K., Arnold, F. H. "Chemomimetic Biocatalysis: Exploiting the Synthetic Potential of Cofactor-Dependent Enzymes to Create New Catalysts." *J. Am. Chem. Soc.* **2015**, *137*, 13992–14006.

[26] Arnold, F. H. "Innovation by Evolution: Bringing New Chemistry to Life (Nobel Lecture)" *Angew. Chem. Int. Ed.* **2019**, *58*, 14420-14426.

[27] Bornscheuer, U. T.; Hauer, B., Jaeger, K. E., Schwaneberg, U. "Directed Evolution Empowered Redesign of Natural Proteins for the Sustainable Production of Chemicals and Pharmaceuticals" *Angew. Chem. Int. Ed.* **2019**, *58*, 36-40

[28] Wang, Y., Xue, P., Cao, M., Yu, T., Lane, S. T., Zhao, H. "Directed Evolution: Methodologies and Applications" *Chem. Rev.* **2021**, *121*, 12384-12444.

[29] Reetz, M. "Making Enzymes Suitable for Organic Chemistry by Rational Protein Design" *ChemBioChem* **2022**, *23*, e202200049.

[30] Brustad, E. M., Arnold, F. H. "Optimizing non-natural protein function with directed evolution" *Curr. Opin. Chem. Biol.* **2011**, *15*, 201-210.

[31] Huddleston, J. P., Burks, E. A., Whitman, C. P. "Identification and characterization of new family members in the tautomerase superfamily: Analysis and implications." *Arch. Biochem. Biophys.* **2014**, *564*, 189–196.

[32] Guo, C., Saifuddin, M., Saravanan, T., Sharifi, M., Poelarends, G. J. "Biocatalytic Asymmetric Michael Additions of Nitromethane to α,β-Unsaturated Aldehydes via Enzyme-bound Iminium Ion Intermediates." *ACS Catal.* **2019**, *9*, 4369–4373.

addition of nitromethane **17** to various α,β-unsaturated aldehydes **7** and offered a biocatalytic route to the desired enantiomer of pharmaceutical relevant γ-nitroaldehydes **18**. Screening of a collection of single mutants of 4-OT led to the identification of 4-OT F50A, which exhibited a 10-fold increase in specific activity for the Michael addition of nitromethane to cinnamaldehyde compared to the wild-type enzyme. Beyond the initial discovery, further studies suggest the potential for engineered 4-OT variants to catalyze additional reactions. These reactions include cyclopropanation[33] and enantiocomplementary epoxidation[34] reaction using either tBuOOH or H_2O_2 as nucleophiles.

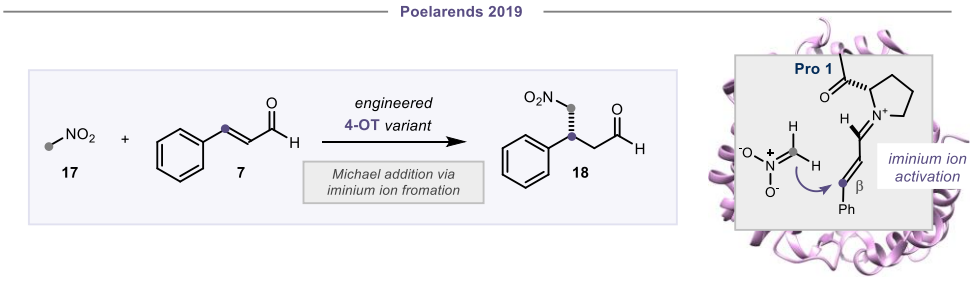

Figure 1.7. Laboratory modifications of the enzyme's structure enhance its traditional catalytic function from tautomerization to stereoselective Michael addition of nitromethane **17** to cinnamaldehyde **7**.

This example highlights how fine-tuning the structure of an enzyme unlocks new possibilities in chiral molecule synthesis. This goes beyond simply enhancing their traditional reactivity. By strategically modifying catalysts, we can achieve entirely new catalytic functions, enabling diverse stereoselective transformations through unique reaction mechanisms.

The combination of biocatalysis and photochemistry has also proven valuable in unveiling novel catalytic functions for established enzymes.[35–37] In 2016, Hyster and coworkers reported a light-induced, novel reactivity for ketoreductase (KRED) enzymes (Figure 1.8).[38] KREDs are naturally occurring enzymes that use NAD(P)H to perform enantioselective reductions of ketones **19**. The study revealed that NAD(P)H can form an EDA complex with bromolactones

[33] Kunzendorf, A., Xu, G., Saifuddin, M., Saravanan, T., Poelarends, G. J. "Biocatalytic Asymmetric Cyclopropanations via Enzyme-Bound Iminium Ion Intermediates." *Angew. Chemie - Int. Ed.* **2021**, *60*, 24059–24063.

[34] Xu, G., Crotti, M., Saravanan, T., Kataja, K. M., Poelarends, G. J. "Enantiocomplementary Epoxidation Reactions Catalyzed by an Engineered Cofactor-Independent Non-natural Peroxygenase." *Angew. Chemie - Int. Ed.* **2020**, *59*, 10374–10378.

[35] Hyster, T. K. "Radical Biocatalysis: Using Non-Natural Single Electron Transfer Mechanisms to Access New Enzymatic Functions" *Synlett* **2020**, *31*, 248-254.

[36] Emmanuel, M. A., Bender, S. G., Bilodeau, C., Carceller, J. M., DeHovitz, J. S., Fu, H., Liu, Y., Nicholls, B. T., Ouyang, Y., Page, C. G., Qiao, T., Raps, F. C., Sorigué, D. R., Sun, S. Z., Turek-Herman, J., Ye, Y., Rivas-Souchet, A., Cao, J., Hyster, T. K. "Photobiocatalytic Strategies for Organic Synthesis." *Chem. Rev.* **2023**, *123*, 5459–5520.

[37] Harrison, W., Huang, X., Zhao, H. Photobiocatalysis for Abiological Transformations. *Acc. Chem. Res.* **2022**, *55*, 1087–1096.

[38] Emmanuel, M. A., Greenberg, N. R., Oblinsky, D. G., Hyster, T. K. "Accessing Non-Natural Reactivity by Irradiating Nicotinamide-Dependent Enzymes with Light" *Nature* **2016**, *540*, 414-417.

21 within the enzyme's active site. Excitation of the EDA complex **X** triggers an intramolecular SET event, leading to the reduction of the bromolactone **21** and the generation of radicals via mesolytic cleavage of the bromide (**XI**). Subsequently, a stereoselective hydrogen atom transfer (HAT) from the NAD(P)H radical cation to the alkyl radical delivers the desired chiral product **22** and regenerates $NAD(P)^+$. The NAD(P)H cofactor is then recycled in the reaction mixture either through a sacrificial reductant or through the biocatalytic oxidation of glucose by gluconolactone dehydrogenase (GHD). This work demonstrated that traditional biocatalysts like KREDs could gain completely new reactivity upon light excitation. Upon light irradiation, KRED catalyzed radical generation and HAT steps, enabling a mechanistically distinct enantioselective protodehalogenation of α-bromolactones – substrates the enzyme would not normally reduce in the ground state.

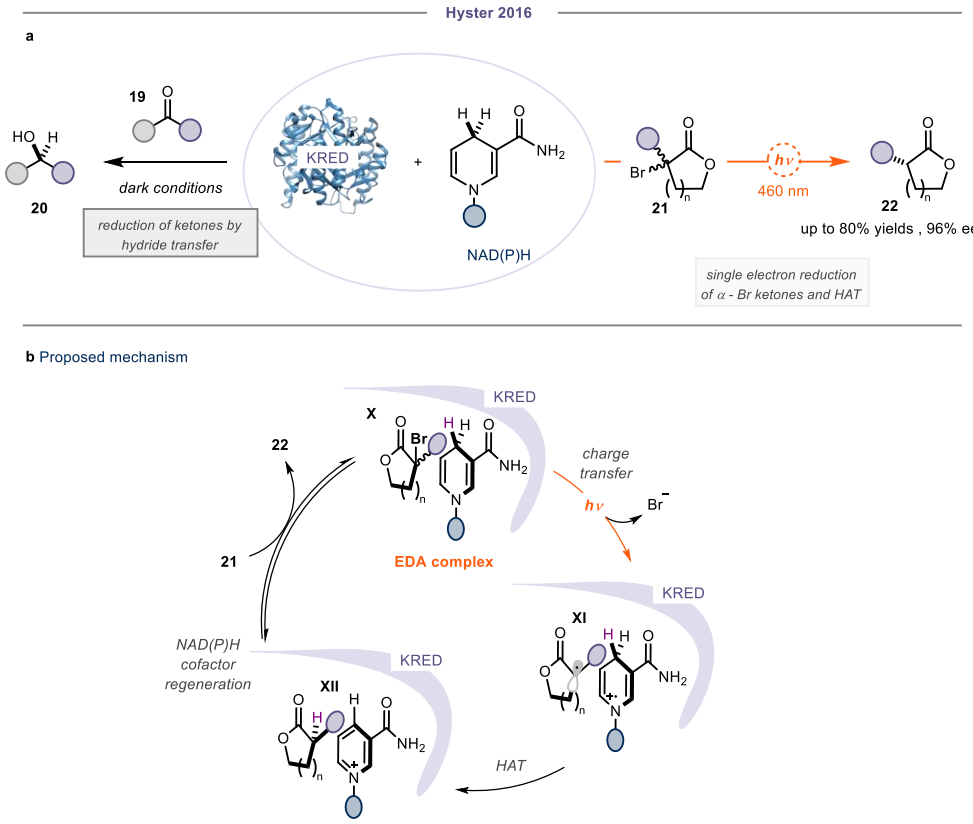

Figure 1.8. a) Visible light irradiation turns a naturally occurring ketoreductase into a photoenzyme that promotes the SET reduction of α-bromo ketones; b) proposed mechanism. KRED = ketoreductase; NAD(P)H = nicotinamide adenine dinucleotide (phosphate); HAT = hydrogen atom transfer; EDA complex = electron donor acceptor complex.

The presented example highlights the potential of photoexcitation as a transformative strategy in biocatalysis. This approach offers the possibility of unlocking entirely new reaction pathways, enabling the synthesis of challenging chiral compounds that were previously difficult to access.

1.2 General Objectives of the Thesis

The general objective of this thesis was to develop new-to-nature biocatalytic processes to enable the stereoselective synthesis of complex chiral substrates. The main idea was to translate known organocatalytic and photochemical activation strategies in a biological setting. The first chapter focused on the development of two stereoselective biocascade processes via the engineering of a single multifunctional enzyme and using the classical polar chemistry of enamines and iminium ions, but within an enzyme's active site. Chapter III introduced a novel photochemical strategy of substrate activation for biocatalysis, enabling a stereospecific radical coupling via direct excitation of an enzyme-bound iminium ion.

1.2.1 Enantioselective Biocascade Catalysis Using a Single Multifunctional Enzyme

In Chapter II, the development of a stereoselective biocascade using a single enzyme performing mechanistically distinct steps of the sequence is discussed (Figure 1.9).[39] Cascade reactions utilizing a single multifunctional catalyst for each step are a powerful strategy in organocatalysis.[40,41] The most advanced example combining two different activation strategies, enamine and iminium ion activation, in one sequence is the complex three-component cascade of Enders in 2006.[18] In contrast, biocatalytic cascade reactions using a single multifunctional enzyme are less explored. This project aimed to develop such asymmetric multicomponent biocascade processes, specifically targeting the elegant triple cascade reaction by Enders. We identified and engineered a multifunctional enzyme capable of sequentially performing enamine activation of aldehydes **5** and iminium ion activation of enals **7** to deliver complex chiral products **8**. The resulting cyclohexene carbaldehyde products **8** exhibited high yields, diastereomeric ratios, and enantiomeric excess, matching or even surpassing the efficacy and stereoselectivity of traditional organocatalytic strategy in certain instances.

[39] Tseliou, V., Faraone, A., Kqiku, L., Vilím, J., Simionato, G., Melchiorre, P. "Enantioselective Biocascade Catalysis With a Single Multifunctional Enzyme", *Angew. Chem. Int. Ed.* **2022**, *61*, e202212176.

[40] Grondal, C., Jeanty, M., Enders, D. "is" *Nat. Chem.* **2010**, *2*, 167-178.

[41] Jones, S. P., Simmons, B., Mastracchio, A., MacMillan, D. W. C. "Collective synthesis of natural products by means of organocascade catalysis" *Nature* **2011**, *475*, 183-188.

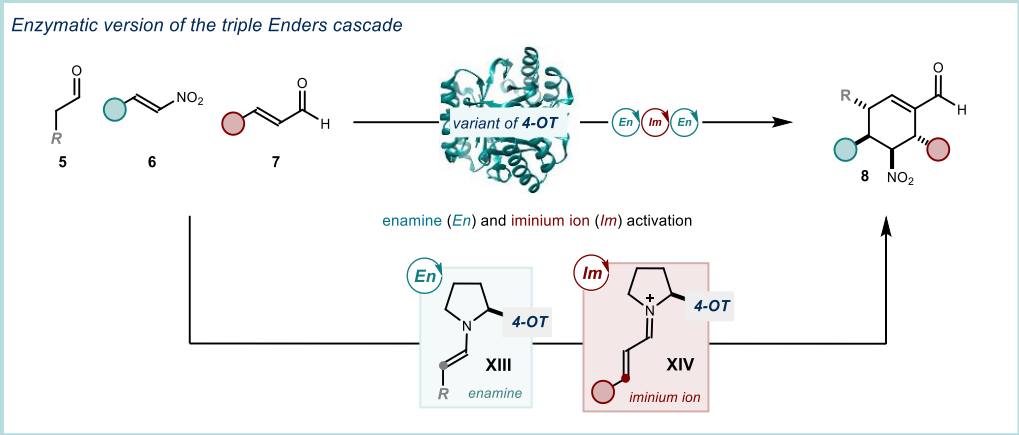

Figure 1.9. A multifunctional variant of the 4-oxalocrotonate tautomerase (4-OT) enzyme, capable of sequentially activating substrates **5** and **7** through enamine and iminium ion formation, was utilized to develop a novel single-enzyme triple biocascade reaction, effectively creating the enzymatic version of the classic organocatalyzed Enders triple cascade.

1.2.2 Stereospecific Radical Coupling Enabled by a Non-Natural Photodecarboxylase

Chapter III introduces a novel photoenzymatic strategy that significantly diverges from existing photobiocatalytic methodologies.[42] We developed a non-natural photodecarboxylase employing a unique mechanism of photoactivation *via* excitation of enzyme-bound catalytic intermediates **XV** (Figure 1.10). Specifically, this strategy exploits the photoproperties of iminium ions **XV**, transiently formed from enals **7** within the active site of an engineered class I aldolase. The formed iminium ion absorbs violet light, acting as SET oxidant to drive the oxidation of chiral carboxylic acid **23**. Upon subsequent decarboxylation, the resulting chiral radical **XVII** undergoes stereospecific cross-coupling with β-enaminyl radical **XVI**, yielding products **24** with two stereocenters. By using the appropriate enantiopure chiral substrate, the desired diastereomeric product was selectively formed with complete enantiocontrol. This finding underscores the active site's ability to transfer stereochemical information from the chiral radical precursor into the product, effectively preventing racemization of prochiral radicals. The resulting 'memory of chirality' scenario[43] is a rarity in enantioselective radical chemistry. This work highlights the potential for novel light-driven radical methodologies based on the photoexcitation of enzyme-bound intermediates. The confined environment of the active site offers a promising strategy to address challenges in asymmetric catalysis.

[42] Tseliou, V., Kqiku, L., Berger, M., Schiel, F, Melchiorre, P. "Stereospecific Radical Coupling Enabled by a Non-Natural Photodecarboxylase." *Under revision*.
[43] Gloor, C. S., Dénès, F., Renaud, P. "Memory of chirality in reactions involving monoradicals." *Free Radic. Res.* **2016**, *50*, 102–111.

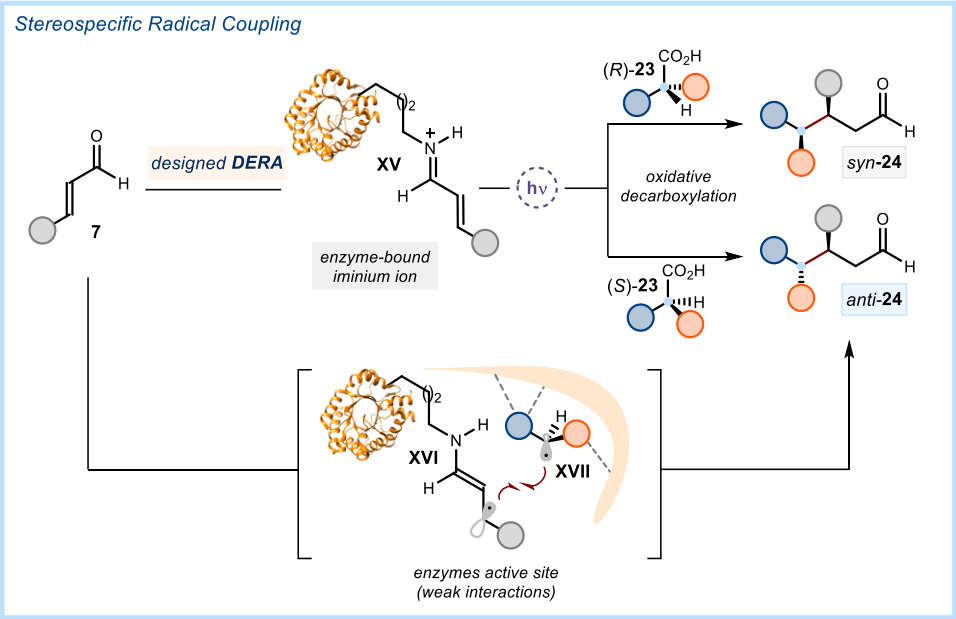

Figure 1.10. A stereospecific radical coupling of enals **7** with chiral carboxylic acids **23** using an unnatural photodecarboxylase.

Chapter II

Enantioselective Biocascade Catalysis Using a Single Multifunctional Enzyme

Target

Developing a highly enantioselective two-and-three-component cascade reaction enabled by a single multifunctional enzyme.

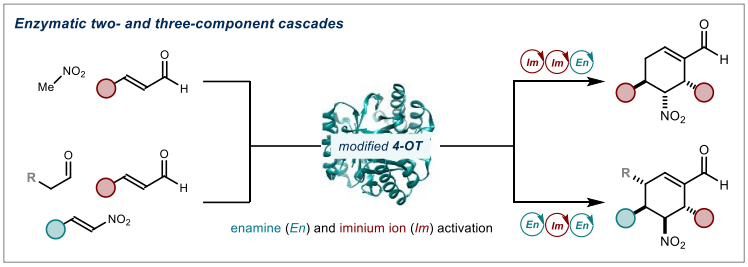

Tools

Leveraging the unique catalytic versatility of the terminal proline residue in 4-oxalocrotonate tautomerase enzymes enables reactions to proceed through both enamine and iminium ion activation pathways.[1]

2.1 Introduction

Biocatalysis, organocatalysis and transition metal catalysis are the pillars of asymmetric catalysis. While the mechanisms of organocatalysis have some similarities with specific natural enzymes (e.g., class I aldolases), the connections between these two fields have remained scarce. The term organocatalysis refers to the acceleration of chemical reactions by adding a substochiometric amount of an organic compound. While sporadic examples of chemical transformations[2] using organic catalysts have been reported over the last century, the field experienced explosive growth thanks to the groundbreaking work of Barbas, Lerner, and List as well as MacMillan's contributions in the early 2000s.[3,4] Today, organocatalysis is

[1] The project discussed in this chapter was conducted in collaboration with Dr. Vasilis Tseliou, Dr. Adriana Faraone, Dr. Jan Vilím, and Gianluca Simionato. The biochemical work was directed by Dr. Vasilis Tseliou and Dr. Jan Vilím, who conducted also the optimization studies. Adriana Faraone and I were involved in the synthetic work, optimization studies and investigation of the scope of the three processes. Adriana Faraone was also involved in the mechanistic studies. Part of the work has been published in: Tseliou, V., Faraone, A., Kqiku, L., Vilím, J., Simionato, G., Melchiorre, P. "Enantioselective Biocascade Catalysis With a Single Multifunctional Enzyme", *Angew. Chem. Int. Ed.* **2022**, *61*, e202212176.

[2] Bredig G, Fiske P. *Biochem Z.* **1912**, *46*, 7-20.

[3] List, B., Lerner, R. A., Barbas, C. F. "Proline-Catalyzed Direct Asymmetric Aldol Reactions", *J. Am. Chem. Soc.* **2000**, *122*, 2395-2396.

[4] Ahrendt, K. A., Borths, C. J., MacMillan D. W. C. "New Strategies for Organic Catalysis: The First Highly Enantioselective Organocatalytic Diels−Alder Reaction", *J. Am. Chem. Soc.* **2000**, *122*, 4243-4244.

a thriving research area in synthetic chemistry. A key factor in its success has been the identification of generic mechanisms of substrate activation in organocatalysis, which can be categorized into two main groups: 'covalent' and 'noncovalent' organocatalysis. In the former scenario, a covalent bond forms between the substrate(s) and the organic catalyst during the catalytic cycle. This is exemplified by proline-catalyzed aldol reactions, which involve enamine intermediates, or reactions like cycloadditions and conjugate additions that utilize iminium ions derived from enal substrates and a chiral amine catalyst, which enable stereoinduction. These mechanisms of 'covalent' activation will be discussed below.

2.1.1 Enamine-Mediated Catalysis

Enamines are remarkably reactive neutral carbon nucleophiles.[5–7] They readily engage with a diverse array of electrophiles, catalyzing various reactions such as aldol, Mannich or Michael additions.

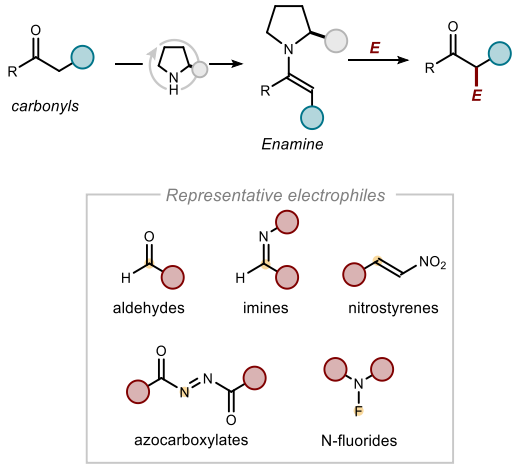

Figure 2.1. The polar reactivities of enamines. Grey circles represent the chiral catalyst scaffolds. Orange circles represent position of nucleophilic attack

The term "enamine" was coined by Wittig, although at that time, enamines were not regarded as reactive intermediates.[8] In 1964, Rutter proposed the initial enamine-based mechanism for a reaction conducted by an aldolase enzyme.[9] This mechanistic proposal gained acceptance in

[5] Stork, G., Terrell, R., Szmuszkovicz, J. "A new synthesis of 2-alkyl and 2-acyl ketones." *J. Am. Chem. Soc.* **1954**, *76*, 2029–2030.

[6] Rappoport, Z. "The chemistry of enamines" Wiley & Sons, 1994.

[7] Hickmott, P. W. "Enamines: recent advances in synthetic, spectroscopic, mechanistic, and stereochemical aspects—I." *Tetrahedron* **1982**, *38*, 1975–2050.

[8] Wittig, G., Blumenthal, H. "Über die Einwirkung von Ammoniak und Ammoniak-Derivaten auf o-Acetylaceto-phenole. " *Berichte der Dtsch. Chem. Gesellschaft* **1927**, *60*, 1085–1094.

[9] Rutter, W. J. „Evolution of Aldolase." *Fed. Proc. Am. Soc. Exp. Biol.*. **1964**, *23*, 1248–1257.

the realm of enzymatic enamine catalysis.

Over the following decades, some sporadic examples of small chiral organic molecules performing enamine catalysis were reported. For instance, in the early 1970s, a pioneering contribution to the field of asymmetric catalysis was made by Hajos and Parrish (Figure 2.2a).[10] They demonstrated that (*S*)-proline **A** can catalyze the cyclization of the achiral triketone **1**, resulting in the enantioselective formation of enone **2**. However, it took until the 2000s, with the groundbreaking contributions of Barbas, Lerner, and List, that the concept of enamine-mediated catalysis, particularly in the context of intermolecular aldol reactions with proline, became widely acknowledged. They reported the development of the first enantioselective intermolecular aldol reaction using the amino acid proline as organocatalyst (Figure 2.2b).[3] In this process, proline **A** activates acetone **3**, forming an enamine intermediate that catalyzes the aldol addition of acetone **3** to a substituted benzaldehyde **4**, yielding the aldol addition product **5** with moderate yield and enantioselectivity. The five-membered ring of proline significantly contributes to the nucleophilic nature of the corresponding enamine intermediate.

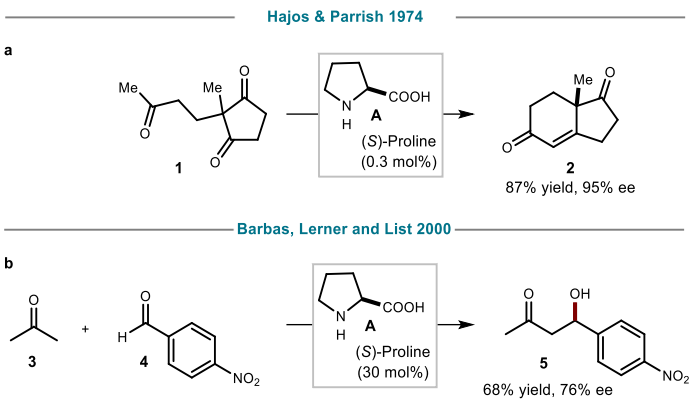

Figure 2.2. a) Prioneering contribution of Hajosh & Parrish b) Barbas, Lerner and List's landmark reaction in enamine catalysis.

The nucleophilicity of enamines varies depending on the extent of delocalization of the nitrogen lone pair, which is influenced by the structure of the amine catalyst. Enamines derived from cyclic five-membered ring amines, such as pyrrolidine, exhibit greater nucleophilicity compared to those derived from six-membered rings.[11]

[10] Hajos, Z. G; Parrish, D. R. "Asymmetric Synthesis of Bicyclic Intermediates of Natural Product Chemistry" *J. Org. Chem.* **1974**, *39*, 1615-1621

[11] Kempf, B., Hampel, N., Ofial, A. R., Mayr, H. "Structure - Nucleophilicity relationships for enamines." *Chem. - A Eur. J.* **2003**, *9*, 2209–2218.

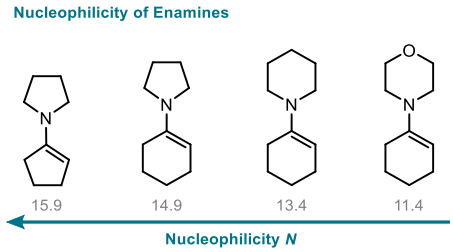

Figure 2.3. Nucleophilicity of various enamines.

Consequently, the reactivity trend of enamines follows: pyrrolidine-derived > acyclic amine-derived > piperidine-derived enamines.

Generally, the mechanism of enamine-mediated catalysis initiates with the reversible formation of an enamine *via* the condensation of a secondary or primary amine with an aldehyde or ketone **6**, yielding imines or iminium ions **I** (Figure 2.4a). Upon deprotonation of the acidic α-proton, the nucleophilic enamine **II** is formed, which then can attack an electrophile ***E***. Hydrolysis of the imine **III** leads the α-substituted product **7**. Compared to the enol counterpart, the enamine exhibits a higher energy of the highest occupied molecular orbital (HOMO) (Figure 2.4b), enabling its reaction with various electrophiles in solution.

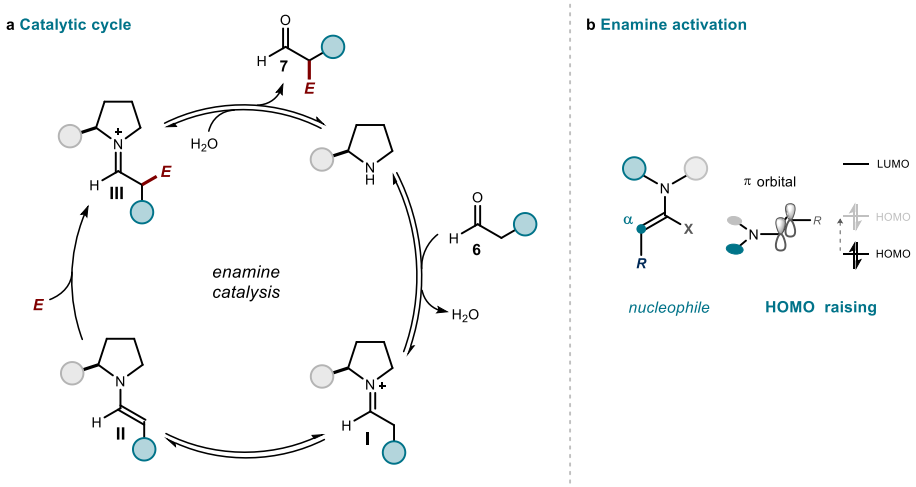

Figure 2.4. a) Schematic enamine catalytic cycle. b) enamine activation.

2.1.2 Iminium-Ion-Mediated Catalysis

Iminium ion-based catalysis is as a potent approach to activate α,β-unsaturated carbonyl compounds for nucleophilic additions and finds widespread application in two key reactions: cycloaddition and conjugate addition of nucleophiles (Figure 2.5).[12] This activation mode relies on the condensation of an amine catalyst under acidic conditions, forming iminium ion intermediates, with enhanced electrophilicity compared to the corresponding α,β-unsaturated carbonyl compound, to enable otherwise challenging or previously unknown reactions.

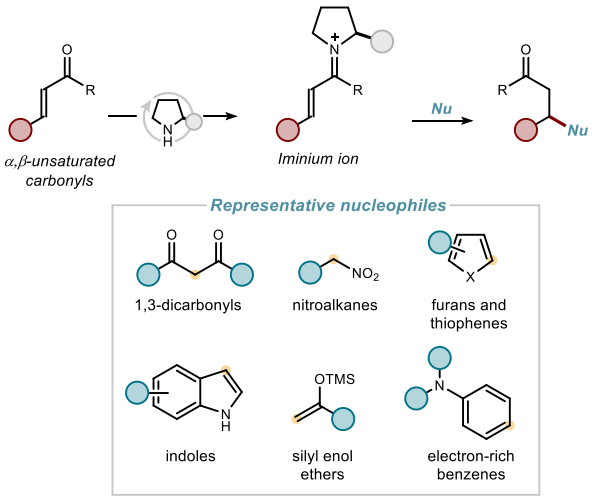

Figure 2.5. The polar reactivity of iminium ions. Grey circles represent the chiral catalyst scaffolds. Orange circles represent position of electrophilic attack.

The foundational concept of iminium ion catalysis was introduced in a seminal study by MacMillan in 2000, wherein he described an asymmetric Diels-Alder cycloaddition (Figure 2.6a).[4] The condensation of a chiral imidazolidinone catalyst **B** with α,β-unsaturated aldehyde **8** led to the reversible formation of a chiral electron-deficient iminium ion. This iminium ion served as a chiral dienophile, engaging in a Diels-Alder cycloaddition with a diene **9**. Its formation mimics the π-electronic behavior and equilibrium dynamics conventionally associated with Lewis acid activation, thereby lowering the energy of the lowest unoccupied molecular orbital (LUMO) of the π-system with respect to the corresponding enal, facilitating subsequent reaction with nucleophiles (Figure 2.6b).

[12] Lelais, G., MacMillan, D. W. C. "Enantioselective Organocatalysis" Wiley-VCH, Weinheim, 2007.

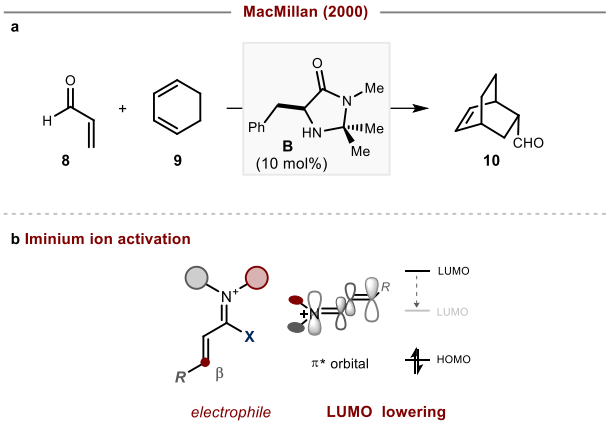

Figure 2.6. a) MacMillan's landmark reaction in iminium ion catalysis. b) Iminium ion activation.

The typical mechanism of action for the conjugate addition involves the condensation of the chiral aminocatalyst with enal **11**, yielding a chiral electrophilic iminium ion intermediate **IV**. The nucleophile attacks at the electrophilic β-position of **IV** to generate an enamine intermediate **V**, which, upon α-protonation and hydrolysis, furnishes the enantioenriched chiral β-functionalized aldehyde **12**. The versatility of iminium ion activation is evidenced by the multitude of enantioselective transformations developed over the past two decades.[13]

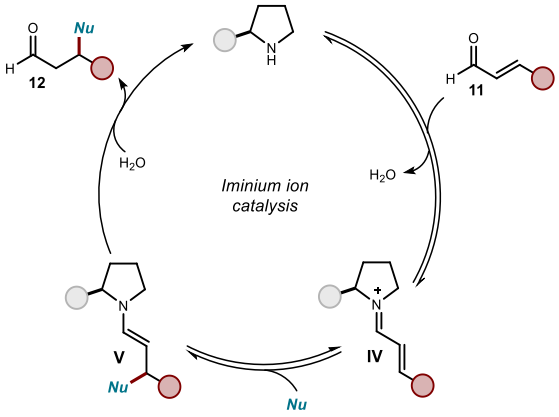

Figure 2.7. Schematic iminium ion catalytic cycle.

While the majority of transformations reported in the literature utilizing the LUMO-lowering iminium ion activation concept employ secondary amines as catalysts, it is worth noting that under the acidic conditions inherent to this mode of activation, primary amines can also serve as efficient catalysts, with the active species being a protonated imine.

[13] Hayashi, Y. "Catalytic Asymmetric Synthesis" John Wiley & Sons, Inc., Hoboken, 2022.

2.1.3 Organocascade Reactions combining Enamine and Iminium Ion Catalysis

Organocatalysis has provided new opportunities to develop asymmetric multicomponent reactions,[14–16] aiming to convert simple starting compounds into complex chiral products in a single step. This approach requires the ability of a single catalyst to promote different mechanisms of substrate transformation, activating different substrates through divergent mechanisms. One notable example is the use of small amine catalysts in organocascade processes, where both iminium and enamine activations of carbonyl substrates are harnessed within the same reaction sequence. This approach enabled cascade processes using a single amine catalyst in one-pot and a sequential fashion. For example, as exemplified in Figure 2.8, when unsaturated iminium ions react with nucleophiles, they afford enamines. the latter intermediates, being nucleophilic in character, can then intercept electrophiles to generate a final product with multiple stereocenters. In these reactions, an iminium-ion/enamine sequence is operational.

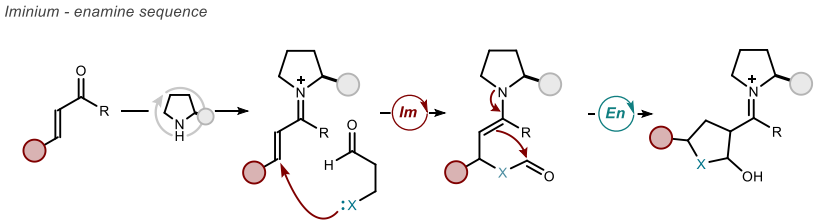

Figure 2.8. Generic organocatalytic cascade strategy: iminium ion – enamine sequence.

Two pioneering examples of organocascade processes that harnessed a sequence of iminium ion and enamine activation were reported by Yamamoto and MacMillan. Yamamoto developed an enantioselective organocascade employing a sequence of enamine-iminium ion reactions using cyclic enones **13** and aromatic nitroso compounds **14** (Figure 2.9a).[17] The cyclic enone **13** condensed with the secondary amine catalyst **C** to form an enamine which was prone to trap the electrophilic oxygen of the nitroso compound **14**. This led to the intramolecular cyclization at the iminium ion to yield the Diels-Alder product **15**.

In the second work, MacMillan demonstrated a three-component cascade reaction via an iminium ion-enamine activation sequence, resulting in a difunctionalized product **19** (Figure

[14] Guillena, G., Ramón, D. J., Yus, M. "Organocatalytic enantioselective multicomponent reactions (OEMCRs)" *Tetrahedron Asymmetry* **2007**, *18*, 693–700.

[15] Simmons, B., Walji, A. M., MacMillan, D. W. C. "Cycle-specific organocascade catalysis: Application to olefin hydroamination, hydro-oxidation, and amino-oxidation, and to natural product synthesis." *Angew. Chemie - Int. Ed.* **2009**, *48*, 4349–4353.

[16] Enders, D., Grondal, C., Hüttl, M. R. M. "Asymmetric organocatalytic domino reactions." *Angew. Chemie - Int. Ed.* **2007**, *46*, 1570–1581.

[17] Yamamoto, Y., Momiyama, N.,Yamamoto, H. "Enantioselective Tandem O-Nitroso Aldol/Michael Reaction." *J. Am. Chem. Soc.* **2004**, *126*, 5962–5963.

2.9b).[15] This involved the conjugate addition of nucleophilic heterocycles **17** to a range of α,β-unsaturated enals **16**, followed by α-chlorination of the resulting enamine with an electrophilic chlorinating agent **18**. This process yielded the *syn*-products **19** with high yields and enantiomeric excess. Independently, Jøergensen reported a similar domino sequence with different nucleophile-electrophile partners.[18]

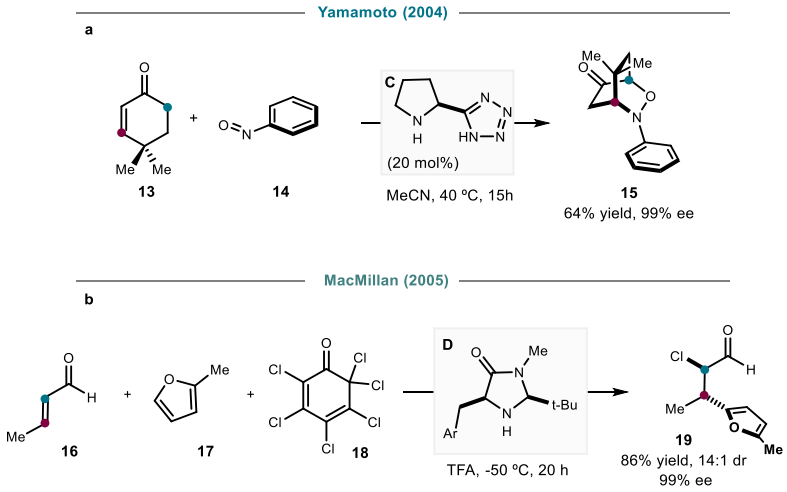

Figure 2.9. Seminal reports on asymmetric organocatalyzed enamine-iminium or iminium ion-enamine cascades reported by a) Yamamoto and b) MacMillan.

In a landmark report in 2006, Enders introduced an organocatalytic triple cascade to construct four stereogenic centers in a single operation via an enamine-iminium ion-enamine activation sequence (Figure 2.10).[19] This work marked a significant advancement in the field of organocatalytic asymmetric multicomponent reactions. Linear aldehydes like butanal **20** underwent enamine-catalyzed Michael additions to β-nitrostyrenes **21**, followed by iminium ion-catalyzed addition of the resulting nitro aldehyde **24**. The resulting enamine then underwent cyclization and aldol condensation yielding cyclic carbaldehyde **23** as a mixture of only two diastereomers (epimers at C5) and a single enantiomer.

[18] Marigo, M., Schulte, T., Franzén, J., Jørgensen, K. A. "Asymmetric Multicomponent Domino Reactions and Highly Enantioselective Conjugated Addition of Thiols to α,β-Unsaturated Aldehydes" *J. Am. Chem. Soc.* **2005**, *127*, 15710-15711.

[19] Enders, D., Hüttl, M. R. M., Grondal, C., Raabe, G. "Control of Four Stereocentres in a Triple Cascade Organocatalytic Reaction" *Nature* **2006**, *441*, 861-863.

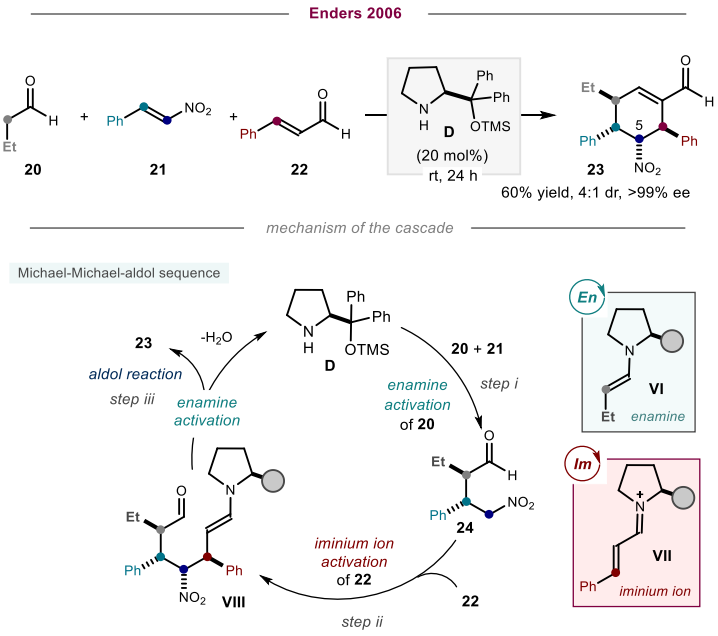

Figure 2.10. Asymmetric three-component cascade reaction operating through a Michael-Michael-aldol sequence reported by Enders in 2006.

In 2009, Enders developed a mechanistically related yet simpler two-component cascade based on an iminium ion-iminium-ion-enamine activation sequence (Figure 2.11).[20] This involved two Michael addition steps and an aldol reaction, resulting in cyclohexene carbaldehydes **26** with three stereocenters. The mechanism involved the formation of an iminium ion **VII** upon condensation of cinnamaldehyde **22** with the diphenylprolinol catalyst **D**, followed by Michael addition of nitromethane **25** to yield intermediate **27**. This nucleophilic intermediate then underwent another Michael addition to a second equivalent of cinnamaldehyde **22**, generating enamine-intermediate **IX**. Subsequent intramolecular aldol reaction yielded the product **26**. In this case, the cyclohexene carbaldehyde **26** featured identical substituents at carbon 4 and 6, since it was not possible to discriminate between different enals using catalyst **D**. This two-component process exemplified another instance of a complex cascade protocol, driven by the same multifunctional organocatalyst **D** that facilitated the earlier triple cascade reaction. Consequently, this catalyst displayed the capability to activate various substrate classes through mechanistically distinct activation strategies.

[20] Enders, D., Jeanty, M., Bats, J. W. "Organocatalytic asymmetric triple domino reactions of nitromethane with α,β-unsaturated aldehydes." *Synlett* **2009**, *19*, 3175–3178.

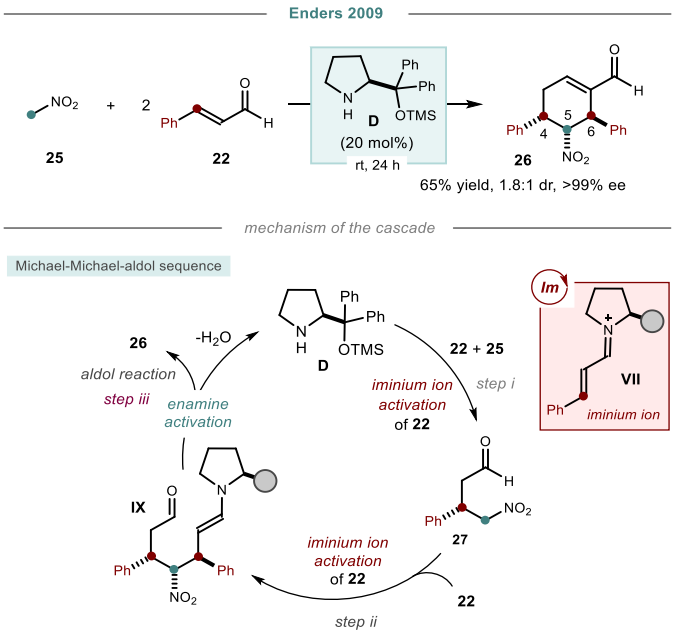

Figure 2.11. Asymmetric two-component cascade reaction operating through a Michael-Michael-aldol sequence reported by Enders in 2009.

2.1.4 Transformations of enzymes by enamine catalysis

Enamine catalysis draws inspiration from naturally occurring biological processes, particularly the carbon-carbon bond formation strategy employed by aldolase enzymes. The elucidation of the class I aldolase mechanism in the 1960s and 1970s revealed the key role of an enamine intermediate formed between a specific lysine residue within the enzyme and a carbonyl group of the substrate.[9,21] For instance, class I aldolases can utilize this intermediate to facilitate reversible aldol reactions between aldehydes and ketones yielding β-hydroxyketones.[22] This enzymatic process exemplifies the concept of aminocatalytic activation in biological systems. In the 1990s, Lerner and Barbas III designed antibodies capable of catalyzing intermolecular aldol reactions.[23] These antibodies were able to mimic the function of class I aldolase enzymes by employing the amine group of a lysine residue within their active sites. This amine moiety forms an enamine intermediate with the substrate **3**, which subsequently reacts with an aldehyde **28** to complete the aldol reaction. Notably, in their study catalytic antibody 38C2 demonstrated a broad range of compatible substrates and

[21] Lai, C. Y., Nakai, N., Chang, D. "Amino Acid Sequence of Rabbit Muscle Aldolase and the Structure of the Active Center." *Science* **1974**, *183*, 1204–1206.

[22] Clapés, P., Garrabou, X. "Current trends in asymmetric synthesis with aldolases." *Adv. Synth. Catal.* **2011**, *353*, 2263–2283.

[23] Wagner, J., Lerner, R. A., Barbas, C. F. "Efficient Aldolase Catalytic Antibodies That Use the Enamine Mechanism of Natural Enzymes." *Science* **1995**, *270*, 1797–1800.

yielded products **29** with high enantioselectivity (Figure 2.12).[24]

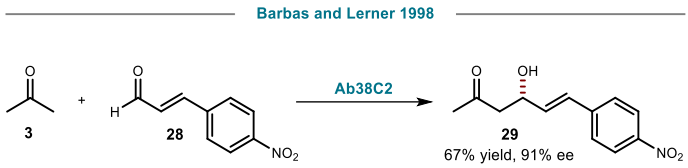

Figure 2.12. Intermolecular aldol addition catalyzed by an antibody.

With the discovery of numerous organocatalytic reactions over the last two decades, transitioning catalytic systems, like enamine catalysis, back to enzymatic platforms holds significant promise for developing novel biocatalysts. For example, researchers have successfully engineered and repurposed enzymes to engage in enamine catalysis for specific synthetic transformations. An illustrative instance is the engineering of the artificial aldolase RA95.5-8 to enable enamine catalysis for C-C bond formation reactions. Hilvert and colleagues developed the asymmetric synthesis of γ-nitroketones **30** through a Michael-type reaction.[25] The condensation of acetone **3** with the active site lysine (K83) generated an enamine species **X**, which enabled the addition to nitrostyrenes **21**. Subsequent protein engineering led to the development of the variant RA95.5-8 S233F, proficient in catalyzing the Michael addition of acetone **3** to various substituted nitrostyrenes **21**, yielding the corresponding γ-nitroketones **30** in moderate to good yields, with up to 76% enantiomeric excess for the (*S*)-enantiomer of product **30** (Figure 2.13).

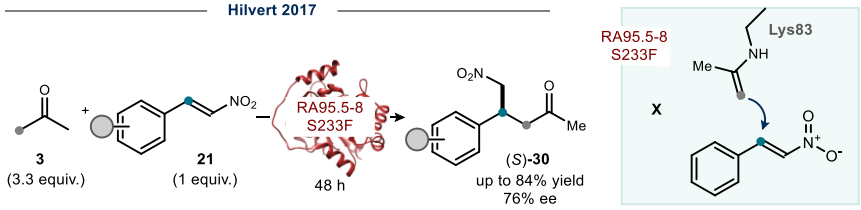

Figure 2.13. Michael addition of acetone **3** to nitrostyrene **21** using a computationally designed enzyme.

Another enzyme demonstrated to catalyze enamine reactions is 4-OT. In 2011, Poelarends reported the novel promiscuous activity of 4-OT enzymes in catalyzing the aldol condensation of acetaldehyde **31** with benzaldehyde **32**, yielding cinnamaldehyde **22**, albeit with extended

[24] Hoffmann, T., Zhong, G., List, B., Shabat, D., Anderson, J., Gramatikova, S., Lerner, R. A., Barbas, C. F., "Aldolase Antibodies of Remarkable Scope." *J. Am. Chem. Soc.* **1998**, *120*, 2768-2779.

[25] Garrabou, X., Verez, R., Hilvert, D. "Enantiocomplementary synthesis of γ-nitroketones using designed and evolved carboligases." *J. Am. Chem. Soc.* **2017**, *139*, 103–106.

reaction times of up to 14 days (Figure 2.14).[26] The authors proposed the formation of an enamine intermediate **XI** within the active site of 4-OT upon the condensation of acetaldehyde **31** with the catalytically active residue proline 1. The nucleophilic enamine thus generated within the active site of 4-OT reacted with benzaldehyde **32**. The intermediate was stabilized by arginine residue 11. Protonation of this intermediate, followed by subsequent hydrolysis, resulted in the formation of product **22**. This study underscored the ability of the proline 1 residue in 4-OT enzymes to activate aldehydes through the formation of an enamine intermediate. This enamine formation within the active site of 4-OT was directly observed trough crystallographic X-ray analysis.[27]

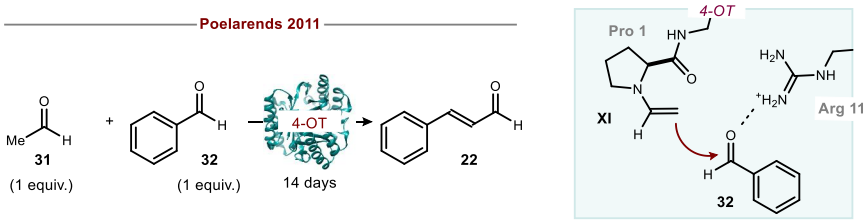

Figure 2.1. Novel promiscuous activity of 4-OT tautomerase as an aldolase catalyst.

In addition to its promiscuous activities as both an aldolase and a retro-aldolase enzyme,[28] the same research group documented the catalytic role of 4-OT as a "Michaelase" in the reaction of acetaldehyde **31** with trans-β-nitrostyrene **21**, yielding γ-nitroaldehydes **27** with commendable stereoselectivity (Figure 2.15).[29] They proposed that the proline 1 residue initiated a condensation reaction with substrate **31**, generating intermediate **XI**. The resulting nucleophilic enamine then reacted with the electrophilic β-nitrostyrene **21**, stabilized by non-covalent interactions with arginine 11, forming the new C-C bond.

[26] Zandvoort, E., Baas, B. J., Quax, W. J., Poelarends, G. J. "Systematic Screening for Catalytic Promiscuity in 4-Oxalocrotonate Tautomerase: Enamine Formation and Aldolase Activity." *ChemBioChem* **2011**, *12*, 602–609.

[27] Poddar, H., Rahimi, M., Geertsema, E. M., Thunnissen, A. M. W. H., Poelarends, G. J. "Evidence for the formation of an enamine species during aldol and Michael-type addition reactions promiscuously catalyzed by 4-oxalocrotonate tautomerase." *ChemBioChem* **2015**, *16*, 738–741.

[28] Zandvoort, E., Geertsema, E. M., Quax, W. J., Poelarends, G. J. "Enhancement of the Promiscuous Aldolase and Dehydration Activities of 4-Oxalocrotonate Tautomerase by Protein Engineering." *ChemBioChem* **2012**, *13*, 1274–1277.

[29] Zandvoort, E., Geertsema, E. M., Baas, B. J., Quax, W. J., Poelarends, G. J. "Bridging between organocatalysis and biocatalysis: Asymmetric addition of acetaldehyde to β-nitrostyrenes catalyzed by a promiscuous proline-based tautomerase." *Angew. Chemie - Int. Ed.* **2012**, *51*, 1240–1243.

Diversely substituted aromatic trans-β-nitrostyrenes,[30] aliphatic nitroalkenes,[31] and different aldehydes[32] were successfully employed in the Michael addition, yielding highly enantioenriched γ-nitroaldehydes.

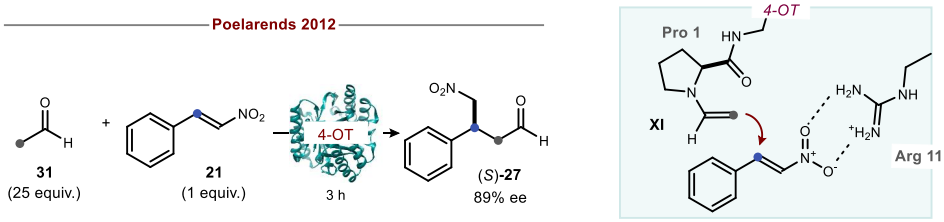

Figure 2.15. Novel promiscuous activity of 4-OT as a "Michaelase" catalyst.

Moreover, a comprehensive mutagenesis study of 4-OT was conducted, exploring all possible single-point mutations along the 62-amino acid sequence of the enzyme monomers.[33] This investigation revealed a greater influence of residue Arg39 over Arg11 in the direct substrate binding within the active site of 4-OT. This likely played a crucial role in the protonation step of the nitronate intermediate subsequent to the addition of **31** to **21**. Furthermore, the mutagenesis study led to the identification of two novel 4-OT mutants (A33D and M45Y/F50A) exhibiting enhanced "Michaelase" activity and high stereoselectivity for the opposite (*R*)-product in the acetaldehyde addition to nitrostyrene derivatives **21**.

Furthermore, DERA and FSA enzymes have been identified as catalysts for various aldol addition reactions involving aldehydes and ketones, facilitating the formation of C-C bonds *via* enamine catalysis.[22,34,35] In 2015, Clapés reported an example of a multicomponent asymmetric biocascade reaction catalyzed by a single enzyme (Figure 2.16).[36] Various

[30] Miao, Y., Tepper, P. G., Geertsema, E. M., Poelarends, G. J. "Stereochemical Control of Enzymatic Carbon–Carbon Bond-Forming Michael-Type Additions by 'Substrate Engineering'." *European J. Org. Chem.* **2016**, *14*, 5350–5354.

[31] Kunzendorf, A., Saifuddin, M., Poelarends, G. J. "Enantiocomplementary Michael Additions of Acetaldehyde to Aliphatic Nitroalkenes Catalyzed by Proline-Based Carboligases." *ChemBioChem* **2022**, *23*, 15–17.

[32] Miao, Y., Geertsema, E. M., Tepper, P. G., Zandvoort, E., Poelarends, G. J. "Promiscuous Catalysis of Asymmetric Michael-Type Additions of Linear Aldehydes to β-Nitrostyrene by the Proline-Based Enzyme 4-Oxalocrotonate Tautomerase." *ChemBioChem* **2013**, *14*, 191–194.

[33] Van Der Meer, J. Y., Poddar, H., Baas, B. J., Miao, Y., Rahimi, M., Kunzendorf, A., Van Merkerk, R., Tepper, P. G., Geertsema, E. M., Thunnissen, A. M. W. H., Quax, W. J., Poelarends, G. J. "Using mutability landscapes of a promiscuous tautomerase to guide the engineering of enantioselective Michaelases." *Nat. Commun.* **2016**, *7*, 1-16.

[34] Mifsud, M., Szekrényi, A., Joglar, J., Clapés, P. "In situ aldehyde generation for aldol addition reactions catalyzed by d-fructose-6-phosphate aldolase." *J. Mol. Catal. B Enzym.* **2012**, *84*, 102–107.

[35] Roldán, R., Hernández, K., Joglar, J., Bujons, J., Parella, T., Fessner, W. D., Clapés, P. "Aldolase-Catalyzed Asymmetric Synthesis of N-Heterocycles by Addition of Simple Aliphatic Nucleophiles to Aminoaldehydes." *Adv. Synth. Catal.* **2019**, *361*, 2673–2687.

[36] Szekrenyi, A., Garrabou, X., Parella, T., Joglar, J., Bujons, J., Clapés, P. "Asymmetric assembly of aldose carbohydrates from formaldehyde and glycolaldehyde by tandem biocatalytic aldol reactions." *Nat. Chem.* **2015**, *7*, 724–729.

engineered variants of the aldolase FSA from *E.coli* demonstrated the ability to combine two molecules of glycoaldehyde **34** with one molecule of a small aldehyde **33**, including a simple C1 synthon like formaldehyde, in a sequential aldol cascade, yielding aldose sugars **36** with moderate to good yields and high stereocontrol. In these reactions, one molecule of substrate **34** was activated as an enamine intermediate by the catalytically active lysine residue within FSA. The aldehyde functioned as the acceptor in the initial aldol addition. Subsequently, another molecule of substrate **34** was activated through enamine intermediate formation in FSA's active site, while the intermediate **35** from the preceding step served as the aldehyde acceptor. Through a single spontaneous cyclization, the hemiacetal products **36** were obtained. In this study, the enzyme showcased its capability to involve more than two molecules of small, achiral substrates in constructing chiral compounds through a series of consecutive steps. Nevertheless, the multistep process depended on a *single*, consistently *repeated activation mechanism*—enamine activation.

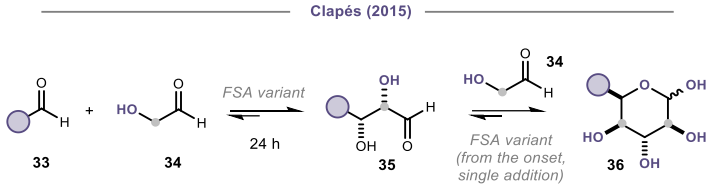

Figure 2.16. Multicomponent aldol cascade for the synthesis of sugars mediated by engineered FSA aldolases.

2.1.5 Transformations of Enzymes by Iminium Ion Catalysis

In contrast to enamine catalysis, iminium ion catalysis is not employed in nature. While iminium ion formation is a component of the catalytic cycle in pyridoxal phosphate (PLP)-dependent enzymes and class I aldolases, natural enzymes with iminium ion catalysis capability are uncommon.[37,38] Consequently, researchers have redirected their focus towards repurposing both natural and computationally designed enzymes containing catalytic lysine or N-terminal proline residues for iminium ion biocatalysis. Through repurposing existing enzymes or construction of artificial enzymes, a diverse array of biocatalysts for iminium ion catalysis has been engineered and fine-tuned *via* protein engineering to facilitate non-natural transformations.[39]

For instance, Poelarends explored the potential of 4-oxatocrotonate tautomerase (4-OT) for

[37] Di Salvo, M. L., Remesh, S. G., Vivoli, M., Ghatge, M. S., Paiardini, A., D'Aguanno, S., Safo, M. K., Contestabile, R. "On the catalytic mechanism and stereospecificity of *Escherichia coli* l -threonine aldolase." *FEBS J.* **2014**, *281*, 129–145.

[38] Haridas, M., Abdelraheem, E. M. M., Hanefeld, U. "2-Deoxy-D-ribose-5-phosphate aldolase (DERA): Applications and Modifications." *Appl. Microbiol. Biotechnol.* **2018**, *102*, 9959–9971.

[39] Xu, G., Poelarends, G. J. "Unlocking New Reactivities in Enzymes by Iminium Catalysis." *Angew. Chemie - Int. Ed.* **2022**, *61*, e202203613.

iminium ion catalysis.[40] 4-OT possesses a *N*-terminal proline (Pro-1) within the active site. By engineering 4-OT they successfully enabled iminium ion catalysis. The modified 4-OT demonstrated enantioselective Michael addition of nitromethane **25** to various α,β-unsaturated aldehydes **22** *via* enzyme-bound iminium-ion intermediates (Figure 2.17). Through screening of a library of single mutants of 4-OT, they identified that the F50A mutation significantly enhanced the catalytic efficiency for the Michael addition reaction, yielding γ-nitroaldehydes **27** with excellent yield and high enantiopurity from diverse α,β-unsaturated aldehydes **22**. It was proposed that by replacing phenylalanine 50 with alanine, the rate of hydrolysis was enhanced for the enamine intermediate formed upon addition of **22** to **XII**, facilitating product release. This mutation created a water-accessible cavity within the active site, reducing its hydrophobicity without affecting the pKa of crucial *N*-terminal proline.[28] Notably, 4-OT F50A increased the enantioselectivity to 98% ee, a significant improvement compared to the wild-type 4-OT enzyme (35% yield, 72% ee).

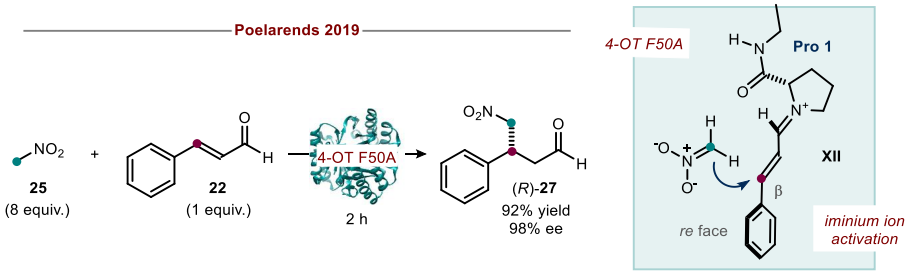

Figure 2.17. Iminium ion activation in a 4-OT mutant.

Another enzyme displaying promiscuous activity towards iminium ion catalysis is 2-deoxy-D-ribose-5-phosphate aldolase (DERA), a class I aldolase widely utilized in biocatalysis for its ability to forge C-C bonds. Poelarends and colleagues engineered an efficient biocatalyst for the conjugate addition of nitromethane **25** to enals **22** by subjecting DERA to 11 rounds of mutagenesis and thereby replacing twelve amino acids (Figure 2.18).[41] This resulted in an enzyme with a remarkable 190-fold increase in catalytic activity compared to the parental enzyme. High-resolution crystal structure of DERA-MA revealed the formation of an iminium ion intermediate **XIII** between the cinnamaldehyde **22** and the catalytic residue Lys-167. Notably, directed evolution played a crucial role in reshaping two loops of the enzyme, creating a dedicated binding pocket for the covalently bound substrate.

[40] Guo, C., Saifuddin, M., Saravanan, T., Sharifi, M., Poelarends, G. J. "Biocatalytic Asymmetric Michael Additions of Nitromethane to α,β-Unsaturated Aldehydes via Enzyme-bound Iminium Ion Intermediates." *ACS Catal.* **2019**, *9*, 4369–4373.

[41] Kunzendorf, A., Xu, G., van der Velde, J. J. H., Rozeboom, H. J., Thunnissen, A. M. W. H., Poelarends, G. J. "Unlocking Asymmetric Michael Additions in an Archetypical Class I Aldolase by Directed Evolution." *ACS Catal.* **2021**, *11*, 13236–13243.

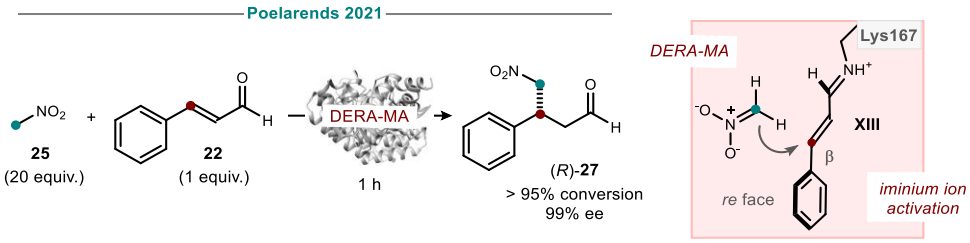

Figure 2.18. Iminium ion activation using genetically modified DERA.

Furthermore, enzyme-mediated iminium catalysis can also be achieved through computational design and evolution of enzymes toward desired reactivity.[25,42]

2.1.6 Multifunctional Biocatalysts

While some biocatalysts exhibit remarkable versatility, handling a wide range of substrates and catalyzing multiple transformations, designing systems where enzymes perform diverse catalytic activities within a single sequence remains a challenge. Multifunctional biocatalysts hold immense potential for streamlining chemical synthesis by minimizing steps and reducing the number of enzymes required.[43] However, there are significant hurdles to overcome when an enzyme attempts to catalyze mechanistically distinct reactions: (*i*) the biocatalyst needs to effectively bind and orient structurally related molecules, as the product from one reaction becomes the substrate for the next. (*ii*) the catalytic active site must possess residues capable of participating in diverse non-bonding interactions (e.g. proton donors and acceptors) for different reactions and (*iii*) in some cases, multiple cofactors might be necessary to mediate distinct processes, such as reduction of both C=O and C=N bonds. These multifunctional biocatalysts catalysts perform two or more chemically distinct reactions within a single active site, seamlessly converting a substrate into a final product.

A recent example of a multifunctional biocatalyst is the Ene-IRED discovered by Turner, an enzyme able to catalyze the conjugate alkene reduction and subsequent reductive amination or imine reduction (Figure 2.19).[44] The Ene-IRED was identified through a large screening of a metagenomic library focused on imine reductases (IREDs).[45] This variant was capable of accepting iminium ion intermediates generated upon spontaneous condensation of

[42] Garrabou, X., Beck, T., Hilvert, D. "A promiscuous de Novo retro-aldolase catalyzes asymmetric michael additions via Schiff base intermediates." *Angew. Chemie - Int. Ed.* **2015**, *54*, 5609–5612.

[43] Thorpe, T. W., Marshall, J. R., Turner, N. J. "Multifunctional Biocatalysts for Organic Synthesis." *J. Am. Chem. Soc.* **2024**, *146*, 7876–7884.

[44] Thorpe, T. W., Marshall, J. R., Harawa, V., Ruscoe, R. E., Cuetos, A., Finnigan, J. D., Angelastro, A., Heath, R. S., Parmeggiani, F., Charnock, S. J., Howard, R. M., Kumar, R., Daniels, D. S. B., Grogan, G., Turner, N. J. "Multifunctional biocatalyst for conjugate reduction and reductive amination." *Nature* **2022**, *604*, 86–91.

[45] Marshall, J. R., Yao, P., Montgomery, S. L., Finnigan, J. D., Thorpe, T. W., Palmer, R. B., Mangas-Sanchez, J., Duncan, R. A. M., Heath, R. S., Graham, K. M., Cook, D. J., Charnock, S. J., Turner, N. J. "Screening and characterization of a diverse panel of metagenomic imine reductases for biocatalytic reductive amination." *Nat. Chem.* **2021**, *13*, 140–148.

cyclohexenones **37** with amines **38** in the active site. The enzyme facilitated sequentially the asymmetric conjugate reduction of the C-C double bonds in iminium ions **39** (acting as an ene-reductase, EneRED), followed by the asymmetric reduction of C-N double bonds (IRED activity) in iminium ion intermediates **40**. This resulted in the production of enantioenriched chiral amines **41** with moderate to high levels of both chemo- and stereoselectivity. The novelty of the EneIRED enzyme lies in its exceptional ability to execute two distinct mechanistic steps. Intriguingly, experiments showed that the C-C bond reduction (*step one)* would not occur on the cyclohexenone **37** alone, requiring the presence of the amine **38**. Thus, the identified EneIRED variant exhibited selectivity in activating only iminium ion functionalities while demonstrating restrained substrate promiscuity.

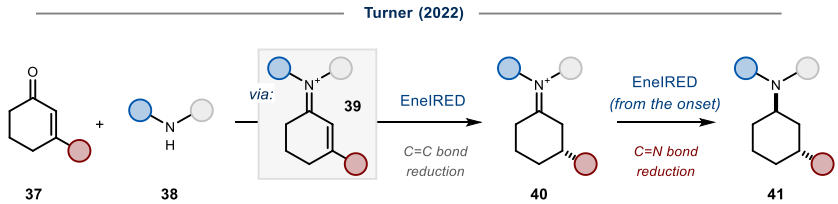

Figure 2.19. A recently discovered multifunctional imine reductase (EneIRED) enzyme drives a sequential two-step cascade characterized by two distinct reactivities.

Another example of a multifunctional biocatalyst is 4-OT, as demonstrated by Poelarends, who developed a one-pot cascade process combining multiple activities of 4-OT to facilitate the conversion of aldehydes **31** and **32** into nitroaldehydes **27** (Figure 2.20).[40] In this sequence, 4-OT initially forms a nucleophilic enamine intermediate **XIII** between the aliphatic aldehyde and the N-terminal proline, enabling aldol addition to the aromatic aldehyde **32**. Subsequently, it catalyzes the dehydration of the intermediate to yield the corresponding α,β-unsaturated aldehyde **22**. This enal is then activated by the same proline residue as an electrophilic unsaturated iminium ion intermediate **IX**, facilitating the subsequent Michael addition of nitromethane **25** to produce a nitroaldehyde **27**. Variant 4-OT F50A emerged as a potent catalyst for these reactions in a one-pot setting. This system was used to form γ-nitroaldehydes **27**, subsequently oxidized to the corresponding γ-nitrocarboxylic acids **42** with yields of 53% and excellent enantioselectivities of 99% ee.

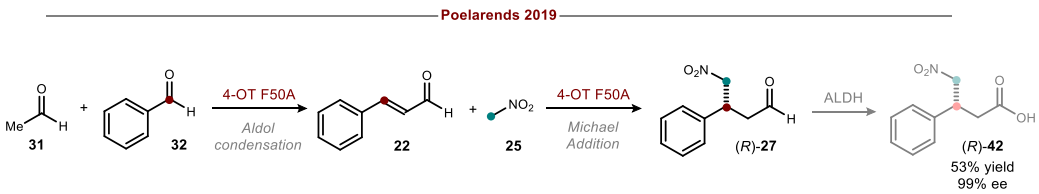

Figure 2.20. Biocascade using 4-OT F50A as multifunctional biocatalyst performing a sequence of aldol condensation and Michael addition.

Identifying and engineering multifunctional biocatalysts offer a means to simplify biocatalytic routes by reducing the number of required biocatalysts. By utilizing different substrate activation mechanisms, a wide array of complex stereoenriched functionalized products can be prepared.

2.2 Target of the Project

The present study was motivated by our interest in developing a multifunctional biocatalyst that promotes several steps of a cascade in a stereoselective fashion. We specifically targeted the intriguing triple cascade reaction reported by Enders in 2006,[19] which is likely the most sophisticated cascade process implemented using a single organic catalyst able to sequentially exploit orthogonal activation mechanisms of substrates. Our aim was to implement a *biocatalytic* version of this strategy. To achieve this goal, we needed to identify an enzyme with several key abilities: *i*) activating aldehydes **20** by forming an enamine intermediate, *ii*) activating enals **22** by forming an iminium ion intermediate, and *iii*) combining these two activation principles in a regulated sequence necessary to achieve the Enders triple cascade. This sequential activation would ultimately lead to the desired complex products **23**. In the ideal scenario, our biocatalytic protocol for the implementation of the Enders cascade processe would not only match, but even outperform the original organocatalytic method in terms of efficiency and selectivity for synthesizing the desired complex product.

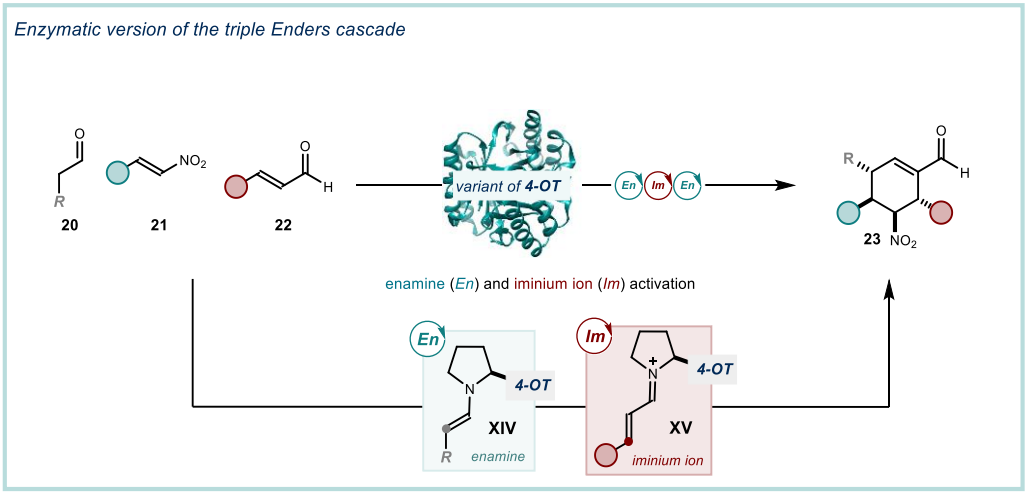

Figure 2.21. Target of the project: enzymatic version of the Enders cascade.

2.3 Results and Discussion

2.3.1 Identification of a Suitable Enzyme Family

Developing an enzymatic version of the Enders triple cascade, a remarkable example of organocatalysis, presented a challenge. We needed to find a biocatalyst that could efficiently generate both enamine and iminium ion intermediates from aldehydes. This ability mirrors the multifunctional behavior of the diphenylprolinol organocatalyst depicted in Figures 2.10 and 2.11. We were inspired by the innovative work of Poelarends and colleagues. They showed that natural 4-oxalocrotonate tautomerases (4-OT) from *Pseudomonas putida* (Pp-4OT) and their engineered variants hold exciting potential. These enzymes can be used to develop various non-natural carbon-carbon bond-forming processes, mimicking the catalytic mechanisms of classical organocatalysis with high stereoselectivity.[39,46] 4-Oxalocrotonate tautomerase (4-OT, EC 5.3.2.X) is a subgroup within the larger tautomerase superfamily.[47] One well-studied example is 4-OT from the soil bacterium *Pseudomonas putida* (Pp-4OT, EC 5.3.2.6).[47] In its natural activity, Pp-4OT plays a part in the microbial degradation of aromatic hydrocarbons. It catalyzes the conversion of these hydrocarbons into intermediates of the Krebs cycle. Specifically, Pp-4OT catalyzes the isomerization of 4-oxalocrotonate **43** into 2-oxo-3-hexene-1,6-dioate **44** through the intermediate 2-hydroxymuconate **45** (Figure 2.22).

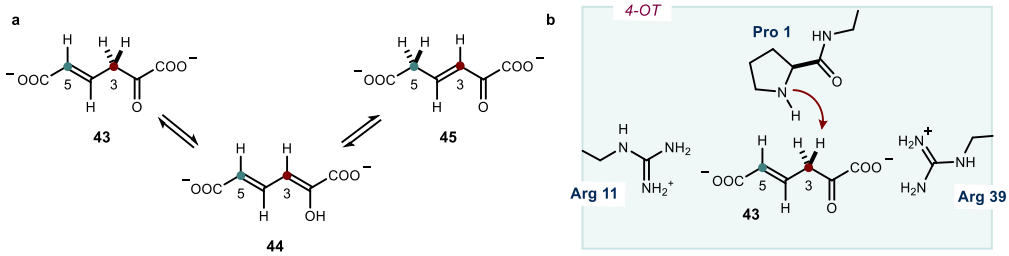

Figure 2.22. a) Natural reactivity of the Pp-4-OT enzyme: the isomerization of 4-oxalocrotonate **43**; b) proposed mechanism.[48]

[46] Miao, Y., Rahimi, M., Geertsema, E. M., Poelarends, G. J. "Recent developments in enzyme promiscuity for carbon-carbon bond-forming reactions." *Curr. Opin. Chem. Biol.* **2015**, *25*, 115–123.

[47] Davidson, R., Baas, B. J., Akiva, E., Holliday, G. L., Polacco, B. J., LeVieux, J. A., Pullara, C. R., Zhang, Y. J., Whitman, C. P., Babbitt, P. C. "A global view of structure–function relationships in the tautomerase superfamily." *J. Biol. Chem.* **2018**, *293*, 2342–2357.

[48] Whitman, C. P. "The 4-oxalocrotonate tautomerase family of enzymes: How nature makes new enzymes using a β-α-β structural motif." *Arch. Biochem. Biophys.* **2002**, *402*, 1–13.

In 1992, the configuration of this enzyme was elucidated and in another study confirmed by X-ray crystallography.[49,50] The enzyme was shown to be a homohexamer comprising six small monomers, each composed of 62 amino acid residues (Figure 2.23c). These monomers adopt a β-α-β structural motif, starting with a β-sheet β-1 at the *N*-terminus, followed by an α-helix α-1, a small 310 helix, and a second β-sheet β-2 and ends with two β-3 and β-4 strands at the *C*-terminus (see Figure 2.23a). Two monomers unite to form a dimer, where the β strands and α helices are oriented in an anti-parallel manner (see Figure 2.23b). The hexamer is constituted by the interaction of three such dimers, facilitated by non-covalent bonding between the β strands of one dimer and the C-terminal β hairpins of another. Each dimer exposes regions consisting of four anti-parallel β sheets toward the center of the hexameric structure, forming a hydrophobic cavity (see Figure 2.23c).

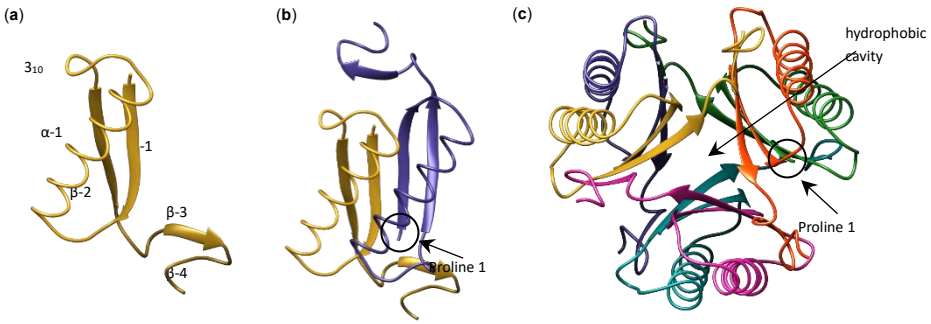

Figure 2.23. Crystal structure of the a) monomer, b) dimer, c) hexamer of 4-oxalocrotonate tautomerase isolated from Pseudomonas sp. CF600: reported by Subramanya et al. in 1996 (PDB 1OTF). All structures were plotted by UCSF Chimera 1.15.

4-OT's activity hinges on the N-terminal proline residue (Pro-1). Notably, the pKa of this proline within the active site is significantly reduced to around 6.4 compared to the free amino acid (pKa ~ 10.6).[51] This allows the Pro-1 residue under physiological pH to act as a general base in the isomerization of its natural substrate via the abstraction of the pro-R proton in carbon 3 of **43** and as an acid via protonation of carbon 5 in **44**.[48] Beyond Pro-1, a network of cationic residues plays a critical role. The positively charged residues, such as arginine 11 from one anti-parallel monomer of the dimer, and arginine 39 from another dimeric structure, were identified as crucial for stabilizing the carboxylic groups in **43** and facilitating the

[49] Chen, L. H., Kenyon, G. L., Curtin, F., Harayama, S., Bembenek, M. E., Hajipour, G., Whitman, C. P. "4-Oxalocrotonate tautomerase, an enzyme composed of 62 amino acid residues per monomer." *J. Biol. Chem.* **1992**, *267*, 17716–17721.

[50] Subramanya, H. S., Roper, D. I., Dauter, Z., Dodson, E. J., Davies, G. J., Wilson, K. S., Wigley, D. B. "Enzymatic Ketonization of 2-Hydroxymuconate: Specificity and Mechanism Investigated by the Crystal Structures of Two Isomerases." *Biochemistry* **1996**, *35*, 792–802.

[51] Czerwinski, R. M., Harris, T. K., Massiah, M. A., Mildvan, A. S., Whitman, C. P. "The structural basis for the perturbed pKa of the catalytic base in 4-oxalocrotonate tautomerase: Kinetic and structural effects of mutations of Phe-50." *Biochemistry* **2001**, *40*, 1984–1995.

accumulation of the resultant negative charge during deprotonation to yield intermediate **44**. The active site architecture of 4-OT exemplifies impressive inter-subunit cooperation. Residues from three distinct monomers (Pro-1, Arg-11, and Arg-39) act in concert to perform the catalytic transformation. This synergistic interplay is essential for 4-OT's remarkable catalytic activity. Recent studies have shown the promiscuity of 4-OT enzymes. Beyond its natural function, 4-OT can perform aldol condensations and Michael additions *via* enamine activation. This Michael addition of acetaldehyde **31** to nitrostyrene **21** resembles *step i* of the Enders triple cascade (Figure 2.10), yielding intermediate **27**. This intermediate is also the product of *step i* in the Enders two-component process (Figure 2.11).

Furthermore, Poelarends created a single-mutation variant of 4-OT capable of activating α,β-unsaturated aldehyde **22** *via* an iminium ion intermediate. This reaction, as we highlighted, corresponds to *step i* of the Enders two-component process depicted in Figure 2.11. The researchers extended this reactivity to show that the engineered 4-OT variants can efficiently catalyse diverse reactions, through iminium ion activation mode, with various nucleophiles, including epoxidations with peroxides[52] and cyclopropanations with halogenated malonates.[53] These findings demonstrate the remarkable versatility of 4-OT enzymes. They can activate carbonyl substrates for Michael additions through both enamine and iminium ion intermediates, facilitated by condensation with the terminal proline residue. While these activation modes are common in organocatalysis, it is unusual that an enzyme can perform both modes within the same active site.

Overall, 4-OT tautomerases emerge as remarkably versatile biocatalysts. They exhibit broad substrate scope, activating both linear aliphatic and α,β-unsaturated aldehydes through either enamine or iminium ion intermediates. This versatility extends to catalysing diverse reactions like Michael additions and aldol condensations, which are the crucial steps in the Enders cascade processes that form the basis of this work. Consequently, 4-OT enzymes present themselves as ideal multifunctional catalysts for developing a biocatalytic approach to the Enders cascade reactions.

2.3.2 Preliminary Results and Optimization

To validate the potential of 4-OT enzymes to combine enamine and iminium ion activation in a single cascade, we initially focused on a simpler, mechanistically related two-component process reported by Enders in 2009.[19] This reaction served as a testbed for our approach. The enzymatic process is shown in Figure 2.24. The reaction converts nitromethane **25** and cinnamaldehyde **22** to tri-substituted cyclohexene carbaldehyde **26**, which possesses three

[52] Xu, G., Crotti, M., Saravanan, T., Kataja, K. M., Poelarends, G. J. "Enantiocomplementary Epoxidation Reactions Catalyzed by an Engineered Cofactor-Independent Non-natural Peroxygenase." *Angew. Chemie - Int. Ed.* **2020**, *59*, 10374–10378.

[53] Kunzendorf, A., Xu, G., Saifuddin, M., Saravanan, T., Poelarends, G. J. "Biocatalytic Asymmetric Cyclopropanations via Enzyme-Bound Iminium Ion Intermediates." *Angew. Chemie - Int. Ed.* **2021**, *60*, 24059–24063.

contiguous stereogenic centers. This process proceeds through a sequence of Michael-Michael-aldol reactions, similar to the organocatalytic mechanism shown in Figure 2.11. The 4-OT enzyme activates enal **22** by generating the iminium ion intermediate **XV**. Then, a Michael addition of **25** to **XV** occurs. The resulting Michael product **27** undergoes a second Michael addition with its nitro-bearing nucleophilic carbon to another iminium ion **XV** intermediate. Finally, an enamine-driven aldol cyclization and dehydration furnish product **26**.

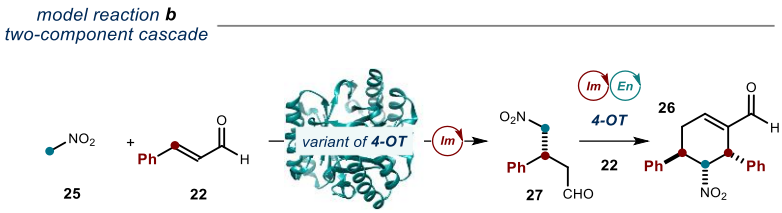

Figure 2.24. Biocatalytic approach for the two-component cascade reaction.

We investigated this two-component cascade reaction as a stepping stone towards developing the more intricate triple cascade reported by Enders in 2006 (Figure 2.10).[19] Our selection was driven by several key observations: firstly, 4-OT enzymes have been shown to facilitate the Michael addition of nitromethane **25** to cinnamaldehyde **22**, the initial step in the two-component process (see *chapter 2.1.5*). Secondly, the resulting Michael adduct **27** is identical to the intermediate formed during the *second step* of the Enders triple cascade. Notably, the mechanisms for the second and third steps in the two-component reaction mirror those of the more complex triple cascade, making it an ideal simplified model for our studies.

Our initial investigation focused on testing the wild-type Pp-4OT enzyme from *Pseudomonas putida* for its ability to activate cinnamaldehyde **22** via iminium ion formation. We cloned the gene encoding this enzyme into pET20b plasmids, expressed it in *E. coli* BL21(DE3) competent cells, and purified it following a published protocol.[26] To assess Pp-4OTs "Michaelase" activity, we incubated the enzyme with cinnamaldehyde **22** (5 mM) and an excess of nitromethane **25** (50 mM) for 24 at 30 °C (Table 2.1, entry 1). Gratifyingly, we observed the formation of the desired (*R*)-**27** product in 44% yield with 99% *ee*, along with trace amounts of the final cascade product **26**. This result supported the feasibility of our approach but also indicated the need for further optimization of the enzyme or reaction conditions to favor the complete cascade towards the final product **26**.

Table 2.1. Initial screening to test the activity of different 4-OT variants in the iminium ion activation of cinnamaldehyde **22**.[a]

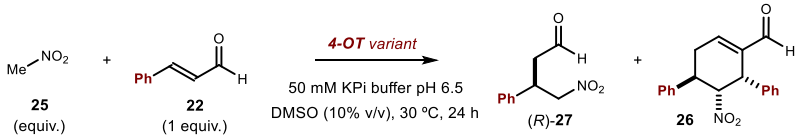

entry	enzyme (loading)	equiv. **25**	yield **27** (%)	*ee* **27** (%)[b]	yield **26** (%)	dr **26**[c]	*ee* **26** (%)[c]
1	**Pp**-4OT (4 mol%)	10	44	99	<5	*n.d.*	*n.d.*
2	**Ps**-4OT (4 mol%)	10	38	37	0	*n.d.*	*n.d.*
3	**Ml**-4OT (4 mol%)	10	41	12	0	*n.d.*	*n.d.*
4	**Tb**-4OT (4 mol%)	10	27	22	0	*n.d.*	*n.d.*
5	**DERA-MA** (4 mol%)	10	50	99	0	*n.d.*	*n.d.*
6	**Pp**-4OT (4 mol%)	1	13	99	49	>20:1	96
7	**Ps**-4OT (4 mol%)	1	22	37	7	*n.d.*	*n.d.*
8	**Ml**-4OT (4 mol%)	1	12	12	6	*n.d.*	*n.d.*
9	**Tb**-4OT (4 mol%)	1	18	22	6	*n.d.*	*n.d.*
10	**DERA-MA** (4 mol%)	1	38	99	7	*n.d.*	*n.d.*
11	-	1	0	*n.d.*	0	*n.d.*	*n.d.*

[a]Reactions performed on a 2.5 µmol scale (5 mM) at 30 °C. Analytical yields of **27** and **26** determined by GC-FID analysis (calibration using mesitylene as internal standard) and by HPLC analysis (calibration using 1,3,5-methoxybenzene as internal standard). [b]Enantiomeric excess (ee) value determined by UPC² analysis. [c]Diastereomeric ratio (dr) and enantiomeric excess (ee) measured by HPLC analysis. *n.d.* = not determined; KPi = potassium phosphate.

To enhance the cascade reaction's efficiency, we explored additional 4-OT enzymes. We employed PSI-BLAST,[54] a protein sequence similarity search method, to identify enzymes sharing over 75% sequence identity with Pp-4OT. Notably, all selected enzymes retained the *N*-terminal proline residue at position 1 due to its crucial role in catalysis. We then cloned, expressed, and purified a collection of 4-OT enzymes, including Ml-4OT from *Marinobacter lipolyticus* SM19 (NCBI accession: txid1318628, 85.7% sequence identity with Pp-4OT), Tb-4OT from *Thiolapillus brandeum* (NCBI accession: txid1076588, 79.4% sequence identity), and Ps-4OT from *Pseudomonas sagittaria* (NCBI accession: txid1135990, 93.7% sequence identity). The cloning, expression, and purification procedures employed were identical to those used for Pp-4OT.

Unfortunately, incubating the other 4-OT variants (*Ml*-4OT, *Tb*-4OT, *Ps*-4OT) under the same reaction conditions resulted in lower product yield and enantioselectivity compared to Pp-4OT (Table 2.1, entries 2-4). Notably, no formation of the cascade product **26** was observed

[54] Altschul, S. F., Madden, T. L., Schäffer, A. A., Zhang, J., Zhang, Z., Miller, W., Lipman, D. J. "Gapped BLAST and PSI-BLAST: A new generation of protein database search programs." *Nucleic Acids Res.* **1997**, *25*, 3389–3402.

with these variants. We then shifted our focus to an engineered variant of deoxyribose-phosphate aldolase, DERA-MA. This variant was recently reported to outperform Pp-4OT in the iminium ion-mediated addition of nitromethane **25** to cinnamaldehyde **22**.[41] We incubated a 10:1 ratio of nitromethane **25** (5 mM) to cinnamaldehyde **22** with 4 mol% DERA-MA in 50 mM KPi buffer pH 6.5 (10% DMSO) for 24 hours at 30 °C. While the Michael addition product (*R*)-**27** was obtained in good yield (50%) and excellent enantioselectivity (99% ee), the desired cascade product **26** was again absent (Table 2.1, entry 5). Having evaluated the ability of 4-OT variants and DERA-MA to activate **22** and promote the Michael addition to form **27**, we next aimed to optimize the reaction conditions to favor the complete cascade reaction and enhance the formation of the final product **26**. This involved adjusting the substrate stoichiometry of nitromethane **25** to cinnamaldehyde **22** from the initial 10:1 ratio to a more balanced 1:1 ratio. We hypothesized that increasing the cinnamaldehyde concentration relative to nitromethane could promote the cascade sequence, as **22** participates in two reaction steps. To test this, we re-evaluated all enzymes under these new conditions. Gratifyingly, Pp-4OT yielded 49% of the final cascade product **26** with excellent diastereo- and enantioselectivity (>20:1 dr, 96% ee). A minor amount of intermediate **27** (13% yield) was also observed (Table 2.1, entry 6). The other 4-OT variants produced lower yields of **27**, and only trace amounts of **26** were detected (Table 2.1, entries 7-9). Interestingly, DERA-MA also yielded only traces of **26** under these conditions, *suggesting its inability to further engage intermediate **25** into the cascade process* (Table 2.1, entry 10). A control experiment lacking the enzyme produced no detectable amounts of **27** or **26** (Table 2.1, entry 11). Analytical yields in Table 2.1 were determined using authentic samples of **26** prepared following the Enders procedure.[20]

The enzymatic process exhibited a key advantage over the organocatalytic reaction reported by Enders in 2009 (Figure 2.11). While the Enders reaction produced a mixture of diastereomers of compound **26** at a ratio of 1.8:1, the 4-OT enzyme selectively catalyzed the formation of the minor diastereomer with excellent enantiopurity. This demonstrates the superior diastereoselectivity of the enzymatic pathway and its ability to provide access to a previously poorly accessible stereisomer.

2.3.3 Construction of Fused 4-OT Variants

Encouraged by these findings, we chose Pp-4OT for further engineering. We hypothesized that incorporating a polyhistidine-tag (His-Tag) into its amino acid sequence would streamline Pp-4OT purification using metal ion affinity chromatography. This would provide us with a catalyst with higher purity. Additionally, the His-tagged enzyme could hold promise for immobilization and applications in organic solvents, where high reactant concentrations are often necessary. His-Tag technology relies on the interaction between the imidazole groups of histidine residues on the peptide and immobilized metal ions (typically nickel) on a chromatography column.[55] It is important to note that previous studies have shown that a His-

Tag positioned at the C-terminus of 4-OT enzymes is detrimental for their catalytic activity.[56] To avoid potential activity reduction, we opted to incorporate the His-Tag within the enzyme's internal sequence. We used a naturally occurring trimeric 4-OT from *Burkholderia lata* (PDB 6BLM) as a template. This enzyme shares 59% sequence similarity with Pp-4OT. Inspired by this natural design and recent findings by Poelarends, we engineered a tandem 4-OT by fusing the *C*-terminus of one Pp-4OT monomer to the *N*-terminus of another (a detailed description of 4-OT structure is provided in the *Experimental Section 2.2*). This approach resulted in a trimeric enzyme, a significant difference from the native hexameric structure of Pp-4OT. Poelarends' work on tandem-fused 4-OT enzymes demonstrated increased activity in the iminium ion activation, supporting the potential benefits of our design.[57]

The fused 4-OT design offers two key advantages: increased space for genetic manipulations and the ability to integrate an internal His-Tag within the protein sequence. To create the fused enzyme, we inserted a flexible linker sequence (GAGGSL) between the *C*-terminus of one Pp-4OT monomer and the *N*-terminus of the second monomer. This linker, similar to the naturally occurring GAPPSL linker found in *Burkholderia lata* 4-OT (PDB 6BLM), enhances flexibility compared to the wild-type enzyme. This is achieved by replacing the proline residues in the linker with glycine.[58] Additionally, the last three residues (VRR) of Pp-4OT were removed to further enhance linker flexibility and match the length of the natural *Burkholderia lata* enzyme (127 amino acids). Pp-4OT-F_1 was successfully expressed and evaluated in the model cascade reaction under the conditions described in Table 2.1, entry 5. Gratifyingly, the fused variant maintained its catalytic activity (Table 2.2), delivering the desired cascade product **26** in a slightly improved yield of 55% compared to the wild-type enzyme (49%, Table 2.1, entry 6). Importantly, Pp-4OT-F_1 also displayed excellent diastereomeric ratio and enantiomeric excess (entry 1).

[55] Porath, J. "Immobilized Metal Ion Affinity Chromatography" *Protein Expr. Purif.* **1992**, *3*, 263-281.

[56] Lukesch, M. S., Pavkov-Keller, T., Gruber, K., Zangger, K., Wiltschi, B. "Substituting the catalytic proline of 4-oxalocrotonate tautomerase with non-canonical analogues reveals a finely tuned catalytic system." *Sci. Rep.* **2019**, *9*, 1–9.

[57] Xu, G., Kunzendorf, A., Crotti, M., Rozeboom, H. J., Thunnissen, A. M. W. H., Poelarends, G. J. "Gene Fusion and Directed Evolution to Break Structural Symmetry and Boost Catalysis by an Oligomeric C-C Bond-Forming Enzyme" *Angew. Chem. Int. Ed.* **2022**, *61*. DOI: e20211397.

[58] Caparco, A. A., Bommarius, A. S., Champion, J. A. "Effect of Peptide Linker Length and Composition on Immobilization and Catalysis of Leucine Zipper-Enzyme Fusion Proteins" *AIChE J.* **2018**, *64*, 2934-2946.

Table 2.2. Screening of fused 4-OT variants in the model biocascade process.[a]

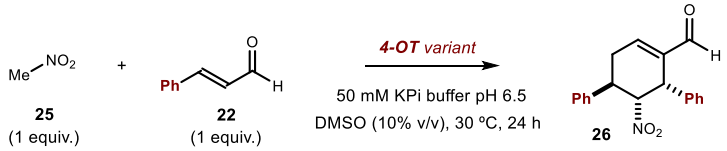

entry	enzyme (loading)	yield **26** (%)	dr **26**	*ee* **26** (%)
1	**Pp**-4OT-**F**$_1$ (4 mol%)	55	>20:1	99
2	**Pp**-4OT-**F**$_2$ (4 mol%)	8	*n.d.*	*n.d.*
3	**Pp**-4OT-**F**$_3$ (4 mol%)	57	>20:1	99

[a]Reactions performed on a 2.5 µmol scale (5 mM) at 30 °C. Analytical yields of **26** determined by GC-FID analysis (calibration using mesitylene as internal standard); dr and ee of **26** measured by HPLC analysis. *n.d.* = not determined; KPi = potassium phosphate.

Having confirmed the efficiency of the fused variant Pp-4OT-F$_1$, we generated a homology model of the enzyme structure with the YASARA software (Figure 2.25) to better evaluate where to include the His-Tag. Loop regions exposed to the aqueous environment were targeted. Consequently, we designed three additional variants: Pp-4OT-F$_2$ with a His-Tag at positions 57-62 near the GAGGSL linker, Pp-4OT-F$_3$ with a His-Tag at positions 12-17 in the β1-α1 loop, and Pp-4OT-F$_4$ with a *C*-terminal His-Tag at positions 130-135. All His-tagged and fused Pp-4OT enzymes were successfully expressed and purified using nickel affinity chromatography, yielding 45-50 mg of protein per gram of cell pellet (details on the procedure and protein purity are available in the *Experimental Section*).

Evaluation in our model reaction revealed that Pp-4OT-F$_2$ displayed significantly reduced activity, giving only 8% yield of product **26** (Table 2.2, entry 2). Conversely, Pp-4OT-F$_3$ exhibited improved performance compared to previous variants, yielding product **26** in 57% with excellent stereoselectivity, favoring the same diastereomer as the unfused Pp-4OT (Table 2.2, entry 3). Unfortunately, Pp-4OT-F$_4$ immediately precipitated upon purification. This aligns with previous reports indicating activity loss for *C*-terminal His-tagged unfused 4-OT enzymes.[56] Figure 2.25 visually compares the crystal structure of wild-type Pp-4OT (PDB: 4x19)[27] with the homology model of the most successful multifunctional enzyme, the His-tagged fused Pp-4OT-F$_3$.

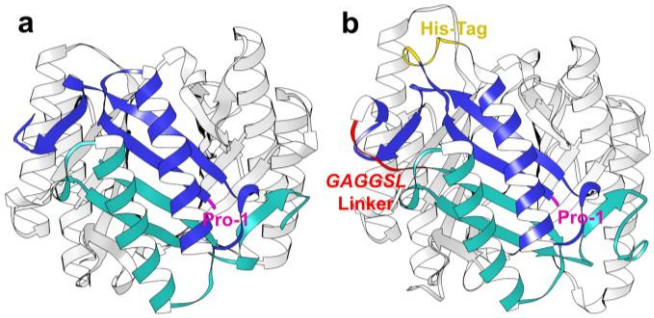

Figure 2.25. a) Crystal structure of wild type Pp-4OT (PDB: 4X19); b) homology model of Pp-4OT-F_3 created with YASARA structure. UCSF Chimera software was used for visualization.

The crystal structure of Pp-4OT shows its homo-hexameric arrangement, where each subunit (colored blue or green in Figure 2.25) adopts a β1-α-β2 fold. The homology model of Pp-4OT-F_3 predicts the location of the His-Tag within the β1-α1 loop of the fused subunit, specifically at residues 12-17 (highlighted yellow in Figure 2.25b). This placement keeps the His-Tag spatially distant from the critical proline 1 residue (shown in magenta), minimizing potential negative effect on the catalytic activity of the enzyme. The linker sequence connecting the *N*-terminus (green) and *C*-terminus (blue) of the original monomers introduces a new loop structure (residues 67-72) depicted in red in Figure 2.25b.

The crystal structure of Pp-4OT shows the homo-hexameric three-dimensional space arrangement of the enzyme, where each monomer (blue or green in Figure 2.25) displays a β1-α-β2 structure. The homology model created for Pp-4OT-F_3 predicts the location of the His-Tag in the loop connecting the β1 and the α1 of each of the three subunits, in position 12-17 (shown in yellow in Figure 2.25b). The His-Tag is far in space from the proline 1 residue (shown in magenta in Figure 2.25) and therefore should not affect its catalytic activity. The linker connecting the *N*-terminus (shown in green) with the *C*-terminus (shown in blue) of the two original monomers creates a loop (position 67-72) highlighted in red in Figure 2.25.

2.3.4 Optimization Studies

Encouraged by the superior performance of Pp-4OT-F_3, we sought to further optimize the model reaction with this fused variant. We investigated the effects of enzyme loading and reaction time (Table 2.3). Increasing the enzyme concentration from 4 mol% to 5 mol% did not lead to a significant improvement in yield (entry 3 vs. entry 2 in Table 2.3). Reducing the loading to 2 mol% resulted in a slightly lower yield of product **26** (44% compared to 57%, entries 1 and 2, respectively).

Table 2.3. Screening of the catalyst loading and the reaction time in the model biocascade process.[a]

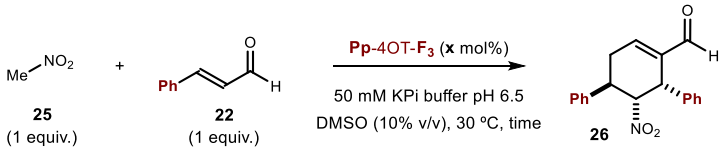

entry	x	time (h)	yield **26** (%)	dr **26**	*ee* **26** (%)
1	2 mol%	24	44	>20:1	99
2	4 mol%	24	57	>20:1	99
3	5 mol%	24	49	>20:1	99
4	4 mol%	6	40	>20:1	99
5	4 mol%	16	45	>20:1	99
6	4 mol%	48	58	>20:1	99

[a]Reactions performed on a 2.5 µmol scale (5 mM) at 30 °C. Analytical yields of **26** determined by GC-FID analysis (calibration using mesitylene as internal standard); dr and ee of **26** measured by HPLC analysis. KPi = potassium phosphate.

We further investigated the impact of reaction time on the yield. Extending the reaction to 48 hours did not afford any significant improvement (entry 6, Table 2.3). Conversely, shorter reaction times of 6 and 16 hours resulted in lower yields of 40% and 45%, respectively (entries 4 and 5). Based on these results, we chose 4 mol% enzyme loading and a 24 hour reaction time for subsequent optimization.

The next round focused on the reaction medium (buffer and pH) and substrate stoichiometry (data shown in Table 2.4). Increasing the pH to 7.5 resulted in a significant decrease in yield, and further elevation to pH 9 completely abolished product formation (entries 1 and 2). Conversely, increasing the equivalents of cinnamaldehyde **22** proved beneficial for the cascade process. The optimal conditions employed 3 equivalents of **22**, affording product **26** in 80% yield with excellent stereoselectivity (entry 5). A further increase to 4 equivalents did not offer any substantial improvement (entry 6).

Table 2.4. Screening of the buffer, the pH and the equivalents of cinnamaldehyde in the model biocascade process.[a]

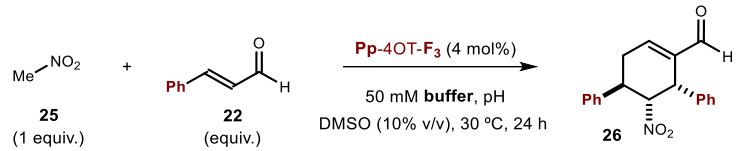

entry	equiv. of **22**	buffer (pH)	yield **26** (%)	dr **26**	*ee* **26** (%)
1	1	NaH_2PO_4 (7.5)	29	11:1	99
2	1	NaH_2PO_4 (9)	<5	*n.d.*	*n.d.*
3	1	KPi (6.5)	57	>20:1	99
4	2	KPi (6.5)	60	>20:1	99
5	3	KPi (6.5)	80	>20:1	99
6	4	KPi (6.5)	81	>20:1	99

[a]Reactions performed on a 2.5 µmol scale (5 mM) at 30 °C. Analytical yields of **26** determined by GC-FID analysis (calibration using mesitylene as internal standard); dr and ee of **26** measured by HPLC analysis. *n.d.* = not determined; KPi = potassium phosphate.

The conditions in entry 5 of Table 2.4 were selected for further screenings. We further explored the reaction medium by investigating the impact of co-solvents (data presented in Table 2.5). DMF and EtOH functioned similarly to DMSO, delivering the cascade product in comparable yields of 80% and 75%, respectively (entries 2 and 3). The reaction also exhibited tolerance towards other alcohols, including ethylene glycol (EG) and MeOH. However, these resulted in slightly lower yields of 71% and 69%, respectively (entries 4 and 5).

Table 2.5. Screening of solvents in the model biocascade process.[a]

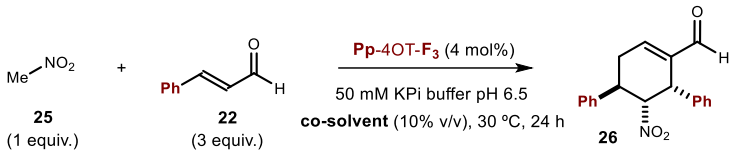

entry	co-solvent	yield **26** (%)	dr **26**	*ee* **26** (%)
1	DMSO	80	>20:1	99
2	DMF	80	>20:1	99
3	EtOH	75	>20:1	99
4	EG	71	>20:1	99
5	MeOH	69	>20:1	99

[a]Reactions performed on a 2.5 µmol scale (5 mM) at 30 °C. Analytical yields, dr and ee of **26** determined by HPLC analysis (calibration using 1,3,5-trimethoxybenzene as internal standard). KPi = potassium phosphate; EG = ethylene glycol.

Importantly, all reactions furnished product **26** with excellent stereoselectivity, isolated as a single, highly enantioenriched diastereomer. Therefore, the reaction conditions from entries 1 or 2 of Table 2.5 were chosen for evaluating the biocatalytic cascade's substrate scope.

2.3.5 Scope of the Two-Component Biocascade

A collection of enals that performed well in the biocascade process with nitromethane **25** are shown in Figure 2.26. Analytical yields for products **26** were determined after instrument calibration using authentic samples prepared following the methods detailed in the *Experimental Section*. Notably, the established organocatalytic Enders procedure was generally unsuitable for obtaining these authentic samples. This method yielded only trace amounts of the cascade product as a mixture of various diastereomers. Consequently, most calibration samples were prepared by running a semi-preparative (milligram scale) enzymatic reaction as described in *section 2.5.5*. Our findings demonstrate that Pp-4OT-F_3 exhibits a broad substrate scope, accepting various *ortho*-, *meta*-, and *para*-substituted cinnamaldehydes **22b-h** with both electron-donating and electron-withdrawing substituents. This enzyme efficiently catalyzes the formation of the corresponding cascade products (**26b-h**) in moderate to high yields (44-89%), good to excellent diastereoselectivity (dr ranging from 3:1 to over 20:1), and with full enantioselectivity (>99% ee) in all cases. Among the tested cinnamaldehydes, *para*-fluoro **26b** and *meta*-methoxy **26c** substitutions resulted in the highest yields (89% and 88%, respectively) with perfect stereocontrol (diastereomeric ratio >20:1). *Ortho*-methyl substitution provided product **26d** in a moderate yield (63%) with good diastereoselectivity (dr 9:1). This yield could be further improved to 77% using ethanol as a co-solvent, although at the expense of slightly lower diastereoselectivity (dr 7:1). *Ortho*-

chloro substitution afforded product **26f** in a lower yield (44%) with modest diastereoselectivity (dr 3:1). Attempts to improve this outcome using different co-solvents were unsuccessful. *Meta*-bromo and *meta*-chloro-substituted cinnamaldehydes (**26e** and **26g**) provided the products in good yields (**26e**: 73% and **26g**: 68%). Interestingly, the yield of **26g** could be increased to 84% using DMF as a co-solvent, but this came at the cost of reduced diastereoselectivity (dr 10:1 compared to >20:1). Notably, Pp-4OT-F_3 also accepted heteroaromatic α,β-unsaturated aldehyde **22i**, affording product **26i** in modest yield (20%) with moderate diastereoselectivity (dr 3:1). Aliphatic enals and substituted nitroalkanes were not suitable for this biocatalytic cascade. Additionally, other nucleophiles, such as malonates, were explored but no reactivity was observed.

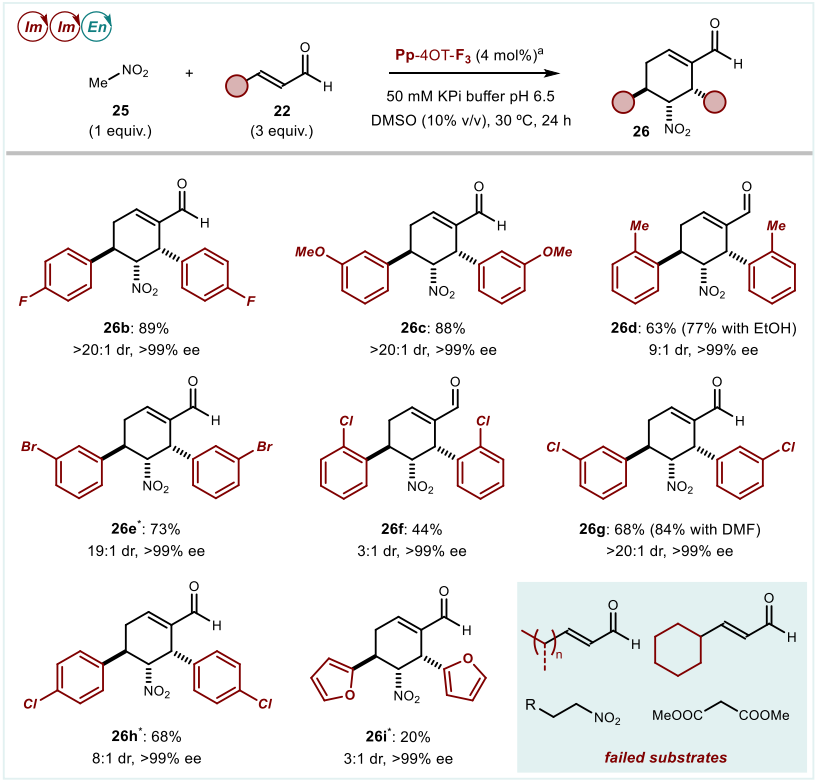

Figure 2.26. Scope of the enals **22** that can participate in the biocascade process. [a]Reactions performed on a 2.5 µmol scale (5 mM) at 30 °C over 24 h. Analytical yields of **26** determined as an average of two runs by HPLC analysis (calibration using 1,3,5-trimethoxybenzene as internal standard); dr and ee of **26** measured by HPLC analysis. *Reactions run with DMF as co-solvent.

2.3.6 Semi-Preparative Enzymatic Cascade Reactions

To evaluate the scalability of the biocascade and fully characterize the isolated products **26**, we scaled up some enzymatic reactions. We used 150 µmol of substrate **25**, 30 mL of *E.coli* cell-free extracts (CFE) in 50mM KPi buffer containing approximately 75 mg of enzyme

(corresponding to ~3 mol% catalyst loading or 2.5 mg enzyme per mL of reaction). Using the crude enzyme from the CFE, we successfully isolated products **26a** and **26b** as pure stereoisomers in good to excellent yields (61% for **26a**, 28 mg; 88% for **26b**, 46 mg) after column chromatography (see Figure 2.27). This larger reaction scale enabled us to obtain single crystals of the major stereoisomer of product **26f**. X-ray crystallographic analysis unambiguously confirmed its relative and absolute configuration.[59] Further analysis using through-space ^{1}H NMR experiments (described in the *Experimental Section*) identified the minor stereoisomer of **26f** as the epimer at the carbon 5 bearing the nitro group. Overall, isolated products **26** exhibited good to excellent diastereoselectivity (see Figure 2.27) with moderate yields. Notably, the only exception was product **26i**, which was obtained as a 1:1 mixture of diastereomers.

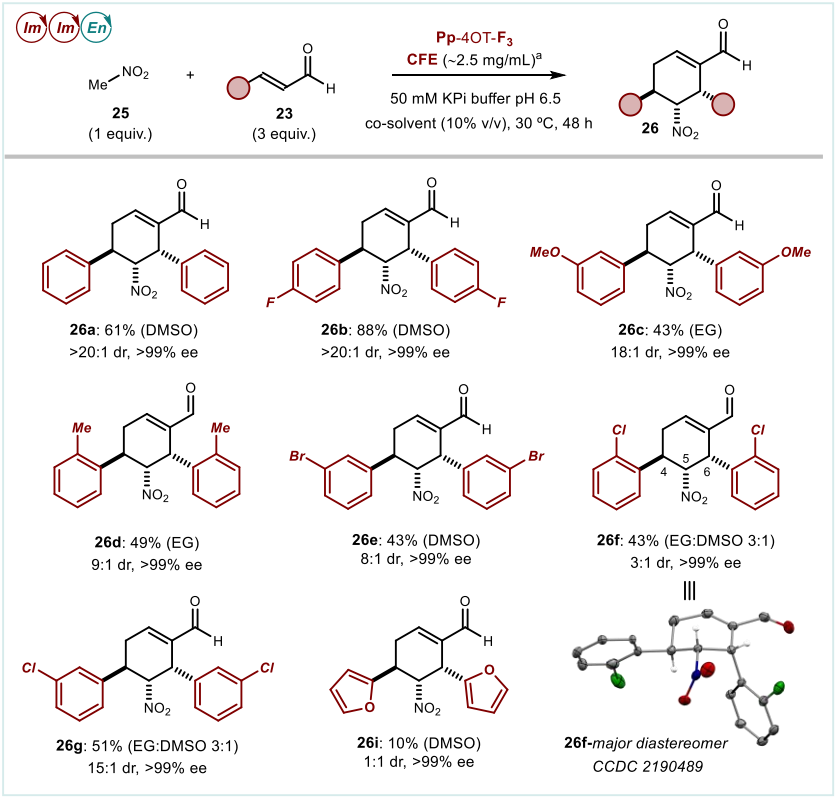

Figure 2.27. Scope of the semi-preparative scale biocascade process. [a]Reactions performed on a 150 µmol scale (5 mM) at 30 °C over 48 h in 30 mL of reaction volume with cell-free-extract containing Pp-4OT-F$_3$ (2.5 mg mL^{-1}) and the co-solvent or mixture of co-solvents indicated in parenthesis. Isolated yields of **26** determined after column chromatography; dr and ee of **26** measured by HPLC analysis. CFE = cell-free extracts.

[59] The crystal structure has been deposited at the Cambridge Crystallographic Data Centre, under deposition number CCDC2190489.

2.3.7 Sequential Double-Enzyme Cascade Process

So far, the C4 and C6 substituents on the cascade products **26** have been identical because they originated from the same cinnamaldehyde substrate **22**. To create products with different substituents at these positions, two distinct cinnamaldehydes would be necessary. However, achieving such selective activation within the same enzyme is challenging. The biocatalyst would need to differentiate and activate two different enals **22** during the two consecutive iminium ion steps of the cascade. *This goal proved unachievable using organocatalysis* (Figure 2.11),[20] since the chiral diphenylprolinol catalyst lacked the ability to distinguish and precisely control the individual steps in the cascade sequence.

A potential solution might lie in a sequential one-pot biocascade process employing two enzymes working in sequence. We aimed to identify an enzyme capable of catalyzing *only* the first Michael addition of **25** to **22** yielding product **27** without further reacting it towards the cascade product **26**. Following this initial step, a different enal **22'** could be introduced along with the Pp-4OT-F_3 variant, which is instead able to further react intermediate **27** and form non-symmetric cascade products **46** (Figure 2.28). This approach draws inspiration from our observation that DERA-MA effectively catalyzed the iminium-ion-mediated Michael addition of nitromethane **25** to cinnamaldehyde **22**, generating intermediate (*R*)-**27**, but failed to produce the final cascade product **26** (see entry 10 in Table 2.1).

This sequential biocatalytic cascade was successfully implemented by combining DERA-MA and Pp-4OT-F_3 (Figure 2.28). After incubating nitromethane **25** and cinnamaldehyde **22** with 4 mol% DERA-MA for 5 hours to selectively generate intermediate **27**, the addition of Pp-4OT-F_3 and a different enal **22'** led to the target non-symmetric products **46**. This approach is applicable to various substituted cinnamaldehydes **22'**. We obtained products **52a-c**, all featuring three consecutive stereocenters, in moderate to good yields (45-74%) with excellent diastereoselectivity (diastereomeric ratio 13:1 to >20:1) and near-perfect enantioselectivity (>99% ee).

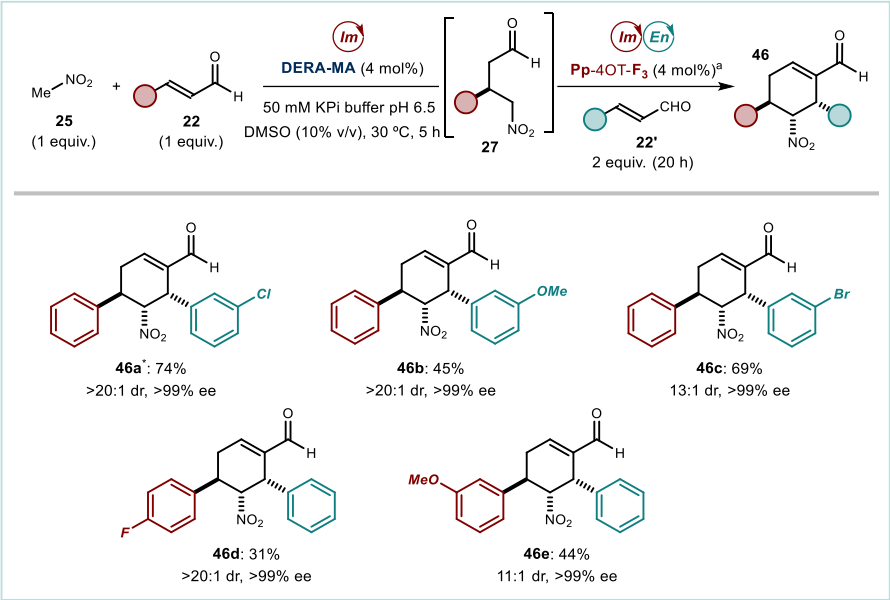

Figure 2.28. Scope of the sequential one-pot two-enzyme cascade for the synthesis of non-symmetric products **46**. [a]Reactions performed on a 2.5 µmol scale of **25** (5 mM) at 30 °C in two steps; first step performed in the presence of DERA-MA (4 mol%), enal **22** (5 mM) and **25** (5 mM) for 5 h; second step performed by adding *in situ* 2 equivalents of a different enal **22'** (10 mM) together with Pp-4OT-F3 (4 mol%) and run for additional 20 h. Analytical yields of **46** determined as an average of two runs by HPLC analysis (calibration using 1,3,5-trimethoxybenzene as internal standard); dr and ee of **46** measured by HPLC analysis. *Reactions run with DMF as co-solvent.

In the first step of the sequential cascade, using substituted cinnamaldehydes **22b** and **22c** followed by cinnamaldehyde **22a** in the second step, products **46d** and **46e** were obtained with moderate yields and good to excellent diastereoselectivity (Figure 2.28). Analytical yields were determined after instrument calibration using authentic product samples prepared according to the methods in the *Experimental Section*.

2.3.8 Development of the Enders Triple Cascade

Building on the success of 4-OTs as versatile biocatalysts in cascade reactions, and having established a two-component enzymatic cascade process, we focused on our ultimate goal: developing a biocatalytic version of the Enders triple cascade reported in 2006 (Figure 2.29).[19]

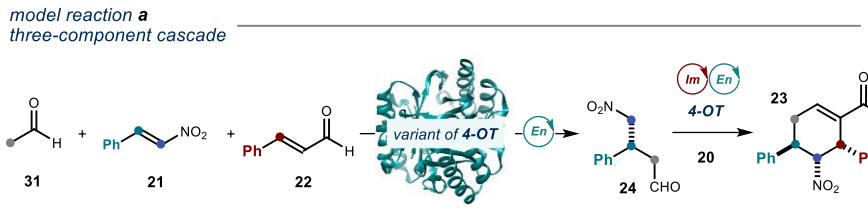

Figure 2.29. Model reaction: enzymatic version of the triple cascade reported by Enders in 2006.

Given the success of Pp-4OT-F_3 in the two-component biocascade, we investigated its potential to achieve the Enders triple cascade with acetaldehyde **31**, nitrostyrene **21** and cinnamaldehyde **22** (Figure 2.29). The proposed mechanism involved initial enamine activation of acetaldehyde **31** followed by a Michael addition to nitrostyrene **21**. This approach was supported by prior studies demonstrating the ability of 4-OT enzymes to catalyze such an enamine-mediated reaction.[29] Importantly, the resulting intermediate **25** is identical to the one formed in the first step of the two-component cascade. We hypothesized that Pp-4OT-F_3 could then utilize intermediate **24** and participate in the same iminium ion-enamine sequence, ultimately leading to cascade product **23** from these different starting materials.

To test this idea, all available 4-OT variants were subjected to a model reaction (Figure 2.30) using acetaldehyde **31**, β-nitrostyrene **21a**, and cinnamaldehyde **22a**. The enzymes (4 mol%) were incubated with the substrates **21a** (1.25 µmol, 2.5 mM), **30** (4-10 equiv.) and **22a** (3-4 equiv.) under optimized conditions (50 mM KPi buffer, pH 6.5, 10% DMSO, 30 °C, 24 hours to 3 days, Figure 2.30). However, disappointingly, none of the reactions yielded the desired cascade product **23**.

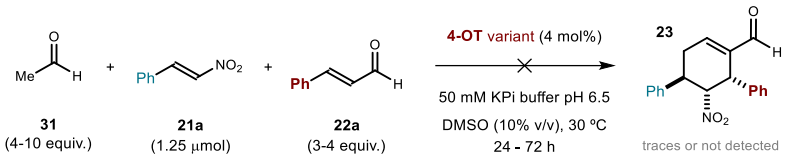

Figure 2.30. Initial attempts for the enzymatic Enders triple cascade

We carefully investigated the catalytic behavior focused of Pp-4OT-F_3, the most effective multifunctional enzyme for the two-component cascade. We confirmed its ability to catalyze the enamine-mediated addition of acetaldehyde **31** to nitrostyrene **21a**. With an excess of acetaldehyde **31** (10 equiv.) and Pp-4OT-F_3 (4 mol%), the Michael product (*S*)-**24** was obtained in 37% yield with 81% ee (Figure 2.31a). However, Pp-4OT-F_3 failed to promote the complete triple cascade reaction. Intrigued by this observation, we recognized a key difference: Pp-4OT-F_3 generates intermediate **24** with an absolute (*S*)-configuration when reacting

acetaldehyde **31** with nitrostyrene **21a** (Figure 2.31a). Conversely, in the two-component cascade, the same enzyme produces the opposite enantiomer (*R*)-**24** when reacting nitromethane **25** and cinnamaldehyde **22a** (Figure 2.31b). We suspected the absolute configuration of intermediate **24** might be critical for the cascade to progress. In theory, this intermediate should be accepted by the enzyme's active site and further react with the iminium ion-activated cinnamaldehyde **22** in the second step. However, enzymes are highly selective towards chiral substrates. We hypothesized that a very strong "matched-mismatched effect" could explain Pp-4OT-F_3's inability to drive the triple cascade, where the generated intermediate (*S*)-**24** in the first step might not be accommodated to drive the subsequent step. To investigate this possibility, we prepared enantiopure samples of both (*S*) and (*R*)-enantiomer of intermediate **24** (97% and 99% ee, respectively). These were then subjected to the second part of the cascade reaction with cinnamaldehyde **22a** in the presence of Pp-4OT-F_3. Importantly, only trace amounts of the cascade product **23** were formed when using the (*S*)-**24** intermediate (Figure 2.31c). Conversely, the (*R*)-**24** isomer yielded the desired triple cascade product **23** in 62% yield with excellent diastereo- and enantioselectivity (Figure 2.31d). Control experiments without enzyme confirmed that Pp-4OT-F_3 is essential for both steps of the cascade process.

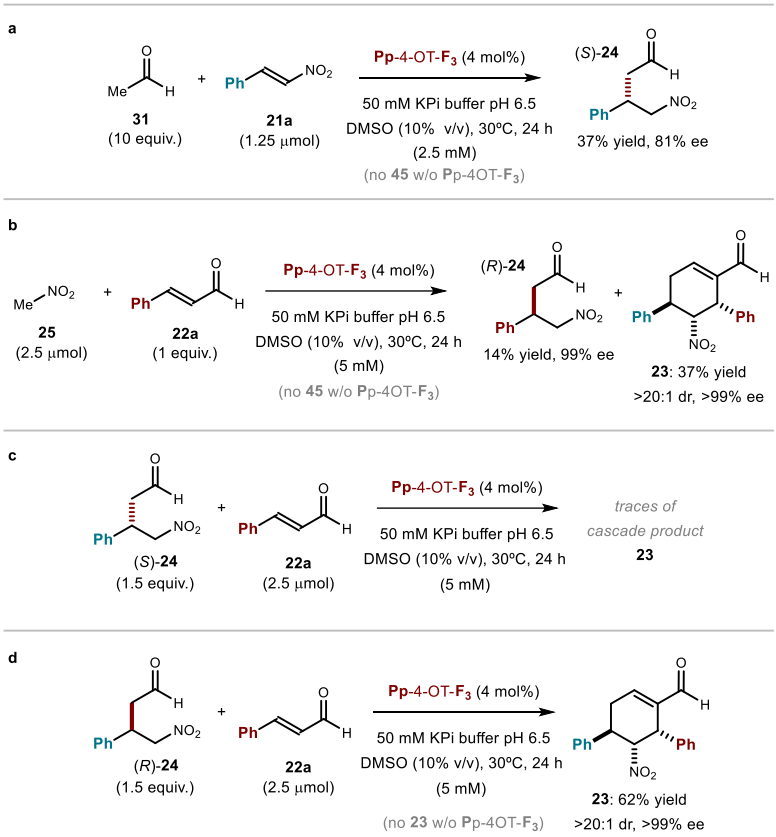

Figure 2.31. Mechanistic experiments for the development of the enzymatic triple cascade.

This finding suggests, that the observed selectivity accounts for Pp-4OT's inability to complete the triple cascade due to a strong "matched-mismatched effect." This would mean that the enzyme can not bind the (*S*) enantiomer of intermediate **24a** in the optimal orientation for subsequent reaction with the iminium ion. Conversely, the (*R*)-enantiomer **24a** would bind more effectively in the active site, facilitating the reaction. This 'extreme' matched-mismatched effect, where a single bifunctional catalyst governs a highly enantioselective first step but is unsuitable for the second, has been observed in other organocatalytic multicomponent reactions.[60,61]

To understand this preference, docking studies using YASARA Structure software were performed. We modeled both enantiomers of intermediate **24** within Pp-4OT-F_3's active site,

[60] Varga, S., Jakab, G., Drahos, L., Holczbauer, T., Czugler, M., Soós, T. "Double Diastereocontrol in Bifunctional Thiourea Organocatalysis: Iterative Michael-Michael-Henry Sequence Regulated by the Configuration of Chiral Catalysts" *Org. Lett.* **2011**, *13*, 5416-5419.

[61] Varga, S., Jakab, G., Csámpai, A., Soós, T. "Iterative Coupling of Two Different Enones by Nitromethane Using Bi-functional Thiourea Organocatalysts. Stereocontrolled Assembly of Cyclic and Acyclic Structures" *J. Org. Chem.* **2015**, *80*, 8990-8996.

considering interactions with the iminium ion derived from cinnamaldehyde **20** bound to proline 1. Two potential binding poses were found for each enantiomer (Figure 2.32). A productive binding requires a distance of about 3.6 Å between the reactive γ-carbon of **24** and the β-carbon of the iminium ion (corresponding to the sum of their van der Waals radii).[62] All identified binding poses for (*S*)-**24** showed distances exceeding 6 Å, suggesting a non-productive interaction (Figure 2.32b depicts one such favored pose). Conversely, the most favorable binding pose for (*R*)-**24** displayed a suitable distance of 3.4 Å for a productive reaction (Figure 2.32a).

Furthermore, residue R46 (arginine 46, corresponding to arginine 39 in wild-type 4-OT - see *Chapter 2.3.1*) stabilizes intermediate **24** within the active site through non-covalent interactions between its positively charged side chain of R46 and the negatively charged oxygen atoms of the nitro group.

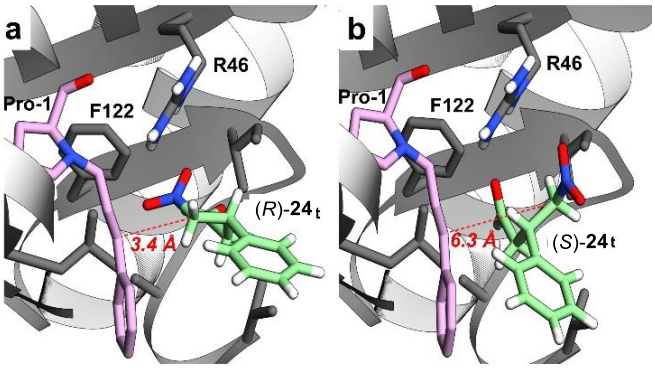

Figure 2.32. a) Docking of (*R*)-**24** in the active site of Pp-4OT-F_3, binding energy: 4.00 Kcal mol^{-1}; b) docking of (*S*)-**24** in the active site of Pp-4OT-F_3, binding energy: 4.31 kcal mol^{-1}. The iminium ion is shown in purple while intermediate **24** is in green. The dashed red line shows the distance between the two reactive carbons for C-C bond formation. All docking simulations were performed with YASARA Structure. UCSF Chimera software was used for visualization.

Having identified the reason behind the inability of (*S*)-**24** to promote the Ender's triple cascade, we sought to identify a 4-OT variant that could generate the desired (*R*)-enantiomer of intermediate **24**, which would be suitable for the cascade reaction. Previous studies demonstrated that mutations M45Y and F50A in wild-type 4-OT enabled the formation of (*R*)-**24**, when performing the Michael addition of acetaldehyde **31** with β-nitrostyrene **21a**.[33] We hypothesized that introducing these mutations into our fused F_3 variant might reverse the intermediate's absolute configuration in the first step. Consequently, the corresponding mutations were introduced on the second half of the fused F_3 variant, becoming M117Y and F122A (sequence provided in the *Experimental Section*). The resulting Pp-4OT-$F_3^{M117Y/F122A}$

[62] Rowland, R. S., Taylor, R. "Intermolecular Nonbonded Contact Distances in Organic Crystal Structures: Comparison with Distances Expected from van Der Waals Radii" *J. Phys. Chem.* **1996**, *100*, 7384-7391.

variant was successfully expressed and purified using the same protocol as Pp-4OT-F_3. Pleasingly, when the enzyme was incubated with acetaldehyde **31** and β-nitrostyrene **21a** under optimized conditions (Figure 2.33a), Pp-4OT-$F_3^{M117Y/F122A}$ produced the desired (*R*)-**24** intermediate in 10% yield with 85% enantioselectivity.

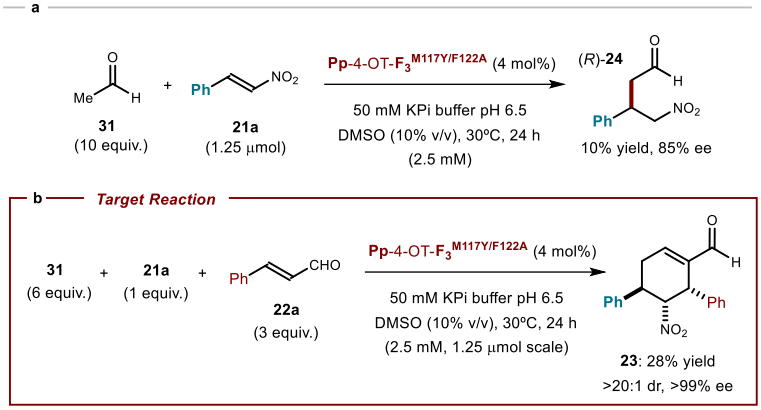

Figure 2.33. a) Michael addition between **31** and **21a** driven by the M117Y/F122A variant of the fused 4-OT. b) Successful implementation of the target reaction: triple cascade enabled by the M117Y/F122A variant of the fused 4-OT.

Importantly, upon incubation with acetaldehyde **31**, β-nitrostyrene **21a** and cinnamaldehyde **22a** (Figure 2.33b), the new variant Pp-4OT-F3$^{M117Y/F122A}$ (4 mol%) effectively catalyzed the triple cascade reaction. The desired product **23** was obtained in 28% yield with excellent diastereo- and enantioselectivity (complete stereocontrol). Interestingly, increasing the acetaldehyde equivalents to 10 had a negative impact, reducing the yield of product **23** to less than 10%. These observations support our hypothesis: Pp-4OT-$F_3^{M117Y/F122A}$ produces the desired (*R*)-enantiomer of intermediate **24**, which then further engages in a subsequent Michael addition with cinnamaldehyde **22a** within the active site of the enzyme, ultimately leading to the triple cascade product **23**.

2.3.9 Scope of the Three-Component Cascade

Having established Pp-4OT-$F_3^{M117Y/F122A}$'s ability to drive the Enders triple cascade, we explored its compatibility with various substrates (Figure 2.34). Using butanal **20** instead of acetaldehyde in the three-component reaction with β-nitrostyrene **21a** and cinnamaldehyde **22a**, product **23a** was obtained in 50% yield with moderate diastereoselectivity (3.7:1 dr) and excellent enantioselectivity (>99% ee). Notably, the major stereoisomer from the enzymatic reaction matched the relative configuration and exhibited comparable selectivity (4:1 dr) for the same major diastereomer obtained in the organocatalytic Enders protocol.[19] Increasing the enzyme loading to 6 mol% further improved the yield of **23a** to 64%. The new variant also tolerated substituted β-nitrostyrene derivative **21b** and cinnamaldehyde **22b**, affording the

corresponding products **23b** and **23c** in moderate yields and diastereoselectivity (Figure 2.34). Furthermore, the reaction could be scaled up to 150 µmol (30 mL reaction volume) using *E.coli* cell-free extracts containing approximately 2.5 mg/mL of Pp-4OT-$F_3^{M117Y/F122A}$. This approach gave product **23c** in 23% yield after column chromatography. Importantly, our enzymatic method achieved comparable efficiency and stereoselectivity to the reported organocatalytic protocol for the synthesis of product **23**.[19]

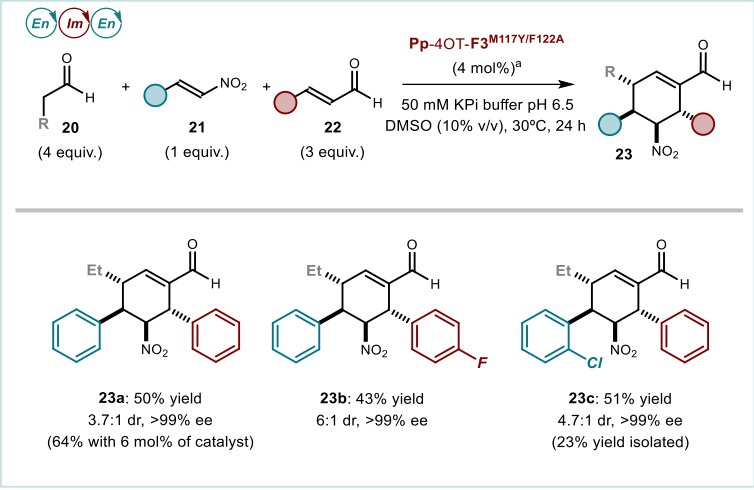

Figure 2.34. Scope of the three-component enzymatic cascade. [a]Reactions performed on a 1.25 µmol scale of nitrostyrene **21** (2.5 mM) for 24 hours at 30°C. Analytical yields of products **23** are given as an average of two runs and determined by HPLC analysis (calibration using 1,3,5-trimethoxybenzene as the internal standard). The dr and ee of **23** were measured via chiral HPLC or UPC² analysis. The yield in parenthesis refers to the isolated product for the reaction on a 150 µmol scale.

Similar to Enders' organocatalytic protocol, the enzymatic reaction yielded very low product quantities when longer-chain alkyl aldehydes **23** were employed. Additionally, alkyl-substituted Michael acceptors were not compatible with the process. Unsuccessful or low-yielding substrates are listed in Figure 2.35.

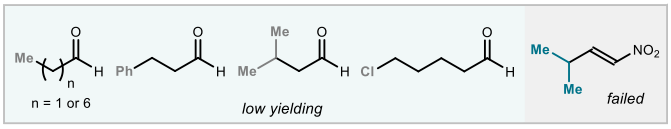

Figure 2.35. Survey of unsuccessful substrates in the triple biocascade.

2.3.10 Deuterium Labelling Experiment

To investigate the mechanism further, we sought to determine whether the final step of both cascades, the aldol condensation, is catalyzed by the enzyme or occurs spontaneously outside of the active site. Former control experiments (Table 2.1 and Figure 2.31) already confirmed that the enzyme Pp-4OT-F_3 is essential for both previous steps in the cascade reactions: the *first step* (iminium ion formation in the two-component or the enamine activation in the triple cascade), and the *second step* (iminium ion activation) in both pathways. Therefore, we wanted to perform the reaction with pre-aldol intermediate **XVI** in enzyme-free environment (Figure 2.36a). However, the execution of the initially planned control experiment was not successful, hence the isolation of the pre-aldol intermediate **XVI** was unsuccessful. To investigate Pp-4OT-F_3's role in the final aldol step of the cascade, a deuterium labeling experiment was performed (Figure 2.36b). β-Deuterated cinnamaldehyde **d-22** and (*R*)-**24** were incubated with *E.coli* cell-free extracts. The reaction was performed on a 158 µmol scale. The isolated product, **d-23**, showed complete incorporation of the deuterium atom at carbon 6, with a yield of 34%.

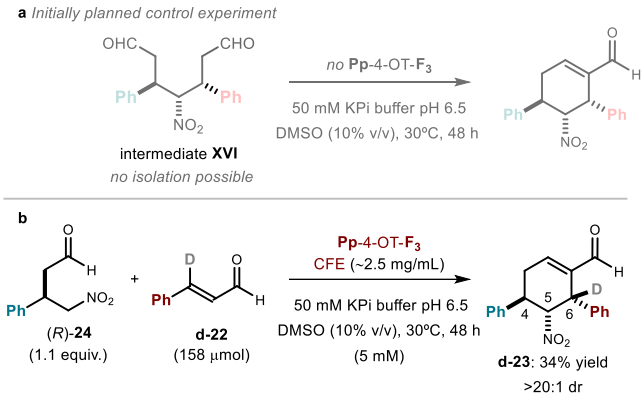

Figure 2.36. a) Initial idea of the control experiment. b) Deuterium labelling experiment on a semi-preparative scale. CFE = cell-free extracts.

If the pre-aldol enamine intermediate **XVI** (Figure 2.37a) formed upon the Michael addition of (*R*)-**24** to β-deuterated cinnamaldehyde **d-22** underwent hydrolysis to intermediate **XVII** followed by spontaneous aldol cyclization outside the enzyme's active site, the product **d-22** would possess the deuterium label at both C4 and C6 (Figure 2.37b). This is because both released aldehydes **XVII** (from intermediate **XVI**) could participate in the aldol addition through *paths i* or *ii*. However, the observed complete deuterium incorporation at C6 in product **23** suggests that the aldol cyclization likely occurs within the enzyme's active site, facilitated by the enzyme-bound enamine **XVI**.

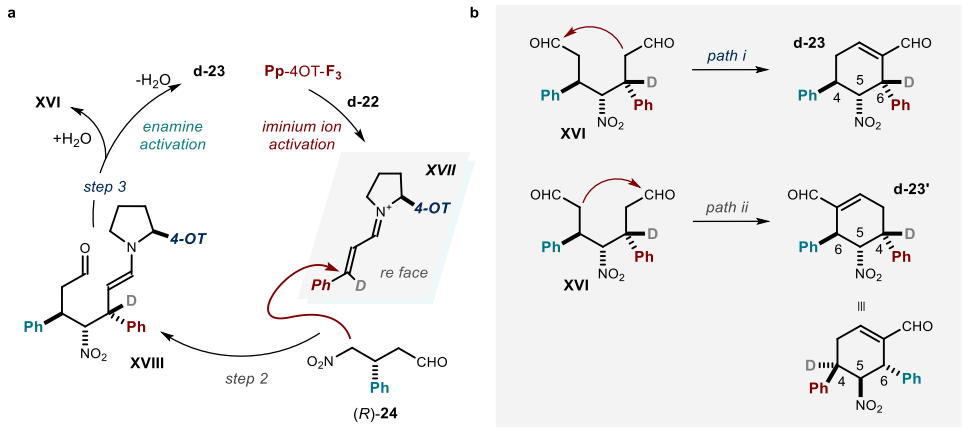

Figure 2.37. a) Mechanism of the reaction between intermediate (*R*)-**24** and deuterated cinnamaldehyde **d-22**; b) possible mechanisms for the spontaneous aldol cyclization of intermediate **XVI**.

2.4 Conclusions

We presented here rare examples of asymmetric multicomponent biocascade reactions driven by a single multifunctional enzyme. The identified enzymes catalysed each step of the cascade in a one-pot fashion, simplifying the processes. Specifically, we have engineered two genetically modified 4-OT enzyme mutants to facilitate triple cascade reactions. In certain instances, this biocatalytic approach not only complements but also surpasses organocatalytic methods in terms of efficiency and stereoselectivity. Through mechanistic experiments, we addressed the initial poor reactivity in the enzymatic three-component cascade and identified key mutations essential for advancing this biocatalytic process. Furthermore, we targeted the synthesis of products **46** with diverse substituents on carbons C4 and C6, which were inaccessible through the organocatalytic route. We designed a distinct double-enzyme tandem process to achieve this class of compounds, showcasing the greater versatility of the enzymatic cascade strategy compared to the organocatalytic approach.

2.5 Experimental Section

2.5.1 General Information

The NMR spectra are available in the published manuscript[1] and are not reported in the present dissertation.

The NMR spectra were recorded at 300 MHz, 400 MHz, and 500 MHz for ^{1}H, at 75 MHz, 101 MHz and 125 MHz for ^{13}C, at 376 MHz for ^{19}F and at 162 and 202 MHz for ^{31}P. The chemical shifts (δ) for ^{1}H and ^{13}C are given in ppm relative to residual signals of the solvents ($CHCl_3$ @ 7.26 ppm ^{1}H NMR, 77.16 ppm ^{13}C NMR; DMSO @ 2.54 ppm ^{1}H NMR, 40.45 ppm ^{13}C NMR). Coupling constants (*J*) are given in Hz, and are quoted to the nearest 0.5 Hz. The following abbreviations are used to indicate the multiplicity: s, singlet; d, doublet; t, triplet; q, quartet; sext, sextet; hept, heptet; m, multiplet. Additionally, signals can be described as broad (br) and apparent (app).

High-resolution mass spectra (HRMS) were obtained from the ICIQ High Resolution Mass Spectrometry Unit on MicroTOF Focus and Maxis Impact (Bruker Daltonics) with electrospray ionization. Optical rotations were measured on a Polarimeter Jasco P-1030 and are reported as follows: $[\alpha]_D^T$ (c in g per 100 mL, solvent).

Cell growing and enzyme expression were performed in a standard INFORS-HT multitron incubator with an orbital of 50 mm. Cells lysis was performed with a Thermo Fisher ultrasonicator 120 W. Centrifugation was performed with a Thermo Fisher SORVALL ST16R centrifuge equipped with different rotors. When applicable, enzyme concentration was determined using a Nanodrop™ One from Thermo Fisher Scientific. The optical density (OD) was measured in a Cell Density Meter Model 40 from Thermo Fisher. LB broth was sterilized with a 75 L Autoclave Sterilmatic (AE-75-DRY) from Thermo Fisher. Biocatalytic transformations on the analytical scale were performed in a 1.5 mL Thermoshaker from Thermo Scientific equipped with a temperature control. Mini-PROTEAN™ SDS-Acrylamide Electrophoresis equipment was purchased from BIO-RAD.

General Procedures. Biochemical reactions were set up in standard 2 mL Eppendorf tubes under air. Synthesis and HPLC grade solvents were used as purchased. Anhydrous solvents were taken from a commercial SPS solvent dispenser. Chromatographic purification of products was accomplished using force-flow chromatography (FC) on silica gel (230-400 mesh). For thin layer chromatography (TLC) analyses throughout this work, Merck precoated TLC plates (silica gel 60 GF_{254}, 0.25 mm) were employed. UV light was used as the visualizing agent, and either an ethanol solution of phosphomolybdic acid or basic aqueous potassium permanganate ($KMnO_4$), and heat served as developing agents. Organic solutions were concentrated under reduced pressure on a Büchi rotary evaporator (in vacuo at 40 ºC, ~5 mbar).

Determination of Enantiomeric Purity. HPLC analyses on chiral stationary phase were performed on an Agilent 1200 series HPLC, using Daicel Chiralpak IB-3 and IC-3 column. UPC^2 analyses on chiral stationary phases were performed on a Waters ACQUITY® UPC^2 instrument, using Daicel Chiralpak IC-3 chiral column. For each compound, the exact conditions for the analysis are specified within the characterization section. HPLC/UPC^2 traces were compared to the mixtures of the two enantiomers prepared by running the reactions under the conditions specified in the reference compounds synthesis.

Materials. HisTrap™ HP chromatography columns for enzyme purification were purchased from Cytiva. HiTrap™ DEAE FF columns for ion exchange chromatography were purchased from GE Healthcare. PD-10 columns containing Sephadex™ G-25 M for buffer exchange were purchased from Cytiva. LB Broth powder was purchased from Nzytech. Customized genes encoding for the enzymes used in this study were purchased from GenScript. BL21(DE3) competent cells were purchased from New England BioLabs$_{Inc}$. Coomassie R250 powder was purchased from BIO-RAD. Protein ladders and standard markers were purchased from BIO-RAD. Commercial grade reagents and solvents were purchased at the highest commercial quality from Sigma Aldrich or Alfa Aesar and used as received, unless otherwise stated. Cinnamaldehyde was purchased from Sigma Aldrich, distilled prior to use and stored in a closed vial under argon at -20 ºC. Butanal was purchased from Sigma Aldrich, distilled prior to use and stored at -20ºC.

2.5.2 Enzyme Preparation

For heterologous expression of all enzymes, *E.coli* BL21(DE3) (New England BioLabs, NEB) was used as host organism. All enzymes except of DERA-MA were cloned in pET20b vector between NdeI and XhoI. DERA-MA was cloned in pET26b vector with a C-terminus His-Tag and without the pelB signal peptide. Transformations were performed at 42 ˚C for 10 seconds according to the standard protocol (NEB). For expression of all enzymes except of DERA-MA the following protocol was used: 400 mL of LB medium, supplemented with ampicillin (100 μg mL^{-1}) were inoculated with 7 mL of pre-culture. The cells were allowed to grow at 37 °C until an OD_{600} of 0.7-1 was reached. Expression of the enzymes were performed by inducing the main cultures with 1 mM of isopropyl β-D-1-thiogalactopyranoside (IPTG) and cultures were grown overnight at 37 °C with shaking at 170 rpm. The next day, the cells were harvested by centrifugation (4.700 g, 20 min, 4 °C), resuspended in 10 mM NaH_2PO_4 pH 8 and lysed by ultrasonication. For DERA-MA, 400 mL of LB medium, supplemented with kanamycin (50 μg mL^{-1}) were inoculated with 7 mL of pre-culture and cells were grown at 37 °C until the OD_{600} was between 0.7-1. Expression of the enzyme was performed by the addition of 0.1 mM IPTG and cultures were grown overnight at 25 °C with shaking at 170 rpm. The cells were harvested by centrifugation (4.700 g, 20 min, 4 °C), resuspended in lysis buffer (50 mM KH_2PO_4, 300 mM NaCl, 10 mM imidazole, pH 8.0) and lysed by

ultrasonication. For protein purification of Pp-4OT, Ps-4OT, Ml-4OT and Tb-4OT the lysate was centrifuged (18.000 rpm, 50 min, 4 °C) and filtered through a 0.45 µm filter. After that, 1.5 M of $(NH_4)_2SO_4$ was added into the supernatant which was stirred for 6 h. Protein solution was centrifuged (12.000 g, 20 min, 4 °C) and the supernatant was dialyzed overnight against the 10 mM NaH_2PO_4 pH 8. Dialyzed sample was loaded into a column containing DEAE sepharose (GE Healthcare) for an anion exchange chromatography when Pp-4OT, Ps-4OT and Ml-4OT enzymes were purified. For Tb-4OT the dialyzed sample was loaded into a HiTrap™ CM FF column (Cytiva) for cation exchange. The column was pre-equilibrated with 10 column volumes (CV) of 10 mM NaH_2PO_4 pH before loading of the protein. After the loading of the enzymatic solutions, the column was washed with 3 CV using the loading buffer and the elution was performed with the same buffer supplemented with 90 mM Na_2SO_4. Elution fractions were collected and analyzed by SDS-PAGE. Fractions containing the enzyme were combined and concentrated using centricon with 6-8 kDa cutoff. Buffer exchange was performed with PD-10 desalting columns (cytiva). The protein concentration was determined using Biuret assay. For His-Tagged Pp-4OT-$F_{2\text{-}4}$ and DERA-MA, protein purification was performed by Ni-NTA affinity chromatography using pre-packed Ni-NTA HisTrap FF columns (GE Healthcare) according to the manufacturer's instructions. First the cell pellet was resuspended in lysis buffer (50 mM KH_2PO_4, 300 mM NaCl, 10 mM imidazole, pH 8.0). After sonication the enzyme solution was filtrated with a 0.45 µm filter and loaded into the column which has been previously equilibrated with lysis buffer. After loading of the filtered lysate, the column was washed with sufficient amounts of washing buffer (50 mM KH_2PO_4, 300 mM NaCl, 25 mM imidazole, pH 8.0), and bound protein was recovered with elution buffer (50 mM KH_2PO_4, 300 mM NaCl, 300 mM imidazole, pH 8.0). The process of purification was monitored with SDS-PAGE and fractions containing pure protein were pooled and dialyzed overnight against potassium phosphate buffer (50 mM, pH 6.5). Protein solutions were concentrated, and the concentration was determined either spectrophotometrically using the extinction coefficient at 280 nm or the Biuret assay. Typically, a protein yield of 50 mg per gram of cell culture was obtained. All amino acid sequences of the enzymes are shown in Table 3.6. The purity of the enzymes was verified by SDS-PAGE (Figure 2.38).

Table 2.1. The amino acid sequences of the enzymes used in this study.

Enzyme	Amino acid sequence
Pp-4OT	PIAQIHILEGRSDEQKETLIREVSEAISRSLDAPLTSVRVIITEMAKGHFGIGG ELASKVRR
Ml-4OT	PIAQINIMEGRSDEQKEALIVEVTAAISRALDAPEQNIRVLIQELPRQNWGIAG QSAKKLGR
Ps-4OT	PIAHVQIMEGRSDEQKEAMIREVSEALARTLDSPLDRVRVLITEVPKSHWGIAG

	EPASKVR
Tb-4OT	PFAQISILEGRSDEKKAELIREVTEAIHRSLGAPREAIRVALYEVKKTEWGIGG ETAKKLGR
Pp-4OT-F_1	PIAQIHILEGRSDEQKETLIREVSEAISRSLDAPLTSVRVIITEMAKGHFGIGG ELASK**GAGGSL**PIAQIHILEGRSDEQKETLIREVSEAISRSLDAPLTSVRVIIT EMAKGHFGIGGELASKVRR
Pp-4OT-F_2	PIAQIHILEGRSDEQKETLIREVSEAISRSLDAPLTSVRVIITEMAKGHFGIGG EL**HHHHHH**GSLPIAQIHILEGRSDEQKETLIREVSEAISRSLDAPLTSVRVIIT EMAKGHFGIGGELASKVRR
Pp-4OT-F_3	PIAQIHILEGA**HHHHHH**GSDEQKETLIREVSEAISRSLDAPLTSVRVIITEMAK GHFGIGGELASK**GAGGSL**PIAQIHILEGRSDEQKETLIREVSEAISRSLDAPLT SVRVIITEMAKGHFGIGGELASKVRR
Pp-4OT-F_4	PIAQIHILEGRSDEQKETLIREVSEAISRSLDAPLTSVRVIITEMAKGHFGIGG ELASK**GAGGSL**PIAQIHILEGRSDEQKETLIREVSEAISRSLDAPLTSVRVIIT EMAKGHFGIGGELASKVRRLG**HHHHHH**
Pp-4OT-$F_3^{M117Y/F122A}$	PIAQIHILEGAHHHHHHGSDEQKETLIREVSEAISRSLDAPLTSVRVIITEMAK GHFGIGGELASKGAGGSLPIAQIHILEGRSDEQKETLIREVSEAISRSLDAPLT SVRVIITE**Y**AKGH**A**GIGGELASKVRR
DERA-MA	MTDLKASSLRALKLMDLSTLNGDYTDEKVIALCHQAKTPVGNTAAISIYPRSIP IARKTLKEQGTPEIRIATVTNFPHGNDDIDIALAETRAAIAYGADEVDVVFPYR ALMAGNEQVGFDLVKACKEACAAANVLLKVIIESGELKDEALIRKASEISIKAG ADFIKTSTGLVAVNATPESARIMMEVIRDMGVEKSVGFKVTGGARTAEDAQKYL AIADELFGADWADARHYRFGASGLLASLLKALGHGDGKSASSYLEHHHHHH

Genetic alterations of Pp-4OT variants with respect to the wild type enzyme are shown in bold. MI-4OT is from *Marinobacter lipolyticus* SM19 (NCBI:[63] txid1318628), Tb-4OT is from *Thiolapillus brandeum* (NCBI: txid1076588) Ps-4OT is from *Pseudomonas sagittaria* (NCBI: txid1135990).

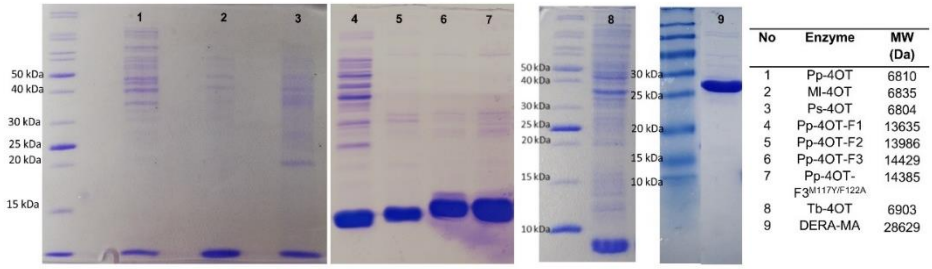

No	Enzyme	MW (Da)
1	Pp-4OT	6810
2	MI-4OT	6835
3	Ps-4OT	6804
4	Pp-4OT-F1	13635
5	Pp-4OT-F2	13986
6	Pp-4OT-F3	14429
7	Pp-4OT-$F3^{M117Y/F122A}$	14385
8	Tb-4OT	6903
9	DERA-MA	28629

Figure 2.38. Purity of enzymes used in this study.

[63] Schoch, C. L., Ciufo, S., Domrachev, M., Hotton, C. L., Kannan, S., Khovanskaya, R., Leipe, D., McVeigh, R., O'Neill, K., Robbertse, B., Sharma, S., Soussov, V., Sullivan, J. P., Sun, L., Turner, S., Karsch-Mizrachi, I. "NCBI Taxonomy: A Comprehensive Update on Curation, Resources and Tools" Database 2020, 2020.

2.5.3 Substrate Synthesis

GP1 – General Procedure for the Synthesis of Enals ***22***

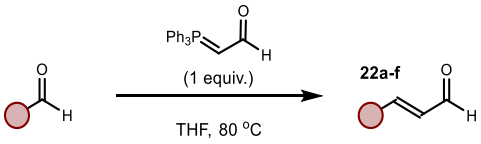

The general procedure for the synthesis of the enals **22** was adapted from a reported procedure.[64] A suspension of (triphenylphosphoranylidene)acetaldehyde (1 equiv.) and the corresponding aldehyde (1 equiv.) in anhydrous THF (0.35 M) was refluxed overnight at 80 ºC until complete conversion of the aldehyde was inferred by TLC analysis. The resulting mixture was cooled down to ambient temperature and dried under reduced pressure. Purification of the crude material by flash column chromatography on silica gel provided the enal products **22b-g** and **d-22**.

(*E*) 3-(4-fluorophenyl)acrylaldehyde (22b)

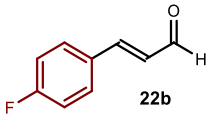

Prepared according to *GP1*, using 4-fluorobenzaldehyde (760 µL, 7.10 mmol) and (triphenylphosphoranylidene)acetaldehyde (2.2 g, 7.70 mmol) in THF (20 mL). The crude mixture was purified by flash column chromatography (isocratic 10% EtOAc in hexane) to afford product **22b** (456 mg, 43% yield) as a yellow liquid. The product was stored at -20 ºC under an argon atmosphere. The characterization of the title compound was consistent with the data available in the literature.[65]

^{1}H NMR (500 MHz, $CDCl_3$): δ 9.69 (d, J = 7.7 Hz, 1H), 7.61 – 7.53 (m, 2H), 7.45 (d, J = 16.0 Hz, 1H), 7.17 – 7.09 (m, 2H), 6.65 (dd, J = 16.0, 7.6 Hz, 1H).

^{19}F NMR (471 MHz, $CDCl_3$): δ -107.7.

^{13}C NMR (126 MHz, $CDCl_3$): δ 193.6, 164.6 (d, $J_{C\text{-}F}$ = 253.2 Hz), 151.4, 130.6 (d, $J_{C\text{-}F}$ = 8.7 Hz), 130.5 (d, $J_{C\text{-}F}$ = 3.3 Hz), 128.5 (d, $J_{C\text{-}F}$ = 2.3 Hz), 116.5 (d, $J_{C\text{-}F}$ = 22.1 Hz).

(*E*) 3-(3-methoxyphenyl)acrylaldehyde (22c)

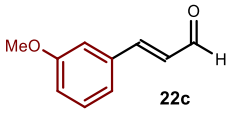

Prepared according to *GP1*, using 3-methoxybenzaldehyde (600 µL, 4.92 mmol) and (triphenylphosphoranylidene)acetaldehyde (2.25 g, 7.38 mmol, 1.5 equiv.) in THF (10 mL). The crude mixture was

[64] Zu, L., Zhang, S., Xie, H., Wang, W. "Catalytic Asymmetric oxa-Michael-Michael Cascade for Facile Construction of Chiral Chromans via an Aminal Intermediate" *Org. Lett.* **2009**, *11*, 1627-1630.

[65] Huang, H., Yu, C., Li, X., Zhang, Y., Zhang, Y., Chen, X., Mariano, P. S., Xie, H., Wang, W. "Synthesis of Aldehydes by Organocatalytic Formylation Reactions of Boronic Acids with Glyoxylic Acid" *Angew. Chem. Int. Ed.* **2017**, *56*, 8201-8205.

purified by flash column chromatography (isocratic 10% EtOAc in hexane) to afford product **22c** (310 mg, 39% yield) as a yellow oil. The product was stored at -20 ºC. The characterization of the title compound was consistent with the data available in the literature.[65]

^{1}H NMR (400 MHz, $CDCl_3$): δ 9.71 (d, *J* = 7.8 Hz, 1H), 7.45 (d, *J* = 15.9 Hz, 1H), 7.35 (t, *J* = 7.9 Hz, 1H), 7.16 (d, *J* = 7.6 Hz, 1H), 7.08 (t, *J* = 2.1 Hz, 1H), 7.00 (dd, *J* = 8.3, 2.5 Hz, 1H), 6.71 (dd, *J* = 15.9, 7.7 Hz, 1H), 3.85 (s, 3H).

^{13}C NMR (101 MHz, $CDCl_3$): δ 193.8, 160.2, 152.8, 135.5, 130.2, 129.0, 121.4, 117.2, 113.4, 55.5.

(*E*) 3-(2-methylphenyl)acrylaldehyde (22d)

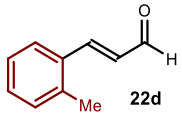

22d

Prepared according to *GP1*, using 2-methylbenzaldehyde (810 µL, 7.00 mmol) and (triphenylphosphoranylidene)acetaldehyde (2.13 g, 7.00 mmol) in THF (20 mL). The crude mixture was purified by flash column chromatography (isocratic 5% EtOAc in hexane) to afford product **22d** (321 mg, 31% yield) as a pale yellow oil. The product was stored at -20ºC. The characterization of the title compound was consistent with the data available in the literature.[66]

^{1}H NMR (500 MHz, $CDCl_3$): δ 9.73 (d, *J* = 7.7 Hz, 1H), 7.78 (d, *J* = 15.8 Hz, 1H), 7.64 – 7.50 (m, 1H), 7.37 – 7.30 (m, 1H), 7.28 – 7.23 (m, 2H), 6.67 (dd, *J* = 15.8, 7.7 Hz, 1H), 2.48 (s, 3H).

^{13}C NMR (126 MHz, $CDCl_3$): δ 194.0, 150.4, 138.1, 133.0, 131.2, 131.2, 129.8, 127.0, 126.8, 19.9.

(*E*) 3-(3-bromophenyl)acrylaldehyde (22e)

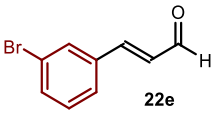

22e

Prepared according to *GP1*, using 3-bromobenzaldehyde (900 µL, 7.7 mmol) and (triphenylphosphoranylidene)acetaldehyde (2.35 g, 7.7 mmol) in THF (22 mL). The crude mixture was purified by flash column chromatography (isocratic 10% EtOAc in hexane) to afford product **22e** (894 mg, 55% yield) as a yellow solid. The product was stored at -20ºC. The characterization of the title compound was consistent with the data available in the literature.[67]

^{1}H NMR (400 MHz, $CDCl_3$): δ 9.71 (d, *J* = 7.6 Hz, 1H), 7.71 (t, *J* = 1.8 Hz, 1H), 7.57 (ddd, *J* = 8.0, 2.0, 1.0 Hz, 1H), 7.52 – 7.47 (m, 1H), 7.40 (d, *J* = 16.0 Hz, 1H), 7.31 (t, *J* = 7.9 Hz, 1H), 6.70 (dd, *J* = 16.0, 7.6 Hz, 1H).

^{13}C NMR (101 MHz, $CDCl_3$): δ 193.4, 150.8, 136.2, 134.1, 131.4, 130.8, 129.8, 127.0, 123.4.

[66] Liu, J., Zhu, J., Jiang, H., Wang, W., Li, J. "Pd-catalyzed cascade Heck-Saegusa: direct synthesis of enals from aryl iodides and allyl alcohol" *Chem. Commun.* **2010**, *46*, 415-417.

[67] Zhang, X., Jiang, G., Lei, S., Shan, X., Qu, J., Kang, Y. "Iron-Catalyzed α,β-Dehydrogenation of Carbonyl Compounds" *Org. Lett.* **2021**, *23*, 1611-1615.

(*E*) 3-(2-chlorophenyl)acrylaldehyde (22f)

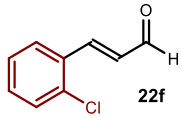

22f

Prepared according to *GP1*, using 2-chlorobenzaldehyde (800 µL, 7.10 mmol) and (triphenylphosphoranylidene)acetaldehyde (2.16 g, 7.10 mmol) in THF (20 mL). The crude mixture was purified by flash column chromatography (isocratic 10% EtOAc in hexane) to afford product **22f** (579 mg, 49% yield) as a pale yellow solid. The product was stored at -20ºC. The characterization of the title compound was consistent with the data available in the literature.[65]

^{1}H NMR (500 MHz, $CDCl_3$): δ 9.77 (d, J = 7.7, 1H), 7.94 (d, J = 16.0 Hz, 1H), 7.67 (dd, J = 7.7, 1.8 Hz, 1H), 7.51-7.43 (m, 1H), 7.41-7.29 (m, 2H), 6.71 (dd, J = 16.1, 7.7 Hz, 1H).

^{13}C NMR (126 MHz, $CDCl_3$): δ 193.7, 148.1, 135.4, 132.2, 132.1, 130.7, 130.5, 128.0, 127.5.

(*E*) 3-(3-chlorophenyl)acrylaldehyde (22g)

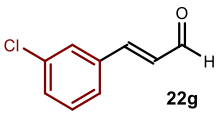

22g

Prepared according to *GP1*, using 3-chlorobenzaldehyde (560 µL, 4.98 mmol) and (triphenylphosphoranylidene)acetaldehyde (1.52 g, 4.98 mmol) in THF (15 mL). The crude mixture was purified by flash column chromatography (isocratic 10% EtOAc in hexane) to afford product **22g** (472 mg, 56% yield) as a yellow solid. The product was stored at -20 ºC. The characterization of the title compound was consistent with the data available in the literature.[65]

^{1}H NMR (500 MHz, $CDCl_3$): δ 9.72 (d, J = 7.6 Hz, 1H), 7.55 (t, J = 1.9 Hz, 1H), 7.47-7.35 (m, 4H), 6.71 (dd, J = 16.0, 7.5 Hz, 1H).

^{13}C NMR (126 MHz, $CDCl_3$): δ 193.4, 150.9, 135.9, 135.3, 131.2, 130.5, 129.8, 128.4, 126.5.

(*E*) cinnamaldehyde-3-d (d-22)

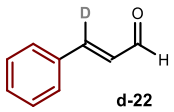

d-22

Prepared according to *GP1*, using benzaldehyde-d_1 (500 µL, 4.92 mmol) and (triphenylphosphoranylidene)acetaldehyde (2.25 g, 7.30 mmol) in THF (12 mL). The crude mixture was purified by flash column chromatography (isocratic 10% EtOAc in hexane) to afford product **d-20** (110 mg, 16% yield) as a yellow liquid. The product was stored at -20 ºC. The characterization of the title compound was consistent with the data available in the literature.[68]

^{1}H NMR (300 MHz, $CDCl_3$): δ 9.72 (d, J = 7.8 Hz, 1H), 7.63 – 7.52 (m, 2H), 7.49 – 7.39 (m, 3H), 6.73 (dt, $J_{H\text{-}H}$ = 7.7, $J_{H\text{-}D}$ = 2.4 Hz, 1H).

^{13}C NMR (75 MHz, $CDCl_3$): δ 193.9, 134.1, 131.4, 129.3, 129.1, 128.7, 128.6.

---

[68] Chavhan, S. W., Cook, M. J. "Silicon-Directed Rhenium-Catalyzed Allylic Carbaminations and Oxidative Fragmentations of γ-Silyl Allylic Alcohols" *Chem. Eur. J.* **2014**, *20*, 4891-4895.

[69] Gotoh, H., Ishikawa, H., Hayashi, Y. "Diphenylprolinol Silyl Ether as Catalyst of an Asymmetric, Catalytic, and Direct Michael Reaction of Nitroalkanes with α,β-Unsaturated Aldehydes" *Org.Lett.* **2007**, *9*, 5307-5309.

GP2 – General Procedure for the Synthesis of Intermediates **27a-c**

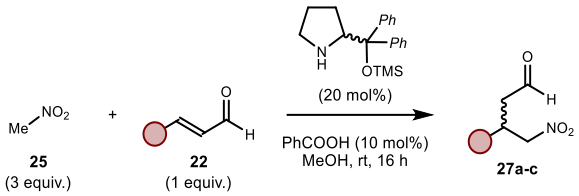

The general procedure for the synthesis of the intermediates **27** was adapted from a reported procedure.[69] To a solution of benzoic acid (20 mol%) in MeOH (0.5 M) were added an approximately 1:1 (*R*) and (*S*) mixture of the diphenylprolinol TMS ether as the organocatalyst (10 mol%), the corresponding enal **22** (1 equiv.) and nitromethane **25** (3 equiv.). After stirring the reaction at room temperature for 16 hours, the resulting mixture was quenched with saturated aqueous $NaHCO_3$ and extracted twice with ethyl acetate. The combined organic extracts were dried over anhydrous $MgSO_4$, filtered and concentrated under reduced pressure. Purification of the crude material by flash column chromatography on silica gel provided the corresponding compounds as racemic mixtures.

4-nitro-3-phenyl-butanal (27a)

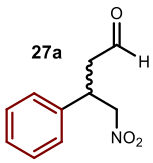

Prepared according to *GP2*, using cinnamaldehyde **22a** (465 µL, 3.70 mmol) and nitromethane **25** (600 µL, 11.1 mmol) in MeOH (7.4 mL). The crude mixture was purified by flash column chromatography (gradient from 10 to 20% EtOAc in hexane) to afford product **27a** (290 mg, 40% yield) as a yellow liquid. The product was stored at -20 ºC. The characterization of the title compound was consistent with the data available in the literature.[69]

^{1}H NMR (500 MHz, $CDCl_3$): δ 9.70 (t, *J* = 1.1 Hz, 1H), 7.38 – 7.31 (m, 2H), 7.31 – 7.27 (m, 1H), 7.25 – 7.20 (m, 2H), 4.71 – 4.58 (m, 2H), 4.05 (p, *J* = 7.3 Hz, 1H), 2.94 (ddd, *J* = 6.9, 3.1, 1.1 Hz, 2H).

^{13}C NMR (101 MHz, $CDCl_3$): δ 199.1, 138.3, 129.3 (2C), 128.3 (2C), 127.5, 79.5, 46.5, 38.1.

4-nitro-3-(4-fluorophenyl)-butanal (27b)

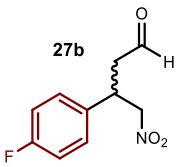

Prepared according to *GP2*, using 4-fluorocinnamaldehyde **22b** (60.1 mg, 0.40 mmol) and nitromethane **25** (65 µL, 1.20 mmol) in MeOH (800 µL). The crude mixture was purified by flash column chromatography (isocratic 30% EtOAc in hexane) to afford product **27b** (32 mg, 38% yield) as a yellow liquid. The product was stored at -20ºC. The characterization of the title compound was consistent with the data available in the literature.[70]

[70] Chen, W., Fang, H., Xie, K., Oestreich, M. "The Cyclohexa-2,5-dienyl Group as a Placeholder for Hydrogen: Organocatalytic Michael Addition of an Acetaldehyde Surrogate" *Chem. Eur. J.* **2020**, *26*, 15126-15129.

^{1}H NMR (400 MHz, $CDCl_3$): δ 9.70 (t, J = 1.0 Hz, 1H), 7.26 – 7.16 (m, 2H), 7.11 – 6.96 (m, 2H), 4.67 (app dd, J = 12.6, 6.9 Hz, 1H), 4.58 (app dd, J = 12.5, 7.9 Hz, 1H), 4.07 (p, J = 7.2 Hz, 1H), 2.94 (dd, J = 7.1, 1.0 Hz, 2H).
^{19}F NMR (376 MHz, $CDCl_3$): δ -113.81.
^{13}C NMR (101 MHz, $CDCl_3$): δ 198.6, 162.5 (d, $J_{C\text{-}F}$ = 246.3 Hz), 134.1 (d, $J_{C\text{-}F}$ = 3.4 Hz), 129.2 (d, $J_{C\text{-}F}$ = 8.2 Hz), 116.3 (d, $J_{C\text{-}F}$ = 21.6 Hz), 46.7, 37.4.

4-nitro-3-(3-methoxyphenyl)-butanal (27c)

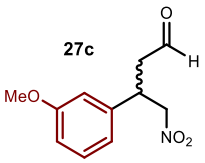

Prepared according to *GP2*, using 3-methoxycinnamaldehyde **22c** (65 mg, 0.40 mmol) and nitromethane **25** (65 µL, 1.20 mmol) in MeOH (800 µL). The crude mixture was purified by flash column chromatography (isocratic 30% EtOAc in hexane) to afford product **27c** (29 mg, 32% yield) as a yellow liquid. The product was stored at -20ºC. The characterization of the title compound was consistent with the data available in the literature.[71]
^{1}H NMR (400 MHz, $CDCl_3$): δ 9.71 (t, J = 1.1 Hz, 1H), 7.31 – 7.22 (m, 1H), 6.82 (dtd, J = 7.0, 3.5, 3.0, 1.4 Hz, 2H), 6.76 (t, J = 2.1 Hz, 1H), 4.71 – 4.56 (m, 2H), 4.04 (q, J = 7.3 Hz, 1H), 3.80 (s, 3H), 2.94 (ddd, J = 6.9, 4.1, 1.1 Hz, 2H).
^{13}C NMR (101 MHz, $CDCl_3$): δ 198.9, 160.2, 139.8, 130.5, 119.6, 113.8, 113.3, 79.5, 55.4, 46.5, 38.2.

Synthesis and Characterization of Enantiopure Intermediates **27**
(*R*) and (*S*)-**27**were prepared following the general procedure *GP2* using, respectively, the (*R*) or (*S*) enantiomer of the diphenylprolinol TMS ether as the organocatalyst.

(*R*)-4-nitro-3-phenyl-butanal (27a)

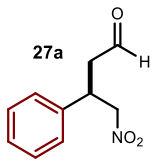

Prepared according to *GP2*, using cinnamaldehyde **22a** (126 µL, 1.00 mmol), nitromethane **25** (161 µL, 3.00 mmol) and (*R*)-2-(diphenyl((trimethylsilyl)oxy)methyl)-pyrrolidine (32 mg, 100 µmol) in MeOH (2 mL). The crude mixture was purified by flash column chromatography (gradient from 10 to 20% EtOAc in hexane) to afford product **27a** (122 mg, 60% yield, >99% ee) as a yellow liquid. The enantiomeric ratio was determined by UPC^2 analysis on a Daicel Chiralpak IG-3 column: isocratic CO_2/i-PrOH 97:3, flow rate 2 mL/min, λ = 210 nm: τ_{minor} = 5.5 min, τ_{major} = 6.2 min. The product was stored at -20 ºC. The characterization of the title compound was consistent with the data available in the literature.[69]

[71] Zu, L., Xie, H., Li, H., Wang, J., Wang, W. "Highly Enantioselective Organocatalytic Conjugate Addition of Nitromethane to α,β-Unsaturated Aldehydes: Three-Step Synthesis of Optically Active Baclofen" *Adv. Synth. Catal.* **2007**, *349*, 2660-2664.

(*S*)-4-nitro-3-phenyl-butanal (27a)

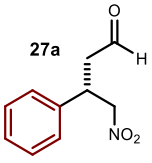

Prepared according to *GP2*, using cinnamaldehyde **22a** (126 µL, 1.00 mmol), nitromethane **25** (161 µL, 3.00 mmol) and (S)-2-(diphenyl((trimethylsilyl)oxy)methyl)pyrrolidine (32 mg, 100 µmol) in MeOH (2 mL). The crude mixture was purified by flash column chromatography (gradient from 10 to 20% EtOAc in hexane) to afford product **27a** (96 mg, 50% yield, 97% ee) as a yellow liquid. The enantiomeric ratio was determined by UPC[2] analysis on a Daicel Chiralpak IG-3 column: isocratic CO_2/i-PrOH 97:3, flow rate 2 mL/min, λ = 210 nm: τ_{major} = 5.5 min, τ_{minor} = 6.2 min. The product was stored at -20ºC. The characterization of the title compound was consistent with the data available in the literature.[69]

(*R*)-**27b** and (*R*)-**27c** were prepared following the general procedure *GP2* using, the (*R*) enantiomer of the diphenylprolinol TMS ether as the organocatalyst.

2.5.4 Synthesis of Reference Compounds

GP3 – General Procedure for the Organocatalyzed Synthesis of Reference Compounds **26**

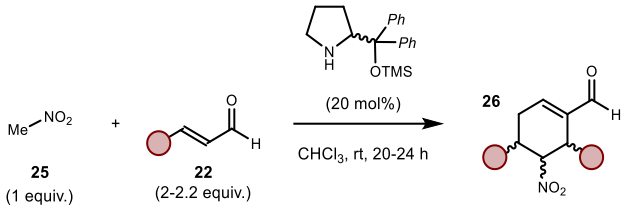

Racemic compounds **26** were synthesized following a reported literature procedure.[20] To a 10 mL screw-cup vial were added, in sequence, an approximately 1:1 (*R*) and (*S*) mixture of the diphenylprolinol TMS ether as the organocatalyst (20 mol%), the corresponding enal **22** (2.2 equiv.), if solid, and chloroform (1 M). To the resulting mixture were added nitromethane **25** (1 mmol, 1 equiv.) and the corresponding enal **22** (2.2 equiv.), if liquid, under argon atmosphere. The reaction mixture was stirred at ambient temperature for 20 to 24 hours. The crude mixture was diluted with dichloromethane and washed with water. The combined organic extracts were dried over anhydrous $MgSO_4$, filtered and concentrated under reduced pressure. Purification of the crude material by flash column chromatography on silica gel provided the corresponding reference compounds **26** as mixtures of two main diastereomers. The relative configuration of the two main diastereomers were assigned by comparison with the reported data for compound **26**.[44] These diastereomers are the same obtained in the biocatalytic semi-preparative scale reactions described below and were used for the determination of the diastereomeric ratio and the enantiomeric excess of the products obtained in both semi-preparative and analytical scale biocatalytic reactions.

4,6-bis-(4-chlorophenyl)-5-nitrocyclohex-1-ene carbaldehyde (26h)

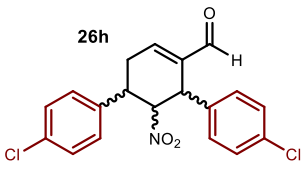

Prepared according to *GP3*, using nitromethane **25** (54 µL, 1.00 mmol), the racemic diphenylprolinol catalyst (65 mg, 200 µmol) and 4-chlorocinnamaldehyde **22h** (333 mg, 2.00 mmol) in anhydrous chloroform (1 mL). The crude mixture was purified by flash column chromatography (gradient from 10 to 30% EtOAc in hexane) to afford product **26h** as a mixture of two diastereomers ***d1*** and ***d2*** (240 mg, 64% yield, 1:1.4 dr ***d1***:***d2***) as orange solids. The enantiomers were separated by HPLC analysis on a Daicel Chiralpak IB-3 column: isocratic 100% hexane for 2 min; gradient from 100% hexane to 90:10 hexane/*i*-PrOH for 8 min; gradient from 90:10 to 70:30 hexane/*i*-PrOH for 2 min; isocratic hexane/*i*-PrOH 70:30 for 23 min, flow rate 1.0 mL/min, λ = 215 nm: ***d1***: τ = 24 min and τ = 25 min; ***d2***: τ = 18 min and τ = 19 min. The relative configurations were assigned by comparison with compound **26a**.

^{1}H NMR (**26h-*d1***, 400 MHz, $CDCl_3$): δ 9.57 (s, 1H), 7.40 – 7.33 (m, 3H), 7.32 – 7.22 (m, 2H), 7.21 – 7.11 (m, 2H), 7.03 – 6.95 (m, 2H), 4.86 (dd, *J* = 3.3, 2.0 Hz, 1H), 4.50 (s, 1H), 3.32 (ddd, *J* = 9.7, 5.8, 3.3 Hz, 1H), 3.28 – 3.14 (m, 1H), 2.90 (dt, *J* = 19.9, 5.3 Hz, 1H).

^{13}C NMR (**26h -*d1***, 101 MHz, $CDCl_3$): δ 191.5, 150.2, 138.0, 137.3, 136.2, 134.3, 134.2, 129.6 (2C), 129.4 (2C), 129.3 (2C), 128.8 (2C), 90.9, 42.5, 37.0, 28.0.

HRMS (ESI) Exact mass calculated for **26h-*d1***, $C_{19}H_{15}Cl_2NNaO_3$ $[M+Na]^+$: 398.0321, found: 398.0315.

^{1}H NMR (**26h-*d2***, 400 MHz, $CDCl_3$): δ 9.53 (s, 1H), 7.37 – 7.24 (m, 5H), 7.19 – 7.09 (m, 2H), 7.10 – 6.99 (m, 2H), 5.21 (dd, *J* = 12.4, 5.8 Hz, 1H), 4.69 (d, *J* = 5.9 Hz, 1H), 3.55 (ddd, *J* = 12.4, 10.8, 6.5 Hz, 1H), 3.11 (ddd, *J* = 20.9, 6.5, 4.6 Hz, 1H), 2.64 (ddt, *J* = 20.9, 10.8, 2.2 Hz, 1H).

^{13}C NMR (**26h-*d2***, 101 MHz, $CDCl_3$): δ 190.6, 148.0, 139.9, 138.3, 134.8, 133.8, 133.7, 129.9 (2C), 129.4 (2C), 129.2 (2C), 128.7 (2C), 89.1, 42.0, 37.4, 35.2.

HRMS (ESI) Exact mass calculated for **26h-*d1***, $C_{19}H_{15}Cl_2NNaO_3$ $[M+Na]^+$: 398.0321, found: 398.0315.

Reference compounds **26a-g** and **26i** were synthesized using the general procedure *GP3*. The main diastereomers obtained for these compounds using the general procedure above are the same diastereomers obtained in the biocatalytic semi-preparative scale reactions detailed below. Therefore, their full characterization is provided below.

GP4 – General Procedure for the Organocatalyzed Synthesis of Reference Compounds **46**

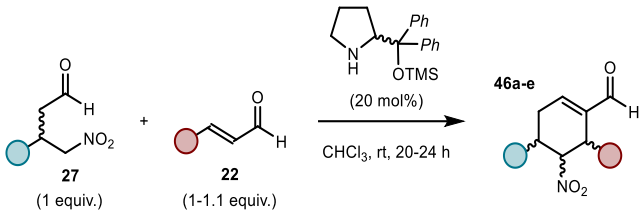

To a 10 mL screw-cup vial were added, in sequence, the intermediate **27** (1.0 equiv.), an approximately 1:1 (*R*) and (*S*) mixture of the diphenylprolinol TMS ether as the organocatalyst (20 mol%) and chloroform (1 M). To the resulting mixture was added the corresponding enal **22** (1-1.1 equiv.) under argon atmosphere. The reaction mixture was stirred at ambient temperature for 20 to 24 hours. The crude mixture was diluted with dichloromethane and washed with water. The combined organic extracts were dried over anhydrous $MgSO_4$, filtered and concentrated under reduced pressure. Purification of the crude material by flash column chromatography on silica gel provided the corresponding reference compounds **46** as mixtures of two main diastereomers. The relative configurations of the two main diastereomers were assigned by comparison with compound **26**. These diastereomers are the same obtained in the biocatalytic semi-preparative scale reactions detailed below. Therefore, the full characterization of compounds **46a-e** is provided further below. The isolated products **46** were used for the determination of the diastereomeric ratio and the enantiomeric excess of the products obtained in both semi-preparative and analytical scale biocatalytic reactions.

GP5 – General Procedure for the Organocatalyzed Synthesis of Reference Compounds **23**

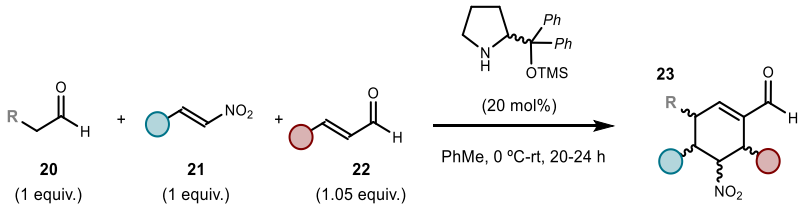

Reference compounds **23** were synthesized following a reported literature procedure.[19] To a 10 mL screw-cup vial were added, in sequence, an approximately 1:1 (*R*) and (*S*) mixture of the diphenylprolinol TMS ether as the organocatalyst (20 mol%), the corresponding trans-β-nitrostyrene **21** (1 mmol, 1 equiv.), the corresponding enal **22** (1.05 equiv.), if solid, and anhydrous toluene (1.25 M). To the resulting mixture were added at 0ºC the aliphatic aldehyde **20** (1 equiv.) and the corresponding enal **22** (1.05 equiv.), if liquid, under argon atmosphere. The reaction mixture was allowed to reach the ambient temperature for approximately 1 hour

and left stirring for additional 20 to 24 hours. The crude mixture was concentrated under reduced pressure. Purification of the crude material by flash column chromatography on silica gel provided the corresponding reference compounds **23** as mixtures of two main diastereomers. The relative configurations of the two main diastereomers were assigned by comparison with the reported data for compound **23**.[19,72]

3-ethyl-5-nitro-4,6-diphenylcyclohex-1-ene carbaldehyde (23a)

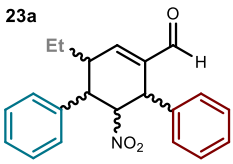

Prepared according to *GP5*, using trans-β-nitrostyrene **21a** (106 mg, 710 µmol), the (*R*) and (*S*) mixture of the diphenylprolinol catalyst (46 mg, 142 µmol), butanal **20** (64 µL, 710 µmol) and cinnamaldehyde **22a** (94 µL, 746 µmol) in anhydrous toluene (600 µL). The crude mixture was purified by flash column chromatography (gradient from 10 to 30% EtOAc in hexane) to afford product **23a** as a mixture of two diastereomers ***d1*** and ***d2*** (197 mg, 60% yield, 3:1 dr ***d1***:***d2***) as yellow solids. The enantiomers were separated by HPLC analysis on a Daicel Chiralpak IB-3 column: isocratic 100% hexane for 5 min; gradient from 100% hexane to 95:5 hexane/*i*-PrOH for 10 min; gradient from 95:5 to 80:20 hexane/*i*-PrOH for 5 min; isocratic hexane/*i*-PrOH 80:20 for 10 min, flow rate 1.0 mL/min, λ = 215 nm: ***d1***: τ = 16 min and τ = 19 min; ***d2***: τ = 24 min and τ = 29 min. The relative and absolute configurations were assigned by comparison with the data reported in the literature.[19,72]

^{1}H NMR (**23a-*d1***, 400 MHz, $CDCl_3$): δ 9.62 (s, 1H), 7.47 – 7.15 (m, 9H), 7.06 – 6.96 (m, 2H), 4.89 (dd, *J* = 3.5, 1.8 Hz, 1H), 4.47 (s, 1H), 3.38 – 3.28 (m, 1H), 3.06 (dd, *J* = 10.5, 3.5 Hz, 1H), 1.77 (dqd, *J* = 13.8, 7.6, 4.1 Hz, 1H), 1.55 – 1.40 (m, 1H), 1.07 (t, *J* = 7.5 Hz, 3H).

^{13}C NMR (**23a-*d1***, 101 MHz, $CDCl_3$): δ 192.0, 154.4, 138.9, 137.9, 137.4, 129.3 (2C), 129.2 (2C), 128.2, 128.1 (2C), 127.9 (2C), 127.0, 92.7, 43.2, 42.9, 38.3, 25.2, 10.8.

^{1}H NMR (**23a-*d2***, 400 MHz, $CDCl_3$): δ 9.54 (s, 1H), 7.37 – 7.20 (m, 6H), 7.20 – 7.15 (m, 2H), 7.14 – 7.06 (m, 3H), 5.28 (dd, *J* = 12.4, 5.9 Hz, 1H), 4.69 – 4.63 (m, 1H), 3.27 (dd, *J* = 12.4, 10.2 Hz, 1H), 2.70 (dddq, *J* = 10.3, 8.4, 4.3, 1.9 Hz, 1H), 1.78 (dqd, *J* = 13.9, 7.6, 4.1 Hz, 1H), 1.51 (ddd, *J* = 13.8, 8.0, 7.1 Hz, 1H), 1.09 (t, *J* = 7.5 Hz, 3H).

^{13}C NMR (**23a-*d2***, 101 MHz, $CDCl_3$): δ 191.2, 152.0, 139.6, 139.0, 137.9, 135.4, 128.9 (2C), 128.8 (2C), 128.7 (2C), 128.5, 127.8, 127.0, 90.3, 45.8, 43.0, 42.7, 24.7, 11.0.

[72] Jia, Y., Mao, Z., Wang, R. "Asymmetric triple cascade organocatalytic reaction in water: construction of polyfunctional cyclohexene building blocks having multiple stereocenters" Tetrahedron: Asymmetry 2011, 22, 2018-2023.

3-ethyl-6-(4-fluorophenyl)-5-nitro-4-phenylcyclohex-1-ene carbaldehyde (23b)

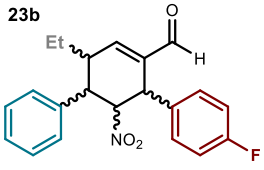

Prepared according to *GP5*, using trans-β-nitrostyrene **21a** (75 mg, 500 µmol), the (*R*) and (*S*) mixture of the diphenylprolinol catalyst (46 mg, 140 µmol), butanal **20** (54 µL, 600 µmol) and 4-fluoro-cinnamaldehyde **22b** (79 mg, 525 µmol) in anhydrous toluene (400 µL). The crude mixture was purified by flash column chromatography (gradient from 10 to 30% EtOAc in hexane) to afford product **23b** as a mixture of several compounds with ***d*₁** as the main diastereomer and traces amount of ***d*₂** (29 mg, 16% yield for **23b-*d*₁**) as a yellow oil. The enantiomers were separated by HPLC analysis on a Daicel Chiralpak IB-3 column: isocratic 100% hexane for 2 min; gradient from 100% hexane to 90:10 hexane/*i*-PrOH for 8 min; gradient from 90:10 to 80:20 hexane/*i*-PrOH for 2 min; isocratic hexane/*i*-PrOH 80:20 for 23 min, flow rate 1.0 mL/min, λ = 215 nm: τ = 11 min, τ = 12 min. The relative and absolute configurations were assigned by comparison with compound **23a**.

^{1}H NMR (**23b-*d*₁**, 400 MHz, $CDCl_3$): δ 9.60 (s, 1H), 7.33 (dd, *J* = 2.7, 0.9 Hz, 1H), 7.31 – 7.27 (m, 3H), 7.23 – 7.14 (m, 2H), 7.14 – 7.02 (m, 2H), 7.05 – 6.96 (m, 2H), 4.83 (dd, *J* = 3.5, 1.9 Hz, 1H), 4.44 (s, 1H), 3.38 – 3.26 (m, 1H), 3.03 (dd, *J* = 10.4, 3.5 Hz, 1H), 1.85 – 1.69 (m, 1H), 1.47 (dt, *J* = 13.7, 7.4 Hz, 1H), 1.06 (t, *J* = 7.4 Hz, 3H).

^{19}F NMR (**23b-*d*₁**, 376 MHz, $CDCl_3$): δ -114.13.

^{13}C NMR (**23b-*d*₁**, 101 MHz, $CDCl_3$): δ 192.0, 162.4 (d, J_{C-F} = 247.4 Hz), 154.6, 137.9, 137.2, 134.7, 129.7 (d, J_{C-F} = 8.2 Hz), 129.3, 128.3, 127.9, 116.3 (d, J_{C-F} = 21.7 Hz), 92.6, 43.0, 42.4, 38.4, 25.3, 10.9.

HRMS (ESI) Exact mass calculated for **23b-*d*₁**, $C_{21}H_{20}FNNaO_3$ $[M+Na]^+$: 376.1319, found: 376.1319.

^{1}H NMR (**23b-*d*₂**, 400 MHz, $CDCl_3$): δ 9.54 (s, 1H), 7.32 – 7.20 (m, 3H), 7.20 – 7.14 (m, 2H), 7.11 (d, *J* = 2.6 Hz, 1H), 7.09 – 6.97 (m, 4H), 5.26 (dd, *J* = 12.4, 5.9 Hz, 1H), 4.63 (d, *J* = 5.9 Hz, 1H), 3.21 (dd, *J* = 12.4, 10.2 Hz, 1H), 2.74 – 2.65 (m, 1H), 1.77 (dtd, *J* = 15.1, 7.6, 4.2 Hz, 1H), 1.48 (dd, *J* = 14.4, 7.3 Hz, 1H), 1.08 (t, *J* = 7.5 Hz, 3H).

^{19}F NMR (**23b-*d*₂**, 376 MHz, $CDCl_3$): δ -113.8.

^{13}C NMR (**23b-*d*₂**, 101 MHz, $CDCl_3$): δ 190.9, 164.0, 152.1, 139.4, 138.6, 131.0, 130.1 (d, J_{C-F} = 8.2 Hz), 128.9, 128.0, 127.8, 115.8 (d, J_{C-F} = 21.5 Hz), 90.0, 45.6, 42.8, 41.8, 24.1, 10.8.

The synthesis of the reference compound **23c** using the general procedure *GP5* only afforded a mixture of several diastereomers in traces amount. Further attempts to synthesize these compounds were not undertaken since the amount obtained was in general sufficient for HPLC detection and chiral separation of the desired diastereomers.

2.5.5 Semi-Preparative Scale Biocatalytic Reactions

GP6 – General Procedure for the Semi-Preparative Scale Enzymatic Synthesis of Enantiopure Products **23**

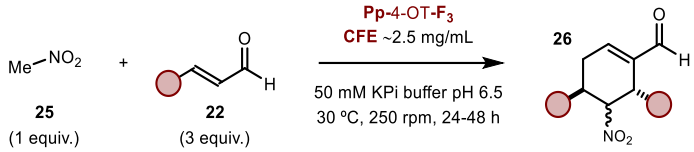

In typical procedure for the Pp-4-OT-F_3-catalyzed biosynthesis of compounds **26** on a semi-preparative scale, 1.5 g of *E. coli* cells containing the overexpressed Pp-4OT-F_3 enzyme were resuspended in 27 mL of 50 mM KPi buffer pH 6.5 and sonicated for 20 min. The lysate was cleared by centrifugation for 20 min at 4ºC and the supernatant collected and used without further purification. In a 50 mL Falcon tube a solution of nitromethane **25** (0.15 mmol, final concentration of 5 mM) and enal **22** (0.45 mmol, final concentration of 15 mM) in DMSO was added to the supernatant to reach the final volume of 30 mL (10% v/v DMSO/water buffer). The reaction mixture was shaken in an incubator at 30 ºC and 250 rpm for 24 to 48 hours (see Figure 2.39a). The crude mixture was quenched with 1 mL of 1M HCl and extracted twice with 30 mL of ethyl acetate. The combined organic extracts were dried over anhydrous $MgSO_4$, filtered and concentrated under reduced pressure. Purification of the crude material by flash column chromatography on silica gel provided the corresponding enantiopure reference compounds.

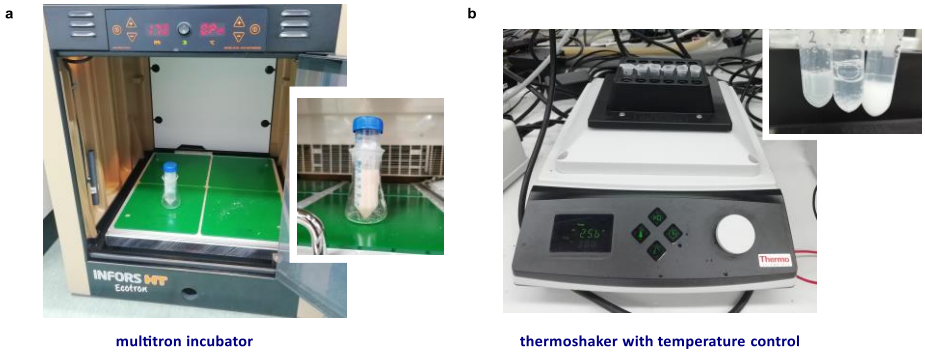

Figure 2.39. a) Set-up for the semi-preparative scale enzymatic reactions (150 µmol scale); b) set-up for the analytical scale enzymatic reactions (2.50 µmol scale).

(4*R*,5*R*,6*S*)-5-nitro-4,6-diphenylcyclohex-1-ene carbaldehyde (26a)

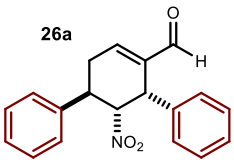

Prepared according to *GP6*, using nitromethane **25** (8.2 uL, 150 µmol) and cinnamaldehyde **22a** (57 µL, 450 µmol) as the substrates in DMSO as solvent. The crude mixture was purified by flash column chromatography (gradient from 10 to 30% EtOAc in hexane) to afford product **26a** as a major diastereomer ***d1*** and traces of a second diastereomer ***d2*** (28 mg, 61% yield, >20:1 dr ***d1*:*d2***, >99% ee) as a white solid. The enantiomeric excess was determined by HPLC analysis on a Daicel Chiralpak IB-3 column: isocratic 100% hexane for 2 min; gradient from 100% hexane to 90:10 hexane/*i*-PrOH for 8 min; gradient from 90:10 to 70:30 hexane/*i*-PrOH for 2 min; isocratic hexane/*i*-PrOH 70:30 for 23 min, flow rate 1.0 mL/min, λ = 215 nm: τ_{major} = 26 min, τ_{minor} = 29 min; $[\alpha]_D^{26}$ = +373 (c = 0.0012, CH_2Cl_2, >99% ee). The relative and absolute configurations were assigned by comparison with compound **26f** and the data reported in the literature.[20]

^{1}H NMR (**26a-*d1***, 500 MHz, $CDCl_3$): δ 9.52 (s, 1H), 7.35 – 7.16 (m, 8H), 7.15 – 7.07 (m, 3H), 5.27 (dd, *J* = 12.4, 5.8 Hz, 1H), 4.71 (d, *J* = 5.8 Hz, 1H), 3.61 (ddd, *J* = 12.4, 10.7, 6.6 Hz, 1H), 3.11 (ddd, *J* = 21.0, 6.6, 4.6 Hz, 1H), 2.66 (dddd, *J* = 21.0, 10.7, 2.9, 1.8 Hz, 1H).

^{13}C NMR (**26a-*d1***, 126 MHz, $CDCl_3$): δ 190.8, 148.1, 140.2, 140.1, 135.3, 129.1, 128.9, 128.7, 128.6, 127.8, 127.3, 89.3, 42.7, 37.9, 35.5.

HRMS (ESI) Exact mass calculated for **26a-*d1***, $C_{19}H_{17}NNaO_3$ $[M+Na]^+$: 330.1101, found: 330.1097.

^{1}H NMR (**26a-*d2***, 500 MHz, $CDCl_3$): δ 9.60 (s, 1H), 7.41 – 7.35 (m, 3H), 7.35 – 7.21 (m, 6H), 7.09 – 7.01 (m, 2H), 4.97 (dd, *J* = 3.3, 1.8 Hz, 1H), 4.54 (s, 1H), 3.43 – 3.35 (m, 1H), 3.28 (ddt, *J* = 20.1, 11.3, 2.4 Hz, 1H), 2.91 (dt, *J* = 20.0, 5.3 Hz, 1H).

^{13}C NMR (**26a-*d2***, 126 MHz, $CDCl_3$): δ 191.8, 150.5, 138.9, 138.2, 138.1, 129.4, 129.1, 128.2, 128.1, 127.4, 91.3, 43.3, 37.3, 28.0.

(4*R*,5*R*,6*S*)- 4,6-bis-(4-fluorophenyl)-5-nitrocyclohex-1-ene carbaldehyde (26b)

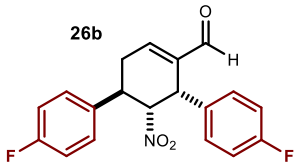

Prepared according to *GP6*, using nitromethane **25** (8.2 uL, 150 µmol) and 4-fluorocinnamaldehyde **22b** (68 mg, 450 µmol) as the substrates in DMSO as solvent. The crude mixture was purified by flash column chromatography (gradient from 10 to 50% EtOAc in hexane) to afford product **26b** as a single diastereomer (46 mg, 88% yield, >99% ee) as colorless crystals. The enantiomeric excess was determined by HPLC analysis on a Daicel Chiralpak IB-3 column: isocratic 100% hexane for 2 min; gradient from 100% hexane to 90:10 hexane/*i*-PrOH for 8 min; gradient from 90:10 to 80:20 hexane/*i*-PrOH for 2 min; isocratic hexane/*i*-PrOH 80:20 for 23 min, flow rate 1.0 mL/min, λ = 215 nm: τ_{minor} = 25 min, τ_{major} = 26 min; $[\alpha]_D^{26}$ = +310 (c = 0.0012, CH_2Cl_2, >99% ee). The relative and absolute configurations were assigned by comparison with compound **26f**.

^{1}H NMR (400 MHz, $CDCl_3$): δ 9.53 (s, 1H), 7.26 – 6.91 (m, 9H), 5.21 (dd, *J* = 12.4, 5.8 Hz, 1H), 4.70 (d, *J* = 6.2 Hz, 1H), 3.65 – 3.49 (m, 1H), 3.11 (ddd, *J* = 21.0, 6.5, 4.6 Hz, 1H), 2.65 (ddt, *J* = 21.1, 10.9, 2.4 Hz, 1H).
^{19}F NMR (376 MHz, $CDCl_3$): δ -113.5, -114.4.
^{13}C NMR (101 MHz, $CDCl_3$): δ 190.6, 162.8 (d, J_{C-F} = 247.9 Hz), 161.1 (d, J_{C-F} = 246.8 Hz), 147.8, 140.0, 135.4 (d, J_{C-F} = 3.2 Hz), 130.9 (d, J_{C-F} = 3.3 Hz), 130.2 (d, J_{C-F} = 8.3 Hz), 128.8 (d, J_{C-F} = 8.1 Hz), 116.0 (d, J_{C-F} = 20 Hz), 115.8 (d, J_{C-F} = 20 Hz), 89.2, 41.8, 37.1, 35.2.
HRMS (ESI) Exact mass calculated for $C_{19}H_{15}F_2NNaO_3$ $[M+Na]^+$: 366.0912, found: 366.0911.

(4*R*,5*R*,6*S*)- 4,6-bis-(3-methoxyphenyl)-5-nitrocyclohex-1-ene carbaldehyde (26c)

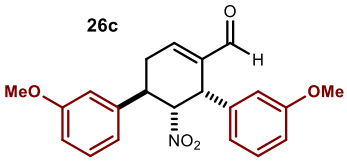

Prepared according to *GP6*, using nitromethane **25** (8.2 uL, 150 µmol) and 3-methoxycinnamaldehyde **22c** (73 mg, 450 µmol) as the substrates in ethylene glycol as solvent. The crude mixture was purified by flash column chromatography (gradient from 10 to 30% EtOAc in hexane) to afford product **26c** as the major diastereomer ***d1*** and traces of ***d2*** (24 mg, 43% yield, 18:1 dr ***d1*:*d2***, >99% ee) as a white solid. The enantiomeric excess was determined by HPLC analysis on a Daicel Chiralpak IB-3 column: isocratic 100% hexane for 2 min; gradient from 100% hexane to 90:10 hexane/*i*-PrOH for 8 min; gradient from 90:10 to 40:60 hexane/*i*-PrOH for 2 min; isocratic hexane/*i*-PrOH 40:60 for 23 min, flow rate 1.0 mL/min, λ = 215 nm: τ_{major} = 27 min, τ_{minor} = 23 min; $[\alpha]_D^{26}$ for **26c-*d1*** = +314 (c = 0.0010, CH_2Cl_2, >99% ee). The relative and absolute configurations were assigned by comparison with compound **26f**.
^{1}H NMR (**26c-*d1***, 400 MHz, $CDCl_3$): δ 9.51 (s, 1H), 7.22 (dt, *J* = 12.8, 8.1 Hz, 2H), 7.11 – 7.05 (m, 1H), 6.84 (ddd, *J* = 8.3, 2.6, 0.9 Hz, 1H), 6.80 – 6.73 (m, 2H), 6.73 – 6.66 (m, 2H), 6.64 – 6.59 (m, 1H), 5.23 (dd, *J* = 12.4, 5.8 Hz, 1H), 4.67 (d, *J* = 5.8 Hz, 1H), 3.78 (s, 3H), 3.76 (s, 3H), 3.59 (ddd, *J* = 12.4, 10.6, 6.5 Hz, 1H), 3.09 (ddd, *J* = 21.0, 6.4, 4.7 Hz, 1H), 2.63 (dddd, *J* = 21.0, 10.6, 2.9, 1.9 Hz, 1H).
^{13}C NMR (**26c-*d1***, 126 MHz, $CDCl_3$): δ 190.9, 160.1, 159.7, 148.1, 141.8, 140.1, 136.8, 130.2, 129.8, 121.2, 119.3, 115.2, 113.6, 113.1, 112.9, 89.1, 55.4, 55.3, 42.6, 37.92, 35.5.
HRMS (ESI) Exact mass calculated for **26c-*d1***, $C_{21}H_{21}NNaO_5$ $[M+Na]^+$: 390.1312, found: 390.1311.

^{1}H NMR (**26c-*d2***, 500 MHz, $CDCl_3$): δ 9.58 (s, 1H), 7.34 (dd, *J* = 4.8, 2.8 Hz, 1H), 7.29 (t, *J* = 7.9 Hz, 1H), 7.21 (t, *J* = 8.0 Hz, 1H), 6.88 – 6.78 (m, 4H), 6.65 (dd, *J* = 7.7, 1.7 Hz, 1H), 6.60 (t, *J* = 2.2 Hz, 1H), 4.97 (dd, *J* = 3.3, 1.8 Hz, 1H), 4.50 (s, 1H), 3.81 (s, 3H), 3.75 (s, 3H), 3.36 (ddd, *J* = 11.3, 6.0, 3.3 Hz, 1H), 3.24 (ddt, *J* = 20.0, 11.4, 2.3 Hz, 1H), 2.89 (dt, *J* = 20.1, 5.5 Hz, 1H).
^{13}C NMR (**26c-*d2***, 126 MHz, $CDCl_3$): δ 191.8, 160.2, 160.0, 150.5, 140.5, 139.7, 138.1, 130.4, 130.1, 120.4, 119.6, 114.5, 113.9, 112.9, 112.7, 91.1, 55.4, 43.2, 37.4, 28.0.

(4*R*,5*R*,6*S*)- 4,6-bis-(2-tolyl)-5-nitrocyclohex-1-ene carbaldehyde (26d)

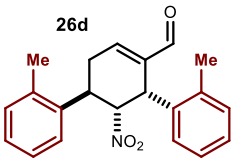

Prepared according to *GP6*, using nitromethane **25** (8.2 uL, 150 µmol) and 2-methylcinnamaldehyde **22d** (66 mg, 450 µmol) as the substrates in ethylene glycol as solvent. The crude mixture was purified by flash column chromatography (gradient from 10 to 30% EtOAc in hexane) to afford product **26d** as a mixture of two diastereomers ***d1*** and ***d2*** (27 mg, 49% yield, 9:1 dr ***d1***:***d2***, >99% ee) as white solids. The enantiomeric excess was determined by HPLC analysis on a Daicel Chiralpak IB-3 column: isocratic 100% hexane for 2 min; gradient from 100% hexane to 90:10 hexane/*i*-PrOH for 8 min; gradient from 90:10 to 80:20 hexane/*i*-PrOH for 2 min; isocratic hexane/*i*-PrOH 80:20 for 23 min, flow rate 1.0 mL/min, λ = 215 nm: τ_{major} = 27 min, τ_{minor} = 25 min; $[\alpha]_D^{26}$ for **26d-*d1*** = +389 (c = 0.0009, CH_2Cl_2, >99% ee). The relative and absolute configurations were assigned by comparison with compound **26f**.

^{1}H NMR (**26d-*d1***, 500 MHz, $CDCl_3$): δ 9.47 (s, 1H), 7.20 – 7.13 (m, 5H), 7.13 – 7.10 (m, 2H), 7.10 – 7.03 (m, 2H), 5.36 (dd, *J* = 12.4, 5.8 Hz, 1H), 5.16 (d, *J* = 5.6 Hz, 0H), 4.18 (ddd, *J* = 12.6, 10.6, 6.4 Hz, 1H), 3.07 (ddd, *J* = 21.0, 6.4, 4.6 Hz, 1H), 2.58 (ddt, *J* = 21.0, 10.7, 2.4 Hz, 1H), 2.40 (s, 3H), 2.32 (s, 3H).

^{13}C NMR (**26d-*d1***, 126 MHz, $CDCl_3$): δ 191.0, 147.5, 141.7, 138.6, 138.2, 136.9, 134.0, 131.4, 131.1, 128.0, 128.0, 127.4, 127.0, 125.6, 88.8, 37.6, 34.5, 19.8, 19.4.

HRMS (ESI) Exact mass calculated for **26d-*d1***, $C_{21}H_{21}NNaO_3$ $[M+Na]^+$: 358.1419, found: 358.1414.

^{1}H NMR (**26d-*d2***, 500 MHz, $CDCl_3$): δ 9.62 (s, 1H), 7.45 (dd, *J* = 4.8, 2.4 Hz, 1H), 7.32 – 7.29 (m, 1H), 7.25 (td, *J* = 7.4, 1.4 Hz, 1H), 7.21 – 7.14 (m, 4H), 7.12 – 7.09 (m, 1H), 7.03 (dd, *J* = 7.6, 1.4 Hz, 1H), 4.69 (s, 1H), 4.63 (dd, *J* = 3.0, 1.1 Hz, 1H), 3.69 (ddd, *J* = 12.0, 5.7, 3.0 Hz, 1H), 3.36 (ddt, *J* = 20.1, 12.0, 2.3 Hz, 1H), 2.79 (dt, *J* = 20.1, 5.4 Hz, 1H), 2.53 (s, 3H), 1.68 (s, 3H).

^{13}C NMR (**26d-*d2***, 126 MHz, $CDCl_3$): δ 192.0, 151.2, 138.7, 136.9, 136.3, 135.9, 135.7, 131.7, 131.2, 128.2, 128.0, 126.8, 126.8, 126.4, 126.3, 88.0, 40.2, 33.0, 27.5, 19.5, 18.6.

HRMS (ESI) Exact mass calculated for **26d-*d2***, $C_{21}H_{21}NNaO_3$ $[M+Na]^+$: 358.1414, found: 358.1418.

(4*R*,5*R*,6*S*)- 4,6-bis-(3-bromophenyl)-5-nitrocyclohex-1-ene carbaldehyde (26e)

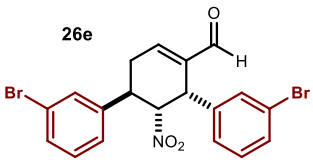

Prepared according to *GP6*, using nitromethane **25** (8.2 uL, 150 µmol) and 3-bromocinnamaldehyde **22e** (95 mg, 450 µmol) as the substrates in DMSO as solvent. The crude mixture was purified by flash column chromatography (gradient from 10 to 30% EtOAc in hexane) to afford product **26e** as a mixture of two diastereomers ***d1*** and ***d2*** (30 mg, 43% yield, 8:1 dr ***d1***:***d2***, >99% ee) as white solids. The enantiomeric excess was determined by HPLC analysis on a Daicel

Chiralpak IB-3 column: isocratic 100% hexane for 2 min; gradient from 100% hexane to 90:10 hexane/*i*-PrOH for 8 min; gradient from 90:10 to 70:30 hexane/*i*-PrOH for 2 min; isocratic hexane/*i*-PrOH 70:30 for 23 min, flow rate 1.0 mL/min, λ = 215 nm: ***d1***: τ_{major} = 24 min, τ_{minor} = 28 min; ***d2***: τ_{minor} = 17 min, τ_{major} = 20 min; $[\alpha]_D^{26}$ for **26e-*d1*** = +349 (c = 0.0011, CH_2Cl_2, >99% ee). The relative and absolute configurations were assigned by comparison with compound **26g**.

^{1}H NMR (**26e-*d1***, 500 MHz, $CDCl_3$): δ 9.51 (s, 1H), 7.45 (ddd, *J* = 8.1, 1.9, 1.0 Hz, 1H), 7.41 – 7.33 (m, 2H), 7.23 – 7.09 (m, 5H), 7.04 (dt, *J* = 7.8, 1.4 Hz, 1H), 5.20 (dd, *J* = 12.4, 5.9 Hz, 1H), 4.66 (dd, *J* = 5.8, 1.7 Hz, 1H), 3.52 (ddd, *J* = 12.5, 10.7, 6.5 Hz, 1H), 3.11 (ddd, *J* = 21.0, 6.6, 4.6 Hz, 1H), 2.63 (ddt, *J* = 21.0, 10.7, 2.4 Hz, 1H).

^{13}C NMR (**26e-*d1***, 126 MHz, $CDCl_3$): δ 190.5, 148.1, 142.1, 139.6, 137.4, 131.9, 131.2, 131.2, 130.8, 130.7, 130.5, 127.7, 125.9, 123.2, 123.0, 88.8, 42.1, 37.7, 35.2.

HRMS (ESI) Exact mass calculated for **26e-*d1***, $C_{19}H_{15}Br_2NNaO_3$ $[M+Na]^+$: 485.9311, found: 485.9308.

^{1}H NMR (**26d-*d2***, 500 MHz, $CDCl_3$): δ 9.59 (s, 1H), 7.48 (ddd, *J* = 8.0, 2.0, 1.1 Hz, 1H), 7.42 (ddd, *J* = 8.0, 2.0, 1.0 Hz, 1H), 7.40 – 7.35 (m, 1H), 7.34 (t, *J* = 1.9 Hz, 1H), 7.31 – 7.24 (m, 1H), 7.23 – 7.15 (m, 3H), 7.03 – 6.98 (m, 1H), 4.91 (dd, *J* = 3.2, 1.9 Hz, 1H), 4.52 (s, 1H), 3.35 – 3.19 (m, 2H), 2.93 (dt, *J* = 19.7, 5.2 Hz, 1H).

^{13}C NMR (**26e-*d2***, 126 MHz, $CDCl_3$): δ 191.5, 150.3, 141.0, 140.0, 137.7, 131.6, 131.5, 131.0, 131.0, 130.7, 130.7, 126.9, 126.0, 123.6, 123.2, 90.5, 42.8, 37.0, 27.8.

HRMS (ESI) Exact mass calculated for **26e-*d2***, $C_{19}H_{15}Br_2NNaO_3$ $[M+Na]^+$: 485.9311, found: 485.9308.

(4*R*,5*R*,6*S*)- 4,6-bis-(2-chlorophenyl)-5-nitrocyclohex-1-ene carbaldehyde (26g)

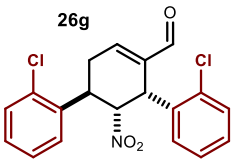

Prepared according to *GP6*, using nitromethane **25** (8.2 uL, 150 µmol) and 2-chlorocinnamaldehyde **22g** (75 mg, 450 µmol) as the substrates in ethylene glycol:DMSO 3:1 as solvent mixture. The crude mixture was purified by flash column chromatography (gradient from 10 to 30% EtOAc in hexane) to afford product **26g** as a mixture of two diastereomers ***d1*** and ***d2*** (24 mg, 43% yield, 3:1 dr ***d1***:***d2***, >99% ee) as white solids. The enantiomeric excess was determined by HPLC analysis on a Daicel Chiralpak IB-3 column: isocratic 100% hexane for 2 min; gradient from 100% hexane to 90:10 hexane/*i*-PrOH for 8 min; gradient from 90:10 to 70:30 hexane/*i*-PrOH for 2 min; isocratic hexane/*i*-PrOH 70:30 for 23 min, flow rate 1.0 mL/min, λ = 215 nm: ***d1***: τ_{major} = 25 min, τ_{minor} = 33 min; ***d2***: τ_{minor} = 17 min, τ_{major} = 20 min; $[\alpha]_D^{26}$ for **26g-*d1*** = +261 (c = 0.0018, CH_2Cl_2, >99% ee). Crystals of derivatives **26g-*d1***, suitable for X-ray diffraction analysis, were obtained upon slow evaporation of a CH_2Cl_2 solution of the title compound. This enabled the unambiguous determination of the absolute and relative stereochemical configurations for product **26g-*d1***. NMR conformational studies detailed below further confirmed the relative configuration of

compounds **26g-*d*$_1$** and **26g-*d*$_2$**.

^{1}H NMR (**26g-*d*$_1$**, 500 MHz, $CDCl_3$): δ 9.52 (s, 1H), 7.44 – 7.39 (m, 1H), 7.40 – 7.35 (m, 1H), 7.31 – 7.19 (m, 5H), 7.16 (td, *J* = 7.3, 3.0 Hz, 2H), 5.61 – 5.42 (m, 2H), 4.44 – 4.27 (m, 1H), 3.22 (ddd, *J* = 20.9, 6.2, 4.6 Hz, 1H), 2.74 – 2.55 (m, 1H).

^{13}C NMR (**26g-*d*$_1$**, 126 MHz, $CDCl_3$): δ 190.5, 148.0, 140.7, 136.7, 136.2, 134.2, 133.2, 130.6, 130.4, 129.7, 129.5, 129.1, 127.9, 126.7, 86.9, 37.8, 35.4, 33.1.

HRMS (ESI) Exact mass calculated for **26g-*d*$_1$**, $C_{19}H_{15}Cl_2NNaO_3$ $[M+Na]^+$: 398.0321, found: 398.0322.

^{1}H NMR (**26g-*d*$_2$**, 500 MHz, $CDCl_3$): δ 9.62 (s, 1H), 7.49 (dd, *J* = 7.7, 1.6 Hz, 1H), 7.43 (dd, *J* = 5.2, 2.5 Hz, 1H), 7.37 – 7.15 (m, 6H), 7.06 (dd, *J* = 7.5, 1.9 Hz, 1H), 5.06 (dd, *J* = 3.1, 1.2 Hz, 1H), 5.00 (s, 1H), 3.84 (ddd, *J* = 12.3, 5.5, 2.9 Hz, 1H), 3.18 (ddt, *J* = 19.8, 12.3, 2.3 Hz, 1H), 2.78 (dt, *J* = 19.8, 5.3 Hz, 1H).

^{13}C NMR (**26g-*d*$_2$**, 126 MHz, $CDCl_3$): δ 191.4, 150.7, 138.3, 135.4, 135.0, 134.3, 133.7, 130.4, 130.1, 129.4, 129.2, 128.8, 128.0, 127.3, 127.1, 85.9, 40.1, 34.2, 26.6.

HRMS (ESI) Exact mass calculated for **26g-*d*$_2$**, $C_{19}H_{15}Cl_2NNaO_3$ $[M+Na]^+$: 398.0321, found: 398.0328.

(4*R*,5*R*,6*S*)-4,6-bis-(3-chlorophenyl)-5-nitrocyclohex-1-ene carbaldehyde (26h)

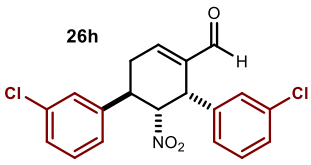

Prepared according to *GP6*, using nitromethane **25** (8.2 uL, 150 µmol) and 3-chlorocinnamaldehyde **22h** (75 mg, 450 µmol) as the substrates in ethylene glycol:DMSO 3:1 as solvent mixture. The crude mixture was purified by flash column chromatography (gradient from 10 to 30% EtOAc in hexane) to afford product **26h** as a mixture of two diastereomers ***d*$_1$** and ***d*$_2$** (29 mg, 51% yield, 15:1 dr ***d*$_1$**:***d*$_2$**, >99% ee) as white solids. The enantiomeric excess was determined by HPLC analysis on a Daicel Chiralpak IB-3 column: isocratic 100% hexane for 2 min; gradient from 100% hexane to 90:10 hexane/*i*-PrOH for 8 min; gradient from 90:10 to 70:30 hexane/*i*-PrOH for 2 min; isocratic hexane/*i*-PrOH 70:30 for 23 min, flow rate 1.0 mL/min, λ = 215 nm: ***d*$_1$**: τ_{major} = 23 min, τ_{minor} = 26 min; ***d*$_2$**: τ_{minor} = 17 min, τ_{major} = 19 min; $[\alpha]_D^{26}$ for **26h-*d*$_1$** = +268 (c = 0.0010, CH_2Cl_2, >99% ee). The relative and absolute configurations were assigned by comparison with compound **26g**.

^{1}H NMR (**26h-*d*$_1$**, 400 MHz, $CDCl_3$): δ 9.54 (s, 1H), 7.36 – 7.19 (m, 5H), 7.18 – 6.98 (m, 4H), 5.24 (dd, *J* = 12.4, 5.9 Hz, 1H), 4.70 (dd, *J* = 5.5, 1.7 Hz, 1H), 3.56 (ddd, *J* = 12.4, 10.7, 6.5 Hz, 1H), 3.14 (ddd, *J* = 21.0, 6.5, 4.6 Hz, 1H), 2.73 – 2.58 (m, 1H).

^{13}C NMR (**26h-*d*$_1$**, 101 MHz, $CDCl_3$): δ 190.4, 148.0, 141.7, 139.5, 137.1, 134.9, 134.7, 130.4, 130.1, 128.9, 128.3, 128.1, 127.6, 127.1, 125.3, 88.7, 42.0, 37.6, 35.0.

HRMS (ESI) Exact mass calculated for **26h-*d*$_1$**, $C_{19}H_{15}Cl_2NNaO_3$ $[M+Na]^+$: 398.0321, found: 398.0317.

^{1}H NMR (**26h-*d*$_2$**, 500 MHz, $CDCl_3$): δ 9.61 (s, 1H), 7.42 – 7.15 (m, 7H), 7.08 (d, *J* = 2.1 Hz,

1H), 6.98 (dt, *J* = 7.0, 1.8 Hz, 1H), 4.94 (dd, *J* = 3.2, 1.9 Hz, 1H), 4.55 (s, 1H), 3.38 – 3.22 (m, 2H), 2.95 (dt, *J* = 19.8, 5.2 Hz, 1H).

^{13}C NMR (**26h-*d*$_2$**, 126 MHz, $CDCl_3$): δ 191.3, 150.2, 140.6, 139.7, 137.6, 135.2, 134.9, 130.6, 130.3, 128.5, 128.4, 128.0, 127.7, 126.3, 125.4, 90.4, 42.6, 36.9, 27.6.

HRMS (ESI) Exact mass calculated for **26h-*d*$_2$**, $C_{19}H_{15}Cl_2NNaO_3$ $[M+Na]^+$: 398.0321, found: 398.0333.

(4*R*,5*R*,6*S*)- 4,6-bis-(2-furyl)-5-nitrocyclohex-1-ene carbaldehyde (26i)

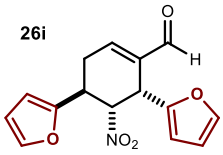

Prepared according to *GP6*, using nitromethane **25** (8.2 uL, 150 µmol) and (E)-3-(furan-2-yl)acrylaldehyde **22i** (55 mg, 450 µmol) as the substrates in DMSO as solvent. The crude mixture was purified by flash column chromatography (gradient from 10 to 30% EtOAc in hexane) to afford product **26i** as a mixture of two diastereomers ***d*$_1$** and ***d*$_2$** (4.3 mg, 10% yield, 1:1 dr ***d*$_1$**:***d*$_2$**, >99% ee) as brown oils. The enantiomeric excess of **26i-*d*$_1$** was determined by HPLC analysis on a Daicel Chiralpak IB-3 column: isocratic 100% hexane for 2 min; gradient from 100% hexane to 90:10 hexane/*i*-PrOH for 8 min; isocratic hexane/*i*-PrOH 90:10 for 25 min, flow rate 1.0 mL/min, λ = 215 nm: ***d*$_1$**: τ_{major} = 27 min, τ_{minor} = 26 min; ***d*$_2$**: τ = 16 min. The enantiomeric excess of **26i-*d*$_2$** was determined by HPLC analysis on a Daicel Chiralpak IC-3 column: isocratic 100% hexane for 2 min; gradient from 100% hexane to 90:10 hexane/*i*-PrOH for 8 min; gradient from 90:10 to 40:60 hexane/*i*-PrOH for 2 min; isocratic hexane/*i*-PrOH 40:60 for 23 min, flow rate 1.0 mL/min, λ = 215 nm: τ_{major} = 19 min, τ_{minor} = 20 min; $[\alpha]_D^{26}$ for **26i-*d*$_1$** = +145 (c = 0.0008, CH_2Cl_2, >99% ee). The relative and absolute configurations were assigned by comparison with compound **26h**.

^{1}H NMR (**26i-*d*$_1$**, 500 MHz, $CDCl_3$): δ 9.50 (s, 1H), 7.35 (dd, *J* = 1.9, 0.8 Hz, 1H), 7.30 (dd, *J* = 1.9, 0.8 Hz, 1H), 7.04 – 6.99 (m, 1H), 6.29 (ddd, *J* = 16.9, 3.2, 1.8 Hz, 2H), 6.17 (ddd, *J* = 10.0, 3.2, 0.8 Hz, 2H), 5.08 (dd, *J* = 12.1, 5.5 Hz, 1H), 4.79 (dd, *J* = 5.3, 1.6 Hz, 1H), 4.00 (ddd, *J* = 12.1, 10.4, 6.6 Hz, 1H), 3.07 (ddd, *J* = 20.9, 6.6, 4.6 Hz, 1H), 2.83 (dddd, *J* = 20.9, 10.4, 3.0, 1.8 Hz, 1H).

^{13}C NMR (**26i-*d*$_1$**, 126 MHz, $CDCl_3$): δ 190.4, 152.2, 148.3, 148.1, 143.6, 142.3, 137.8, 110.9, 110.7, 110.3, 107.7, 86.6, 36.5, 33.0, 31.9.

HRMS (ESI) Exact mass calculated for **26i-*d*$_1$**, $C_{15}H_{13}NNaO_5$ $[M+Na]^+$: 310.0686, found: 310.0682.

^{1}H NMR (**26i-*d*$_2$**, 500 MHz, $CDCl_3$): δ 9.56 (s, 1H), 7.37 (dd, *J* = 14.7, 1.9 Hz, 2H), 7.17 (t, *J* = 3.8 Hz, 1H), 6.32 (td, *J* = 3.6, 1.8 Hz, 2H), 6.17 (d, *J* = 3.3 Hz, 1H), 6.10 (d, *J* = 3.4 Hz, 1H), 5.36 (dd, *J* = 3.4, 1.9 Hz, 1H), 4.68 (s, 1H), 3.64 (ddd, *J* = 10.4, 7.1, 3.4 Hz, 1H), 3.07 – 2.89 (m, 2H).

^{13}C NMR (**26i-*d*$_2$**, 126 MHz, $CDCl_3$): δ 191.4, 151.8, 150.8, 149.2, 143.0, 142.5, 136.8, 110.9, 110.6, 109.0, 107.0, 84.7, 36.3, 33.0, 26.8.

HRMS (ESI) Exact mass calculated for **26i-*d*$_2$**, $C_{15}H_{13}NNaO_5$ $[M+Na]^+$: 310.0686, found:

310.0682.

GP7 – General Procedure for the Semi-Preparative Scale Enzymatic Synthesis of Enantiopure Compounds ***46***

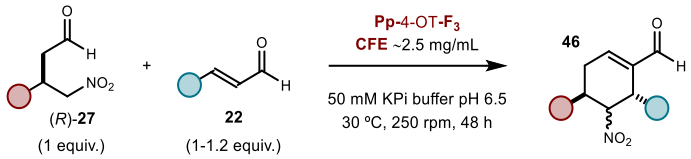

In typical procedure for the Pp-4-OT-F_3-catalyzed biosynthesis of compounds **46** on a semi-preparative scale, 1.5 g of *E. coli* cells containing the overexpressed Pp-4OT-F_3 enzyme were resuspended in 27 mL of 50 mM KPi buffer pH 6.5 and sonicated for 20 min. The lysate was cleared by centrifugation (20 min, 4ºC) and the supernatant collected and used without further purification. In a 50 mL Falcon tube a solution of intermediate **27** (0.12 mmol, final concentration of 5 mM) and enal **22** (0.12-0.14 mmol, final concentration of 5-6 mM) in DMSO was added to the supernatant to reach the final volume of 25 mL (10% v/v DMSO/water buffer). The reaction mixture was shaken in an incubator at 30 ºC and 250 rpm for 48 hours (see Figure 2.39a). The crude mixture was quenched with 1 mL of 1M HCl and extracted twice with 30 mL of ethyl acetate. The combined organic extracts were dried over anhydrous $MgSO_4$, filtered and concentrated under reduced pressure. Purification of the crude material by flash column chromatography on silica gel provided the corresponding enantiopure reference compounds **46**.

(4*R*,5*R*,6*S*)-6-(3-chlorophenyl)-5-nitro-4-phenylcyclohex-1-ene carbaldehyde (46a)

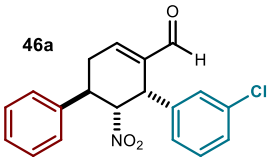

Prepared according to *GP7*, using intermediate (*R*)-**27a** (23 mg, 120 µmol) and 3-chlorocinnamaldehyde **22g** (28 mg, 145 µmol) as the substrates in DMSO as solvent. The crude mixture was purified by flash column chromatography (gradient from 10 to 20% EtOAc in hexane) to afford product **46a** as diastereomer ***d*$_1$** and traces amount of ***d*$_2$** (16 mg, 38% yield, 12:1 dr ***d*$_1$**:***d*$_2$**, >99% ee) as a white solid. The enantiomeric excess was determined by HPLC analysis on a Daicel Chiralpak IC-3 column: isocratic 100% hexane for 2 min; gradient from 100% hexane to 90:10 hexane/*i*-PrOH for 8 min; gradient from 90:10 to 70:30 hexane/*i*-PrOH for 2 min; isocratic hexane/*i*-PrOH 70:30 for 40 min, flow rate 0.5 mL/min, λ = 215 nm: τ_{major} = 30 min, τ_{minor} = 29 min; $[\alpha]_D^{26}$ for **46a-*d*$_1$** = +380 (c = 0.0010, CH_2Cl_2, >99% ee). The relative and absolute configurations were assigned by comparison with compound **26h**.

^{1}H NMR (**46a-*d*$_1$**, 500 MHz, $CDCl_3$): δ 9.52 (s, 1H), 7.35 – 7.27 (m, 3H), 7.27 – 7.21 (m, 2H), 7.22 – 7.18 (m, 2H), 7.16 – 7.13 (m, 1H), 7.06 (t, *J* = 1.9 Hz, 1H), 7.01 (dt, *J* = 7.5, 1.5 Hz,

1H), 5.26 (dd, *J* = 12.4, 5.9 Hz, 1H), 4.67 (d, *J* = 5.9 Hz, 1H), 3.56 (ddd, *J* = 12.4, 10.7, 6.5 Hz, 1H), 3.13 (ddd, *J* = 21.0, 6.5, 4.6 Hz, 1H), 2.67 (dddd, *J* = 21.1, 10.7, 2.9, 1.9 Hz, 1H).
^{13}C NMR (**46a-*d*$_1$**, 126 MHz, $CDCl_3$): δ 190.7, 148.7, 139.7, 139.7, 137.4, 134.7, 130.2, 129.2, 128.9, 128.5, 127.9, 127.3, 89.1, 42.2, 37.9, 35.4.
HRMS (ESI) Exact mass calculated for **46a-*d*$_1$**, $C_{19}H_{16}ClNNaO_3$ $[M+Na]^+$: 364.0711, found: 364.0716.

^{1}H NMR (**46a-*d*$_2$**, 400 MHz, $CDCl_3$): δ 9.59 (s, 1H), 7.39 (m, 1H), 7.36 – 7.26 (m, 5H), 7.22 – 7.10 (m, 2H), 7.06 (m, 2H), 4.94 (dd, *J* = 3.2, 2.0 Hz, 1H), 4.50 (d, *J* = 2.0 Hz, 1H), 3.36 (ddd, *J* = 11.1, 5.5, 3.2 Hz, 1H), 3.27 (dddd, *J* = 19.8, 11.0, 2.8, 1.8 Hz, 1H), 2.94 (dt, *J* = 19.7, 5.5 Hz, 1H).
^{13}C NMR (**46a-*d*$_2$**, 101 MHz, $CDCl_3$): δ 191.7, 151.0, 141.0, 137.7, 137.7, 135.2, 130.6, 129.1, 128.5, 128.3, 128.2, 127.4, 126.5, 90.9, 42.8, 37.5, 28.0.
HRMS (ESI) Exact mass calculated for **46a-*d*$_2$**, $C_{19}H_{16}ClNNaO_3$ $[M+Na]^+$: 364.0711, found: 364.0715.

(4*R*,5*R*,6*S*)-6-(3-methoxyphenyl)-5-nitro-4-phenylcyclohex-1-enecarbaldehyde (46b)

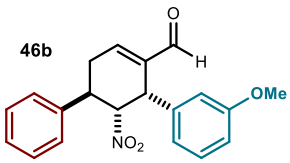

Prepared according to *GP7*, using intermediate (*R*)-**27a** (23 mg, 120 µmol) and 3-methoxycinnamaldehyde **22c** (23 mg, 120 µmol) as the substrates in DMSO as solvent. The crude mixture was purified by flash column chromatography (gradient from 10 to 30% EtOAc in hexane) to afford product **46b** as a single diastereomer (12 mg, 30% yield, >99% ee) as a colorless oil. The enantiomeric excess was determined by UPC^2 analysis on a Daicel Chiralpak IC-3 column: isocratic 100% CO_2 for 1 min; gradient CO_2/MeOH from 100% CO_2 to 60:40 over 5 minutes, curve 6, flow rate 2 mL/min, λ = 210: τ_{major} = 4.2 min and τ_{minor} = 4.7 min; $[\alpha]_D^{26}$ = +311 (c = 0.00085, CH_2Cl_2, >99% ee). The relative and absolute configuration were assigned by comparison with compound **26h**.

^{1}H NMR (500 MHz, $CDCl_3$): δ 9.52 (s, 1H), 7.32 – 7.26 (m, 2H), 7.25 – 7.17 (m, 4H), 7.12 – 7.08 (m, 1H), 6.84 (ddd, *J* = 8.3, 2.6, 0.9 Hz, 1H), 6.71 – 6.67 (m, 1H), 6.62 (t, *J* = 2.1 Hz, 1H), 5.24 (dd, *J* = 12.4, 5.8 Hz, 1H), 4.67 (d, *J* = 5.8 Hz, 1H), 3.79 (s, 3H), 3.62 (ddd, *J* = 12.4, 10.7, 6.6 Hz, 1H), 3.09 (ddd, *J* = 21.0, 6.5, 4.7 Hz, 1H), 2.64 (dddd, *J* = 21.0, 10.6, 2.9, 1.8 Hz, 1H).
^{13}C NMR (126 MHz, $CDCl_3$): δ 190.9, 159.8, 148.1, 140.2, 136.8, 129.9, 129.1, 127.8, 127.4, 121.3, 115.2, 113.2, 89.3, 55.4, 42.6, 37.9, 35.5.
HRMS (ESI) Exact mass calculated for $C_{20}H_{19}NNaO_4$ $[M+Na]^+$: 360.1206, found: 360.1209.

(4*R*,5*R*,6*S*)-6-(3-bromophenyl)-5-nitro-4-phenylcyclohex-1-ene carbaldehyde (46c)

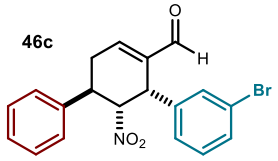

Prepared according to *GP7*, using intermediate (*R*)-**27a** (23 mg, 120 µmol) and 3-bromocinnamaldehyde **22e** (30 mg, 120 µmol) as the substrates in DMSO as solvent. The crude mixture was purified by flash column chromatography (gradient from 10 to 20% EtOAc in hexane) to afford product **46c** as diastereomer ***d*$_1$** and traces amount of ***d*$_2$** (15 mg, 32% yield, >20:1 dr ***d*$_1$**:***d*$_2$**, >99% ee) as a white solid. The enantiomeric excess was determined by HPLC analysis on a Daicel Chiralpak IC-3 column: isocratic 100% hexane for 2 min; gradient from 100% hexane to 90:10 hexane/*i*-PrOH for 8 min; gradient from 90:10 to 70:30 hexane/*i*-PrOH for 2 min; isocratic hexane/*i*-PrOH 70:30 for 23 min, flow rate 1.0 mL/min, λ = 215 nm: τ_{major} = 18 min and τ_{minor} =19 min; $[\alpha]_D^{26}$ = +297 (c = 0.0013, CH_2Cl_2, >99% ee). The relative and absolute configuration were assigned by comparison with compound **26h**.

^{1}H NMR (**46c-*d*$_1$**, 500 MHz, $CDCl_3$): δ 9.52 (s, 1H), 7.44 (ddd, *J* = 7.9, 2.0, 1.0 Hz, 1H), 7.33 – 7.27 (m, 2H), 7.26 – 7.17 (m, 5H), 7.17 – 7.13 (m, 1H), 7.05 (dt, *J* = 7.8, 1.4 Hz, 1H), 5.25 (dd, *J* = 12.4, 6.0 Hz, 1H), 4.65 (dd, *J* = 6.0, 1.7 Hz, 1H), 3.55 (ddd, *J* = 12.4, 10.7, 6.5 Hz, 1H), 3.13 (ddd, *J* = 20.7, 6.5, 4.6 Hz, 1H), 2.66 (dddd, *J* = 21.1, 10.7, 2.9, 1.9 Hz, 1H).
^{13}C NMR (**46c-*d*$_1$**, 126 MHz, $CDCl_3$): δ 190.7, 148.7, 139.7, 139.7, 137.7, 131.8, 131.3, 130.5, 129.2, 128.0, 127.8, 127.3, 123.0, 89.1, 42.2, 37.9, 35.4.
HRMS (ESI) Exact mass calculated for **52c-*d*$_1$**, $C_{19}H_{16}BrNNaO_3$ $[M+Na]^+$: 408.0206, found: 408.0218.
^{1}H NMR (**46c-*d*$_2$**, 400 MHz, $CDCl_3$): δ 9.59 (s, 1H), 7.46 (ddd, *J* = 7.9, 2.0, 1.1 Hz, 1H), 7.40 (m, 1H), 7.37 – 7.26 (m, 4H), 7.20 (m, 1H), 7.09 – 7.04 (m, 2H), 4.94 (dd, *J* = 3.2, 1.9 Hz, 1H), 4.49 (s, 1H), 3.39 – 3.32 (m, 1H), 3.32 – 3.22 (m, 1H), 2.94 (dt, *J* = 19.2, 4.9 Hz, 1H).
^{13}C NMR (**46c-*d*$_2$**, 101 MHz, $CDCl_3$): δ 191.6, 151.0, 141.3, 137.7, 137.7, 131.4, 131.1, 130.9, 129.2, 128.3, 127.4, 127.0, 123.5, 91.0, 42.7, 37.5, 28.0.

(4*R*,5*R*,6*S*)-4-(4-fluorophenyl)-6-5-nitro-6-phenylcyclohex-1-enecarbaldehyde (46d)

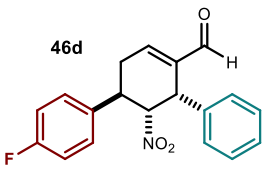

Prepared according to *GP7*, using intermediate (*R*)-**27b** (38 mg, 180 µmol) and cinnamaldehyde **22a** (24 mg, 180 µmol) as the substrates in DMSO as solvent. The crude mixture was purified by flash column chromatography (isocratic 30% EtOAc in hexane) to afford product **46d** as a single diastereomer (30 mg, 51% yield, >99% ee) as a white solid. The enantiomeric excess was determined by HPLC analysis on a Daicel Chiralpak IC-3 column: isocratic 100% hexane for 2 min; gradient from 100% hexane to 70:30 hexane/*i*-PrOH for 8 min; isocratic hexane/*i*-PrOH 70:30 for 40 min, flow rate 1.0 mL/min, λ = 215 nm: τ_{major} = 18 min and τ_{minor} = 20 min; $[\alpha]_D^{26}$ = +285 (c = 0.0019, CH_2Cl_2,

>99% ee). The relative and absolute configuration were assigned by comparison with compound **46h**.

^{1}H NMR (400 MHz, $CDCl_3$): δ 9.51 (s, 1H), 7.31 (dt, *J* = 4.1, 1.6 Hz, 3H), 7.20 – 7.13 (m, 2H), 7.10 (ddt, *J* = 6.1, 4.4, 2.0 Hz, 3H), 7.01 – 6.93 (m, 2H), 5.20 (dd, *J* = 12.4, 5.8 Hz, 1H), 4.73 – 4.66 (m, 1H), 3.60 (ddd, *J* = 12.4, 10.7, 6.5 Hz, 1H), 3.09 (ddd, *J* = 21.0, 6.5, 4.6 Hz, 1H), 2.62 (dddd, *J* = 21.0, 10.7, 2.9, 1.8 Hz, 1H).
^{19}F NMR (376 MHz, $CDCl_3$): δ -114.2.
^{13}C NMR (101 MHz, $CDCl_3$): δ 190.8, 162.2 (d, J_{C-F} = 246.6 Hz), 147.9, 140.1, 135.8 (d, J_{C-F} = 3.3 Hz), 135.1, 129.0 (d, J_{C-F} = 8.2 Hz), 128.9, 128.7, 128.6, 116.0 (d, J_{C-F} = 21.6 Hz), 89.5, 42.7, 37.2, 35.4.
HRMS (ESI) Exact mass calculated for $C_{19}H_{16}FNNaO_3$ $[M+Na]^+$: 348.1006, found: 348.1011.

(4*R*,5*R*,6*S*)-4-(3-methoxyphenyl)-5-nitro-6-phenylcyclohex-1-enecarbaldehyde (46e)

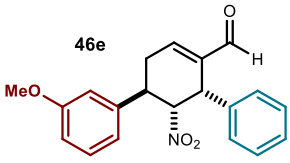

Prepared according to *GP7*, using intermediate (*R*)-**27c** (78 mg, 350 µmol) and cinnamaldehyde **22a** (53 µL, 420 µmol) as the substrates in DMSO as solvent. The crude mixture was purified by flash column chromatography (gradient from 10 to 30% EtOAc in hexane) to afford product **46e** as a major diastereomer ***d1*** and traces amount of ***d2*** (24.5 mg, 21 % yield, 10:1 dr ***d1***:***d2***, >99% ee) as a colorless oil. The enantiomeric excess was determined by HPLC analysis on a Daicel Chiralpak IC-3 column: isocratic 100% hexane for 2 min; gradient from 100% hexane to 90:10 hexane/*i*-PrOH for 8 min; gradient from 90:10 to 70:30 hexane/*i*-PrOH for 2 min; isocratic hexane/*i*-PrOH 70:30 for 40 min, flow rate 0.5 mL/min, λ = 215 nm: ***d1***: τ_{major} = 23 min, τ_{minor} = 24 min; ***d2***: τ_{major} = 22 min, τ_{minor} = 28 min; $[\alpha]_D^{26}$ for **46e-*d1*** = +260 (c = 0.0009, CH_2Cl_2, >99% ee). The relative and absolute configuration were assigned by comparison with compound **26h**.

^{1}H NMR (**46e-*d1***, 500 MHz, $CDCl_3$): δ 9.52 (s, 1H), 7.34 – 7.29 (m, 3H), 7.20 (t, *J* = 8.0 Hz, 1H), 7.13 – 7.09 (m, 3H), 6.80 – 6.73 (m, 2H), 6.73 – 6.70 (m, 1H), 5.25 (dd, *J* = 12.4, 5.8 Hz, 1H), 4.70 (dt, *J* = 5.7, 1.3 Hz, 1H), 3.76 (s, 3H), 3.58 (ddd, *J* = 12.4, 10.6, 6.5 Hz, 1H), 3.11 (ddd, *J* = 21.0, 6.6, 4.7 Hz, 1H), 2.65 (dddd, *J* = 21.1, 10.7, 2.9, 1.8 Hz, 1H).
^{13}C NMR (**46e-*d1***, 126 MHz, $CDCl_3$): δ 190.9, 160.1, 148.1, 141.79, 140.2, 135.3, 130.2, 128.9, 128.7, 128.6, 119.3, 113.6, 112.9, 89.2, 55.4, 42.7, 37.9, 35.5.
HRMS (ESI) Exact mass calculated for **46e-*d1***, $C_{20}H_{19}NNaO_4$ $[M+Na]^+$: 360.1206, found: 360.1213.
^{1}H NMR (**46e-*d2***, 500 MHz, $CDCl_3$): δ 9.59 (s, 1H), 7.39 – 7.34 (m, 2H), 7.34 – 7.29 (m, 1H), 7.26 – 7.17 (m, 4H), 6.80 (ddd, *J* = 8.2, 2.6, 0.9 Hz, 1H), 6.66 – 6.61 (m, 1H), 6.59 (t, *J* = 2.2 Hz, 1H), 4.96 (dd, *J* = 3.2, 1.8 Hz, 1H), 4.53 (s, 1H), 3.75 (s, 3H), 3.35 (ddd, *J* = 11.3, 5.8, 3.3 Hz, 1H), 3.28 (dt, *J* = 11.3, 2.3 Hz, 0H), 2.90 (dt, *J* = 19.9, 5.2 Hz, 1H).

^{13}C NMR (**46e-*d*$_2$**, 126 MHz, $CDCl_3$): δ 191.8, 160.0, 150.5, 139.7, 138.9, 138.2, 130.1, 129.4, 128.2, 128.1, 119.6, 113.9, 112.8, 91.2, 55.4, 43.3, 37.3, 28.1.

Deuterium Labelling Experiment

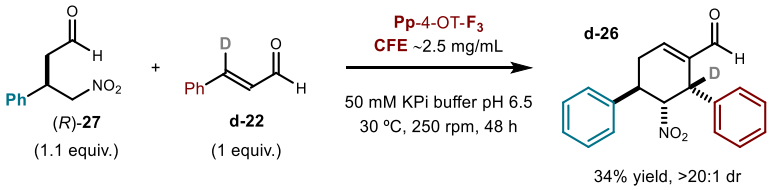

The experimental procedure *GP7* was followed using intermediate (*R*)-**27a** (32 mg, 168 µmol) and cinnamaldehyde-3-d **d-22** (21 mg, 158 µmol) as the substrates in DMSO as co-solvent in KPi buffer pH 6.5. The crude mixture was analyzed by ^{1}H NMR spectroscopy and purified by flash column chromatography (gradient from 10 to 30% EtOAc in hexane) to afford product **d-26** as a *single* diastereomer (18 mg, 34% yield) as a yellow oil. The product was obtained has a >99% deuterium incorporation on carbon C6.

^{1}H NMR (300 MHz, $CDCl_3$): δ 9.47 (s, 1H), 7.42 – 6.93 (m, 11H), 5.22 (d, *J* = 12.4 Hz, 1H), 3.56 (ddd, *J* = 12.4, 10.7, 6.5 Hz, 1H), 3.06 (ddd, *J* = 21.0, 6.6, 4.6 Hz, 1H), 2.60 (ddd, *J* = 21.0, 10.7, 2.8 Hz, 1H).

^{13}C NMR (75 MHz, $CDCl_3$): δ 190.9, 148.2, 140.1, 135.2, 129.1 (2C), 128.9 (2C), 128.7, 128.6, 127.8, 127.3 (2C), 89.2, 42.4 (t), 37.9, 35.5.

*Synthesis of (3R,4R,5S,6S)- 4-(2-chlorophenyl)-3-ethyl-5-nitro-4-phenylcyclohex-1-ene carbaldehyde (**23b**)*

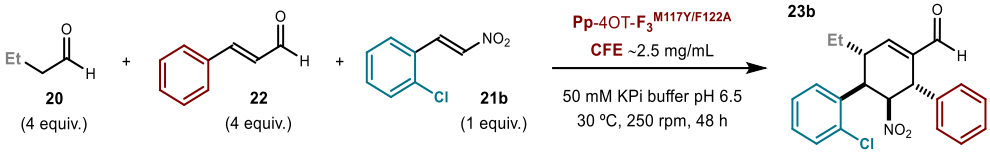

In a 50 mL Falcon tube 1.5 g of *E. coli* cells containing the overexpressed Pp-4OT-$F_3^{M117Y/F122A}$ were resuspended in 27 mL of 50 mM KPi buffer pH 6.5 and sonicated for 20 min. The lysate was cleared by centrifugation for 20 min at 4ºC and the supernatant collected and used without further purification. A solution of trans-2-chloro-β-nitrostyrene **21b** (27 mg, 150 µmol) and cinnamaldehyde **22a** (76 µL, 600 µmol) in DMSO (3 mL) was added to the supernatant (10% v/v DMSO/water buffer). To this mixture, butanal **18** (64 µL, 600 µmol) was added and the reaction mixture was shaken in an incubator at 30 ºC and 250 rpm for 48 hours (see Figure 2.40). The crude mixture was quenched with 1 mL of 1M HCl and extracted

twice with 30 mL of ethyl acetate. The combined organic extracts were dried over anhydrous $MgSO_4$, filtered and concentrated under reduced pressure. Purification of the crude material by flash column chromatography (gradient from 10 to 30% EtOAc in hexane) afforded product **23b** as a mixture of two main diastereomers ***d1*** and ***d2*** (13 mg, 23%, 3.8:1 dr ***d1***:***d2***) as colorless oils. The enantiomers were separated by HPLC analysis on a Daicel Chiralpak IB-3 column: isocratic 100% hexane for 2 min; gradient from 100% hexane to 90:10 hexane/*i*-PrOH for 8 min; gradient from 90:10 to 80:20 hexane/*i*-PrOH for 2 min; isocratic hexane/*i*-PrOH 80:20 for 23 min, flow rate 1.0 mL/min, λ = 215 nm: ***d1***: τ_{minor} = 12 min and τ_{major} = 14 min; ***d2***: τ_{minor} = 17 min and τ_{major} = 21 min; $[\alpha]_D^{26}$ for **23b-*d1*** = -31 (c = 0.0012, CH_2Cl_2, >99% ee). The relative and absolute configurations were assigned by comparison with compound **23a** and the data reported in the literature for similar structures.[19,73]

^{1}H NMR (**23b-*d1***, 400 MHz, $CDCl_3$): δ 9.64 (s, 1H), 7.44 – 7.14 (m, 10H), 4.92 (dd, *J* = 3.2, 1.4 Hz, 1H), 4.55 (s, 1H), 3.75 (dd, *J* = 11.3, 3.2 Hz, 1H), 3.41 – 3.30 (m, 1H), 1.74 (dqd, *J* = 15.0, 7.6, 3.9 Hz, 1H), 1.55 – 1.39 (m, 1H), 1.04 (t, *J* = 7.5 Hz, 3H).

^{13}C NMR (**23b-*d1***, 101 MHz, $CDCl_3$): δ 192.0, 154.2, 138.4, 138.0, 134.7, 134.4, 130.3, 129.2, 129.1 (2C), 128.14 (2C), 128.08, 128.06, 127.5, 90.1, 43.2, 38.0, 37.3, 24.7, 10.5.

HRMS (ESI) Exact mass calculated for **23b-*d1***, $C_{21}H_{20}ClNNaO_3$ $[M+Na]^+$: 392.1024, found: 392.1032.

^{1}H NMR (**23b-*d2***, 400 MHz, $CDCl_3$): δ 9.58 (s, 1H), 7.41 – 7.07 (m, 10H), 5.26 (dd, *J* = 12.3, 5.8 Hz, 1H), 4.72 (d, *J* = 5.7 Hz, 1H), 4.16 (dd, *J* = 12.3, 10.3 Hz, 1H), 2.71 – 2.61 (m, 1H), 1.78 (dqd, *J* = 14.9, 7.3, 4.1 Hz, 1H), 1.68 – 1.46 (m, 1H), 1.15 (t, *J* = 7.4 Hz, 3H).

^{13}C NMR (**23b-*d2***, 126 MHz, $CDCl_3$): δ 190.9, 151.4, 139.4, 137.4, 136.3, 134.2, 130.0, 128.7 (2C), 128.54 (2C), 128.51 (2C), 127.6, 126.1, 90.0, 46.8, 42.9, 37.8, 30.9, 24.1, 11.2.

2.5.6 Analytical scale biocatalytic reactions

GP8 – General Procedure for the Analytical Scale Biocatalytic Synthesis of Compounds **26**

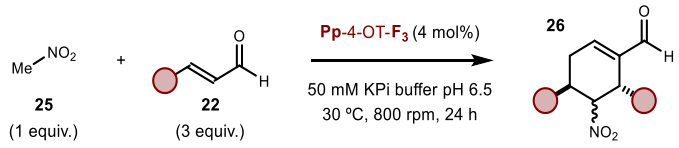

A stock solution of nitromethane **25** (2.50 µmol, final concentration of 5 mM) and a stock solution of the corresponding enal **22** (7.50 µmol, final concentration of 15 mM) in the

[73] Enders, D., Hüttl, M. R. M., Raabe, G., Bats, J. W. "Asymmetric Synthesis of Polyfunctionalized Mono-, Bi-, and Tricyclic Carbon Frameworks via Organocatalytic Domino Reactions" *Adv. Synth. Catal.* **2008**, *350*, 267-279.

selected organic solvent were added to an Eppendorf tube containing the purified enzyme Pp-4-OT-F_3 (200 µmol, 0.04 equiv.) in KPi buffer pH 6.5 to reach the final volume of 500 µL. The reaction mixture was shaken at 800 rpm in a thermoshaker (see Figure 3.10b) at 30 ºC for 24 hours. The crude mixture was quenched with 50 µL of 1M HCl and extracted with 600 µL ethyl acetate containing 5 mM of the internal standard 1,3,5-trimethoxybenzene. The organic extract was dried over anhydrous $MgSO_4$, filtered and analyzed by HPLC chromatography on Daicel Chiralpak IB-3 and IC-3 columns. Calibration curves, not reported in the present dissertation, were obtained using the previously synthesized reference compounds **26** and 1,3,5-trimethoxybenzene as the internal standard. The HPLC data for the analytical scale reactions were fit in the equation to determine the analytical yield and diastereomeric ratio of the enantiopure products reported in Figure 2.27. The enantiomeric excess of products **26** was determined by HPLC analysis by comparison with the (*R*) and (*S*) mixture of the corresponding authentic samples prepared as described earlier.

GP9 – General Procedure for the Analytical Scale Biocatalytic Synthesis of Compounds **46**

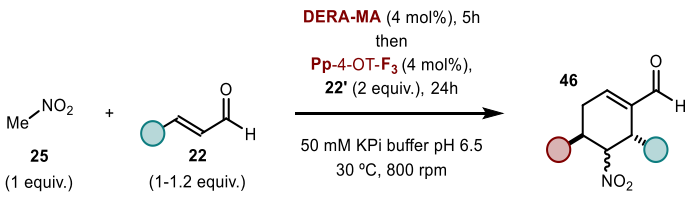

A stock solution of nitromethane **25** (2.50 µmol, final concentration of 5 mM) and a stock solution of the corresponding enal **22** (2.50 µmol, final concentration of 5 mM) in the selected organic solvent were added to an Eppendorf tube containing the purified enzyme DERA-MA (200 µmol, 0.04 equiv.) in KPi buffer pH 6.5. The reaction mixture was shaken at 800 rpm in a thermoshaker (see Figure 3.10b) at 30ºC for 5 hours. Purified enzyme Pp-4-OT-F_3 (200 µmol, 0.04 equiv.) and the second enal **22'** (5.00 µmol, final concentration of 10 mM) were added to the reaction mixture which was left stirring for additional 20 hours. The crude mixture was quenched with 50 µL of 1M HCl and extracted with 600 µL ethyl acetate containing 5 mM of the internal standard 1,3,5-trimethoxybenzene. The organic extract was dried over anhydrous $MgSO_4$, filtered and analyzed by HPLC chromatography on Daicel Chiralpak IB-3 and IC-3 columns and UPC^2 chromatography on Daicel Chiralpak IC-3 column. Calibration curves, not reported in the present dissertation, were obtained using the previously synthesized reference compounds **46** and 1,3,5-trimethoxybenzene as the internal standard. The HPLC data for the analytical scale reactions were fit in the equation to determine the analytical yield of the enantiopure products **46** shown in Figure 2.28. The diastereomeric ratio was determined by HPLC or UPC^2. The enantiomeric excess of products **46** was determined by HPLC analysis by comparison with the (*R*) and (*S*) mixture of the

corresponding authentic samples prepared as described earlier.

GP10 – General Procedure for the Analytical Scale Biocatalytic Synthesis of Compounds **23**

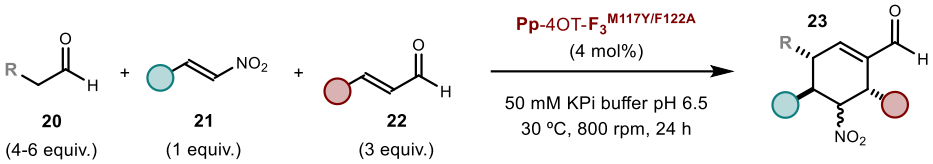

A stock solution of trans-β-nitrostyrene **21** (1.25 µmol, final concentration of 2.5 mM) and a stock solution of the corresponding enal **22** (3.75 µmol, final concentration of 7.5 mM) in DMSO were added to an Eppendorf tube containing the purified protein Pp-4OT-$F_3^{M117Y/F122A}$ (100 µmol, 0.04 equiv.) in KPi buffer pH 6.5 to reach the final volume of 500 µL. A stock solution of the corresponding aldehyde **20** (5.00-7.50 µmol, final concentration of 10-15 mM) in DMSO was added to this mixture and the reaction tube was shaken at 800 rpm in a thermoshaker (see Figure 3.10b) at 30 ºC for 24 hours. The crude mixture was quenched with 50 µL of 1M HCl and extracted once with 600 µL ethyl acetate containing 5 mM of the internal standard 1,3,5-trimethoxybenzene. The organic extract was dried over anhydrous $MgSO_4$, filtered and analyzed by HPLC chromatography on Daicel Chiralpak IB-3 column. Calibration curves, not reported in the present dissertation, were obtained using the previously synthesized reference compounds **23** and 1,3,5-trimethoxybenzene as the internal standard. The HPLC data for the analytical scale reactions were fit in the equation to determine the analytical yield and diastereomeric ratio of the enantiopure products reported in Figure 2.34. The enantiomeric excess of products **23** was determined by HPLC analysis by comparison with the (*R*) and (*S*) mixture of the corresponding authentic samples prepared as described earlier.

2.5.7 NMR Conformational Studies

The relative and absolute configurations of compound **26h-*d*$_1$** were unambiguously determined by X-ray crystallographic analysis (detailed below). The relative configuration was further confirmed by nuclear Overhauser enhancement (NOESY) spectroscopy. The relative configuration of compound **24h-*d*$_2$** was assigned as the one of the epimer of compound **24h-*d*$_1$** at the carbon bearing the nitro group by NOESY.

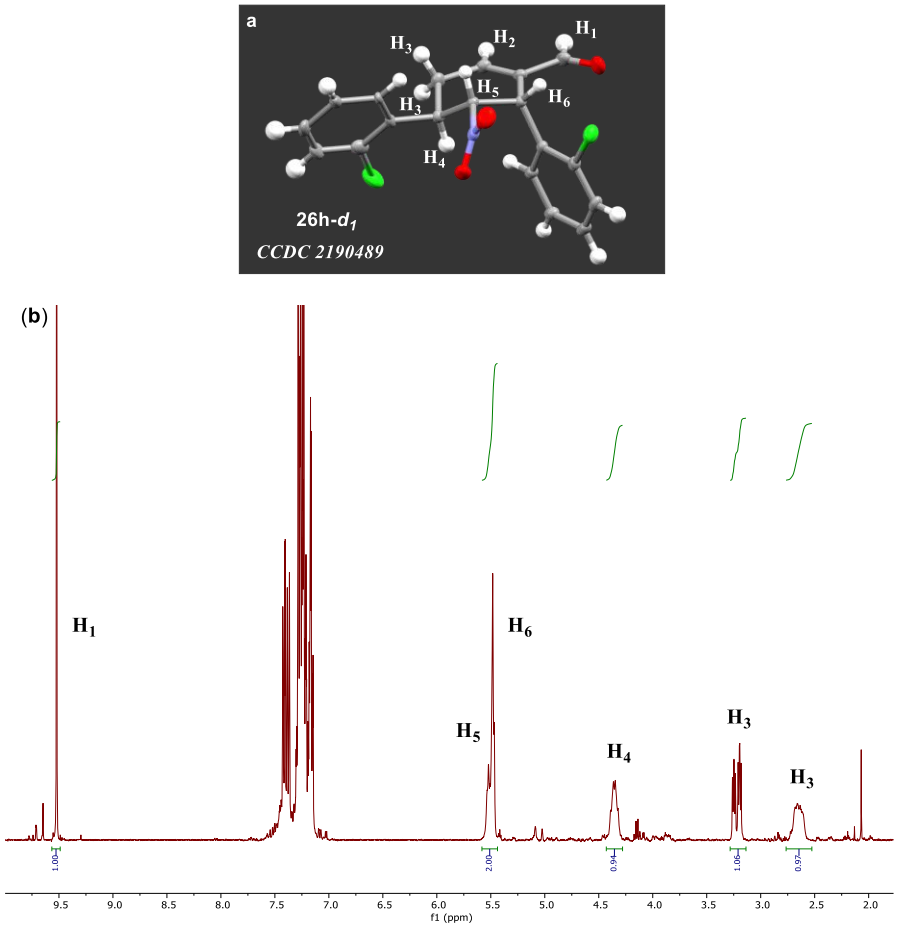

Figure 2.40 a) Crystal structure of the major diastereomer of **26h**; b) ^{1}H NMR of the major diastereomer of **26h** in $CDCl_3$.

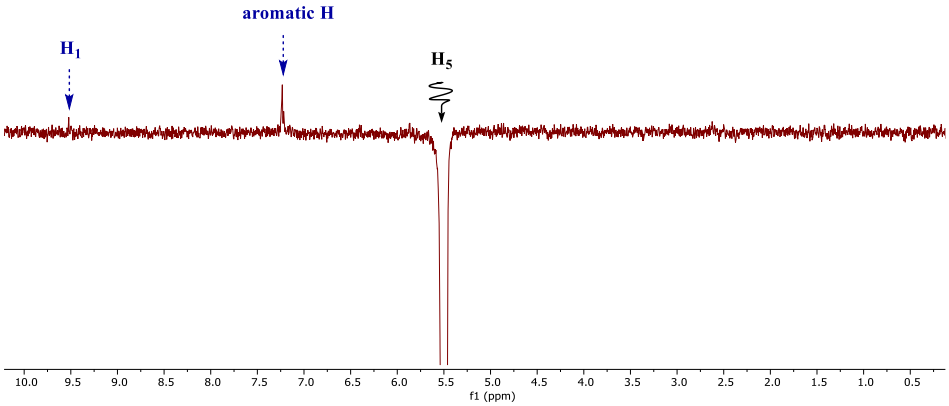

Figure 2.41. NOESY experiment of **26h-*d1*** in $CDCl_3$.

NOESY experiment of 26h-d_1 in $CDCl_3$: Weak Nuclear Overhauser Effects (NOE) are detected when H_5 is selectively irradiated at 5.50 ppm only for aromatic protons of the vicinal phenyl ring and the aldehydic proton H_1 (this correlation is very weak). The correlation is not observed with H_4 due to their *trans* axial relative spatial arrangement. The correlation with H_6 is not observed due to signal overlap.

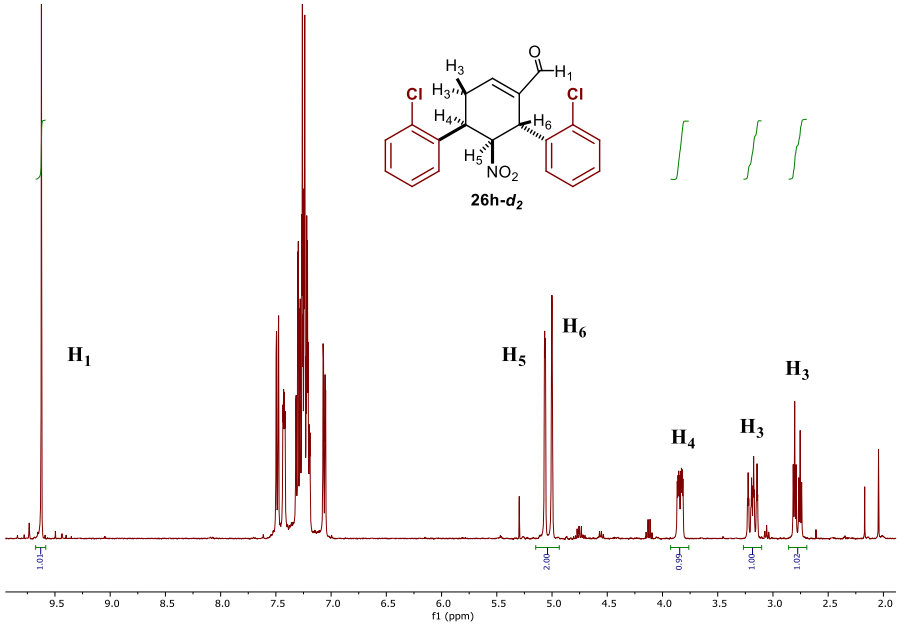

Figure 2.42. ^1H NMR and structure of the minor diastereomer of **26h** in $CDCl_3$.

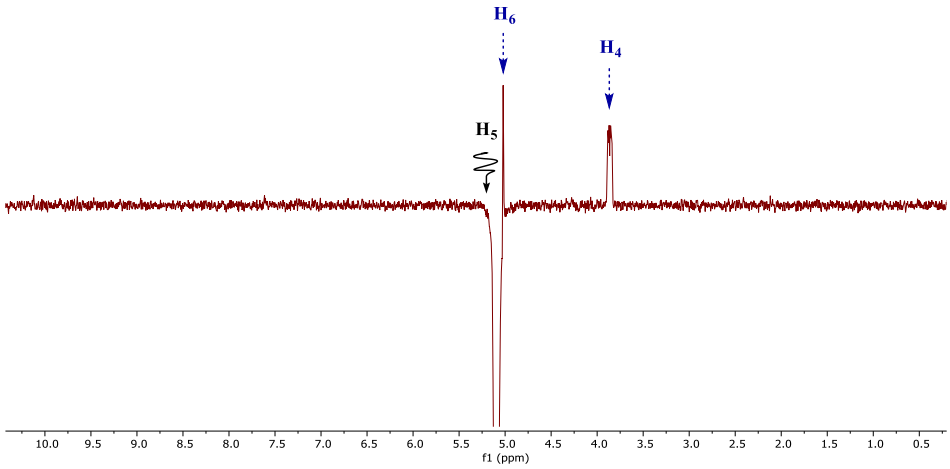

Figure 2.43. NOESY experiment of **26h-d_2** in $CDCl_3$.

NOESY experiment of 26h-*d*$_2$ in $CDCl_3$: Strong Nuclear Overhauser Effects (NOE) are detected when H_5 is selectively irradiated at 5.09 ppm for the vicinal H_6, which is in 1-2 spatial arrangement relative to H_5, and for the vicinal H_4, which is also in 1-2 spatial arrangement relative to H_5. The correlation with the vicinal proton H_4 is absent in the NOE spectra of previously analyzed diastereomer **26h-*d*$_1$** due to a *trans* axial relative spatial arrangement between H_4 and H_5. This suggests a *cis* spatial arrangement between H_4 and H_5 in compound **26h-*d*$_2$**. The relative configuration of compound **26h-*d*$_2$** has been assigned as the one corresponding to the epimer of **26h-*d*$_1$** at the carbon bearing the nitro group. This is in accordance with the relative configuration observed for the minor diastereomer (**26-*d*$_2$**) detected in the biocatalytic synthesis of model compound **26**, confirmed by data reported in the literature,[20] and with an (*R*)-configured intermediate of type **27** leading to both products **26h-*d*$_1$** and **26h-*d*$_2$**.

2.5.8 Computational Studies

The generation of homology models was carried out using the YASARA structure[74] homology model building protocol,[75] which involves multi-template structural model generation. Since the linear amino acid sequence of the target protein was the only given input, the possible templates were identified by running 3 PSI-BLAST[54] iterations to extract a position specific scoring matrix (PSSM) from UniRef90,[76] and then searching the PDB for a match with an E-value below the homology modeling cutoff 0.005. A maximum of 5 templates were allowed. To aid alignment correction and loop modeling, a secondary structure prediction for the target sequence had to be obtained. This was achieved by running PSI-BLAST to create a target sequence profile and feeding it to the PSI-Pred[77] secondary structure prediction algorithm. For each of the found templates, models were built. Either a single model per template was generated, when the alignment was certain, or a number of alternative models were generated, when the alignment was ambiguous. A maximum of 100 conformations per loop were explored. A maximum of 10 residues were added to the termini. Finally, YASARA tried to combine the best parts of the generated models to obtain a hybrid model, with the intension of increasing the accuracy beyond each of the contributors. The quality of the models was evaluated by use of Z-score.[78,79] A Z-score describes how many standard deviations the model

[74] Krieger, E., Koraimann, G., Vriend, G. "Increasing the precision of comparative models with YASARA NOVA-a self-parameterizing force field" *Proteins* **2002**, *47*, 393-402.

[75] Venselaar, H., Joosten, R., Vroling, B., Baakman, C., Hekkelman, M., Krieger, E., Vriend, G. "Homology modelling and spectroscopy, a never-ending love story" *Eur. Biophys. J.* **2010**, *39*, 551-563.

[76] Suzek, B. E., Huang, H., McGarvey, P., Mazumder, R., Wu, C. H. "UniRef: comprehensive and non-redundant UniProt reference clusters" *Bioinformatics* **2007**, *23*, 1282-1288.

[77] Jones, D. T. "Protein secondary structure prediction based on position-specific scoring matrices" *J. Mol. Biol.* **1999**, *292*, 195-202

[78] Laskowski, R. A., MacArthur, M. W., Moss, D. S., Thornton, J. M. "PROCHECK: a program to check the stereochemical quality of protein structures" *J. Appl. Crystallogr.* **1993**, *26*, 283-291

[79] Hooft, R. W., Vriend, G., Sander, C., Abola, E. E. "Errors in protein structures" *Nature* **1996**, *381*, 272.

quality is away from the average high-resolution X-ray structure. The overall Z-scores for all models have been calculated as the weighted averages of the individual Z-scores. The overall score thus captures the correctness of backbone- (Ramachandran plot) and side-chain dihedrals, as well as packing interactions. All in silico modifications were performed using YASARA structure as software with AMBER 03 as force field.[80] After the introduction of a mutation or modification, the energy of the system was minimized following a three-step protocol that enables the adjustment of the model structure without creating any possible unwanted deformation. In step one, only the atoms constituting the mutated amino acid residue were subjected to energy minimization. In step two, the process for energy minimization was repeated by including all the atoms of the amino acid residues that are located within 6 Å distance from the mutated residue. In step three, the energy of the overall structure was minimized.

The molecular dockings were performed using Autodock Vina as tool incorporated into YASARA. The enzyme was used in its reactive binding pose with the cinnamaldehyde bound (Figure 2.45) generating the iminium ion intermediate. The simulation box was placed around the active site of the enzyme 10 Å. 25 VINA docking runs of each ligand to the receptor were run. After clustering the 25 runs, two distinct complex conformations were found for each docking. Results were sorted by binding energy (more positive energies indicate stronger binding). The resulted models were inspected visually.

[80] Oostenbrink, C., Villa, A., Mark, A. E., van Gunsteren, W. F. "A biomolecular force field based on the free enthalpy of hydration and solvation: the GROMOS force-field parameter sets 53A5 and 53A6" *J. Comput. Chem.* **2004**, *25*, 1656-1676.

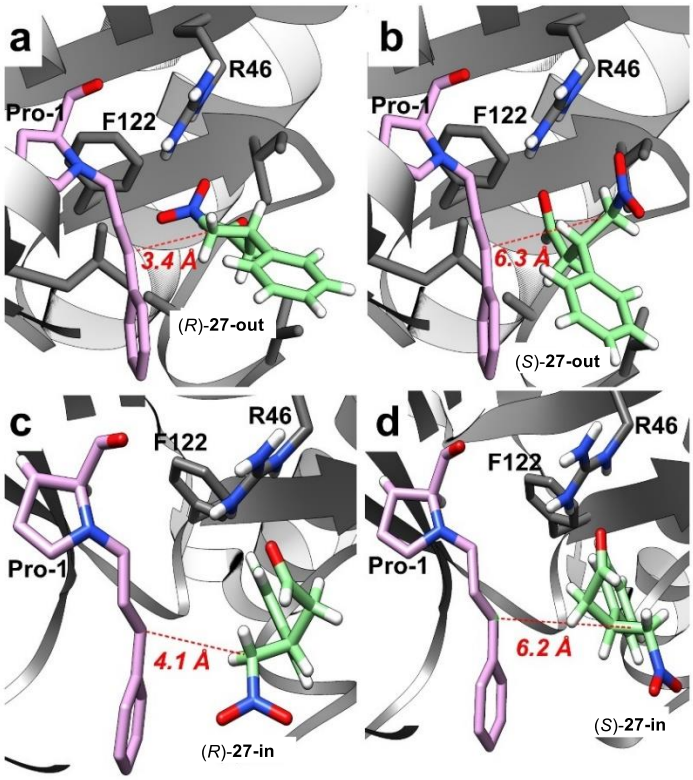

Figure 2.44. Dockings in the active site of Pp-4OT-F_3 of: a) (*R*)-**27** in the (*R*)-**27**-out binding pose (calculated binding energy of 4.00 kcal mol^{-1}); b) (*S*)-**27** in the (*S*)-**27**-out binding pose (calculated binding energy of 4.31 kcal mol^{-1}); c) (*R*)-**27** in the (*R*)-**27**-in binding pose (calculated binding energy of 4.56 kcal mol^{-1}); d) (*S*)-**27** in the (*S*)-**27**-in binding pose (calculated binding energy of 4.50 kcal mol^{-1}). The iminium ion of the Pro-1 with cinnamaldehyde **22** is shown in purple and ligands in green. The dashed red line shows the distance between the two reactive carbons for C-C bond formation. R46 is shown because it stabilizes the ligands in the active site of the enzymes. All dockings were performed with YASARA structure. UCSF Chimera 1.11 was used for visualization.

2.5.9 X-Ray Crystallographic Data

Single Crystal X-Ray Diffraction Data for Product **26h-d_1**

X-ray structure determination: stable colorless crystals of compound **26h-*d_1*** were obtained by slow evaporation of a dichloromethane/hexane mixture at room temperature.

Data Collection: Measurements were made on a Rigaku MicroMax-007HF single crystal X-ray diffractometer equipped with a Pilatus 200K area detector, a Rigaku MicroMax-007HF microfocus rotating anode with $Mo_{K\alpha}$ radiation, Confocal Max Flux optics and an Oxford Cryosystems low temperature device Cryostream 700 plus (T = -173 °C). Full-sphere data collection was used with ω and φ scans.

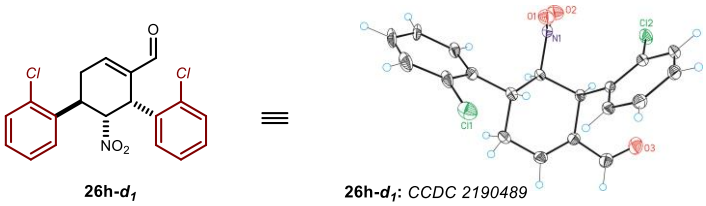

26h-d_1 **26h-d_1**: *CCDC 2190489*

Table 2.2. Crystal data and structure refinement for **26h-d_1**. *CCDC2190489*.

Empirical formula	C19 H15 Cl2 N O3
Formula weight	376.22
Temperature	100(2)K
Wavelength	0.71073 Å
Crystal system	orthorhombic
Space group	P 21 21 21
Unit cell dimensions	α = 8.67030(10)Å α = 90°. β = 11.79300(10)Å β = 90°. γ = 16.8130(2)Å γ = 90°.
Volume	1719.11(3) $Å^3$
Z	4
Density (calculated)	1.454 Mg/m^3
Absorption coefficient	0.396 mm^{-1}
F(000)	776
Crystal size	0.200 x 0.150 x 0.100 mm^3
Theta range for data collection	2.423 to 30.938°.
Index ranges	-12<=h<=12,-16<=k<=17,-24<=l<=23
Reflections collected	29724
Independent reflections	5183[R(int) = 0.0199]
Completeness to theta =30.938°	96.6%
Absorption correction	Multi-scan
Max. and min. transmission	1.00 and 0.84
Refinement method	Full-matrix least-squares on F^2

Data / restraints / parameters	5183/ 215/ 277
Goodness-of-fit on F^2	1.003
Final R indices [I>2sigma(I)]	R1 = 0.0226, wR2 = 0.0644
R indices (all data)	R1 = 0.0233, wR2 = 0.0648
Flack parameter	x =0.018(8)
Largest diff. peak and hole	0.267 and -0.161 e.$Å^{-3}$

Chapter III

Stereospecific Radical Coupling Enabled by a Non-Natural Photodecarboxylase

Target

Developing an artificial photoenzyme that uses light to activate enantiopure chiral carboxylic acids and then couples the resulting chiral radicals with high stereoselectivity, yielding products with two stereocenters

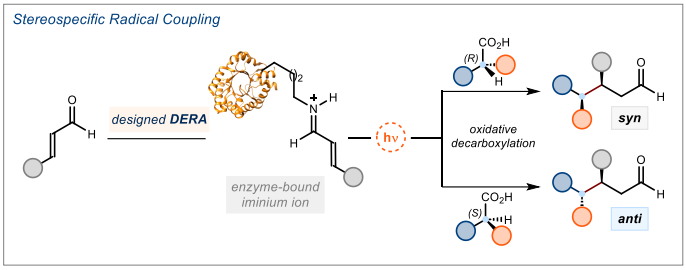

Tools

Exploiting the photoexcitation of iminium ion intermediates, transiently formed within 2-deoxy-*D*-ribose-5-phospate aldolase (DERA), to trigger radical formation and master their stereoselective trap.[1]

3.1 Photochemistry & Biocatalysis

Enzymes have the ability of perform reactions with high stereoselectivity and excellent catalytic efficiency.[2,3] Recent advances in protein engineering have significantly enhanced the synthetic potential of biocatalysis, positioning it as an established alternative to small molecule catalysis, with applications in pharmaceutical and agrochemicals. An ongoing objective to enhance the potential of biocatalysis is to discover new mechanisms of substrate

[1] The project discussed in this chapter was conducted in collaboration with Dr. Vasilis Tseliou, Dr. Martin Berger and Florian Schiel. I was involved in the reaction development, optimization studies, synthetic work, mechanistic experiments and the investigation of the scope. Dr. Vasilis Tseliou was leading the biochemical work related to the project. I was also involved in the biochemical work, performing site-directed mutagenesis, protein expression and purification.

[2] Harrison, W., Huang, X. & Zhao, H. "Photobiocatalysis for Abiological Transformations." *Acc. Chem. Res.* **2022**, *55*, 1087–1096.

[3] M. A. Emmanuel, S. G. Bender, C. Bilodeau, J. M. Carceller, J. S. DeHovitz, H. Fu, Y. Liu, B. T. Nicholls, Y. Ouyang, C. G. Page, T. Qiao, F. C. Raps, D. R. Sorigué, S. Z. Sun, J. Turek-Herman, Y. Ye, A. Rivas-Souchet, J. Cao, T. K. Hyster, "Photobiocatalytic Strategies for Organic Synthesis." *Chem. Rev.* **2023**, *123*, 5459–5520.

activation for performing non-natural transformations.[4] Researchers are primarily directing their efforts towards exploring polar pathways to accomplish this goal.

Meanwhile, over the past decade, the field of small molecule catalysis has undergone substantial exploration into photochemistry and photoredox catalysis.[5,6] Light-mediated electron or energy transfer reactions provide a straightforward access to radicals under mild conditions, enabling reactions inaccessible through traditional two-electron pathways. This approach has facilitated significant advancements in C-H bond functionalizations, C-C cross coupling, and C-N bond formations.[5,7,8] For example, the combination of photochemistry with other established catalytic tools, such as transition metal catalysis or organocatalysis, enabled novel reaction pathways that would remain inaccessible without light.[9,10] It was not long before researchers recognized the potential of combining light-mediated reactivity with enzymes, thus merging the advantages of both fields: the excellent selectivity and efficiency of enzymes with the distinct reactivity offered by photocatalysis. The active site of the protein provides a confined environment where a radical intermediate can be controlled to facilitate the desired stereogenic bond formation. Meanwhile, photocatalysis can overcome the inherent limitation of proteins by providing a mild method to generate radicals, thus enabling diverse reactivity modes to expand the repertoire available to enzymes and address important synthetic challenges. Below, I outline the four primary strategies used in the development of photochemical biocatalysis, along with their mechanistic aspects.[2,3]

3.1.1 New-to-Nature Reactivities of Natural Photoenzymes

The notion of light-triggered enzymes is not novel in nature. So far, three different natural photoenzymes have been discovered.[11] The first one is DNA photolyase, a flavin-dependent enzyme that is involved in DNA repair (Figure 3.1a).[12] The enzyme repairs the cyclobutane dimers formed after UV irradiation of vicinal cytosine or thymine bases. The second natural

---

[4] Renata, H., Wang, Z. J., Arnold, F. H. "Expanding the enzyme universe: Accessing non-natural reactions by mechanism-guided directed evolution." *Angew. Chem., Int. Ed.* **2015**, *54*, 3351–3367.

[5] Romero, N. A., Nicewicz, D. A. "Organic Photoredox Catalysis" *Chem. Rev.* **2016**, *116*, 10075–10166.

[6] Chan, A. Y., Perry, I. B., Bissonnette, N. B., Buksh, B. F., Edwards, G. A., Frye, L. I., Garry, O. L., Lavagnino, M. N., Li, B. X., Liang, Y., Mao, E., Millet, A., Oakley, J. V., Reed, N. L., Sakai, H. A., Seath, C. P., MacMillan, D. W. C. "Metallaphotoredox: The Merger of Photoredox and Transition Metal Catalysis." *Chem. Rev.* **2022**, *122*, 1485–1542.

[7] Shaw, M. H., Twilton, J.,MacMillan, D. W. C. "Photoredox Catalysis in Organic Chemistry." *J. Org. Chem.* **2016**, *81*, 6898–6926.

[8] Strieth-Kalthoff, F., Glorius, F. "Triplet Energy Transfer Photocatalysis: Unlocking the Next Level." *Chem* **2020**, *6*, 1888–1903.

[9] Holmberg-Douglas, N., Nicewicz, D. A. "Photoredox-Catalyzed C–H Functionalization Reactions." *Chem. Rev.* **2022**, *122*, 1925–2016.

[10] Capaldo, L., Ravelli, D., Fagnoni, M. "Direct Photocatalyzed Hydrogen Atom Transfer (HAT) for Aliphatic C-H Bonds Elaboration." *Chem. Rev.* **2022**, *122*, 1875–1924.

[11] Schmermund, L., Jurkaš, V., Özgen, F. F., Barone, G. D., Büchsenschütz, H. C., Winkler, C. K., Schmidt, S., Kourist, R., Kroutil, W. "Photo-Biocatalysis: Biotransformations in the Presence of Light." *ACS Catal.* **2019**, *9*, 4115–4144.

photoenzyme is known as protochlorophyllide reductase (LPOR), which operates as a nicotinamide adenine dinucleotide phosphate (NAD(P)H)-dependent enzyme (Figure 3.1b).[13] LPOR is responsible for the reduction of protochlorophyllide to chlorophyllide in chlorophyll biosynthesis. The photoexcited nicotinamide cofactor reduces protochlorophyllide via *trans*-addition of hydrogen atoms across the C17-C18 double bond. So far, neither of these two enzymes has been utilized in a synthetic setting, likely due to their high specificity and the associated limited substrate scope.

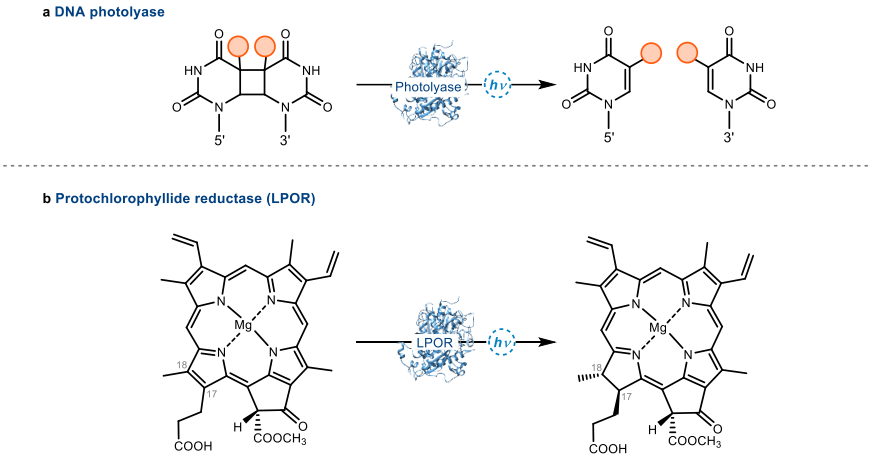

Figure 3.1. Natural photoenzymes and their reactivities: a) DNA photolyase; b) protochlorophyllide reductase.

In 2017, Beisson and coworkers discovered the third photoenzyme, a fatty acid photodecarboxylase (FAP), which catalyzes the hydrodecarboxylation of long-chain fatty acids to yield the corresponding alkanes with one less carbon.[14] They investigated the formation of hydrocarbons in the microalgae *Chlorella variabilis* and identified a protein that can catalyze the decarboxylation of fatty acids in the presence of light. Subsequent studies proposed that the decarboxylation proceeded according to the following mechanism (Figure 3.2). The deprotonated fatty acid **1** binds within the FAP's active site through ionic interactions with the protonated arginine residue 451 (R451), and it is positioned in close proximity to the flavin cofactor (FAD). Upon excitation of the cofactor (λ_{max} = 467 nm) with visible light, a single-electron transfer (SET) from the carboxylate **1** to the excited FAD* occurred. This process leads to decarboxylation, forming an alkyl radical **I** and the reduced

[12] Sancar, A. "Structure and function of DNA photolyase and cryptochrome blue-light photoreceptors" *Chem. Rev.* **2003**, 103, 2203-2237.

[13] Gabruk, M., Mysliwa-Kurdziel, B. Light-Dependent Protochlorophyllide Oxidoreductase: Phylogeny, Regulation, and Catalytic Properties. Biochemistry **2015**, *54*, 5255–5262.

[14] Sorigué, D., Légeret, B., Cuiné, S., Blangy, S., Moulin, S., Billon, E., Richaud, P., Brugière, S., Couté Y., Nurizzo, D., Müller, P., Brettel, K., Pignol, D., Arnoux, P., Li-beisson, Y., Peltier, G., Beisson, F. "An algal photoenzyme converts fatty acids to hydrocarbons" *Science* **2017**, *907*, 903–907.

flavin cofactor ($FAD^{\bullet-}$). For the subsequent radical termination step, the reduction of the alkyl radical by $FAD^{\bullet-}$ and subsequent protonation from the protonated arginine (R451) was proposed.[15] This formed the desired hydrocarbon product **2** and a FAD intermediate (FAD_{RS}). It was proposed that FAD_{RS} arose from the interaction of bicarbonate with FAD. Protonation of arginine, removal of the bicarbonate ion from the active site and exchange of the hydrocarbon **2** by another molecule of fatty acid closed the catalytic cycle. It should be mentioned that another pathway of radical termination by hydrogen atom transfer (HAT) from a cysteine (Cys432) has been proposed.[16]

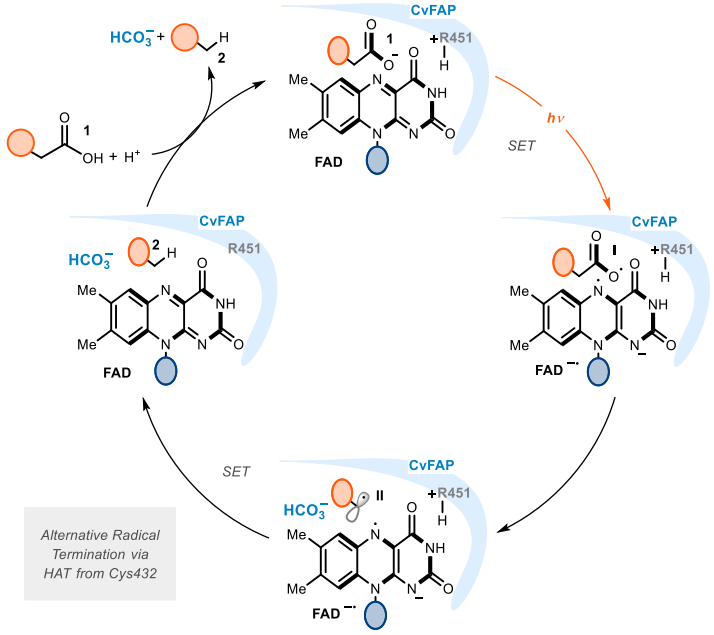

Figure 3.2. Proposed mechanism for the fatty acid photodecarboxylase (*Cv*FAP).

To date, several transformations have been developed using the newly discovered *Cv*FAP. For instance, the group led by Hollman broadened the substrate scope to include medium- to short-chain fatty acids. This expansion was facilitated by a more efficient decarboxylation,

[15] Sorigué, D., Hadjidemetriou, K., Blangy, S., Gotthard, G., Bonvalet, A., Coquelle, N., Samire, P., Aleksandrov, A., Antonucci, L., Benachir, A., Boutet, S., Byrdin, M., Cammarata, M., Carbajo, S., Cuiné, S., Doak, R. B., Foucar, L., Gorel, A., Grünbein, M., Hartmann, E., Hienerwadel, R., Hilpert, M., Kloos, M., Lane, T. J., Légeret, B., Legrand, P., Li-Beisson, Y., Moulin, S. L. Y., Nurizzo, D., Peltier, G., Schirò, G., Shoeman, R. L., Sliwa, M., Solinas, X., Zhuang, B., Barends, T. R. M., Colletier, J. P., Joffre, M., Royant, A., Berthomieu, C., Weik, M., Domratcheva, T., Brettel, K., Vos, M. H., Schlichting, I., Arnoux, P., Müller, P., Beisson, F. "Mechanism and dynamics of fatty acid photodecarboxylase" *Science* **2021**, *372*, eabd5687.

[16] Heyes, D. J., Lakavath, B., Hardman, S. J. O., Sakuma, M., Hedison, T. M., Scrutton, N. S. "Photochemical Mechanism of Light-Driven Fatty Acid Photodecarboxylase" *ACS Catal.* **2020**, *10*, 6691–6696.

achieved by incorporating simple alkanes as 'decoy molecules'.[17] In 2019, Wu and colleagues engineered *Cv*FAP for the photocatalytic kinetic resolution of α-substituted carboxylic acids **3** with an enantioselectivities of up to 99 % ee (Figure 3.3).[18] The engineered variant converted α-hydroxy acids with C6 to C12 alkyl chains and several amino acids. Furthermore, strategies for the kinetic resolution of an herbicide, the decarboxylative deuteration of carboxylic acids or the selective decarboxylation of *trans*-fatty acids were developed using the engineered CvFAP.[19–21]

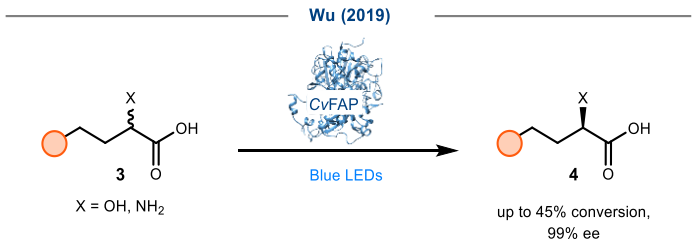

Figure 3.3. Kinetic resolution of α-substituted carboxylic acid using engineered *Cv*FAP.

3.1.2 Photochemical Strategies Based on the Excitation of Cofactor-Dependent Enzymes

The most prominent strategy to date for carrying out a new-to-nature transformation in the field of photobiocatalysis is the irradiation of cofactor-dependent enzymes. There are numerous nicotinamide (NAD(P)H)- or flavin (FAD or FMN)-dependent enzymes in nature that facilitate redox processes within organisms' metabolism. One class of these enzymes are the nicotinamide-dependent ketoreductases (KREDs), whose natural function is to perform the enantioselective reduction of ketones to alcohols. The NAD(P)H cofactor serves as the hydride source (1,4-dihydropyridine moiety) in the reduction. In 1975, Ohnishi demonstrated that irradiating the cofactor with light increased its SET reducing abilities, thereby enabling the reduction of activated olefins.[22] This suggests that, upon light irradiation, NAD(P)H

[17] Zhang, W., Ma, M., Huijbers, M. M. E., Filonenko, G. A., Pidko, E. A., Van Schie, M., De Boer, S., Burek, B. O., J. Z. Bloh, J. Z., Van Berkel, W. J. H., Smith, W. A., Hollmann, F. "Hydrocarbon Synthesis via Photoenzymatic Decarboxylation of Carboxylic Acids" *J. Am. Chem. Soc.* **2019**, *141*, 3116–3120.

[18] Xu, J., Hu, Y., Fan, J., Arkin, M., Li, D., Peng, Y., Xu, W., Lin, X., Wu, Q. "Light-Driven Kinetic Resolution of α-Functionalized Carboxylic Acids Enabled by an Engineered Fatty Acid Photodecarboxylase" *Angew. Chem., Int. Ed.* **2019**, *58*, 8474–8478.

[19] Cheng, F., Li, H., Wu, D. Y., Li, J. M., Fan, Y., Xue, Y. P., Zheng, Y. G. "Light-driven deracemization of phosphinothricin by engineered fatty acid photodecarboxylase on a gram scale" *Green Chem.* **2020**, *22*, 6815–6818.

[20] Xu, J., Fan, J., Lou, Y., Xu, W., Wang, Z., Li, D., Zhou, H., Lin, X., Wu, Q. "Light-driven decarboxylative deuteration enabled by a divergently engineered photodecarboxylase" *Nat. Commun.* **2021**, *12*, 1–10.

[21] Li, D., Han, T., Xue, J., Xu, W., Xu, J., Wu, Q. "Engineering Fatty Acid Photodecarboxylase to Enable Highly Selective Decarboxylation of trans Fatty Acids" *Angew. Chem., Int. Ed.* **2021**, *60*, 20695–20699.

[22] Ohnishi, Y., Kagami, M., Ohno, A. "Reduction by a Model of NAD(P)H. Photo-Activation of NADH and its Model Compounds toward the Reduction of Olefins" *Chem. Lett.* **1975**, *4*, 125–128.

becomes a strong SET reductant. This is in accordance to the calculated redox potential of photoexcited 1-benzyl-1,4-dihydronicotinamide (BNAH, $E_{1/2}^{Red}$[BNAH$^{\bullet+}$/BNAH*] = -2.6 V vs SCE), a simplified model of NADH. In addition, BNAH$^{\bullet+}$ exhibits a low bond-dissociation free energy (32 kcal mol^{-1} in MeCN), facilitating hydrogen atom transfer (HAT) to radicals.[23] In 2016, Hyster and coworkers first employed this notion to develop a novel asymmetric radical process in photobiocatalysis (Figure 3.4).[24] They successfully leveraged the photoinduced SET activity within KRED to develop the light-mediated stereoselective protodehalogenation of α-bromolactones **5** using short-chain dehydrogenase (*Lk*ADH), a ketoreductase found in *Lactobacillus kefiri*. After an engineering campaign, they obtained a *Lk*ADH variant containing three mutations (*Lk*ADH$^{E145F/F147L/Y190C}$) to deliver the dehalogenation product **6** in excellent yield and enantiomeric excess, predominantly as the (*R*)-enantiomer. After screening a new library of wild type KRED variants, they found that *Ras*ADH from *Rastalonia sp.* was highly effective giving access to the opposite (*S*)-enantiomer of **6**.

Mechanistically, it was proposed that the halolactone **5** and the bound nicotinamide cofactor are forming an electron donor acceptor (EDA) complex within the enzyme's active site. An EDA complex[25] is a light-responsive ground-state complex, which results from the association of a colorless electron-rich donor substrate with a colorless electron-acceptor species. This complex was demonstrated to generate open-shell intermediates upon visible light irradiation *via* an intramolecular SET followed by mesolytic cleavage of the C-Br bond. The resulting NAD(P)H radical cation then controlled a selective HAT process to one face of the prochiral radical intermediate **III** (blue insight in the figure) to give the corresponding product **6**. The cofactor was regenerated by either isopropylalcohol or glucose dehydrogenase. The EDA complex was only formed in the presence of the protein, which provided a confined environment suitable for controlling the stereoselective H transfer to the radicals. The enzyme could accept both enantiomers of substrate **5** leading to enantioenriched products **6**.

[23] Zhu, X. Q., Li, H. R., Li, Q., Ai, T., Lu, J. Y., Yang, Y., Cheng J. P. "Determination of the C4-H bond dissociation energies of NADH models and their radical cations in acetonitrile" *Chem. Eur. J.* **2003**, *9*, 871–880.

[24] Emmanuel, M. A., Greenberg, N. R., Oblinsky, D. G. & Hyster, T. K. "Accessing non-natural reactivity by irradiating nicotinamide-dependent enzymes with light" *Nature* **2016**, *540*, 414–417.

[25] Crisenza, G. E. M., Mazzarella, D.,Melchiorre, P. "Synthetic Methods Driven by the Photoactivity of Electron Donor-Acceptor Complexes" *J. Am. Chem. Soc.* **2020**, *142*, 5461–5476.

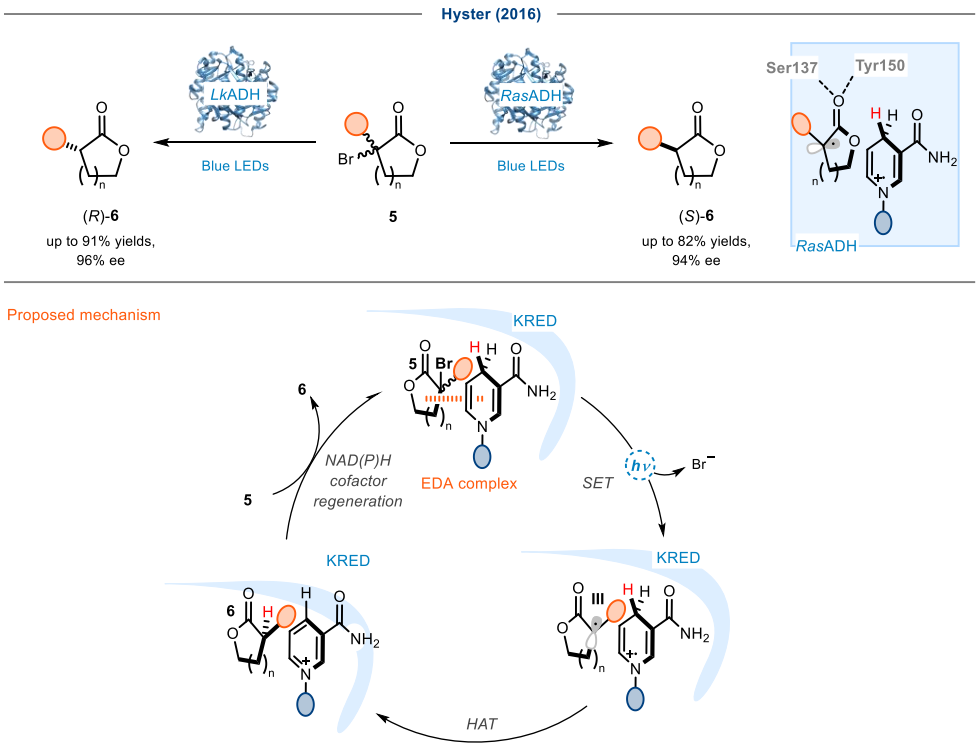

Figure 3.4. Light-mediated dehalogenation using nicotinamide-dependent enzymes and proposed mechanism.

A few years later, the strategy was extended to flavoenzymes. Flavin-dependent "ene"-reductases (EREDs) are biocatalysts often used for the asymmetric hydrogenation of olefins. One of the most prominent EREDs are the old yellow enzymes (OYEs). In 1978, spectroscopic studies from Massey *et. al.* found that when the flavin cofactor is reduced, the enzyme OYE1 can stabilize the flavin semiquinone radical anion (FMN_{sq}).[26] While overlooked for synthetic utilizations at that time, the ability to stabilize an open-shell intermediate paved the way for the use of EREDs as a versatile photoenzyme. In a later study, Massey discovered that after irradiation OYE1 can reduce an organic substrate to the corresponding radical anion via SET from the excited flavin hydroquinone (FMN_{hq}/FMN_{sq} = -230 mV vs SCE, Figure 3.5).[27,28] The generated radical could than abstract a hydrogen atom

[26] Massey, V., Hemmerich, P., Knappe, W. R., Duchstein, H. J., Fenner, H. "Photoreduction of flavoproteins and other biological compounds catalyzed by deazaflavins. Appendix: photochemical formation of deazaflavin dimers" *Biochemistry* **1978**, *17*, 9–17.

[27] Yamano, T., Kuroda, K., Fujii, S., Miura, R. "Characterization of the Electron Acceptors of Old Yellow Enzyme: Mechanistic Approach to the Mode of One Electron Transfer from the Enzyme to Menadione or Dyestuffs1" *J. Biochem.* **1993**, *114*, 879–884.

[28] Stewart, R. C., Massey, V. "Potentiometric studies of native and flavin-substituted old yellow enzyme" *J. Biol. Chem.* **1985**, *260*, 13639–13647.

from the FMN_{sq} (calc. N–H BDE = 59.9 kcal/mol) to form the reduced product and FMN_{ox}.[29]

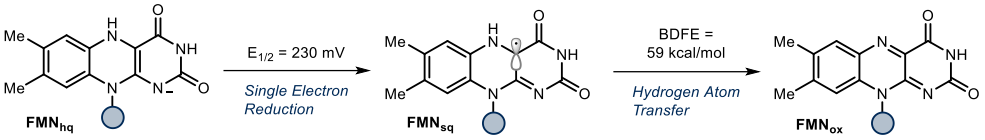

Figure 3.5. Oxidation states of the flavin cofactor.

With the knowledge that EREDs could perform radical reactions, Hyster and coworkers extended the photochemical strategy to flavoenzymes (Figure 3.6),[30] developing a light-mediated radical cyclization of α-chloroamides **7** to lactames **8**. It was proposed that, within the ene-reductase, an EDA complex between **7** and the flavin (FMN_{hq}) was formed. The excitation of this complex enabled an SET from FMN_{hq} to chloroamide **7**. This led to the mesolytic cleavage, cyclization of the α-acyl radical, and subsequent radical termination by HAT to obtain the lactam product **8**. HAT selectively occurred from FMN_{sq} explaining the high enantiomeric excess observed in the reaction. In the following years, the scope of different acceptors participating in EDA complex formation and engaging in intramolecular cyclization was extended to include oximes,[31] alkyliodides,[32] and allyl silanes.[33]

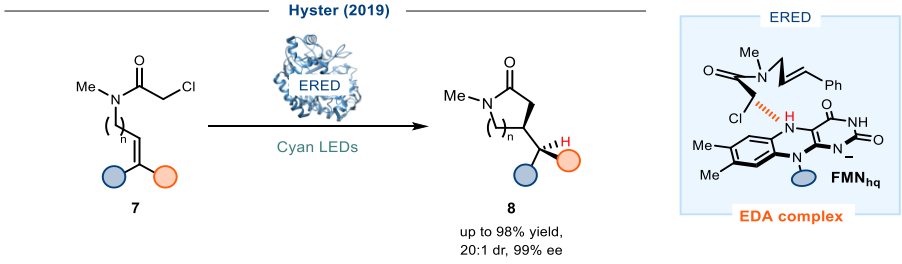

Figure 3.6. Photoenzymatic cyclization of α-chloroamides via the formation of an EDA complex.

This photobiocatalytic approach has thus far been limited to *intramolecular* processes for C-C bond formation, thereby restricting its synthetic utility. In 2020, Zhao and coworkers

[29] Warren, J. J., Tronic, T. A., Mayer, J. M. "Thermochemistry of proton-coupled electron transfer reagents and its implications" *Chem. Rev.* **2010**, *110*, 6961–7001.

[30] Biegasiewicz, K. F., Cooper, S. J., Gao, X., Oblinsky, D. G., Kim, J. H., Garfinkle, S. E., Joyce, L. A., Sandoval, B. A., Scholes, G. D., Hyster, T. K. "Photoexcitation of flavoenzymes enables a stereoselective radical cyclization" *Science* **2019**, *364*, 1166–1169.

[31] Gao, X., Turek-Herman, J. R., Choi, Y. J., Cohen, R. D., Hyster, T. K. "Photoenzymatic Synthesis of α-Tertiary Amines by Engineered Flavin-Dependent 'ene'-Reductases" *J. Am. Chem. Soc.* **2021**, *143*, 19643–19647.

[32] Clayman, P. D., Hyster, T. K. "Photoenzymatic Generation of Unstabilized Alkyl Radicals: An Asymmetric Reductive Cyclization" *J. Am. Chem. Soc.* **2020**, *142*, 15673–15677.

[33] Laguerre, N., Riehl, P. S., Oblinsky, D. G., Emmanuel, M. A., Black, M. J., Scholes, G. D., Hyster, T. K. "Radical Termination via β-Scission Enables Photoenzymatic Allylic Alkylation Using "ene"-Reductases" *ACS Catal.* **2022**, *12*, 9801–9805.

developed the first example of radical *intermolecular* enzymatic process triggered by light (Figure 3.7a). They used OYE1 to perform a light-mediated enantioselective C(sp^3)-C(sp^3) bond formation between an α-halocarbonyl compound **9** and a terminal olefin **10**. The challenge here was that both substrates must be present in the binding pocket of the enzyme before radical formation occurs.[34] Subsequently, Hyster developed an intermolecular hydroalkylation approach to couple activated α-haloacetamides with alkenes.[35] Later, Jia and Xu performed an intermolecular hydroalkylation using diazoesters as electrophiles.[36] Interestingly, in the last two cases, the formation of a photoactive quaternary EDA complex between electrophile, alkene and the flavin cofactor was proposed.

All previously mentioned studies relied on the formation of a photoactive EDA complex within the enzyme's active site, which triggered radical formation. This radical-generation strategy, however, restricted the generality of the methodology since tailored substrates are essential for the formation of charge-transfer complexes. In 2021, Hyster achieved the asymmetric reduction of α,β-unsaturated amides **12** by the direct excitation of flavin hydroquinone (FMN_{hq}) with ultraviolet light (370-410 nm, Figure 3.7b). The excited FMN_{hq} initiated the reaction by SET reduction of substrate **12**, followed by subsequent protonation and HAT from the cofactor, resulting in the formation of product **13**.[37]

[34] Huang, X., Wang, B., Wang, Y., Jiang, G., Feng, J., Zhao, H. "Photoenzymatic enantioselective intermolecular radical hydroalkylation" *Nature* **2020**, *584*, 69–74.

[35] Page, C. G., Cooper, S. J., Dehovitz, J. S., Oblinsky, D. G., Biegasiewicz, K. F., Antropow, A. H., Armbrust, K. W., Ellis, J. M., Hamann, L. G., Horn, E. J., Oberg, K. M., Scholes, G. D., Hyster, T. K. "Quaternary Charge-Transfer Complex Enables Photoenzymatic Intermolecular Hydroalkylation of Olefins" *J. Am. Chem. Soc.* **2021**, *143*, 97–102.

[36] Duan, X., Cui, D., Wang, Z., Zheng, D., Jiang, L., Huang, W. Y., Jia, Y. X., Xu, J. "A Photoenzymatic Strategy for Radical-Mediated Stereoselective Hydroalkylation with Diazo Compounds" *Angew. Chem., Int. Ed.* **2023**, *62*, e202214135.

[37] Sandoval, B. A., Clayman, P. D., Oblinsky, D. G., Oh, S., Nakano, Y., Bird, M., Scholes, G. D., Hyster, T. K. "Photoenzymatic Reductions Enabled by Direct Excitation of Flavin-Dependent "Ene"-Reductases" *J. Am. Chem. Soc.* **2021**, *143*, 1735–1739.

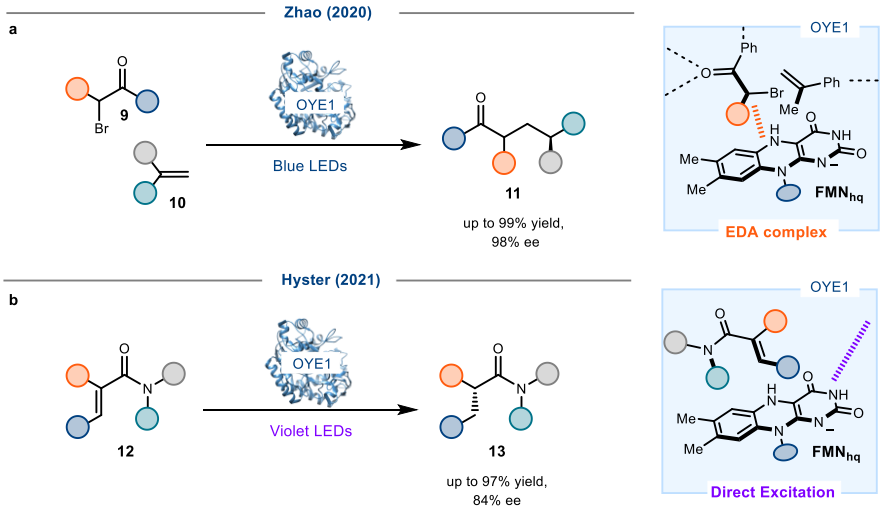

Figure 3.7. a) Intermolecular coupling of α-halocarbonyls and alkenes using OYE1. b) Reduction of α,β-unsaturated amides *via* direct excitation.

In the previously examples, the SET event usually occurred from the cofactor to the substrate either by excitation of an EDA complex or the direct excitation of the cofactor. Until recently, no synthetically useful examples where the cofactor oxidizes a substrate had been reported. In the 1970s, Massey discovered that lactate monooxygenase (LMO) can mediate the photodecarboxylation of various carboxylates under light irradiation and alkylate the flavin cofactor with the formed radical (alkylated flavin adduct).[26] Inspired by this report, Hyster in collaboration with Scholes and Daidone developed a catalytic oxidative photodecarboxylation using engineered lactate monooxygenase (Figure 3.8).[38] After conducting several mechanistic experiments, they proposed the following mechanism. The excitation of the flavin cofactor led to the decarboxylation of the carboxylate. The resulting radical **V** combined with cofactor FMN_{sq} and formed a covalent hemiaminal adduct. In a subsequent step, the enzyme deprotonated the hydroxy group to form aldehyde **15** and cofactor FMN_{hq}. The cofactor was regenerated in the presence of oxygen. $LMO^{H290Q/Y152F}$ performed the photodecarboxylation of mandelic acid **14** to benzaldehyde **15** in 70% yield.

[38] Li, X., Page, C. G., Zanetti-Polzi, L., Kalra, A. P., Oblinsky, D. G., Daidone, I., Hyster, T. K., Scholes, G. D. "Mechanism and Dynamics of Photodecarboxylation Catalyzed by Lactate Monooxygenase" *J. Am. Chem. Soc.* **2023**, *145*, 13232–13240.

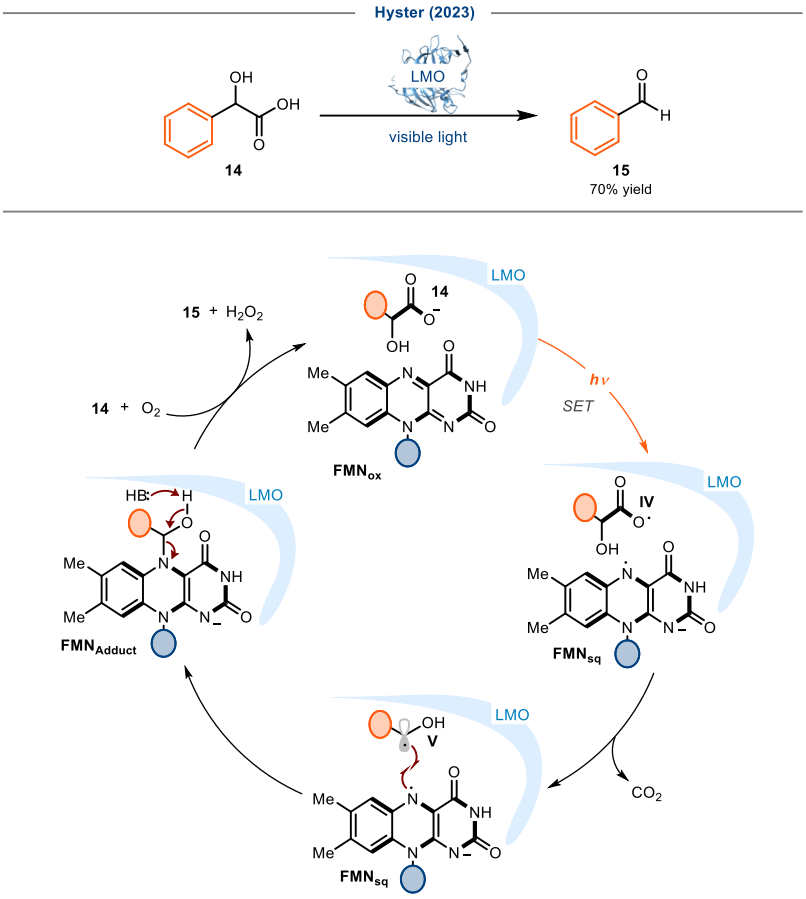

Figure 3.8. Photodecarboxylation using promiscuous lactate monooxygenase and the proposed mechanism.

3.1.3 Artificial Photoenzymes

In addition to the use of enzymes with natural or modified primary structures, artificial enzymes bearing unnatural side chains were also found useful for discovering new photobiocatalytic reactivities. For example, the bioconjugation of metal complexes or photocatalysts to enzymes can give access to new transformations inaccessible by natural cofactor-dependent enzymes. Photoactive motifs can be introduced in the scaffold of an enzyme by covalently linking them to unnatural, non-proteinogenic amino acids. This moiety can alter the photophysical and photocatalytic properties of the enzyme and, by careful engineering it, desired reactivities and selectivities can be achieved. Furthermore, artificial photoenzymes can be engineered by conjugating a photosensitizer close to an immobilized

organometallic complex within a protein scaffold. After light irradiation, the photocatalyst can provide electrons or energy to facilitate organometallic catalysis.[2,39]

In 2015, the group of Lewis developed an artificial photoenzyme for photo-oxidation.[40] This enzyme was constructed by conjugating an acridinium photocatalyst *via* azide-alkyne cycloaddition click chemistry to the propagylic side chain of an unnatural amino acid within a prolyl oligopeptidase. The artificial protein-photocatalyst hybrid was capable to perform the sulfoxidation of thioanisoles **16** to give a racemic mixture of product **17** (Figure 3.9a). However, lower yields were achieved than with the photocatalyst alone.

In 2018, Wang and coworkers constructed an artificial photoenzyme.[39] They used a superfolder yellow fluorescent protein and installed a benzophenone photosensitizer *via* genetic code expansion at position 66. Genetic code expansion is an important technique for protein engineering, which allows the site-specific incorporation of unnatural amino acids with desired properties into proteins.[41] In appropriate distance, they conjugated a nickel bipyridine complex to a cysteine (Cys95) through selective biorthogonal chemistry. With the constructed enzyme PSP-95C-bpy, the researchers could perform the photobiocatalytic reduction of CO_2 to CO. Based on this work, they later developed an artificial dehalogenase for the nickel-catalyzed conversion of aryl halides **18** to phenols **19** (Figure 3.9b).[42] It was found that, when constructing the artificial photoenzyme, the distance between benzophenone and the metal complex was crucial. Deviations from the optimal distance (1.19 nm) were detrimental for the performance of the enzyme. The best variant successfully transformed several aryl halides, like aryl chlorides, bromides and iodides. In contrast to similar work of MacMillan for an organometallic C-O cross-coupling, where photoinduced SET modulated the oxidation states of nickel complex at appropriate steps,[43] an energy transfer reaction mechanism was proposed for the biocatalytic system. According to the authors, benzophenone reaches the triplet state upon excitation within the enzyme. This leads to an energy transfer from the photosensitizer to the Ni^{II} aryl oxide complex, which then drives the reductive elimination step to form the product **19**. However, it should be mentioned that the authors could not rule out the photoinduced Ni^{I}/Ni^{III} cycle.

---

[39] Liu, X., Kang, F., Hu, C., Wang, Z., Xu, L., Zheng, D., Gong, W., Lu, Y., Ma, Y., Wang, J. "A genetically encoded photosensitizer protein facilitates the rational design of a miniature photocatalytic CO2-reducing enzyme" *Nat. Chem.* **2018**, *10*, 1201–1206.

[40] Gu, Y., Ellis-Guardiola, K., Srivastava, P., Lewis, J. C. "Preparation, Characterization, and Oxygenase Activity of a Photocatalytic Artificial Enzyme" *ChemBioChem* **2015**, *16*, 1880–1883.

[41] Shandell, M. A., Tan, Z., Cornish, V. W. "Genetic Code Expansion: A Brief History and Perspective" *Biochemistry* **2021**, *60*, 3455–3469.

[42] Fu, Y., Huang, J., Wu, Y., Liu, X., Zhong, F., Wang, J. "Biocatalytic Cross-Coupling of Aryl Halides with a Genetically Engineered Photosensitizer Artificial Dehalogenase" *J. Am. Chem. Soc.* **2021**, *143*, 617−622.

[43] Terrett, J. A., Cuthbertson, J. D., Shurtleff, V. W., Macmillan, D. W. C. "Switching on elusive organometallic mechanisms with photoredox catalysis" *Nature* **2015**, *524*, 330 –334.

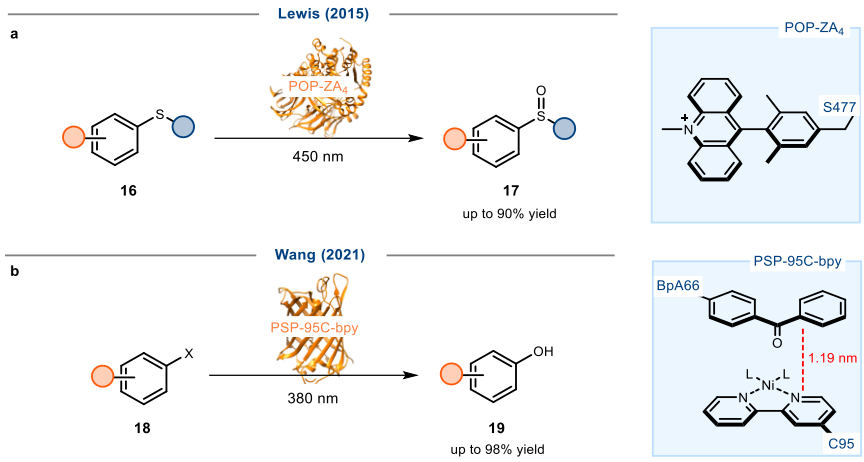

Figure 3.9. a) Design of an artificial photoenzyme by conjugation of an acridinium photocatalyst for the oxidation of **16**. b) Construction of an artificial metalloenzyme using genetically encoded benzophenone for the synthesis of phenols **19**. X=Cl, Br,I.

Another notable example of an artificial photoenzyme is the recent work of Anthony Green (Figure 3.10). His group designed an enzyme capable to perform a photocatalytic, asymmetric [2+2] cycloaddition.[44] As a starting point, they used a computationally designed Diels-Alderase for their engineering campaign. This enzyme was previously constructed to perform thermal [4+2] cycloadditions.[45] Within this scaffold, a noncanonical 4-benzoyl-phenylalanine (BpA) residue was introduced by genetic code expansion. By irradiation of this enzyme with either 365 nm or 395 nm, an asymmetric [2+2] cycloaddition was promoted *via* triplet energy transfer between the installed photosensitizer and the unsaturated amide moiety embedded within substrate **20**. The desired product **21** was obtained in modest enantioselectivity, regioselectivity and yield. After three rounds of directed evolution, the final enzyme was obtained, which performed the reaction with full conversion and enantiocontrol and a regioisomeric ratio up to 15:1. Interestingly, compared to the organocatalytic reaction in a small-molecule setting, the transformation with the enzyme was not sensitive to oxygen. Green and coworkers suggested that the enzyme scaffold might have shielded the photosensitizer from oxygen, therefore limiting the formation of singlet oxygen. Simultaneously and independently, the group of Sun developed a similar approach in which

[44] Trimble, J. S., Crawshaw, R., Hardy, F. J., Levy, C. W., Brown, M. J. B., Fuerst, D. E., Heyes, D. J., Obexer, R., Green, A. P. "A designed photoenzyme for enantioselective [2+2] cycloadditions" *Nature* **2022**, *611*, 709-714.

[45] Siegel, J. B., Zanghellini, A., Lovick, H. M., Kiss, G., Lambert, A. R., St.Clair, J. L., Gallaher, J. L., Hilvert, D., Gelb, M. H., Stoddard, B. L., Houk, K. N., Michael, F. E., Baker, D. "Computational design of an enzyme catalyst for a stereoselective bimolecular diels-alder reaction." *Science* **2010**, *329*, 309–313.

they developed an artificial enzyme with a genetically encoded photosensitizer in the active site to perform [2+2] cycloadditions.[46]

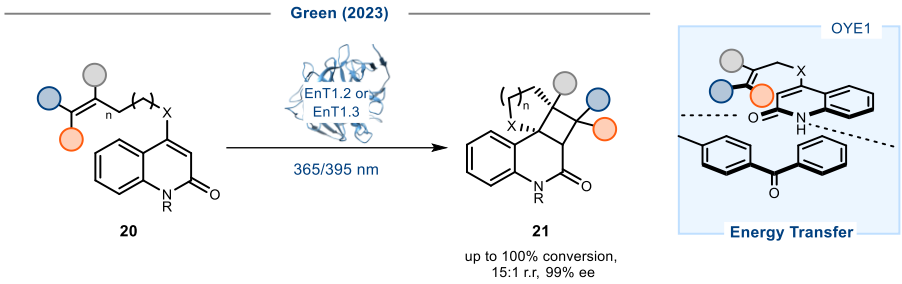

Figure 3.10. Genetically engineered photosensitizer enzyme for the light-mediated asymmetric [2+2]-cycloaddition.

3.1.4 Synergistic Combination of Photocatalysis and Biocatalysis

In this strategy, an enzyme and an external photocatalyst, like metal complexes or organic photocatalysts, are added in one pot to perform a new-to-nature transformation. This can either occur 1) by electron or energy transfer from an exogenous photocatalyst to a substrate located in the active site of an enzyme; or 2) by the combination of a photochemical and a biocatalytic step within a linear cascade.

A prominent example for the first case is the work of Hyster (Figure 3.11).[47] He demonstrated the feasibility of this approach by performing an enantioselective deacetoxylation using a nicotinamide-dependent double bond reductase (*Nt*DBR) and rose bengal as exogenous photocatalyst. Control experiments confirmed that neither the photocatalyst nor the enzyme alone can perform this deacetoxylation reaction. In solution, rose bengal ($E_{1/2}^{Red}$ [RB/RB$^{\bullet-}$] = -0.99 V vs SCE) is incapable of reducing model ketone **22** ($E_{1/2}^{Red}$ = -1.30 V vs SCE).[5] The hydrogen bonding of the enzyme with α-acetoxyketone **22** made the substrate more susceptible toward SET reduction. Based on computational calculations, the authors proposed that the tyrosine residue performed hydrogen-bonding to the carbonyl group of the substrate. This increased the reduction potential of **22**, enabling its facile reduction to ketone **23**.

[46] Sun, N., Huang, J., Qian, J., Zhou, T., Guo, J., Tang, L., Zhang, W., Deng, Y., Zhao, W., Wu, G., Liao, R., Chen, X., Zhong, F., Wu, Y. "Enantioselective [2+2]-cycloadditions with triplet photoenzymes" *Nature* **2022**, *611*, 715-720.

[47] Biegasiewicz, K. F., Cooper, S. J., Emmanuel, M. A., Miller, D. C., Hyster, T. K. "Catalytic promiscuity enabled by photoredox catalysis in nicotinamide-dependent oxidoreductases" *Nat. Chem.* **2018**, *10*, 770–775.

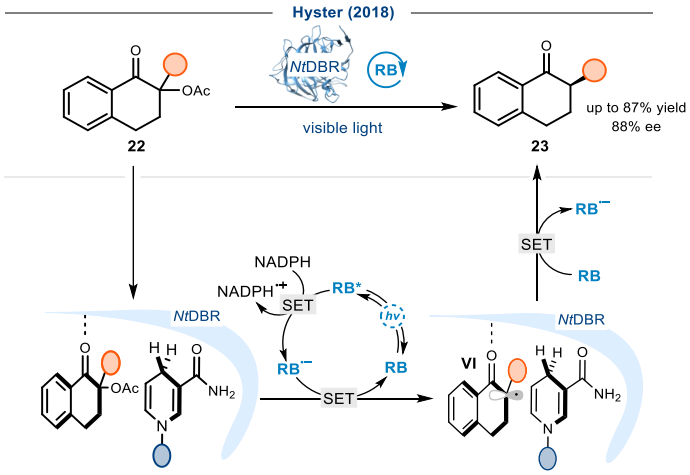

Figure 3.11. Deacetoxylation of ketone **22** by the synergistic combination of NtDBR and rose bengal. Ac: acetyl.

Another recent example of this synergetic approach is the work of Yang and coworkers, where they merged pyridoxal 5′-phosphate (PLP) biocatalysis with photoredox catalysis to enable the stereoselective synthesis of noncanonical amino acids **26** (Figure 3.12).[48] Upon condensation with PLP, β-elimination of serine and other β-hydroxy-α-amino acids (**24**) was achieved to provide intermediate **VII**. Concomitantly, free radical intermediate **V,** which was generated by the photoredox catalyst upon SET oxidation of the trifluoroborate salt **25**, was captured by enzymatically generated covalent intermediate **VIII.** This enabled a stereoselective β-functionalization. In contrast to previous mentioned example, where the light-mediated radical formation and enzymatic radical addition are part of two separated catalytic cycles, in this system the photoredox and biocatalytic cycles are synergistically enabling the reaction.

[48] Cheng, L., Li, D., Mai, B. K., Bo, Z., Cheng, L., Liu, P., Yang, Y. "Stereoselective amino acid synthesis by synergistic photoredox-pyridoxal radical biocatalysis" *Science* **2023**, *381*, 444–451.

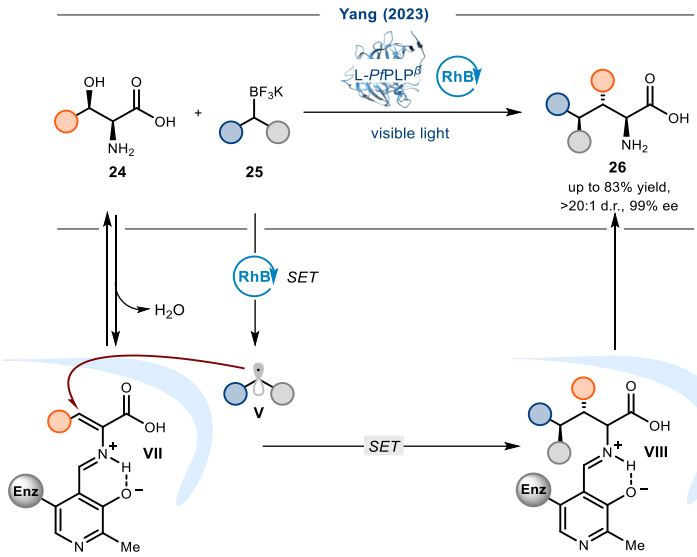

Figure 3.12. Synergistic photobiocatalytic strategy for the asymmetric synthesis of unnatural amino acids.

In contrast to the previously discussed examples, linear cascades of photocatalyst and enzyme can catalyze the steps of a reaction independently. In a collaboration, Hyster and MacMillan developed a linear cascade reaction to target a static (stable) stereocenter of a β-substituted ketone **27** and perform a dynamic kinetic resolution (Figure 3.13).[49] The racemization begins with the amine organocatalyst condensing with the β-stereogenic ketone **27** to form an enamine intermediate **IX**. This intermediate is then oxidized via SET by an excited iridium photocatalyst to produce an enaminyl radical cation **X** with an acidified β-position. Deprotonation at this position leads to the formation of an β-enaminyl radical species **XI**, which subsequently performs a non-stereoselective hydrogen atom transfer from a thiol to racemize the β stereocenter. The resulting racemic enamine **XII** can be hydrolyzed into a racemic ketone **27**. The kinetic resolution of only one enantiomer of the ketone occurs through a ketoreductase, generating enantio- and diastereoenriched 3-substituted alcohol product **28**. The remaining enantiomer was subjected to another round of racemization, thus setting the stage for a dynamic kinetic resolution. The condition was compatible with several ketoreductases, enabling the selective synthesis of each of the four stereoisomers of alcohol **28** depending on the used ketoreductase.

[49] DeHovitz, J. S., Loh, Y. Y., Kautzky, J. A., Nagao, K., Meichan, A. J., Yamauchi, M., MacMillan, D. W. C., Hyster, T. K. "Static to inducibly dynamic stereocontrol: The convergent use of racemic β-substituted ketones" *Science* **2020**, *369*, 1113–1118.

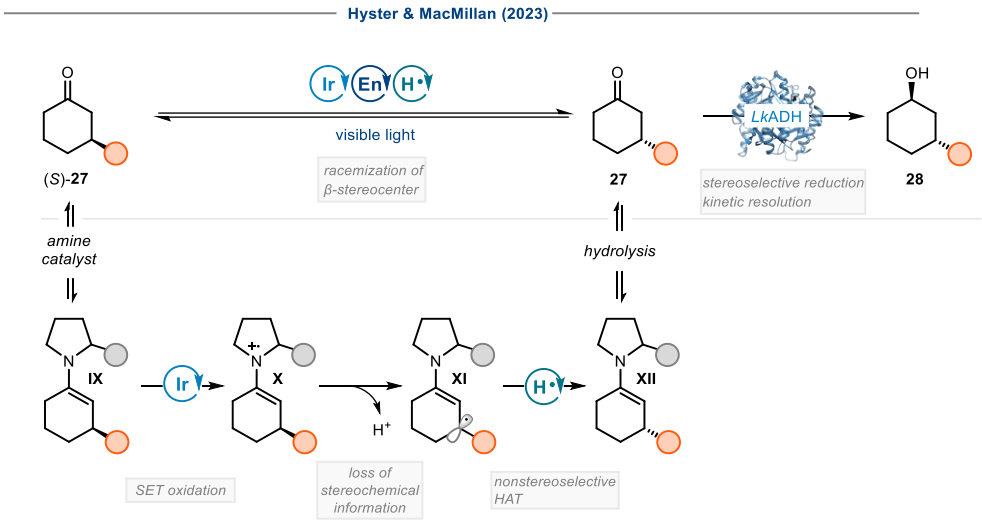

Figure 3.13. Light-mediated organocatalytic deracemization of ketone **28**.

3.2 Iminium Ion Catalysis in the Excited State

In nature, iminium ion photoisomerization plays a crucial role in biological systems. For example, the vision of humans and other higher organism rely on the excitation of an iminium ion. Upon condensation of 11-*cis*-retinal with the lysine residue of opsin, irradiation leads to the photoisomerization.[50] In their excited state, iminium ion intermediates can also act as strong SET oxidants. This has been initially studied by Mariano in the 1980s, where he investigated the reactivity of preformed, stochiometric achiral iminium ions in the excited state (Figure 3.14).[51] Upon excitation with UV light, these intermediates can reach a very high redox potential (E*(**A**$^{\bullet-}$/**A***) up to 3V) allowing them to oxidize several organic molecules, including olefins and arenes *via* SET.

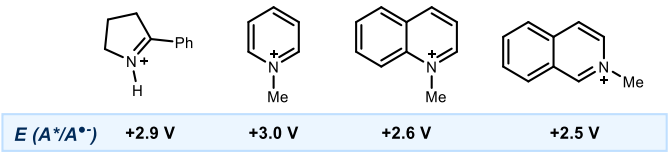

Figure 3.14. Excited-state reduction potential of a selection of preformed iminium ions.

[50] Nathans, J., Thomas, D. & Hogness, D. S. "Molecular genetics of human color vision: the genes encoding blue, green, and red pigments" *Science* **1986**, *232*,193–202.

[51] Mariano, P. S. "The photochemistry of iminium salts and related heteroaromatic systems" *Tetrahedron* **1983**, *39*, 3845–3879.

However, it is only recently that the excitation of iminium ions has found application in enantioselective photocatalysis. By capitalizing on the strongly oxidizing power acquired in the excited state, our research group has successfully applied the photoexcitation of chiral conjugated iminium ions to generate radicals and trap them with high stereoselectivity.[52] Specifically, this strategy was used for the asymmetric catalytic β-benzylation of enals (Figure 3.15). Upon acid-promoted condensation of the aromatic enal **29** with a chiral secondary amine **B**, the achromatic cinnamaldehyde turned into a colored iminium ion **XIII**. Excitation of intermediate **XIII** with visible light furnished a strong oxidant **XIII*** (E*(**XIII**$^{\bullet-}$/**XIII***) = +2.40 V vs Ag/AgCl in MeCN) that triggered the SET oxidation of benzyl silane **30**. This step generated a chiral β-enaminyl radical **XIV** along with a benzylic radical **XV**, which was formed by the irreversible fragmentation of the carbon-silicon bond. Subsequently, the stereocontrolled radical coupling took place to form a new stereogenic center with high enantioselectivity. Hydrolysis of the enamine yielded the β-substituted product **31**. This methodology enabled the functionalization of enals with poor nucleophiles **30**, which did not react under ground-state iminium ion activation.

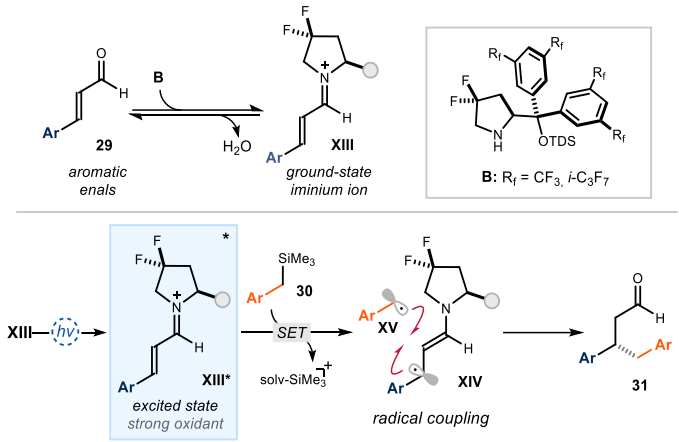

Figure 3.15. Excited-state iminium ion reactivity of aromatic enals **29**. TDS: *tert*-hexyldimethylsilyl.

In subsequent reports, our research laboratory significantly expanded the scope of suitable radical precursors for the asymmetric β-functionalization of enals. Another example was reported in 2019 by the Gilmour group, who developed the β-acylation of enals **29** using α-ketoacids **32** as radical precursors (Figure 3.16).[53] The acidity (pKa = 2.15) of **32** helped facilitating the iminium ion formation, while the resultant carboxylate exhibits an electron-donor ability leading to the formation of an EDA complex between the iminium ion and the

[52] Silvi, M., Verrier, C., Rey, Y. P., Buzzetti, L., Melchiorre, P. "Visible-light excitation of iminium ions enables the enantioselective catalytic β-alkylation of enals" *Nat. Chem.* **2017**, *9,* 868–873.

[53] Morack, T., Mück-Lichtenfeld, C., Gilmour, R. "Bioinspired Radical Stetter Reaction: Radical Umpolung Enabled by Ion-Pair Photocatalysis" *Angew. Chem., Int. Ed.* **2019**, *58*, 1208–1212.

carboxylate. Intracomplex SET upon irradiation led to the decarboxylation of **32** followed by radical coupling yielding racemic β-acylated aldehyde **33**. It is important to note that an asymmetric version of this transformation is yet to be realized.

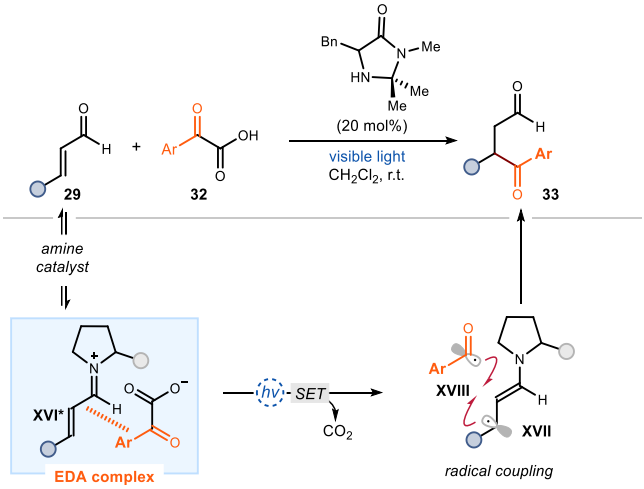

Figure 3.16. Light-mediated decarboxylative acylation of enals **29**.

Beside α-ketoacids[54], the utilization of carboxylic acids as radical precursors in iminium ion photochemistry has thus far been unsuccessful. This is primarily due to the acidic conditions required to facilitate iminium ion formation, which preclude the presence of the redox-active carboxylate moiety.

3.3 Design and Target of the Project

The project described in this chapter was inspired by the desire to develop new-to-nature reactions, thereby expanding the catalytic repertoire available to enzymes. To achieve this goal, we sought to develop a completely new strategy for excitation in photobiocatalysis and apply it within the active site of an enzyme. Specifically, we speculated that the photochemistry of iminium ions, which are known natural enzyme-bound intermediates, could be translated within an enzyme's active site, offering new opportunities to develop otherwise unachievable asymmetric radical transformations (Figure 3.17). Specifically, upon exposure to visible light, catalytic iminium ions **XIX**, transiently formed from enals **29** within enzyme active sites, would drive the SET oxidation of carboxylic acids **34**. This oxidation would lead to decarboxylation, producing a radical **XXI**, which would then couple with the β-enaminyl radical **XX**. The unique environment of the enzyme's active site, facilitated by

[54] Zhao, J. J., Zhang, H. H., Shen, X., Yu, S. "Enantioselective Radical Hydroacylation of Enals with α-Ketoacids Enabled by Photoredox/Amine Cocatalysis" *Org. Lett.* **2019**, *21*, 913–916.

multiple weak interactions, can organize highly ordered transition states, thereby achieving both relative and absolute stereocontrol. Successfully realized, this project would offer a rare example of an *unnatural photodecarboxylase* capable of forging new C-C bonds in a stereoselective fashion.

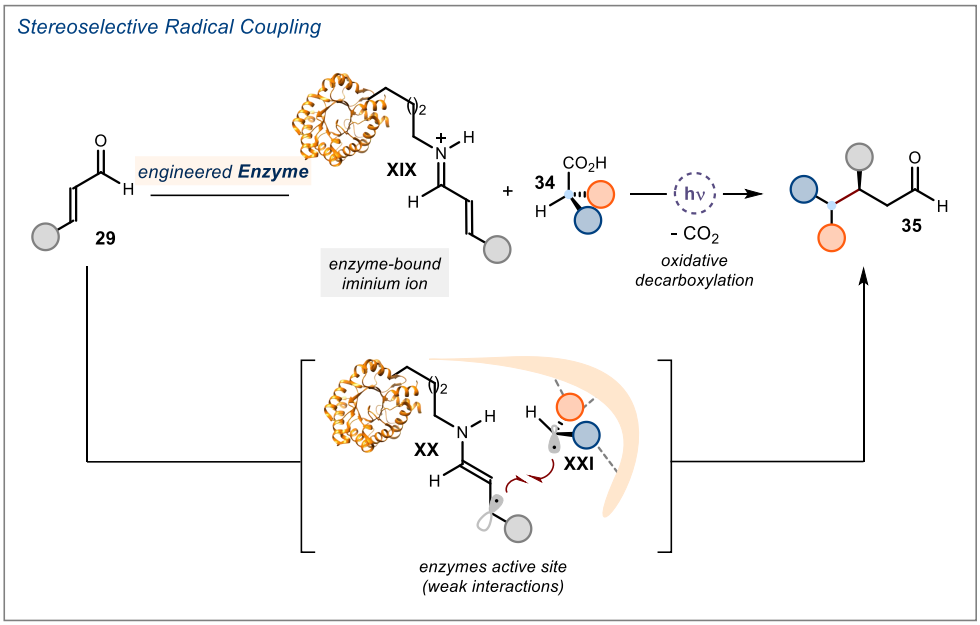

Figure 3.17. Target of the project: stereoselective radical coupling using an unnatural photodecarboxylase.

3.4 Results and Discussion

3.4.1 Identification of a Suitable Enzyme Family

To implement our plan, we needed to identify a suitable enzyme capable of transiently generating iminium ions upon activation of enals. We focused on class I aldolase enzymes[55], as they are known to form covalent enamine and iminium ion intermediates between carbonyl compounds and the ε-amino group of lysine (Lys).

We initially focused on 2-deoxy-*D*-ribose-5-phospate aldolase (DERA), a class I aldolase.[56] This enzyme catalyzes (retro) aldol reactions via iminium ion formation with the ε-amino group of a lysine residue. This activates the donor substrate, enabling attack on an acceptor aldehyde to form the aldol addition product. In particular, DERA promotes the reversible aldol

[55] Windle, C., Müller, M., Nelson, A., Berry, A. "Engineering aldolases as biocatalysts." *Curr. Opin. Chem. Biol.* **2014**, *19*, 25–33.

[56] Haridas, M., Abdelraheem, E. M. M., Hanefeld, U. "Applications and Modifications" *Appl. Microbiol. Biotechnol.* **2018**, *102*, 9959–9971.

addition of acetaldehyde to glyceraldehyde-3-phosphate yielding 2-deoxy-*D*-ribose-5-phospate. DERA is found in various animal and plant tissues, also in humans, where it is expressed mainly in lung and liver cells. Each monomer of DERA exhibits one active site. The monomers of different DERA variants have a common triose-phosphate isomerase (TIM) $(\alpha/\beta)_8$-barrel fold with a similar amino acid sequence and a conserved lysine at position 167 (Figure 3.18a). While length and secondary structure of different DERA enzymes are similar, the oligomeric form can vary (for *Escherichia coli*: Figure 3.18b). Lysine at position 167 is conserved in all DERA homologues and therefore it is hypothesized that this is the lysine residue that is involved in the formation of the iminium ion. Furthermore, lysine at position 201 in close proximity to Lys167 is critical for the catalytic activity of DERA by lowering the pKa of Lys167 to facilitate reactivity.

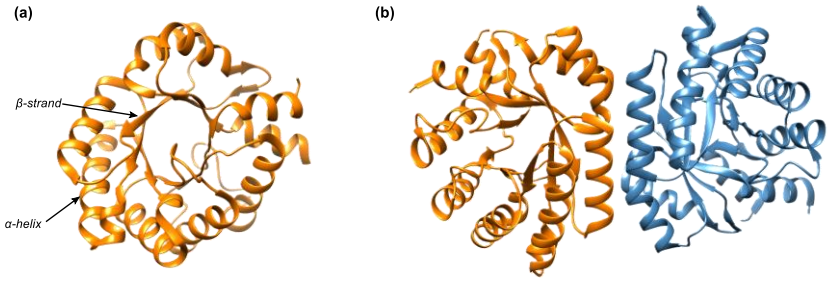

Figure 3.18. Crystal structure of the (a) monomer, (b) dimer of 2-deoxy-D-ribose-5-phospate aldolase isolated from *Escherichia coli* (EC 4.1.2.4) reported by Heine et al. in 2005 (*PDB 1JCL*).[57] All structures were plotted by UCSF Chimera 1.11rc.

Early studies of DERA primarily focused on its natural reactivity and structural properties. Substrate specificity was first examined in the 1960s.[58] While DERA shows broader acceptor tolerance for several small aldehydes and ketones, like propionaldehyde, acetone and fluoroacetone, it is highly specific for the nucleophilic substrate. Despite this specificity, DERA found application in natural product synthesis or for the synthesis of pharmaceutical intermediates.[59–61] Very recently, Poelarends and coworkers demonstrated how variants of

[57] Heine, A., Luz, J. G., Wong, C. H., Wilson, I. A. "Analysis of the class I aldolase binding site architecture based on the crystal structure of 2-Deoxyribose-5-phosphate aldolase at 0.99 Å resolution" *J. Mol. Biol.* **2004**, *343*, 1019–1034.

[58] Pricer, W. E., Horecker, B. L. "Deoxyribose aldolase from Lactobacillus plantarum" *J. Biol. Chem.* **1960**, *235*, 1292–1298.

[59] Liu, J., Wong, C. H. "Aldolase-catalyzed asymmetric synthesis of novel pyranose synthons as a new entry to heterocycles and epothilones" *Angew. Chem., Int. Ed.* **2002**, *41*, 1404–1407.

[60] Müller, M. "Chemoenzymatic synthesis of building blocks for statin side chains" *Angew. Chem., Int. Ed.* **2005**, *44*, 362–365.

[61] Huffman, M. A., Fryszkowska, A., Alvizo, O., Borra-Garske, M., Campos, K. R., Canada, K. A., Devine, P. N., Duan, D., Forstater, J. H., Grosser, S. T., Halsey, H. M., Hughes, G. J., Jo, J., Joyce, L. A., Kolev, J. N., Liang, J., Maloney, K. M., Mann, B. F., Marshall, N. M., Mclaughlin, M., Moore, J. C., Murphy, G. S., Nawrat, C. C., Nazor, J., Novick, S., Patel, N. R., Rodriguez-Granillo, A., Robaire, S. A., Sherer, E. C., Truppo, M. D., Whittaker, A. M., Verma, D., Xiao, L., Xu, Y., Yang, H. "Design of an in vitro biocatalytic cascade for the manufacture of islatravir" *Science* **2019**, *368*, 1255–1259.

DERA could also enable iminium ion-mediated catalytic chemistry to perform the Michael addition between cinnamaldehyde **29** and nitromethane **36** (Figure 3.19), in a manner reminiscent of small-molecule organocatalysis.[62] They observed low promiscuous activity of DERA for the Michael addition. With 11 rounds of directed evolution (focused and random mutagenesis) and in total 12 amino acid substitutions, they could engineer a competent biocatalyst for the iminium ion-mediated Michael addition.

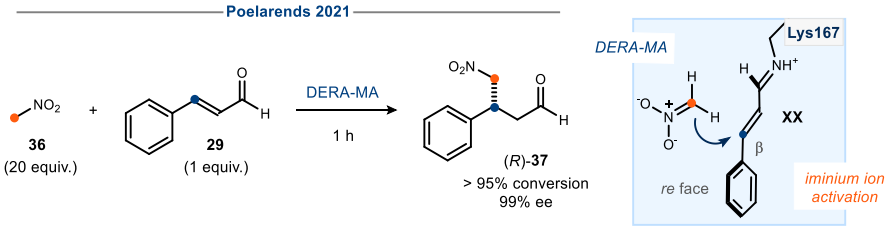

Figure 3.19. Iminium ion activation using genetically modified DERA.

We envisioned this enzyme family as a promising candidate for developing our photobiocatalytic plan via direct excitation of an enzyme-bound iminium ion.

3.4.2 Preliminary Results and Optimization

We initially investigated the suitability of DERA-MA, an engineered variant of the natural DERA class I aldolase, as a catalyst due to its established ability to perform Michael addition via iminium ion activation (see Figure 3.19).[62] We surmised that excitation with purple light (405 nm irradiation) could elicit the required excitation of iminium ion, SET oxidation of the carboxylic acid, and subsequent radical formation. We tested this idea reacting cinnamaldehyde **29** and phenylacetic acid **34a** as model substrates in 50 mM potassium phosphate buffer pH 6.5 using 10% DMSO as a co-solvent to solubilize hydrophobic substrates (Table 3.1). For the irradiation setup, we utilized a commercially available purple LED strip with a maximum emission wavelength (λ_{max}) of 405 nm. To maintain a constant temperature of approximately 30 °C, a fan was positioned 5 cm away from the set up. The detailed configuration of this setup can be found in the Experimental Section (Figure 3.39). Encouragingly, the initial experiment using DERA-MA under purple light (405 nm) delivered the desired benzylation product **35a** in 17% yield with full enantiocontrol (>99% ee, entry 1). To explore potential improvements in reactivity, we screened other enzyme variants. Based on our prior success in developing an efficient Enders cascade using Pp-4OT-F_3 (see *Chapter 2*), we first tested this enzyme as a catalyst.[63] However, Pp-4OT-F_3 resulted in the

[62] Kunzendorf, A., Xu, G., van der Velde, J. J. H., Rozeboom, H. J., Thunnissen, A. M. W. H., Poelarends, G. J. "Unlocking Asymmetric Michael Additions in an Archetypical Class I Aldolase by Directed Evolution" *ACS Catal.* **2021**, *11*, 13236–13243.

[63] Tseliou, V., Faraone, A., Kqiku, L., Vilím, J., Simionato, G., Melchiorre, P. "Enantioselective Biocascade Catalysis with a Single Multifunctional Enzyme" *Angew. Chem., Int. Ed.* **2022**, *61*, e202212176.

formation of the target product **35a** in low yield (2% analytical yield, entry 2). Further screening of Pp-4OT homologs with high sequence similarity (>75%) revealed similar or even lower reactivity (Table 3.1, entries 3-5).

Table 3.1. Initial screening to test the activity toward the photoexcitation of iminium ions.[a]

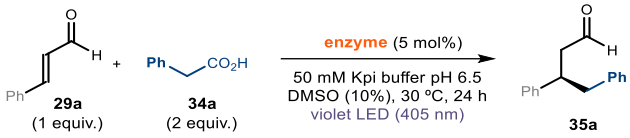

entry	enzyme (loading)	yield **35a** (%)	*ee* **35a** (%)[b]
1	DERA-MA (5 mol%)	17	99
2	**Pp**-4OT-**F$_3$** (5 mol%)	2	*n.d.*
3	**MI**-4OT-**F$_3$** (5 mol%)	<1	*n.d.*
4	**Tb**-4OT (5 mol%)	<1	*n.d.*
5	**Ps**-4OT (5 mol%)	2	*n.d.*

[a]Reactions performed on a 1.25 µmol scale (2.5 mM) at 30 °C. Analytical yield of **35a** was determined by GC-FID analysis (calibration using trimethoxybenzene as internal standard). [b]Enantiomeric excess (ee) value determined by UPC² analysis. *n.d.* = not determined; KPi = potassium phosphate.

We then investigated several reaction parameters, starting with the influence of stoichiometry. Initially, we performed the reaction using an excess of carboxylic acid **34a** with respect to enal **29a** (2:1 ratio, Table 3.1, entry 3). We then examined the effect of an excess of cinnamaldehyde (ratios of 1:1 and 2:1, Table 3.2, entries 1 and 2). In both cases, we observed a significant decrease in the yield of product **35a** (9% and 7% yield, respectively). Increasing the ratio of phenylacetic acid **34a** revealed an optimal ratio of 1:3.5, which afforded product **35a** in 33% yield. Higher substrate ratios led to worse results.

Table 3.2. Screening of substrate ratios in the photobiocatalytic radical coupling.[a]

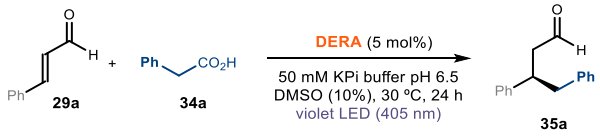

entry	Ratio **29a**/**38a**	yield **35a** (%)	*ee* **35a** (%)[b]
1	2:1	7	*n.d.*
2	1:1	9	*n.d.*
3	1:2	17	99
4	1:3.5	33	99
5	1:5	24	99
6	1:10	17	99

[a]Reactions performed on a 1.25 µmol scale (2.5 mM) at 30 °C. Analytical yield of **35a** was determined by GC-FID analysis (calibration using trimethoxybenzene as internal standard). [b]Enantiomeric excess (ee) value determined by UPC² analysis. *n.d.* = not determined; KPi = potassium phosphate.

We next investigated the influence of four different common co-solvents on the reaction in an aqueous buffer. The use of dimethylformamide (DMF), dimethylacetamide (DMA) and ethylene glycol (EG) as co-solvents was detrimental and led to a decrease in activity (Table 3.3, entries 2-4). Then, different ratios (v/v%) of DMSO (5 – 40%) were tested, showing an optimal ratio of 10 to 20% (Table 3.3, entries 1&6). A lower ratio resulted in reduced yield, potentially due to the poor solubility of the substrate (entry 5), whereas a higher ratio decreases the activity of the enzyme (entry 7). Changing buffers (entries 8-11) or the wavelength of irradiation (entries 12-14) did not improve the reactivity.

Table 3.3. Screening of co-solvents, reaction buffers and wavelength of the light source.[a]

entry	Deviation	yield **35a** (%)	*ee* **35a** (%)[b]
1	none	33	99
2	10% DMF	14	99
3	10% DMA	11	*n.d.*
4	10% EG	15	99
5	5% DMSO	14	99
6	20% DMSO	31	99
7	40% DMSO	5	*n.d.*
8	50 mM TRIS pH 7.4	13	99
9	50 mM MOPS pH 6.5	26	99
10	50 mM MES pH 6.5	22	99
11	50 M ACES pH 6.5	26	99
12	365 nm	10	99
13	380 nm	25	99
14	420 nm	>1	*n.d.*

[a]Reactions performed on a 1.25 µmol scale (2.5 mM) at ambient temperature. Analytical yield of **35a** was determined by GC-FID analysis (calibration using trimethoxybenzene as internal standard). [b]Enantiomeric excess (ee) value determined by UPC² analysis. *n.d.* = not determined; KPi = potassium phosphate.

Several control experiments were conducted to investigate the importance of the enzyme and light. The reactivity was completely lost in the absence of the enzyme or light irradiation, underscoring their essential roles in the process (Table 3.4, entries 2 and 3). This demonstrated that the DERA mutant functions as a photoenzyme, as it requires a continuous input of photons for its activity. Finally, we found that the DERA-MA^{K167L} variant, where the catalytically active lysine was replaced with leucine, was completely inactive (Table 3.4, entry

4), underscoring the crucial role of K167 to activate cinnamaldehyde and form the iminium ion.

Table 3.4. Control experiments for the photobiocatalytic radical coupling.[a]

entry	Deviation	yield **35a** (%)
1	none	33
2	no light	-
3	no enzyme	-
4	DERA-MA K167L	-

[a]Reactions performed on a 1.25 μmol scale (2.5 mM) at ambient temperature. Analytical yield of **35a** was determined by GC-FID analysis (calibration using trimethoxybenzene as internal standard).

3.4.2 Docking Studies and Semi-Rational Engineering

Based on the initial optimization studies, we selected DERA-MA to perform semi-rational mutagenesis. We envisioned targeting specific amino acids in the active site by utilizing information about the structure and sequence of the protein. The amino acids in close proximity to the iminium ion were proposed to exert a more predictable and significant influence. By replacing these amino acids, we believed we could improve our understanding of the reactivity. Molecular docking studies were performed using Autodock Vina and based on a reported crystal structure of the iminium intermediate formed from cinnamaldehyde **29a** and K167 within DERA-MA (PDB: 7P76).[62] Calculations revealed that the preferred binding location and position of phenylacetic acid **34a** with DERA-MA was in the binding pocket of the protein. This binding was stabilized by hydrogen bonding of the carboxylate with the hydroxy groups of serines 18 and 238, as well as π-π stacking between both phenyl substituents of **34a** and the iminium ion **XIX** (Figure 3.20). These interactions secured the positioning of the substrates in close proximity. Computational studies revealed the importance of five amino acids in close proximity to **34a**, which were targeted for semi-rational mutagenesis to alter the binding pose of the acid. The five amino acids included two serines (S18 and S238), a tyrosine at position 19, a leucine at position 172 and threonine at position 203.

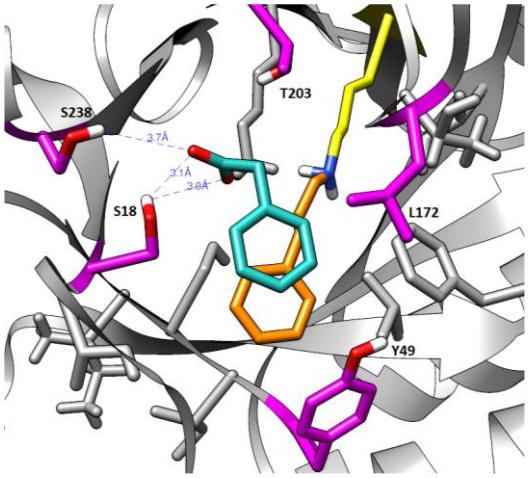

Figure 3.20. Molecular dockings of **34a** into the active site of DERA-MA. The iminium ion formed upon condensation of **29a** with the catalytic K167 is shown in orange. Interacting amino acids are shown in magenta. All dockings were performed with YASARA structure. UCSF Chimera 1.11 was used for visualization.

Based on this model, the influence of each amino acids on reactivity was analysed by substituting them with a more hydrophobic alanine residue (*alanine scan*).[64] Alanine mutants Y49A, L172A, T203A and S238A significantly hampered the reactivity (Table 3.5, entries 3-5). However, the engineered DERA-MA^{S18A} variant afforded product **35a** in greatly improved yield compared to the parental enzyme (Table 3.5, entries 1 and 2), while retaining the high level of stereoinduction. This suggested that, by selectively removing the hydrogen bond interaction of **34a** to Ser18, the acid adopts a less rigid and more productive binding pose. The simulated docking of **34a** to the active site of DERA-MA^{S18A} (Figure 3.21b) suggested also that phenylacetic acid **34a** could get in closer spatial proximity to the iminium ion **XIX**, thus facilitating the reactivity. The introduction of other amino acids with different steric bulk at position 18, such as glycine or valine, resulted in worse reaction outcomes (Table 3.5, entries 7 and 8).

[62] Damián-Almazo, J. Y., Saab-Rincón, G "Site-Directed Mutagenesis as Applied to Biocatalysts." IntechOpen, 2013,

Table 3.5. Semi-rational mutagenesis in the photobiocatalytic radical coupling.[a]

entry	DERA variant	yield **35a** (%)	*ee* **35a** (%)[b]
1	DERA-MA	33	99
2	DERA-MA S18A	57	99
3	DERA-MA Y49A	17	99
4	DERA-MA L172A	15	99
5	DERA-MA T203A	3	*n.d.*
6	DERA-MA S238A	7	*n.d.*
7	DERA-MA S18G	44	99
8	DERA-MA S18V	24	99

[a]Reactions performed on a 1.25 µmol scale (2.5 mM) at ambient temperature. Analytical yield of **35a** was determined by GC-FID analysis (calibration using trimethoxybenzene as internal standard). [b]Enantiomeric excess (ee) value determined by UPC² analysis. *n.d.* = not determined; KPi = potassium phosphate.

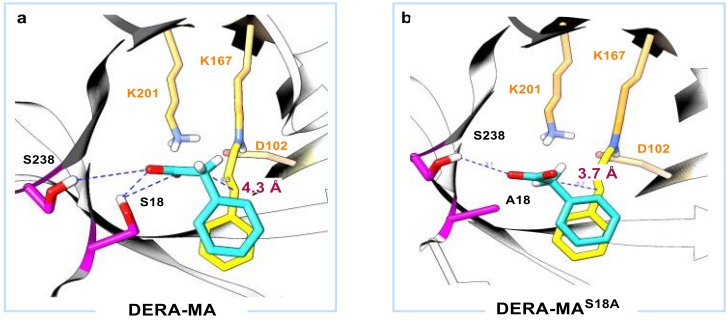

Figure 3.21. Molecular dockings of **35a** (shown in turquoise) into the active site of a) DERA-MA and b) DERA-MA^{S18A}. The iminium ion formed upon condensation of **29a** with the catalytic K167 is shown in yellow. Serine 18 and 238 and S18A are shown in magenta. All dockings were performed with YASARA structure. UCSF Chimera 1.11 was used for visualization.

3.4.3 Scope of the Enantioselective Transformation

Using the optimized conditions with our engineered enzyme DERA-MA^{S18A}, we next explored the generality of the photobiocatalytic process. A range of different aromatic enals **29** and phenylacetic acids **34** were tested (Figure 3.22). Products **35** were formed in mediocre to good yield and full enantiocontrol. DERA-MA^{S18A} tolerated several phenacyl carboxylic acid derivatives with *para*-substitution on the phenyl ring, including methyl, methoxy and halogen substituents (**35b** and **35e-h**). While DERA-MA^{S18A} was able to accommodate *ortho*-

and *meta*-substitutions on the aromatic ring of the carboxylic acid, the parent DERA-MA variant ultimately yielded better results (products **35c** and **35d**). Heteroaromatic scaffolds, including a thiophene and a furan, were tolerated, affording products **35i** and **35j**, respectively. In addition to simple cinnamaldehyde, enals with *para*-substituted phenyl rings were also well accepted, yielding products **35k-m** in moderate to good yields. The photobiocatalytic process was scaled up to 0.075 mmol using a cell-free extract containing DERA-MA^{S18A}, isolating product **35j** in 50% yield. In addition, a semi-preparative enzymatic reaction using purified DERA-MA^{S18A} led to the isolation of **35m** in 29% yield.

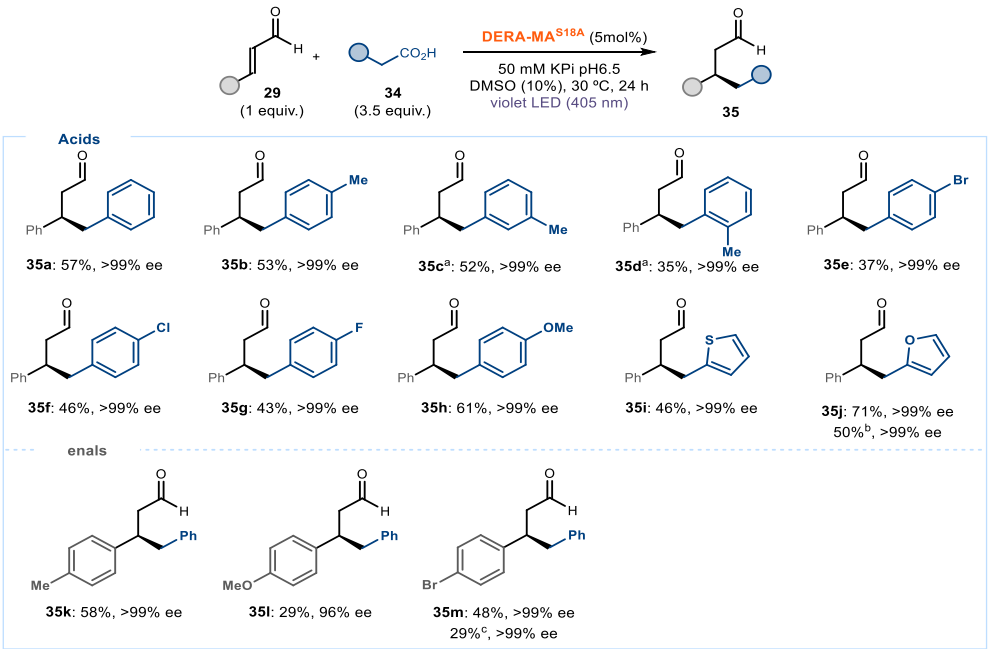

Figure 3.22. Reaction scope: experiments performed using DERA-MA^{S18A} (5 mol%) on a 1.25 µmol scale of **29** (c = 2.5 mM) in phosphate buffer (KPi). Analytical yields are determined as an average of three runs by GC-FID analysis (calibration using 1,3,5-trimethoxybenzene as internal standard); ee was measured by UPC^2 analysis. [a]Using DERA-MA. [b]Yield of isolated **35j** from an upscale reaction using cell-free-extract containing DERA-MA^{S18A} (c = 2.5 mg mL^{-1}). [c]Yield of isolated **35m** from a 75 µmol scale reaction using the purified enzyme (125 µM).

Regarding the limitations of the reaction, aliphatic acids failed to deliver the desired products (Figure 3.23). Carboxylic acids with α-oxy and α-amino-substituents were not tolerated. Acylation of cinnamaldehyde **29a** using phenylglycoxylic acid was observed in low quantities. Reactions using aliphatic or β-substituted enals were not successful. Low reactivity was observed when substituents were introduced at the α-position of cinnamaldehyde. Furthermore, DERA-MA^{S18A} did not accept enones. Overall, the reactivity was limited to aromatic substituted enals and benzylic radical precursors.

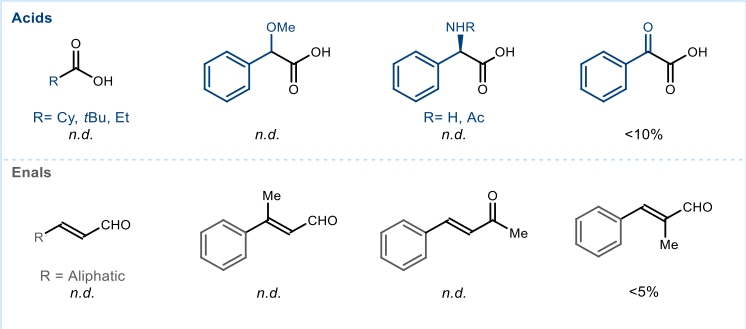

Figure 3.23. Moderately successful and unsuccessful substrates. using DERA-MA^{S18A} (5 mol%) on a 1.25 μmol scale of α,β-unsaturated carbonyl compound (c = 2.5 mM) in phosphate buffer (KPi). Analytical yields are determined by GC-FID analysis (the average response factor was used to calculate the yield). 1,3,5-Trimethoxybenzene as internal standard.

3.4.4 Forging Two Stereocenters via Stereospecific Radical Coupling

The results acquired so far demonstrate the ability of our photoenzyme to achieve perfect enantiocontrol by selecting the face of the iminium ion attacked by the radical. Our next question was whether it would be possible to forge more than one stereocenter enabling the precise control over relative and absolute stereochemistry. Addressing this question required the use of a chiral enantiopure carboxylic acid as the radical precursor. We hoped that the weak interactions of amino acid side chains with the carboxylic acid could stabilize the chiral radical and exert stereoinduction over the radical coupling process. We started our investigation by performing the reaction between enal **29a** and the racemic acid **36** using DERA-MA (Figure 3.24a). Disappointingly, the product **37a** was obtained as a mixture of two diastereomers in almost equal amount (1.1:1 dr, 99% ee). However, when the reaction was performed using the enantiopure radical precursor **36a**, we observed a change in the diastereomeric ratio (Figure 3.24b). Importantly, the opposite diastereomers were obtained when using (*S*)- or (*R*)-acids, suggesting that a stereospecific radical coupling was operational.

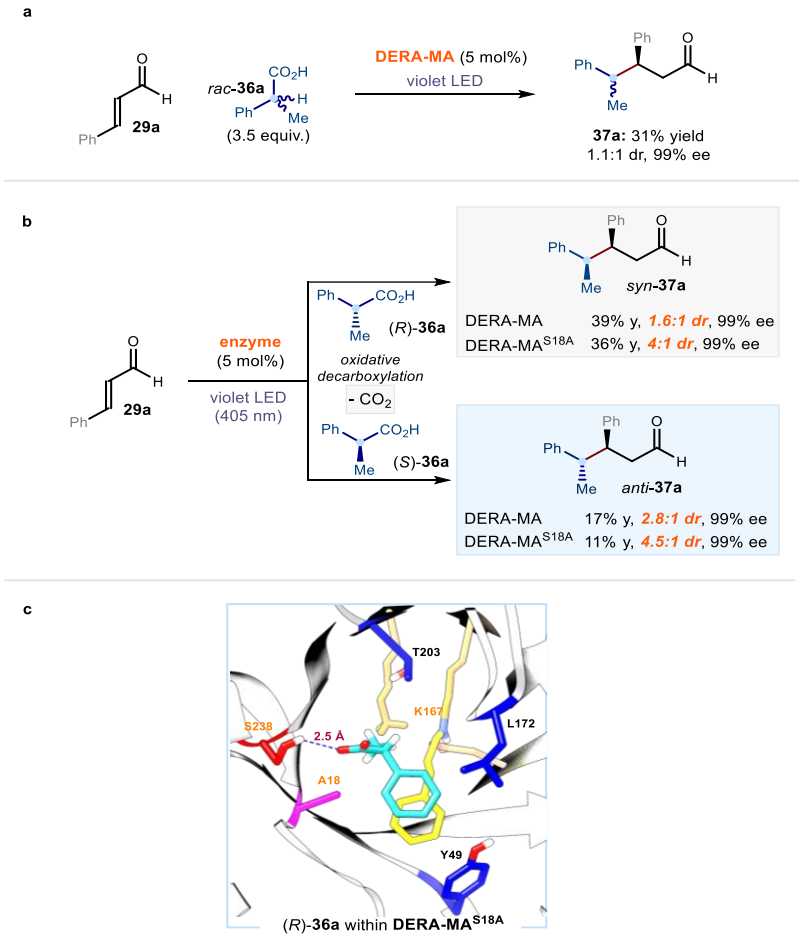

Figure 3.24. Initial experiments for the diastereoselective radical coupling when using a) racemic carboxylic acid **36a** and b) chiral enantiopure carboxylic acid **36a** and observation of 'memory of chirality' c) Docking studies of substrate (*R*)-**36a** within the active site of DERA-MA^{S18A}.

This finding regarding the preservation of stereochemistry was particularly surprising. Most alkyl radicals, upon formation, adopt a pyramidal geometry[65] and exhibit a very low inversion barrier due to sp^2 hybridization.[66] When it comes to chiral radical precursors, and therefore chiral radicals, this characteristic typically leads to rapid racemization. Consequently, asymmetric strategies relying on chiral enantiopure radical precursors are often ineffective. Our results suggest that the enzyme's active site possesses a remarkable ability to transfer stereochemical information from the chiral radical precursor **36** to the product **37**, efficiently

[65] Paddon-Row, M. N., Houk, K. N. "Conformational dependence of the pyramidalization of alkyl radicals." *J. Phys. Chem.* **2015**, *89*, 3771–3774.

[66] Krusic, P. J., Meakin, P. "Barrier to pyramidal inversion in the tert-butyl radical by electron spin resonance." *J. Am. Chem. Soc.* **1976**, *98*, 228–230.

preventing racemization. This 'memory of chirality' scenario[67,68] is uncommon in radical chemistry and highlights a remarkable ability of our photoenzyme.

The reaction was repeated with our best performing enzyme DERA-MA^{S18A} (Figure 3.24b). Enhanced diastereoselectivity was observed: adduct *syn*-**37a** (36% yield, 4:1 dr, 99% ee) was obtained from the (*R*)-enantiomer of substrate **36a**, while the opposite enantiomer (*S*)-**36a** yielded the adduct *anti*-**37a** (11% yield, 4.5:1 dr, 99% ee). These results indicated that acid *(R)*-**36a** was more reactive than the antipode (*S*)-**36a**. This result could be rationalized by analyzing the docking of the (*R*)-enantiomer in the active site of DERA-MA^{S18A} (Figure 3.24c). (*R*)-**36a** is stabilized by S238 via hydrogen bond interaction, leading to a binding pose where the α-methyl group is facing the hydrophobic cavity created by the alanine residue (S18A). Meanwhile, the hydrogen atom of the α-stereogenic carbon is positioned towards the threonine residue 203.

Considering that the (*S*)-enantiomer of **36a** would expose the α-methyl group towards T203, we hypothesized that this specific site could be subject to mutagenesis in order to enhance the binding affinity of (*S*)-**36a** and consequently increase its reactivity. Other residues, namely L172, Y49 and S238, were also found to surround substrate **36a**. To assess the contribution of these amino acids, we performed alanine scanning mutagenesis on the DERA-MA enzyme (Figure 3.25a). Each alanine mutant was then evaluated in the reaction using both (*S*)- and (*R*)-enantiomers of carboxylic acid **36a**. Interestingly, the T203A mutant displayed the most significant improvement in diastereoselectivity, achieving similar stereochemical outcomes as the previously identified S18A mutant and affording product **37a** with different relative configurations depending on the absolute configuration of the carboxylic acid. To potentially leverage the benefits of both mutations, we constructed a double mutant, DERA-MA$^{S18A/T203A}$. This double mutant exhibited enhanced reactivity and stereoselectivity: *anti*-**37a** was obtained in 38% yield (15:1 dr) while *syn*-**37a** was formed in 62% yield (7.5:1 dr) when starting from (*S*)- or (*R*)-**36a**, respectively.

[67] Alezra, V., Kawabata, T. "Recent Progress in Memory of Chirality (MOC): An Advanced Chiral Pool." *Synth.* **2016**, *48*, 2997–3016.

[68] Gloor, C. S., Dénès, F., Renaud, P. "Memory of chirality in reactions involving monoradicals." *Free Radic. Res.* **2016**, *50*, S102–S111.

a

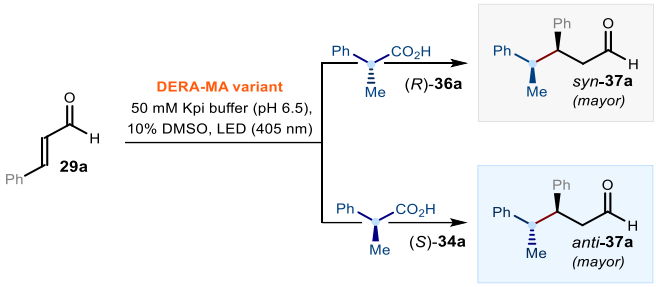

Alanine Scanning	*syn*-**37a** (99% ee)	*anti*-**37a** (99% ee)
mutation	from (*R*)-**36a**	from (*S*)-**36a**
None	39%, 1.6:1 dr	17%, 2.8:1 dr
S18A	36%, **4:1 dr**	11%, **4.5:1 dr**
Y49A	33%, 1:1.3 dr	11%, 2:1 dr
L172A	21%, 1:1.3 dr	7%, 2.4:1 dr
T203A	32%, **4.3:1 dr**	21%, **5.3:1 dr**
S238A	25%, 2:1 dr	6%, 1.4:1 dr
S18A+T203A	62%, **7.5:1 dr**	38%, **15:1 dr**

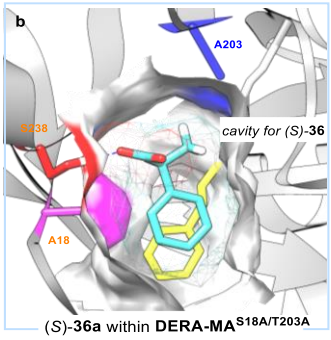

Figure 3.25. a) Alanine scan of DERA-MA. b) Binding pose of (*S*)-**36a** within double mutant DERA-MA$^{S18A/T203A}$. In all dockings, the iminium ion formed from cinnamaldehyde **29a** and lysine K167 is shown in yellow, S18A mutation is shown in magenta, and S238 interaction with substrate **36** is shown with a dashed blue line. Residues identified as suitable for mutagenesis are in blue.

3.4.5 Scope of the Stereospecific Radical Coupling

After optimizing the enzyme, we explored the generality of our photobiocatalytic protocol for the stereospecific radical coupling. The chiral carboxylic acids **36** were obtained *via* asymmetric methylation using chiral oxazolidinones (Evans' auxiliaries, see *Section 3.6.4*). DERA-MA$^{S18A/T203A}$ accepted carboxylic acids **36** with *para*-, *meta*- and *ortho*-substitution and various groups with different electronic properties, affording the corresponding products *syn*-**37** and *anti*-**37**. Furthermore, different enals **29** were well accepted. X-ray crystallographic analysis provided unambiguous evidence for the relative and absolute configurations of products *syn*-**37k** and derivative *syn*-**37e**, which both were obtained starting from the (*R*)-enantiomer of the corresponding carboxylic acid substrate.[69] This analysis established that the radical process proceeded with an overall inversion of the configuration of the carboxylic acid **36**'s stereocenter.

Benzylic carboxylic acids **36** with a bulkier substituent than methyl at the α-carbon reduced the reactivity.

[69] Crystallographic data for compound *syn*-**37k** (accession number CCDC 2280852) and derivative of *syn*-**37e** (accession number CCDC *228164*4) have been deposited with Cambridge Crystallographic Data Centre.

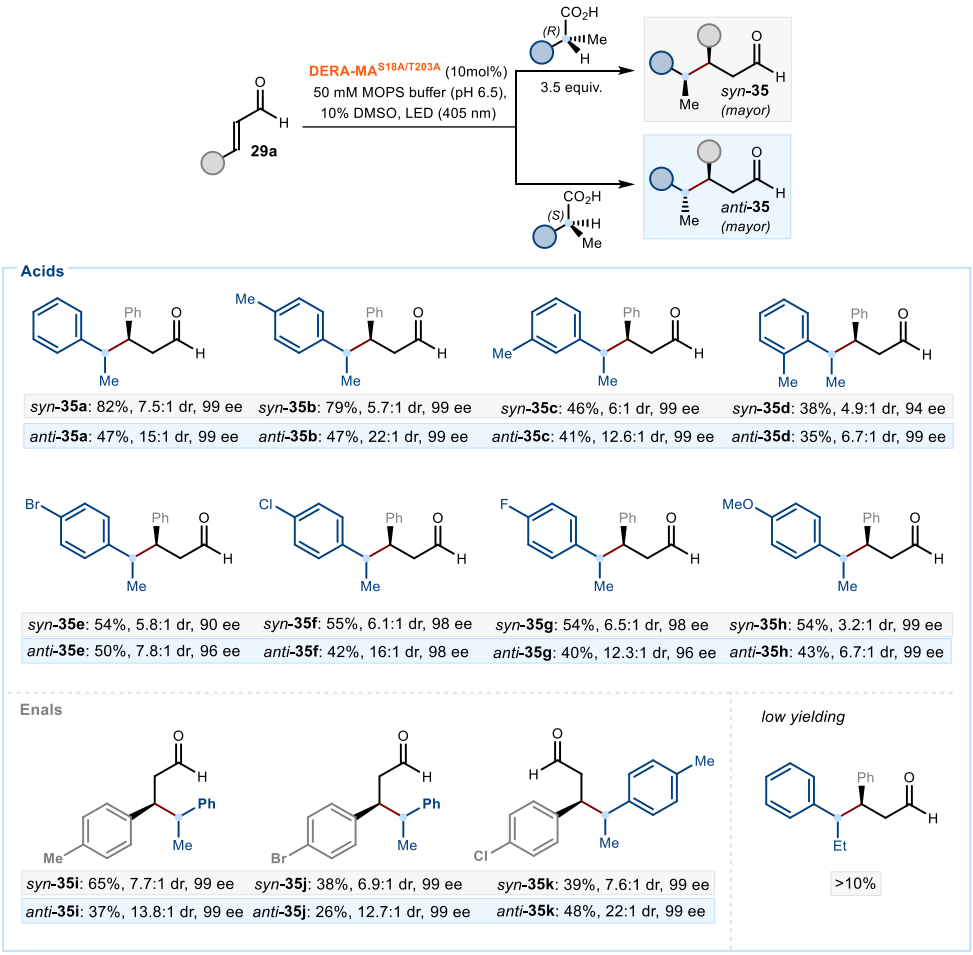

Figure 3.26. Reaction scope of the stereospecific radical coupling. The reactions were performed with either (*S*) or (*R*) enantiomerically pure carboxylic acids **36** using the double mutant DERA-MA$^{S18A/T203A}$ (10 mol%) on a 0.625 µmol scale of **29a** (c = 1.25 mM).

The docking of (*S*)-**36a** within the active site of DERA-MA$^{S18A/T203A}$ (Figure 3.28) provides a rationalization for this lack of reactivity: bulkier alkyl chain than methyl would not fit in the hydrophobic cavity of the active site. Furthermore, it should be mentioned that the aryl moiety was important for reactivity, potentially for the π-π interactions which bring the substrate in close proximity to the iminium ion.

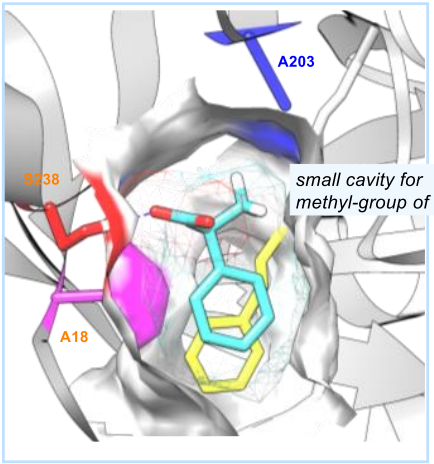

Figure 3.27. Binding pose of (*S*)-**36a** within double mutant DERA-MA$^{S18A/T203A}$. In all dockings, the iminium ion formed from cinnamaldehyde **29a** and lysine K167 is shown in yellow, S18A mutation is shown in magenta, and S238 interaction with substrate **36** is shown with a dashed blue line

3.4.6 Kinetic Resolution

To validate our understanding of the substrate binding within the enzyme, we aimed to modify the active site to alter enzymatic reactivity. We hypothesized that introducing a bulkier residue at position 203, in place of alanine, would block the hydrophobic cavity that accommodates the α-methyl group of (*S*)-**36** (Figure 3.28b). In contrast, carboxylic acid (*R*)-**36** would still fit into the cavity provided by A18. If this hypothesis were correct, the enzyme would facilitate a kinetic resolution (KR) of racemic carboxylic acid **36**, selectively reacting with the (*R*) enantiomer. Three sterically demanding amino acids at position 203 were tested (Figure 3.28a). While the cell free extract of the isoleucine variant did not show any activity and the observed diastereomeric ratio for the leucine was rather low, DERA-MA$^{S18A/T203V}$ showed good diastereocontrol (5.3:1 dr, 99% ee, Figure 3.28). The reaction was repeated using purified DERA-MA$^{S18A/T203V}$, the (*R*)- and the (*S*)- enantiomer and racemic acid **36a**. While (*R*)-**36a** led to product *syn*-**37a** with high reactivity and excellent stereocontrol, (*S*)-**36a** was barely reactive, although the stereospecificity was maintained (*anti*-**37a** formed in 9% yield). Docking studies of (*R*)-**36a** within the active site of DERA-MA$^{S18A/T203V}$ illustrated that substituting alanine with the bulkier valine reduced the available space, thereby hindering the accommodation of (*S*)-**36a**. DERA-MA$^{S18A/T203V}$ was subsequently employed for the kinetic resolution of other racemic carboxylic acids, yielding products *syn*-**37b-c**.

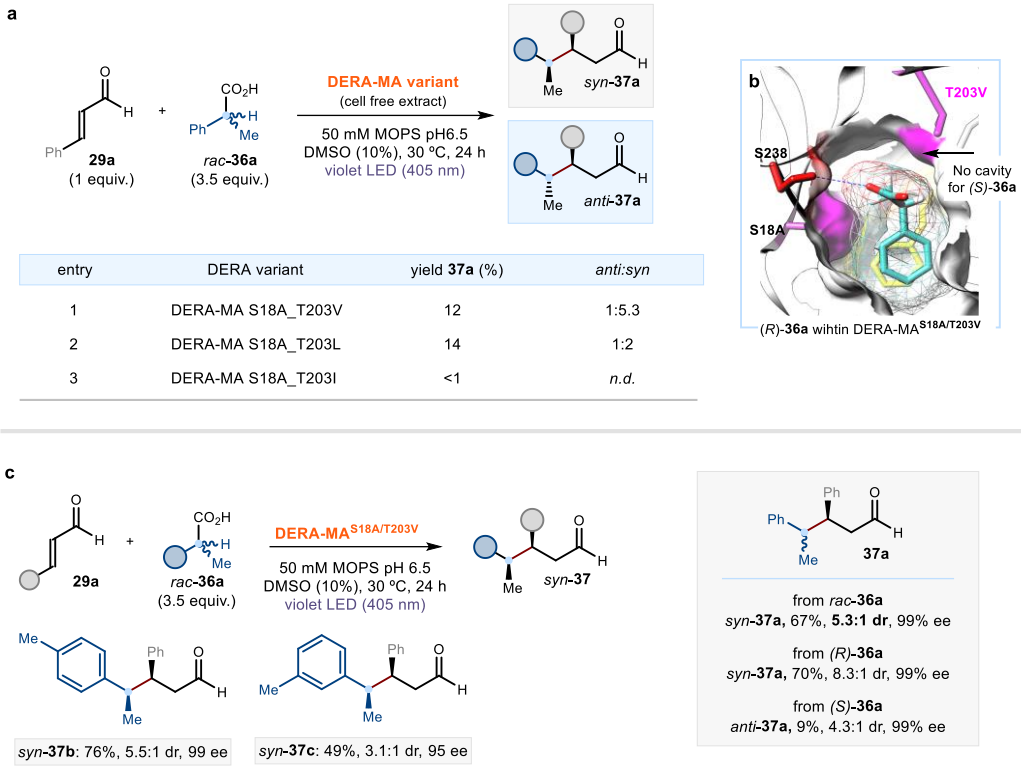

entry	DERA variant	yield **37a** (%)	*anti:syn*
1	DERA-MA S18A_T203V	12	1:5.3
2	DERA-MA S18A_T203L	14	1:2
3	DERA-MA S18A_T203I	<1	*n.d.*

Figure 3.28. a) Screening of DERA-MA variants as cell-free extracts for developing a kinetic resolution. b) Binding pose of (*R*)-**36a** in kinetic resolution enzyme DERA-MA$^{S18A/T203V}$ c) Kinetic resolution reactions performed using DERA-MA$^{S18A/T203V}$ (5 mol%) with racemic acids **36** (3.5 equiv.) on a 1.25 µmol scale of **29** (c = 2.5 mM). All reactions were performed in MOPS buffer at pH 6.5 in 10% of DMSO. Results are the average of two runs. MOPS = 3-(N-morpholino)propane sulfonic acid.

3.4.7 Mechanistic Experiments

3.4.7.1 UV-Vis Studies

We then conducted investigations to gain insight into the catalytic mechanism employed by our photoenzyme. UV/Vis spectroscopic analyses revealed the formation of a new absorption peak at approximately 400 nm (blue trace in Figure 3.29, upper panel) upon addition of cinnamaldehyde **29a** to the enzyme DERA-MA^{S18A}, which we attributed to the formation of an iminium ion. Neither the enzyme nor enal **29a** absorbs at 405 nm. Addition of carboxylic acid **34a** did not induce significant changes in absorbance (orange trace), thus ruling out the formation of any ground-state aggregate. This observation is in agreement with the hypothesis that the enzyme-bound iminium ion is directly excited and is responsible for the observed reactivity.

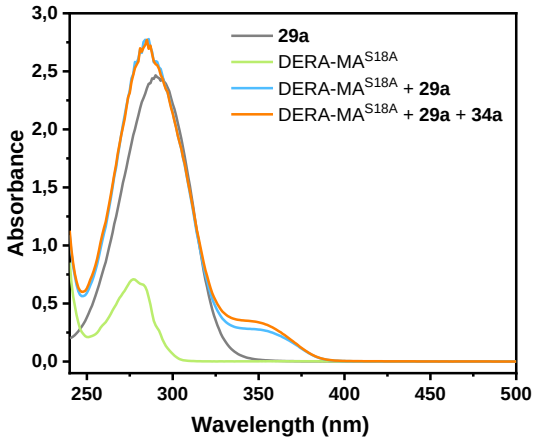

Figure 3.29. UV-Vis spectra of DERA-MA^{S18A} and reagents **29a** and **34a**, and mixtures thereof.

Additional UV-Vis studies were conducted to confirm the essential role of K167 in iminium ion formation. We investigated the variant DERA-MA^{K167L}, in which the critical catalytic lysine residue was substituted. This variant displayed no activity in our model reaction (see *Section 3.4.2*, Table 3.4). When incubated with cinnamaldehyde **29a**, the DERA-MA^{K167L} variant did not show any changes in absorption (Figure 3.30). In contrast, the active variant DERA-MA^{S18A}, which retains K167, exhibited a bathochromic shift upon the addition of **29a** (Figure 3.29), again supportive of iminium ion formation. Therefore, we conclude that iminium ion formation does not occur in the absence of the lysine residue at position 167.

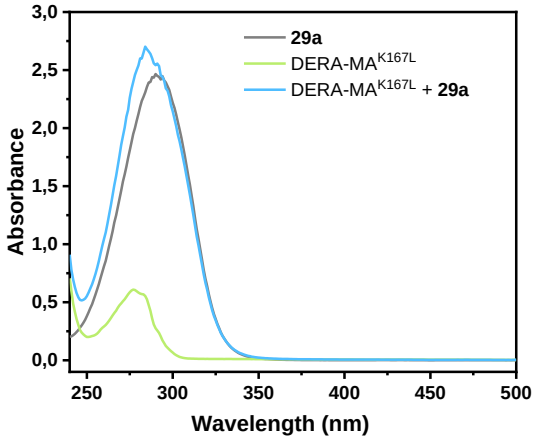

Figure 3.30. UV-Vis spectra of the DERA-MA^{K167L} and reagent **29a**, and a mixture of the two.

3.4.7.2 Light on/off experiment

We also conducted an experiment where the reaction was run for six hours alternating between one hour of light irradiation followed by half an hour in the dark. DERA-MA^{S18A} catalyzed the reaction upon exposure to purple light and stopped immediately after a shift to dark (Figure 3.31). These results demonstrate that the engineered DERA aldolase requires continuous light irradiation to perform the reaction and suggests it functions as a photodecarboxylase.

Entry	Light	Time (h)	Yield **35a** (%)
1	On	0-1	3.4
2	Off	1-1.5	3.2
3	On	1.5-2.5	7.1
4	Off	2.5-3	7.0
5	On	3-4	9.7
6	Off	4-4.5	10.0
7	On	4.5-5.5	12.8
8	Off	5.5-6	12.9

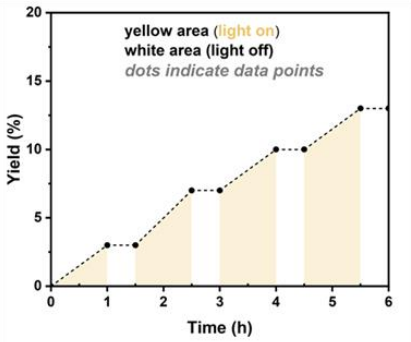

Figure 3.31. Effect of light irradiation on DERA-MA^{S18A} –catalyzed reaction of **29a** and **34a** during the first 6h. Yields were determined by GC-FID analysis using the response factor obtained for compound **35a**.

3.4.8 Mechanistic Proposal

Our proposed mechanism is depicted in Figure 3.32. The condensation of enal **29a** with the ε-amino group of K167 within the enzyme forms the ground-state iminium ion **XIX**. UV-Vis studies demonstrated that this iminium ion can absorb purple light (Figure 3.29), similar to the mechanism observed in small-molecule catalysis.[52] We hypothesize that the excited iminium ion acts as a strong oxidant, enabling SET to the carboxylate **36a**, thereby facilitating decarboxylation. Furthermore, X-ray crystallographic analysis provided clear evidence for the relative and absolute configuration of the syn-**37** products, confirming that the radical process resulted in an overall inversion of configuration at the stereocenter of the chiral carboxylic acid **36**. Leveraging these results and docking studies, Figure 3.32 illustrates a plausible mechanism for this 'memory of chirality' phenomenon. Based on docking studies with (*R*)-**36a**, we propose that specific π-π interactions between the iminium ion and the carboxylic acid, along with selective hydrogen bonding with S238, facilitate the close proximity of the two substrates within the active site. The excitation of iminium ion **XIX*** triggers SET oxidation of **36a**, leading to decarboxylation and the formation of the chiral benzyl radical **XXII**. The stereochemical integrity of **XXII** is maintained through specific interactions, including stabilization of the α-methyl group within the hydrophobic pocket formed by A18.

Overall, this network of weak interactions contributes to a proximity-driven, stereospecific radical coupling of **XXII** with the chiral 5π-enaminyl radical **XXI**, occurring faster than the racemization of the chiral radical.

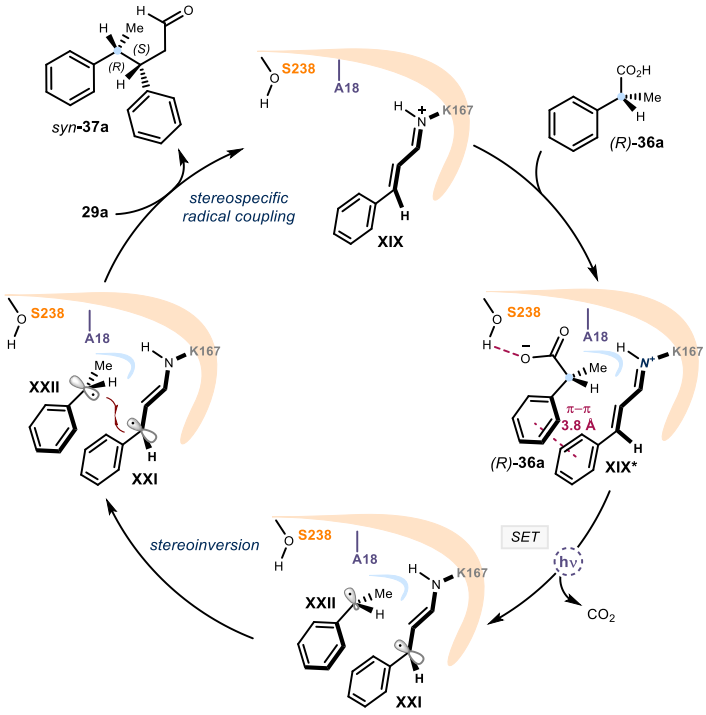

Figure 3.32. Proposed mechanism for the stereospecific radical coupling and observed stereoinversion.

We then performed another experiment to investigate the mechanism. To get evidence for the SET oxidation event, we tested whether the enzyme could also activate alkenoic acid **38** and give *anti*-Markovnikov product **39**, a product only obtained *via* radical pathway. Indeed, we observed the exclusive formation of the chiral γ-lactone **39** in 19% yield and full enantiocontrol. This result is consistent with the proposed radical mechanism enabled by our photoenzyme, as the polar pathway would lead to the Prins-type reactivity (Markovnikov product, Figure 3.33b).[70] This suggests that the radical cyclization of alkenoic acid **38** leads to the formation of radical **XXIII** (Figure 3.33a). This can be initiated by either SET oxidation of the carboxylate or the alkene within substrate **39** (Figure 3.33c).[71]

[70] Hamilton, D. S., Nicewicz, D. A. "Direct catalytic anti-Markovnikov hydroetherification of alkenols" *J. Am. Chem. Soc.* **2012**, *134*, 18577–18580.

[71] Bonilla, P., Rey, Y. P., Holden, C. M., Melchiorre, P. "Photo-Organocatalytic Enantioselective Radical Cascade Reactions of Unactivated Olefins" *Angew. Chem., Int. Ed.* **2018**, *57*, 12819–12823.

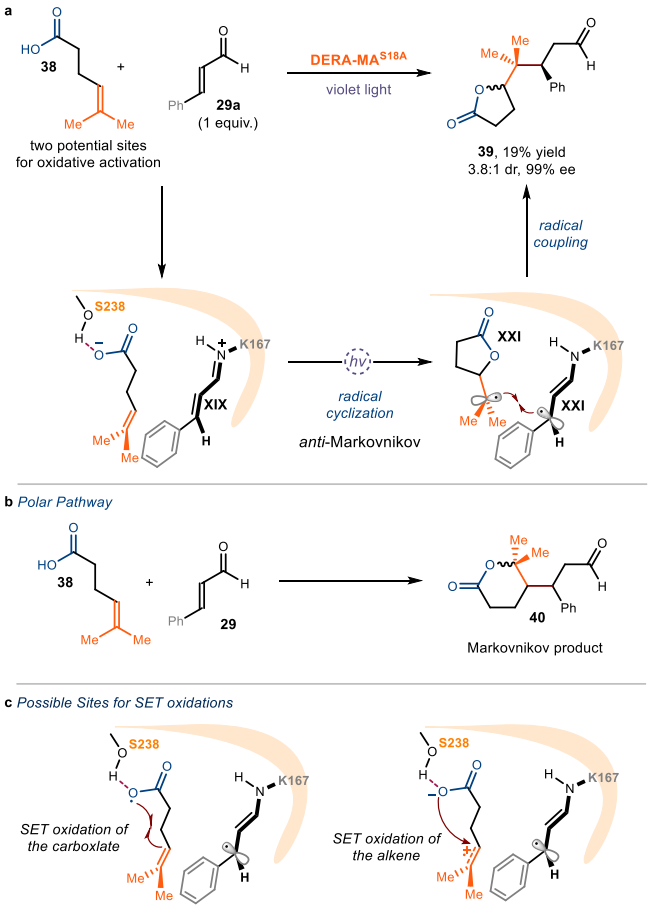

Figure 3.33. a) Proposed radical mechanism for the SET-oxidation of alkenoic acid **38** b) polar cyclization pathway: Markovnikov product **40**. c) possible SET oxidation sites of **38**.

3.4.9 Enzyme Deactivation - Photo-deactivation

The observed low turnover numbers prompted us to investigate the enzyme's stability under light irradiation. This investigation aimed to elucidate if irreversible modifications of the enzyme could be responsible for enzyme deactivation during photocatalysis. Therefore, we contacted the research team of Dr. Andrea Gargano at the University of Amsterdam (UVA, the Netherlands), who is an expert in the field of size-exclusion chromatography (SEC) combined with native mass spectrometry (nMS) to characterize proteins in their native state.[72] SEC-MS analyses of our protein samples were conducted under native conditions before and after photoirradiation. The double mutant DERA-MA$^{S18A/T203A}$ was measured before irradiation, and the deconvoluted mass was found to be 28,451.7 Da (Table 3.6, entry 1, and Figure 3.34a below), in accordance with the calculated mass of 28,452.46 Da for the enzyme (after cleavage of *N*-terminal methionine). The formula below calculates the error range of

the molecular weight obtained by the MS measurement. With this formula, we calculated the error at 26.7 ppm, which is within the error of the method used (50 ppm), confirming the reliability of the measurements.[28]

$$(Theoritical\ MW - Measured\ MW \div Theoritical\ MW) \times 10^6$$

Initially, we confirmed that light irradiation had no effect on the enzyme's mass (Table 3.6, entry 2, and Figure 3.34c), indicating the photostability of our enzyme. We then performed the model reaction of cinnamaldehyde **29a** and acid (*R*)-**36a** under light irradiation for 18 hours (entry 3 and Figure 3.34b). The soluble protein was analyzed by SEC-MS. Notably, in both samples, the observed mass of the major peak increased by 220 Da. We then performed control experiments to understand the origin of this protein change (entries 4-6). All control reactions did not result in a change in the observed protein mass, showing that the modification occurs only under light irradiation and in the presence of both substrates **29a** and (*R*)-**36a**. For example, when only cinnamaldehyde **29a** was present in the reaction mixture (Table 3.6, entry 4), we observed no change in mass, indicating no enzyme modifications. The same result was observed for the control reaction in the dark containing both **29a** and **36a** (entry 6 and Figure 3.34d). These latter experiments also indicated that we could not detect the formation of iminium ions bound in the active site, likely due to the reversible binding of cinnamaldehyde **29a** with lysine K167.

Table 3.6. Samples measured by SEC-MS.

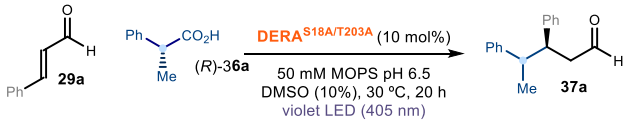

Entry	Enzyme	Light	CA	Acid	Time	Detected Mass [Da]	Mass difference[a]
1	+	-	-	-	0	28451.75	Reference
2	+	+	-	-	18	28451.97	0
3	+	+	+	+	18	28671.86	220.11
4	+	+	+	-	18	28451.98	0
5	+	+	-	+	18	28451.53	0
6	+	-	+	+	18	28451.82	0

[72] Ventouri, I. K., Veelders, S., Passamonti, M., Endres, P., R. Roemling, R., Schoenmakers, P. J., Somsen, G. W., Haselberg, R., Gargano, A. F. G. "Micro-flow size-exclusion chromatography for enhanced native mass spectrometry of proteins and protein complexes" *Anal. Chim. Acta* **2023**, *1266*, 341324.

a) Enzyme- entry 1

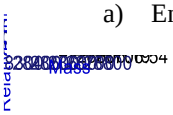

b) Photoenzymatic reaction after 18h- entry 3

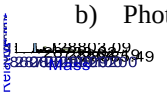

c) Enzyme after irradiation with **29a**- entry 4

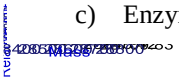

d) Enzymatic reaction after 18h in the dark- entry 6

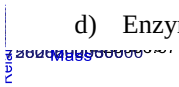

Figure 3.34. SEC-MS spectra of a) DERA-MA$^{S18A/T203A}$, b) the photoenzymatic reaction with both **29a** and (*R*)-**36a** after 18h, c) DERA-MA$^{S18A/T203A}$ with **29a** after light irradiation for 18h, and d) the control reaction in the dark containing enzyme, **29a** and (*R*)-**36a** after 18h.

The observed mass increase of 220 (Figure 3.34, Table 3.6, entry 2) is in accordance to the expected increase after 1,2- or 1,4-addition of the benzylic radical to the iminium ion. However, the latter scenario would lead to the formation of an imine product bound to lysine K167 (Figure 3.35, path A). This path is however unlikely given that previous SEC-MS analyses in the presence of **29a** (entry 4 and entry 6) did not show any mass corresponding to the imine (whose reversible formation cannot be tracked by MS analysis).

These studies are therefore consistent with a radical 1,2-addition to the iminium ion leading to the irreversible modification of the catalytic lysine, forming an amine (Figure 3.35, path B). To further validate this conclusion, we conducted another experiment where, after 18 hours, we added an aliquot of additional cinnamaldehyde **29a**. An exchange of a possible imine product with **29a** would be operational. The measured mass of the enzyme remained at 28,672 Da, further confirming an irreversible modification via 1,2 radical addition leading to an amine product.

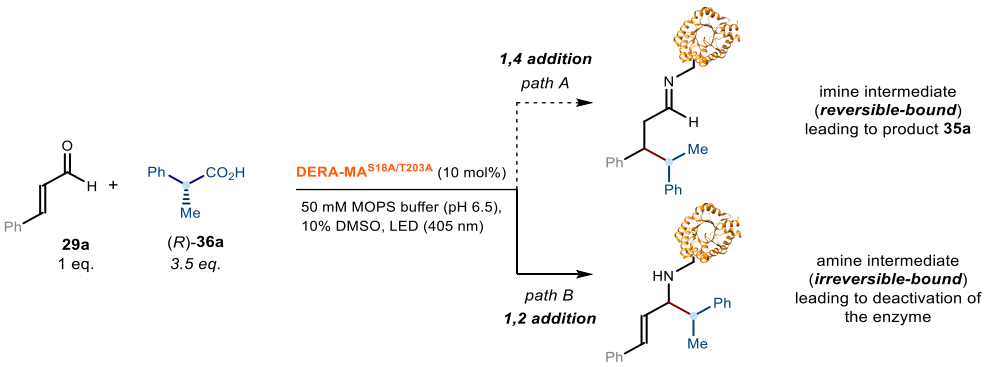

Figure 3.35. Possible pathways leading to the mass increase detected by SEC-MS analyses.

3.5 Conclusion

In summary, this study presents a novel strategy for designing a non-natural photodecarboxylase. It leverages the direct excitation of enzyme-bound iminium ion intermediates, enabling a stereospecific radical coupling reaction through a unique photoactivation mechanism. We used visible light to directly excite the enzyme-bound iminium ion intermediate. This intermediate enabled the SET oxidation of a carboxylic acid, followed by decarboxylation and subsequent radical coupling. In this strategy, we used abundant carboxylic acids as radical precursors. The system enabled full enantiocontrol over the bond forming step, delivering enantiopure β-substituted aldehydes. Furthermore, by employing chiral carboxylic acids as radical precursors, two stereocenters were generated with good to excellent diastereocontrol. By introducing modification in the active site, we could stabilize the chiral carboxylic acids through several weak interactions within the binding pocket, thus preventing racemization of the transient chiral radical. This system preserved the stereochemical information of the sp^3-hybridized radical, allowing for a stereospecific cross-coupling to take place with absolute and relative stereocontrol. Depending on the choice of enantiomer of the radical precursor, the desired diastereomeric product could be selectively accessed at will. Our photobiocatalytic system provided a case of 'memory of chirality',[67] which is a rarity in the context of asymmetric radical chemistry.

3.6 Experimental section

3.6.1 General information

The NMR spectra were recorded at 300 MHz, 400 MHz, and 500 MHz for ^{1}H, at 75 MHz, 101 MHz and 125 MHz for ^{13}C, at 376 MHz for $^{19}F\{1H\}$. The chemical shifts (δ) for ^{1}H and ^{13}C are given in ppm relative to residual signals of the solvents ($CHCl_3$ @ 7.26 ppm ^{1}H NMR, 77.16 ppm ^{13}C NMR). Coupling constants (*J*) are given in Hz, and are quoted to the nearest 0.5 Hz. The following abbreviations are used to indicate the multiplicity: s, singlet; d, doublet; t, triplet; q, quartet; sext, sextet; m, multiplet. Additionally, signals can be described as broad (br) and apparent (app).

High-resolution mass spectra (HRMS) were obtained from the ICIQ High Resolution Mass Spectrometry Unit on MicroTOF Focus and Maxis Impact (Bruker Daltonics) with electrospray ionization. Optical rotations were measured on a Polarimeter Jasco P-1030 and are reported as follows: $[\alpha]_D^T$ (c in g per 100 mL, solvent).

Cell growing and enzyme expression were performed in a standard INFORS-HT multitron incubator with an orbital of 50 mm. Cells lysis was performed with a Thermo Fisher ultrasonicator 120 W. Centrifugation was performed with a Thermo Fisher SORVALL ST16R centrifuge equipped with different rotors. When applicable, enzyme concentration was determined using a Nanodrop™ One from Thermo Fisher Scientific. PCR reactions were performed using MiniAmp thermal cycler from applied biosystems. The optical density (OD) was measured in a Cell Density Meter Model 40 from Thermo Fisher. LB broth was sterilized with a 75 L Autoclave Sterilmatic (AE-75-DRY) from Thermo Fisher. Mini-PROTEAN™ SDS-Acrylamide Electrophoresis equipment was purchased from BIO-RAD.

The authors are indebted to the team of the Research Support Area at ICIQ.

Determination of the Yield and the Diastereomeric Ratio: GC-FID analyses were performed on an Agilent 7890A GC using HP5 column. GC-FID traces of the performed enzymatic analytical scale reactions were compared to the synthesized reference samples of products **35** and **37** (see *section 3.7.5* for the preparation of reference compounds). Yields and diastereomeric ratios were determined using the corresponding response factor (see section I.2 and I.3). The reactions were analyzed using the following conditions: HP5-column 30m x 0.25mm x 0.25µm, constant pressure: 16.4 psi, split ratio: 40:1, T injector: 250 °C. Temperature Program: T initial 50 °C, hold 5 min, gradient 20 °C/min up to 325 °C; hold 5 min.

Determination of Enantiomeric Purity: UPC^2 analyses on chiral stationary phase were performed on a Waters ACQUITY® UPC^2 instrument, using Daicel Chiralpak IC-3, IB-3, IE-3 or IA-3 chiral columns. The exact conditions for the analysis of compounds **35** and **37** are specified within the characterization section. UPC^2 traces were compared to racemic samples

for each diastereomer of compounds **37**, which were prepared by running the reactions under the conditions specified in *Chapter 3.7.5.* Each sample was derivatized before analysis according to following procedure: 25 µL of a stock solution of 2,4-ninitrophenylhydrazin (50 mM) in DMSO and 5 µL of concentrated HCl were added to the extracted analytical scale reaction. The mixture was incubated for 10 min at room temperature under constant shaking (300 rpm) with the orbital shaker. After the incubation period the samples were dried and filtered and analyzed by UPC^2.

Materials

HisTrap™ HP chromatography columns for enzyme purification were purchased from Cytiva. HiTrap™ DEAE FF columns for ion exchange chromatography were purchased from GE Healthcare. PD-10 columns containing Sephadex™ G-25 M for buffer exchange were purchased from Cytiva. LB Broth powder was purchased from Nzytech. Customized genes encoding for the enzymes used in this study were purchased from GenScript. Competent cells BL21(DE3), Monarch plasmid miniprep kit, and Q5 site directed mutagenesis kit were purchased from New England BioLabs$_{Inc}$. QuikChange II-E site-directed mutagenesis Kit was purchased from Agilent. Customized primers were purchased from Biomers. Coomassie R250 powder was purchased from BIO-RAD. Protein ladders and standard markers were purchased from BIO-RAD. Commercial grade reagents and solvents were purchased at the highest commercial quality from Sigma Aldrich or Alfa Aesar and used as received, unless otherwise stated. Cinnamaldehyde **29a** was purchased from Sigma Aldrich, distilled prior to use and stored in a closed vial under argon at -20 ºC. Substrates **29d, 29e**, **34a-i** and chiral acid **36a** were purchased from TCI, Alfa Aesar and Sigma Aldrich, respectively, and used as received. The synthetic procedures for the preparation of substrates **36**, **45** and **46** are reported in *Chapter 3.7* of the Supplementary Information. The synthetic procedures for the preparation of reference products **35** and **37** are reported in *Chapter 3.7.5* of the Supplementary Information.

3.6.2 Mutagenesis Procedures

The DERA-MA variants were obtained by site-directed mutagenesis using either the QuickChange II site-directed mutagenesis kit (Agilent Technologies), according to the procedure A below, or the Q5 site-directed mutagenesis kit (NEB), according to procedure B below. For both procedures the following DNA template (pET26b containing DERA-MA sequence shown in bold) was used after extraction from BL21DE3 *E.coli* cells using the Monarch plasmid miniprep kit (NEB) according to manufacturer´s instructions.

The primers used are shown in Supplementary **Table 3.7**.

Sequences obtain after mutagenesis procedures are shown in **Table 3.8**.

DNA sequence of the pET26b containing DERA-MA:

TGGCGAATGGGACGCGCCCTGTAGCGGCGCATTAAGCGCGGCGGGTGTGGTGGTTACGCGCAGCGTGA
CCGCTACACTTGCCAGCGCCCTAGCGCCCGCTCCTTTCGCTTTCTTCCCTTCCTTTCTCGCCACGTTC
GCCGGCTTTCCCCGTCAAGCTCTAAATCGGGGGCTCCCTTTAGGGTTCCGATTTAGTGCTTTACGGCA
CCTCGACCCCAAAAAACTTGATTAGGGTGATGGTTCACGTAGTGGGCCATCGCCCTGATAGACGGTTT
TTCGCCCTTTGACGTTGGAGTCCACGTTCTTTAATAGTGGACTCTTGTTCCAAACTGGAACAACACTC
AACCCTATCTCGGTCTATTCTTTTGATTTATAAGGGATTTTGCCGATTTCGGCCTATTGGTTAAAAAA
TGAGCTGATTTAACAAAAATTTAACGCGAATTTTAACAAAATATTAACGTTTACAATTTCAGGTGGCA
CTTTTCGGGGAAATGTGCGCGGAACCCCTATTTGTTTATTTTTCTAAATACATTCAAATATGTATCCG
CTCATGAATTAATTCTTAGAAAAACTCATCGAGCATCAAATGAAACTGCAATTTATTCATATCAGGAT
TATCAATACCATATTTTTGAAAAAGCCGTTTCTGTAATGAAGGAGAAAACTCACCGAGGCAGTTCCAT
AGGATGGCAAGATCCTGGTATCGGTCTGCGATTCCGACTCGTCCAACATCAATACAACCTATTAATTT
CCCCTCGTCAAAAATAAGGTTATCAAGTGAGAAATCACCATGAGTGACGACTGAATCCGGTGAGAATG
GCAAAAGTTTATGCATTTCTTTCCAGACTTGTTCAACAGGCCAGCCATTACGCTCGTCATCAAAATCA
CTCGCATCAACCAAACCGTTATTCATTCGTGATTGCGCCTGAGCGAGACGAAATACGCGATCGCTGTT
AAAAGGACAATTACAAACAGGAATCGAATGCAACCGGCGCAGGAACACTGCCAGCGCATCAACAATAT
TTTCACCTGAATCAGGATATTCTTCTAATACCTGGAATGCTGTTTTCCCGGGGATCGCAGTGGTGAGT
AACCATGCATCATCAGGAGTACGGATAAAATGCTTGATGGTCGGAAGAGGCATAAATTCCGTCAGCCA
GTTTAGTCTGACCATCTCATCTGTAACATCATTGGCAACGCTACCTTTGCCATGTTTCAGAAACAACT
CTGGCGCATCGGGCTTCCCATACAATCGATAGATTGTCGCACCTGATTGCCCGACATTATCGCGAGCC
CATTTATACCCATATAAATCAGCATCCATGTTGGAATTTAATCGCGGCCTAGAGCAAGACGTTTCCCG
TTGAATATGGCTCATAACACCCCTTGTATTACTGTTTATGTAAGCAGACAGTTTTATTGTTCATGACC
AAAATCCCTTAACGTGAGTTTTCGTTCCACTGAGCGTCAGACCCCGTAGAAAAGATCAAAGGATCTTC
TTGAGATCCTTTTTTTCTGCGCGTAATCTGCTGCTTGCAAACAAAAAAACCACCGCTACCAGCGGTGG
TTTGTTTGCCGGATCAAGAGCTACCAACTCTTTTTCCGAAGGTAACTGGCTTCAGCAGAGCGCAGATA
CCAAATACTGTCCTTCTAGTGTAGCCGTAGTTAGGCCACCACTTCAAGAACTCTGTAGCACCGCCTAC
ATACCTCGCTCTGCTAATCCTGTTACCAGTGGCTGCTGCCAGTGGCGATAAGTCGTGTCTTACCGGGT
TGGACTCAAGACGATAGTTACCGGATAAGGCGCAGCGGTCGGGCTGAACGGGGGGTTCGTGCACACAG
CCCAGCTTGGAGCGAACGACCTACACCGAACTGAGATACCTACAGCGTGAGCTATGAGAAAGCGCCAC
GCTTCCCGAAGGGAGAAAGGCGGACAGGTATCCGGTAAGCGGCAGGGTCGGAACAGGAGAGCGCACGA
GGGAGCTTCCAGGGGGAAACGCCTGGTATCTTTATAGTCCTGTCGGGTTTCGCCACCTCTGACTTGAG
CGTCGATTTTTGTGATGCTCGTCAGGGGGGCGGAGCCTATGGAAAAACGCCAGCAACGCGGCCTTTTT
ACGGTTCCTGGCCTTTTGCTGGCCTTTTGCTCACATGTTCTTTCCTGCGTTATCCCCTGATTCTGTGG
ATAACCGTATTACCGCCTTTGAGTGAGCTGATACCGCTCGCCGCAGCCGAACGACCGAGCGCAGCGAG
TCAGTGAGCGAGGAAGCGGAAGAGCGCCTGATGCGGTATTTTCTCCTTACGCATCTGTGCGGTATTTC
ACACCGCATATATGGTGCACTCTCAGTACAATCTGCTCTGATGCCGCATAGTTAAGCCAGTATACACT
CCGCTATCGCTACGTGACTGGGTCATGGCTGCGCCCCGACACCCGCCAACACCCGCTGACGCGCCCTG
ACGGGCTTGTCTGCTCCCGGCATCCGCTTACAGACAAGCTGTGACCGTCTCCGGGAGCTGCATGTGTC
AGAGGTTTTCACCGTCATCACCGAAACGCGCGAGGCAGCTGCGGTAAAGCTCATCAGCGTGGTCGTGA
AGCGATTCACAGATGTCTGCCTGTTCATCCGCGTCCAGCTCGTTGAGTTTCTCCAGAAGCGTTAATGT
CTGGCTTCTGATAAAGCGGGCCATGTTAAGGGCGGTTTTTTCCTGTTTGGTCACTGATGCCTCCGTGT
AAGGGGGATTTCTGTTCATGGGGGTAATGATACCGATGAAACGAGAGAGGATGCTCACGATACGGGTT
ACTGATGATGAACATGCCCGGTTACTGGAACGTTGTGAGGGTAAACAACTGGCGGTATGGATGCGGCG
GGACCAGAGAAAAATCACTCAGGGTCAATGCCAGCGCTTCGTTAATACAGATGTAGGTGTTCCACAGG
GTAGCCAGCAGCATCCTGCGATGCAGATCCGGAACATAATGGTGCAGGGCGCTGACTTCCGCGTTTCC
AGACTTTACGAAACACGGAAACCGAAGACCATTCATGTTGTTGCTCAGGTCGCAGACGTTTTGCAGCA
GCAGTCGCTTCACGTTCGCTCGCGTATCGGTGATTCATTCTGCTAACCAGTAAGGCAACCCCGCCAGC
CTAGCCGGGTCCTCAACGACAGGAGCACGATCATGCGCACCCGTGGGGCCGCCATGCCGGCGATAATG
GCCTGCTTCTCGCCGAAACGTTTGGTGGCGGGACCAGTGACGAAGGCTTGAGCGAGGGCGTGCAAGAT
TCCGAATACCGCAAGCGACAGGCCGATCATCGTCGCGCTCCAGCGAAAGCGGTCCTCGCCGAAAATGA
CCCAGAGCGCTGCCGGCACCTGTCCTACGAGTTGCATGATAAAGAAGACAGTCATAAGTGCGGCGACG
ATAGTCATGCCCCGCGCCCACCGGAAGGAGCTGACTGGGTTGAAGGCTCTCAAGGGCATCGGTCGAGA

TCCCGGTGCCTAATGAGTGAGCTAACTTACATTAATTGCGTTGCGCTCACTGCCCGCTTTCCAGTCGG
GAAACCTGTCGTGCCAGCTGCATTAATGAATCGGCCAACGCGCGGGGAGAGGCGGTTTGCGTATTGGG
CGCCAGGGTGGTTTTTCTTTTCACCAGTGAGACGGGCAACAGCTGATTGCCCTTCACCGCCTGGCCCT
GAGAGAGTTGCAGCAAGCGGTCCACGCTGGTTTGCCCCAGCAGGCGAAAATCCTGTTTGATGGTGGTT
AACGGCGGGATATAACATGAGCTGTCTTCGGTATCGTCGTATCCCACTACCGAGATATCCGCACCAAC
GCGCAGCCCGGACTCGGTAATGGCGCGCATTGCGCCCAGCGCCATCTGATCGTTGGCAACCAGCATCG
CAGTGGGAACGATGCCCTCATTCAGCATTTGCATGGTTTGTTGAAAACCGGACATGGCACTCCAGTCG
CCTTCCCGTTCCGCTATCGGCTGAATTTGATTGCGAGTGAGATATTTATGCCAGCCAGCCAGACGCAG
ACGCGCCGAGACAGAACTTAATGGGCCCGCTAACAGCGCGATTTGCTGGTGACCCAATGCGACCAGAT
GCTCCACGCCCAGTCGCGTACCGTCTTCATGGGAGAAAATAATACTGTTGATGGGTGTCTGGTCAGAG
ACATCAAGAAATAACGCCGGAACATTAGTGCAGGCAGCTTCCACAGCAATGGCATCCTGGTCATCCAG
CGGATAGTTAATGATCAGCCCACTGACGCGTTGCGCGAGAAGATTGTGCACCGCCGCTTTACAGGCTT
CGACGCCGCTTCGTTCTACCATCGACACCACCACGCTGGCACCCAGTTGATCGGCGCGAGATTTAATC
GCCGCGACAATTTGCGACGGCGCGTGCAGGGCCAGACTGGAGGTGGCAACGCCAATCAGCAACGACTG
TTTGCCCGCCAGTTGTTGTGCCACGCGGTTGGGAATGTAATTCAGCTCCGCCATCGCCGCTTCCACTT
TTTCCCGCGTTTTCGCAGAAACGTGGCTGGCCTGGTTCACCACGCGGGAAACGGTCTGATAAGAGACA
CCGGCATACTCTGCGACATCGTATAACGTTACTGGTTTCACATTCACCACCCTGAATTGACTCTCTTC
CGGGCGCTATCATGCCATACCGCGAAAGGTTTTGCGCCATTCGATGGTGTCCGGGATCTCGACGCTCT
CCCTTATGCGACTCCTGCATTAGGAAGCAGCCCAGTAGTAGGTTGAGGCCGTTGAGCACCGCCGCCGC
AAGGAATGGTGCATGCAAGGAGATGGCGCCCAACAGTCCCCCGGCCACGGGGCCTGCCACCATACCCA
CGCCGAAACAAGCGCTCATGAGCCCGAAGTGGCGAGCCCGATCTTCCCCATCGGTGATGTCGGCGATA
TAGGCGCCAGCAACCGCACCTGTGGCGCCGGTGATGCCGGCCACGATGCGTCCGGCGTAGAGGATCGA
GATCTCGATCCCGCGAAATTAATACGACTCACTATAGGGGAATTGTGAGCGGATAACAATTCCCCTCT
AGAAATAATTTTGTTTAACTTTAAGAAGGAGATATACAT**ATGACCGACCTGAAGGCGAGCAGCCTGCG**
TGCGCTGAAACTGATGGATCTGAGCACCCTGAACGGCGACTACACCGATGAGAAGGTTATCGCGCTGT
GCCACCAGGCGAAAACCCCGGTGGGTAACACCGCGGCGATCAGCATTTATCCGCGTAGCATCCCGATT
GCGCGTAAGACCCTGAAAGAGCAAGGCACCCCGGAAATCCGTATTGCGACCGTTACCAACTTCCCGCA
CGGTAACGACGATATCGACATTGCGCTGGCGGAAACCCGTGCGGCGATTGCGTACGGCGCGGACGAAG
TGGATGTGGTTTTCCCGTATCGTGCGCTGATGGCGGGCAACGAGCAGGTTGGTTTTGATCTGGTGAAG
GCGTGCAAAGAAGCGTGCGCGGCGGCGAACGTGCTGCTGAAGGTTATCATTGAGAGCGGTGAACTGAA
GGACGAGGCGCTGATCCGTAAAGCGAGCGAAATCAGCATTAAGGCGGGCGCGGATTTCATTAAAACCA
GCACCGGTCTGGTGGCGGTTAACGCGACCCCGGAGAGCGCGCGTATCATGATGGAAGTTATTCGTGAC
ATGGGCGTGGAAAAGAGCGTTGGTTTTAAAGTGACCGGTGGCGCGCGTACCGCGGAGGATGCGCAAAA
ATACCTGGCGATCGCGGATGAGCTGTTTGGTGCGGACTGGGCGGATGCGCGTCACTATCGTTTTGGTG
CGAGCGGTCTGCTGGCGAGCCTGCTGAAGGCGCTGGGTCACGGCGATGGTAAAAGCGCGAGCAGCTAC
CTCGAGCACCACCACCACCACCACTGAGATCCGGCTGCTAACAAAGCCCGAAAGGAAGCTGAGTTGGC
TGCTGCCACCGCTGAGCAATAACTAGCATAACCCCTTGGGGCCTCTAAACGGGTCTTGAGGGGTTTTT
TGCTGAAAGGAGGAACTATATCCGGAT

Procedure A:

Mutagenic primers (**Table 3.7**, 25 ng μL^{-1}) were used in PCR reactions (50 µL) using 25 ng of the template DNA, dNTP mix, *PfuUltra* HF DNA polymerase (2.5 U) and reaction buffer. PCR parameters were: 1 cycle for 35 seconds at 95 ˚C, following by 16 cycles, each one consisted of 30 seconds at 95 ˚C (denaturation), 1 minute at 55 ˚C (annealing) and 6 minutes at 68˚C (extension). After the PCR, the reactions were treated with DpnI enzyme (10 U) to remove the starting template, following by purification of the products with StrataClean resin provided by the kit. Next, 2 µL of the purified product were used to transform electrocompetent XL1 blue *E.coli* cells. In total, 100 µL of the transformation were plated intro LB-agar petri dishes containing kanamycin (50 µg mL^{-1}) and the next day single colonies

were picked. These colonies were used to inoculate LB medium overnight. The resulted overnight cultures were used for plasmid extraction and the mutations introduced were verified with sequencing. After the new sequence was confirmed, the plasmids were used to transform BL21(DE3) competent cells which were used for enzyme expression.

Procedure B:

Mutagenic primers (**Table 3.7**, 0.5 μM) were used in PCR reactions (25 μL) using 20 ng of the template DNA, and Q5 Hot Start High-Fidelity 2X Master Mix provided by the kit. PCR parameters were: 1 cycle for 30 seconds at 98 ˚C, following by 25 cycles, each one consisted of 10 seconds at 98 ˚C (denaturation), 30 seconds at Ta = Tm + 3 (annealing) and 3 minutes at 72˚C (extension). After the PCR the reactions were treated with Kinase, Ligase and DpnI (KLD) enzyme mix for circularization and template removal. Next, 5 μL of the purified product were used to transform competent BL21 (DE3) *E.coli* cells. In total, 100 μL of the transformation were plated intro LB-agar petri dishes containing kanamycin (50 μg mL^{-1}) and the next day single colonies were picked. These colonies were used to inoculate LB medium overnight. The resulted overnight cultures were used for plasmid extraction and for glycerol stock preparation. The mutations introduced were verified with sequencing and the glycerol stocks were used for enzyme expression.

Table 3.7. Primers used for construction of DERA-MA variants. Mutations introduced are shown in bold.

Mutations		**Primer Sequence**
S18A	F	GAAACTGATGGATCTG**gc**CACCCTGAACGGCGAC
	R	GTCGCCGTTCAGGGTG**gc**CAGATCCATCAGTTTC
S18G	F	GATGGATCTG**g**GCACCCTGAAC
	R	AGTTTCAGCGCACGCAGG
S18V	F	CTGAAACTGATGGATCTG**gt**CACCCTGAACGGCGACTA
	R	TAGTCGCCGTTCAGGGTG**ac**CAGATCCATCAGTTTCAG
S238A	F	TTTTGGTGCG**gc**CGGTCTGCTG
	R	CGATAGTGACGCGCATCC
Y49A	F	CACCGCGGCGATCAGCATT**gc**TCCGCGTAGC
	R	GCTACGCGGA**gc**AATGCTGATCGCCGCGGTG
K167L	F	GGATTTCATT**ctg**ACCAGCACCGG
	R	GCGCCCGCCTTAATG
L172A	F	CAGCACCGGT**gc**GGTGGCGGTT
	R	GTTTTAATGAAATCCGCGCCC
T203A	F	TTTTAAAGTG**g**CCGGTGGCGC
	R	CCAACGCTCTTTTCCACG
T203V	F	TTTTAAAGTG**gt**CGGTGGCGCG
	R	CCAACGCTCTTTTCCACG
T203L	F	TTTTAAAGTG**ct**CGGTGGCGCG
	R	CCAACGCTCTTTTCCACG

T203I	F	TTTTAAAGTG**at**CGGTGGCGCG
	R	CCAACGCTCTTTTCCACG
Saturation T203	F	TTTTAAAGTG**nnk**GGTGGCGCGCG
	R	CCAACGCTCTTTTCCACG

Table 3.8. The amino acid and DNA sequences of the enzymes used in this study. Mutations in relation to the parental enzyme DERA-MA are shown in bold.

Enzyme	Amino acid sequence
DERA-MA	MTDLKASSLRALKLMDLSTLNGDYTDEKVIALCHQAKTPVGNTAAISIYPRSIP IARKTLKEQGTPEIRIATVTNFPHGNDDIDIALAETRAAIAYGADEVDVVFPYR ALMAGNEQVGFDLVKACKEACAAANVLLKVIIESGELKDEALIRKASEISIKAG ADFIKTSTGLVAVNATPESARIMMEVIRDMGVEKSVGFKVTGGARTAEDAQKYL AIADELFGADWADARHYRFGASGLLASLLKALGHGDGKSASSYLEHHHHHH
	ATGACCGACCTGAAGGCGAGCAGCCTGCGTGCGCTGAAACTGATGGATCTGAGC ACCCTGAACGGCGACTACACCGATGAGAAGGTTATCGCGCTGTGCCACCAGGCG AAAACCCCGGTGGGTAACACCGCGGCGATCAGCATTTATCCGCGTAGCATCCCG ATTGCGCGTAAGACCCTGAAAGAGCAAGGCACCCCGGAAATCCGTATTGCGACC GTTACCAACTTCCCGCACGGTAACGACGATATCGACATTGCGCTGGCGGAAACC CGTGCGGCGATTGCGTACGGCGCGGACGAAGTGGATGTGGTTTTCCCGTATCGT GCGCTGATGGCGGGCAACGAGCAGGTTGGTTTTGATCTGGTGAAGGCGTGCAAA GAAGCGTGCGCGGCGGCGAACGTGCTGCTGAAGGTTATCATTGAGAGCGGTGAA CTGAAGGACGAGGCGCTGATCCGTAAAGCGAGCGAAATCAGCATTAAGGCGGGC GCGGATTTCATTAAAACCAGCACCGGTCTGGTGGCGGTTAACGCGACCCCGGAG AGCGCGCGTATCATGATGGAAGTTATTCGTGACATGGGCGTGGAAAAGAGCGTT GGTTTTAAAGTGACCGGTGGCGCGCGTACCGCGGAGGATGCGCAAAAATACCTG GCGATCGCGGATGAGCTGTTTGGTGCGGACTGGGCGGATGCGCGTCACTATCGT TTTGGTGCGAGCGGTCTGCTGGCGAGCCTGCTGAAGGCGCTGGGTCACGGCGAT GGTAAAAGCGCGAGCAGCTACCTCGAGCACCACCACCACCACCAC
DERA-MA^{S18A}	MTDLKASSLRALKLMDL**A**TLNGDYTDEKVIALCHQAKTPVGNTAAISIYPRSIP IARKTLKEQGTPEIRIATVTNFPHGNDDIDIALAETRAAIAYGADEVDVVFPYR ALMAGNEQVGFDLVKACKEACAAANVLLKVIIESGELKDEALIRKASEISIKAG ADFIKTSTGLVAVNATPESARIMMEVIRDMGVEKSVGFKVTGGARTAEDAQKYL AIADELFGADWADARHYRFGASGLLASLLKALGHGDGKSASSYLEHHHHHH
	ATGACCGACCTGAAGGCGAGCAGCCTGCGTGCGCTGAAACTGATGGATCTG**GCC** ACCCTGAACGGCGACTACACCGATGAGAAGGTTATCGCGCTGTGCCACCAGGCG AAAACCCCGGTGGGTAACACCGCGGCGATCAGCATTTATCCGCGTAGCATCCCG ATTGCGCGTAAGACCCTGAAAGAGCAAGGCACCCCGGAAATCCGTATTGCGACC GTTACCAACTTCCCGCACGGTAACGACGATATCGACATTGCGCTGGCGGAAACC CGTGCGGCGATTGCGTACGGCGCGGACGAAGTGGATGTGGTTTTCCCGTATCGT GCGCTGATGGCGGGCAACGAGCAGGTTGGTTTTGATCTGGTGAAGGCGTGCAAA GAAGCGTGCGCGGCGGCGAACGTGCTGCTGAAGGTTATCATTGAGAGCGGTGAA CTGAAGGACGAGGCGCTGATCCGTAAAGCGAGCGAAATCAGCATTAAGGCGGGC GCGGATTTCATTAAAACCAGCACCGGTCTGGTGGCGGTTAACGCGACCCCGGAG AGCGCGCGTATCATGATGGAAGTTATTCGTGACATGGGCGTGGAAAAGAGCGTT GGTTTTAAAGTGACCGGTGGCGCGCGTACCGCGGAGGATGCGCAAAAATACCTG GCGATCGCGGATGAGCTGTTTGGTGCGGACTGGGCGGATGCGCGTCACTATCGT TTTGGTGCGAGCGGTCTGCTGGCGAGCCTGCTGAAGGCGCTGGGTCACGGCGAT GGTAAAAGCGCGAGCAGCTACCTCGAGCACCACCACCACCACCAC
	MTDLKASSLRALKLMDL**G**TLNGDYTDEKVIALCHQAKTPVGNTAAISIYPRSIP IARKTLKEQGTPEIRIATVTNFPHGNDDIDIALAETRAAIAYGADEVDVVFPYR ALMAGNEQVGFDLVKACKEACAAANVLLKVIIESGELKDEALIRKASEISIKAG

DERA-MA^{S18G}	ADFIKTSTGLVAVNATPESARIMMEVIRDMGVEKSVGFKVTGGARTAEDAQKYL AIADELFGADWADARHYRFGASGLLASLLKALGHGDGKSASSYLEHHHHHH
	ATGACCGACCTGAAGGCGAGCAGCCTGCGTGCGCTGAAACTGATGGATCTG**GGC** ACCCTGAACGGCGACTACACCGATGAGAAGGTTATCGCGCTGTGCCACCAGGCG AAAACCCCGGTGGGTAACACCGCGGCGATCAGCATTTATCCGCGTAGCATCCCG ATTGCGCGTAAGACCCTGAAAGAGCAAGGCACCCCGGAAATCCGTATTGCGACC GTTACCAACTTCCCGCACGGTAACGACGATATCGACATTGCGCTGGCGGAAACC CGTGCGGCGATTGCGTACGGCGCGGACGAAGTGGATGTGGTTTTCCCGTATCGT GCGCTGATGGCGGGCAACGAGCAGGTTGGTTTTGATCTGGTGAAGGCGTGCAAA GAAGCGTGCGCGGCGGCGAACGTGCTGCTGAAGGTTATCATTGAGAGCGGTGAA CTGAAGGACGAGGCGCTGATCCGTAAAGCGAGCGAAATCAGCATTAAGGCGGGC GCGGATTTCATTAAAACCAGCACCGGTCTGGTGGCGGTTAACGCGACCCCGGAG AGCGCGCGTATCATGATGGAAGTTATTCGTGACATGGGCGTGGAAAAGAGCGTT GGTTTTAAAGTGACCGGTGGCGCGCGTACCGCGGAGGATGCGCAAAAATACCTG GCGATCGCGGATGAGCTGTTTGGTGCGGACTGGGCGGATGCGCGTCACTATCGT TTTGGTGCGAGCGGTCTGCTGGCGAGCCTGCTGAAGGCGCTGGGTCACGGCGAT GGTAAAAGCGCGAGCAGCTACCTCGAGCACCACCACCACCACCAC
DERA-MA^{S18V}	MTDLKASSLRALKLMDL**V**TLNGDYTDEKVIALCHQAKTPVGNTAAISIYPRSIP IARKTLKEQGTPEIRIATVTNFPHGNDDIDIALAETRAAIAYGADEVDVVFPYR ALMAGNEQVGFDLVKACKEACAAANVLLKVIIESGELKDEALIRKASEISIKAG ADFIKTSTGLVAVNATPESARIMMEVIRDMGVEKSVGFKVTGGARTAEDAQKYL AIADELFGADWADARHYRFGASGLLASLLKALGHGDGKSASSYLEHHHHHH
	ATGACCGACCTGAAGGCGAGCAGCCTGCGTGCGCTGAAACTGATGGATCTG**GTC** ACCCTGAACGGCGACTACACCGATGAGAAGGTTATCGCGCTGTGCCACCAGGCG AAAACCCCGGTGGGTAACACCGCGGCGATCAGCATTTATCCGCGTAGCATCCCG ATTGCGCGTAAGACCCTGAAAGAGCAAGGCACCCCGGAAATCCGTATTGCGACC GTTACCAACTTCCCGCACGGTAACGACGATATCGACATTGCGCTGGCGGAAACC CGTGCGGCGATTGCGTACGGCGCGGACGAAGTGGATGTGGTTTTCCCGTATCGT GCGCTGATGGCGGGCAACGAGCAGGTTGGTTTTGATCTGGTGAAGGCGTGCAAA GAAGCGTGCGCGGCGGCGAACGTGCTGCTGAAGGTTATCATTGAGAGCGGTGAA CTGAAGGACGAGGCGCTGATCCGTAAAGCGAGCGAAATCAGCATTAAGGCGGGC GCGGATTTCATTAAAACCAGCACCGGTCTGGTGGCGGTTAACGCGACCCCGGAG AGCGCGCGTATCATGATGGAAGTTATTCGTGACATGGGCGTGGAAAAGAGCGTT GGTTTTAAAGTGACCGGTGGCGCGCGTACCGCGGAGGATGCGCAAAAATACCTG GCGATCGCGGATGAGCTGTTTGGTGCGGACTGGGCGGATGCGCGTCACTATCGT TTTGGTGCGAGCGGTCTGCTGGCGAGCCTGCTGAAGGCGCTGGGTCACGGCGAT GGTAAAAGCGCGAGCAGCTACCTCGAGCACCACCACCACCACCAC
DERA-MA^{S238A}	MTDLKASSLRALKLMDLSTLNGDYTDEKVIALCHQAKTPVGNTAAISIYPRSIP IARKTLKEQGTPEIRIATVTNFPHGNDDIDIALAETRAAIAYGADEVDVVFPYR ALMAGNEQVGFDLVKACKEACAAANVLLKVIIESGELKDEALIRKASEISIKAG ADFIKTSTGLVAVNATPESARIMMEVIRDMGVEKSVGFKVTGGARTAEDAQKYL AIADELFGADWADARHYRFGA**A**GLLASLLKALGHGDGKSASSYLEHHHHHH
	ATGACCGACCTGAAGGCGAGCAGCCTGCGTGCGCTGAAACTGATGGATCTGAGC ACCCTGAACGGCGACTACACCGATGAGAAGGTTATCGCGCTGTGCCACCAGGCG AAAACCCCGGTGGGTAACACCGCGGCGATCAGCATTTATCCGCGTAGCATCCCG ATTGCGCGTAAGACCCTGAAAGAGCAAGGCACCCCGGAAATCCGTATTGCGACC GTTACCAACTTCCCGCACGGTAACGACGATATCGACATTGCGCTGGCGGAAACC CGTGCGGCGATTGCGTACGGCGCGGACGAAGTGGATGTGGTTTTCCCGTATCGT GCGCTGATGGCGGGCAACGAGCAGGTTGGTTTTGATCTGGTGAAGGCGTGCAAA GAAGCGTGCGCGGCGGCGAACGTGCTGCTGAAGGTTATCATTGAGAGCGGTGAA CTGAAGGACGAGGCGCTGATCCGTAAAGCGAGCGAAATCAGCATTAAGGCGGGC GCGGATTTCATTAAAACCAGCACCGGTCTGGTGGCGGTTAACGCGACCCCGGAG AGCGCGCGTATCATGATGGAAGTTATTCGTGACATGGGCGTGGAAAAGAGCGTT GGTTTTAAAGTGACCGGTGGCGCGCGTACCGCGGAGGATGCGCAAAAATACCTG GCGATCGCGGATGAGCTGTTTGGTGCGGACTGGGCGGATGCGCGTCACTATCGT

	TTTGGTGCG**GCC**GGTCTGCTGGCGAGCCTGCTGAAGGCGCTGGGTCACGGCGAT
	GGTAAAAGCGCGAGCAGCTACCTCGAGCACCACCACCACCACCAC
DERA-MA^{Y49A}	MTDLKASSLRALKLMDLSTLNGDYTDEKVIALCHQAKTPVGNTAAISI**A**PRSIP
	IARKTLKEQGTPEIRIATVTNFPHGNDDIDIALAETRAAIAYGADEVDVVFPYR
	ALMAGNEQVGFDLVKACKEACAAANVLLKVIIESGELKDEALIRKASEISIKAG
	ADFIKTSTGLVAVNATPESARIMMEVIRDMGVEKSVGFKVTGGARTAEDAQKYL
	AIADELFGADWADARHYRFGASGLLASLLKALGHGDGKSASSYLEHHHHHH
	ATGACCGACCTGAAGGCGAGCAGCCTGCGTGCGCTGAAACTGATGGATCTGAGC
	ACCCTGAACGGCGACTACACCGATGAGAAGGTTATCGCGCTGTGCCACCAGGCG
	AAAACCCCGGTGGGTAACACCGCGGCGATCAGCATT**GCT**CCGCGTAGCATCCCG
	ATTGCGCGTAAGACCCTGAAAGAGCAAGGCACCCCGGAAATCCGTATTGCGACC
	GTTACCAACTTCCCGCACGGTAACGACGATATCGACATTGCGCTGGCGGAAACC
	CGTGCGGCGATTGCGTACGGCGCGGACGAAGTGGATGTGGTTTTCCCGTATCGT
	GCGCTGATGGCGGGCAACGAGCAGGTTGGTTTTGATCTGGTGAAGGCGTGCAAA
	GAAGCGTGCGCGGCGGCGAACGTGCTGCTGAAGGTTATCATTGAGAGCGGTGAA
	CTGAAGGACGAGGCGCTGATCCGTAAAGCGAGCGAAATCAGCATTAAGGCGGGC
	GCGGATTTCATTAAAACCAGCACCGGTCTGGTGGCGGTTAACGCGACCCCGGAG
	AGCGCGCGTATCATGATGGAAGTTATTCGTGACATGGGCGTGGAAAAGAGCGTT
	GGTTTTAAAGTGACCGGTGGCGCGCGTACCGCGGAGGATGCGCAAAAATACCTG
	GCGATCGCGGATGAGCTGTTTGGTGCGGACTGGGCGGATGCGCGTCACTATCGT
	TTTGGTGCGAGCGGTCTGCTGGCGAGCCTGCTGAAGGCGCTGGGTCACGGCGAT
	GGTAAAAGCGCGAGCAGCTACCTCGAGCACCACCACCACCACCAC
DERA-MA^{L172A}	MTDLKASSLRALKLMDLSTLNGDYTDEKVIALCHQAKTPVGNTAAISIYPRSIP
	IARKTLKEQGTPEIRIATVTNFPHGNDDIDIALAETRAAIAYGADEVDVVFPYR
	ALMAGNEQVGFDLVKACKEACAAANVLLKVIIESGELKDEALIRKASEISIKAG
	ADFIKTSTG**A**VAVNATPESARIMMEVIRDMGVEKSVGFKVTGGARTAEDAQKYL
	AIADELFGADWADARHYRFGASGLLASLLKALGHGDGKSASSYLEHHHHHH
	ATGACCGACCTGAAGGCGAGCAGCCTGCGTGCGCTGAAACTGATGGATCTGAGC
	ACCCTGAACGGCGACTACACCGATGAGAAGGTTATCGCGCTGTGCCACCAGGCG
	AAAACCCCGGTGGGTAACACCGCGGCGATCAGCATTTATCCGCGTAGCATCCCG
	ATTGCGCGTAAGACCCTGAAAGAGCAAGGCACCCCGGAAATCCGTATTGCGACC
	GTTACCAACTTCCCGCACGGTAACGACGATATCGACATTGCGCTGGCGGAAACC
	CGTGCGGCGATTGCGTACGGCGCGGACGAAGTGGATGTGGTTTTCCCGTATCGT
	GCGCTGATGGCGGGCAACGAGCAGGTTGGTTTTGATCTGGTGAAGGCGTGCAAA
	GAAGCGTGCGCGGCGGCGAACGTGCTGCTGAAGGTTATCATTGAGAGCGGTGAA
	CTGAAGGACGAGGCGCTGATCCGTAAAGCGAGCGAAATCAGCATTAAGGCGGGC
	GCGGATTTCATTAAAACCAGCACCGGT**GCG**GTGGCGGTTAACGCGACCCCGGAG
	AGCGCGCGTATCATGATGGAAGTTATTCGTGACATGGGCGTGGAAAAGAGCGTT
	GGTTTTAAAGTGACCGGTGGCGCGCGTACCGCGGAGGATGCGCAAAAATACCTG
	GCGATCGCGGATGAGCTGTTTGGTGCGGACTGGGCGGATGCGCGTCACTATCGT
	TTTGGTGCGAGCGGTCTGCTGGCGAGCCTGCTGAAGGCGCTGGGTCACGGCGAT
	GGTAAAAGCGCGAGCAGCTACCTCGAGCACCACCACCACCACCAC
DERA-MA^{T203A}	MTDLKASSLRALKLMDLSTLNGDYTDEKVIALCHQAKTPVGNTAAISIYPRSIP
	IARKTLKEQGTPEIRIATVTNFPHGNDDIDIALAETRAAIAYGADEVDVVFPYR
	ALMAGNEQVGFDLVKACKEACAAANVLLKVIIESGELKDEALIRKASEISIKAG
	ADFIKTSTGLVAVNATPESARIMMEVIRDMGVEKSVGFKV**A**GGARTAEDAQKYL
	AIADELFGADWADARHYRFGASGLLASLLKALGHGDGKSASSYLEHHHHHH
	ATGACCGACCTGAAGGCGAGCAGCCTGCGTGCGCTGAAACTGATGGATCTGAGC
	ACCCTGAACGGCGACTACACCGATGAGAAGGTTATCGCGCTGTGCCACCAGGCG
	AAAACCCCGGTGGGTAACACCGCGGCGATCAGCATTTATCCGCGTAGCATCCCG
	ATTGCGCGTAAGACCCTGAAAGAGCAAGGCACCCCGGAAATCCGTATTGCGACC
	GTTACCAACTTCCCGCACGGTAACGACGATATCGACATTGCGCTGGCGGAAACC
	CGTGCGGCGATTGCGTACGGCGCGGACGAAGTGGATGTGGTTTTCCCGTATCGT
	GCGCTGATGGCGGGCAACGAGCAGGTTGGTTTTGATCTGGTGAAGGCGTGCAAA
	GAAGCGTGCGCGGCGGCGAACGTGCTGCTGAAGGTTATCATTGAGAGCGGTGAA
	CTGAAGGACGAGGCGCTGATCCGTAAAGCGAGCGAAATCAGCATTAAGGCGGGC

	GCGGATTTCATTAAAACCAGCACCGGTCTGGTGGCGGTTAACGCGACCCCGGAG AGCGCGCGTATCATGATGGAAGTTATTCGTGACATGGGCGTGGAAAAGAGCGTT GGTTTTAAAGTG**GCC**GGTGGCGCGCGTACCGCGGAGGATGCGCAAAAATACCTG GCGATCGCGGATGAGCTGTTTGGTGCGGACTGGGCGGATGCGCGTCACTATCGT TTTGGTGCGAGCGGTCTGCTGGCGAGCCTGCTGAAGGCGCTGGGTCACGGCGAT GGTAAAAGCGCGAGCAGCTACCTCGAGCACCACCACCACCACCAC
DERA-MA^{K167L}	MTDLKASSLRALKLMDLSTLNGDYTDEKVIALCHQAKTPVGNTAAISIYPRSIP IARKTLKEQGTPEIRIATVTNFPHGNDDIDIALAETRAAIAYGADEVDVVFPYR ALMAGNEQVGFDLVKACKEACAAANVLLKVIIESGELKDEALIRKASEISIKAG ADFI**L**TSTGLVAVNATPESARIMMEVIRDMGVEKSVGFKVTGGARTAEDAQKYL AIADELFGADWADARHYRFGASGLLASLLKALGHGDGKSASSYLEHHHHHH
	ATGACCGACCTGAAGGCGAGCAGCCTGCGTGCGCTGAAACTGATGGATCTGAGC ACCCTGAACGGCGACTACACCGATGAGAAGGTTATCGCGCTGTGCCACCAGGCG AAAACCCCGGTGGGTAACACCGCGGCGATCAGCATTTATCCGCGTAGCATCCCG ATTGCGCGTAAGACCCTGAAAGAGCAAGGCACCCCGGAAATCCGTATTGCGACC GTTACCAACTTCCCGCACGGTAACGACGATATCGACATTGCGCTGGCGGAAACC CGTGCGGCGATTGCGTACGGCGCGGACGAAGTGGATGTGGTTTTCCCGTATCGT GCGCTGATGGCGGGCAACGAGCAGGTTGGTTTTGATCTGGTGAAGGCGTGCAAA GAAGCGTGCGCGGCGGCGAACGTGCTGCTGAAGGTTATCATTGAGAGCGGTGAA CTGAAGGACGAGGCGCTGATCCGTAAAGCGAGCGAAATCAGCATTAAGGCGGGC GCGGATTTCATT**CTG**ACCAGCACCGGTCTGGTGGCGGTTAACGCGACCCCGGAG AGCGCGCGTATCATGATGGAAGTTATTCGTGACATGGGCGTGGAAAAGAGCGTT GGTTTTAAAGTGACCGGTGGCGCGCGTACCGCGGAGGATGCGCAAAAATACCTG GCGATCGCGGATGAGCTGTTTGGTGCGGACTGGGCGGATGCGCGTCACTATCGT TTTGGTGCGAGCGGTCTGCTGGCGAGCCTGCTGAAGGCGCTGGGTCACGGCGAT GGTAAAAGCGCGAGCAGCTACCTCGAGCACCACCACCACCACCAC
DERA-MA$^{S18A/T203A}$	MTDLKASSLRALKLMDL**A**TLNGDYTDEKVIALCHQAKTPVGNTAAISIYPRSIP IARKTLKEQGTPEIRIATVTNFPHGNDDIDIALAETRAAIAYGADEVDVVFPYR ALMAGNEQVGFDLVKACKEACAAANVLLKVIIESGELKDEALIRKASEISIKAG ADFIKTSTGLVAVNATPESARIMMEVIRDMGVEKSVGFKV**A**GGARTAEDAQKYL AIADELFGADWADARHYRFGASGLLASLLKALGHGDGKSASSYLEHHHHHH
	ATGACCGACCTGAAGGCGAGCAGCCTGCGTGCGCTGAAACTGATGGATCTG**GCC** ACCCTGAACGGCGACTACACCGATGAGAAGGTTATCGCGCTGTGCCACCAGGCG AAAACCCCGGTGGGTAACACCGCGGCGATCAGCATTTATCCGCGTAGCATCCCG ATTGCGCGTAAGACCCTGAAAGAGCAAGGCACCCCGGAAATCCGTATTGCGACC GTTACCAACTTCCCGCACGGTAACGACGATATCGACATTGCGCTGGCGGAAACC CGTGCGGCGATTGCGTACGGCGCGGACGAAGTGGATGTGGTTTTCCCGTATCGT GCGCTGATGGCGGGCAACGAGCAGGTTGGTTTTGATCTGGTGAAGGCGTGCAAA GAAGCGTGCGCGGCGGCGAACGTGCTGCTGAAGGTTATCATTGAGAGCGGTGAA CTGAAGGACGAGGCGCTGATCCGTAAAGCGAGCGAAATCAGCATTAAGGCGGGC GCGGATTTCATTAAAACCAGCACCGGTCTGGTGGCGGTTAACGCGACCCCGGAG AGCGCGCGTATCATGATGGAAGTTATTCGTGACATGGGCGTGGAAAAGAGCGTT GGTTTTAAAGTG**GCC**GGTGGCGCGCGTACCGCGGAGGATGCGCAAAAATACCTG GCGATCGCGGATGAGCTGTTTGGTGCGGACTGGGCGGATGCGCGTCACTATCGT TTTGGTGCGAGCGGTCTGCTGGCGAGCCTGCTGAAGGCGCTGGGTCACGGCGAT GGTAAAAGCGCGAGCAGCTACCTCGAGCACCACCACCACCACCAC
DERA-MA$^{S18A/T203V}$	MTDLKASSLRALKLMDL**A**TLNGDYTDEKVIALCHQAKTPVGNTAAISIYPRSIP IARKTLKEQGTPEIRIATVTNFPHGNDDIDIALAETRAAIAYGADEVDVVFPYR ALMAGNEQVGFDLVKACKEACAAANVLLKVIIESGELKDEALIRKASEISIKAG ADFIKTSTGLVAVNATPESARIMMEVIRDMGVEKSVGFKV**V**GGARTAEDAQKYL AIADELFGADWADARHYRFGASGLLASLLKALGHGDGKSASSYLEHHHHHH
	ATGACCGACCTGAAGGCGAGCAGCCTGCGTGCGCTGAAACTGATGGATCTG**GCC** ACCCTGAACGGCGACTACACCGATGAGAAGGTTATCGCGCTGTGCCACCAGGCG AAAACCCCGGTGGGTAACACCGCGGCGATCAGCATTTATCCGCGTAGCATCCCG ATTGCGCGTAAGACCCTGAAAGAGCAAGGCACCCCGGAAATCCGTATTGCGACC GTTACCAACTTCCCGCACGGTAACGACGATATCGACATTGCGCTGGCGGAAACC

	CGTGCGGCGATTGCGTACGGCGCGGACGAAGTGGATGTGGTTTTCCCGTATCGT GCGCTGATGGCGGGCAACGAGCAGGTTGGTTTTGATCTGGTGAAGGCGTGCAAA GAAGCGTGCGCGGCGGCGAACGTGCTGCTGAAGGTTATCATTGAGAGCGGTGAA CTGAAGGACGAGGCGCTGATCCGTAAAGCGAGCGAAATCAGCATTAAGGCGGGC GCGGATTTCATTAAAACCAGCACCGGTCTGGTGGCGGTTAACGCGACCCCGGAG AGCGCGCGTATCATGATGGAAGTTATTCGTGACATGGGCGTGGAAAAGAGCGTT GGTTTTAAAGTG**GTC**GGTGGCGCGCGTACCGCGGAGGATGCGCAAAAATACCTG GCGATCGCGGATGAGCTGTTTGGTGCGGACTGGGCGGATGCGCGTCACTATCGT TTTGGTGCGAGCGGTCTGCTGGCGAGCCTGCTGAAGGCGCTGGGTCACGGCGAT GGTAAAAGCGCGAGCAGCTACCTCGAGCACCACCACCACCACCAC
DERA-MA$^{S18A/T203L}$	MTDLKASSLRALKLMDL**A**TLNGDYTDEKVIALCHQAKTPVGNTAAISIYPRSIP IARKTLKEQGTPEIRIATVTNFPHGNDDIDIALAETRAAIAYGADEVDVVFPYR ALMAGNEQVGFDLVKACKEACAAANVLLKVIIESGELKDEALIRKASEISIKAG ADFIKTSTGLVAVNATPESARIMMEVIRDMGVEKSVGFKV**L**GGARTAEDAQKYL AIADELFGADWADARHYRFGASGLLASLLKALGHGDGKSASSYLEHHHHHH
	ATGACCGACCTGAAGGCGAGCAGCCTGCGTGCGCTGAAACTGATGGATCTG**GCC** ACCCTGAACGGCGACTACACCGATGAGAAGGTTATCGCGCTGTGCCACCAGGCG AAAACCCCGGTGGGTAACACCGCGGCGATCAGCATTTATCCGCGTAGCATCCCG ATTGCGCGTAAGACCCTGAAAGAGCAAGGCACCCCGGAAATCCGTATTGCGACC GTTACCAACTTCCCGCACGGTAACGACGATATCGACATTGCGCTGGCGGAAACC CGTGCGGCGATTGCGTACGGCGCGGACGAAGTGGATGTGGTTTTCCCGTATCGT GCGCTGATGGCGGGCAACGAGCAGGTTGGTTTTGATCTGGTGAAGGCGTGCAAA GAAGCGTGCGCGGCGGCGAACGTGCTGCTGAAGGTTATCATTGAGAGCGGTGAA CTGAAGGACGAGGCGCTGATCCGTAAAGCGAGCGAAATCAGCATTAAGGCGGGC GCGGATTTCATTAAAACCAGCACCGGTCTGGTGGCGGTTAACGCGACCCCGGAG AGCGCGCGTATCATGATGGAAGTTATTCGTGACATGGGCGTGGAAAAGAGCGTT GGTTTTAAAGTG**CTC**GGTGGCGCGCGTACCGCGGAGGATGCGCAAAAATACCTG GCGATCGCGGATGAGCTGTTTGGTGCGGACTGGGCGGATGCGCGTCACTATCGT TTTGGTGCGAGCGGTCTGCTGGCGAGCCTGCTGAAGGCGCTGGGTCACGGCGAT GGTAAAAGCGCGAGCAGCTACCTCGAGCACCACCACCACCACCAC
DERA-MA$^{S18A/T203I}$	MTDLKASSLRALKLMDL**A**TLNGDYTDEKVIALCHQAKTPVGNTAAISIYPRSIP IARKTLKEQGTPEIRIATVTNFPHGNDDIDIALAETRAAIAYGADEVDVVFPYR ALMAGNEQVGFDLVKACKEACAAANVLLKVIIESGELKDEALIRKASEISIKAG ADFIKTSTGLVAVNATPESARIMMEVIRDMGVEKSVGFKV**I**GGARTAEDAQKYL AIADELFGADWADARHYRFGASGLLASLLKALGHGDGKSASSYLEHHHHHH
	ATGACCGACCTGAAGGCGAGCAGCCTGCGTGCGCTGAAACTGATGGATCTG**GCC** ACCCTGAACGGCGACTACACCGATGAGAAGGTTATCGCGCTGTGCCACCAGGCG AAAACCCCGGTGGGTAACACCGCGGCGATCAGCATTTATCCGCGTAGCATCCCG ATTGCGCGTAAGACCCTGAAAGAGCAAGGCACCCCGGAAATCCGTATTGCGACC GTTACCAACTTCCCGCACGGTAACGACGATATCGACATTGCGCTGGCGGAAACC CGTGCGGCGATTGCGTACGGCGCGGACGAAGTGGATGTGGTTTTCCCGTATCGT GCGCTGATGGCGGGCAACGAGCAGGTTGGTTTTGATCTGGTGAAGGCGTGCAAA GAAGCGTGCGCGGCGGCGAACGTGCTGCTGAAGGTTATCATTGAGAGCGGTGAA CTGAAGGACGAGGCGCTGATCCGTAAAGCGAGCGAAATCAGCATTAAGGCGGGC GCGGATTTCATTAAAACCAGCACCGGTCTGGTGGCGGTTAACGCGACCCCGGAG AGCGCGCGTATCATGATGGAAGTTATTCGTGACATGGGCGTGGAAAAGAGCGTT GGTTTTAAAGTG**ATC**GGTGGCGCGCGTACCGCGGAGGATGCGCAAAAATACCTG GCGATCGCGGATGAGCTGTTTGGTGCGGACTGGGCGGATGCGCGTCACTATCGT TTTGGTGCGAGCGGTCTGCTGGCGAGCCTGCTGAAGGCGCTGGGTCACGGCGAT GGTAAAAGCGCGAGCAGCTACCTCGAGCACCACCACCACCACCAC

3.6.3 Enzyme Expression and Purification

For heterologous expression of all enzymes, *E. coli* BL21(DE3) (New England BioLabs, NEB) was used as host organism. All enzymes were cloned in pET26b vector with a C-terminus His-Tag and without the pelB signal peptide. Transformations were performed at 42 ˚C for 10 seconds according to the standard protocol (NEB).

For expression of all enzymes, the following protocol was used: 400 mL of LB medium, supplemented with kanamycin (50 μg mL^{-1}) were inoculated with 7 mL of pre-culture. The cells were allowed to grow at 37 °C until an OD_{600} of 0.7-1 was reached. Expression of the enzymes were performed by inducing the main cultures with 0.5 mM of isopropyl β-D-1-thiogalactopyranoside (IPTG) and cultures were grown overnight at 25 °C with shaking at 170 rpm. The next day, the cells were harvested by centrifugation (4.700 g, 20 min, 4 °C), resuspended in lysis buffer (50 mM KH_2PO_4, 300 mM NaCl, 10 mM imidazole, pH 8.0), and lysed by ultrasonication.

Protein purification was performed by Ni-NTA affinity chromatography using pre-packed Ni-NTA HisTrap FF columns (GE Healthcare) according to the manufacturer´s instructions. After sonication, the enzyme solution was filtrated with a 0.45 μm filter and loaded into the column, which has been previously equilibrated with lysis buffer. After loading of the filtered lysate, the column was washed with sufficient amounts of lysis buffer (50 mL) and washing buffer (50 mM KH_2PO_4, 300 mM NaCl, 25 mM imidazole, pH 8.0, 25 mL). The bound protein was recovered with elution buffer (50 mM KH_2PO_4, 300 mM NaCl, 300 mM imidazole, pH 8.0). The process of purification was monitored with SDS-PAGE and fractions containing pure protein were pooled. Pooled fractions were used for buffer exchange using PD-10 columns (Cytiva) and enzymes were obtained in potassium phosphate (KPi) or 3-(*N*-Morpholino)-Propanesulfonic Acid (MOPS) buffer (50 mM, pH 6.5). Protein concentration was determined spectrophotometrically using the extinction coefficient at 280 nm. Typically, a protein yield of 30-50 mg per gram of cell culture was obtained. The purity of the enzymes was examined by SDS-PAGE analysis (Figure 3.36).

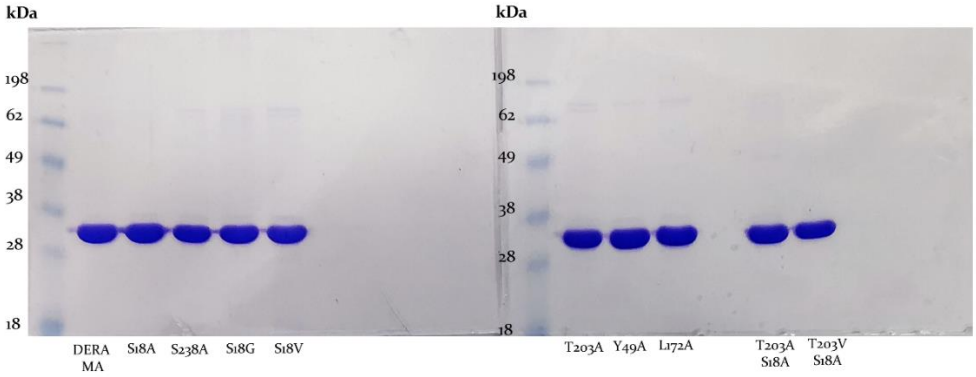

Figure 3.36. SDS-PAGE analysis for purity of the enzymes used in this study. In total 7 μg of each enzyme was loaded into the SDS-PAGE. From left to right: DERA-MA (MW = 28629.7), DERA^{S18A} (MW = 28613.7), DERA^{S238A} (MW = 28613.7), DERA^{S18G} (MW = 28599.7), DERA^{S18V} (MW = 28641.7), DERA^{T203A} (MW = 28599.7), DERA^{Y49A} (MW = 28537.6), DERA^{L172A} (MW = 28587.6), DERA$^{S18A/T203A}$ (MW = 28583.7), DERA$^{S18A/T203V}$ (MW = 28611.7).

3.6.4 Synthesis of the Starting Materials

3.6.4.1 GP1 – General Procedure for the Synthesis of Enantiopure Chiral Acids **36b-36h**

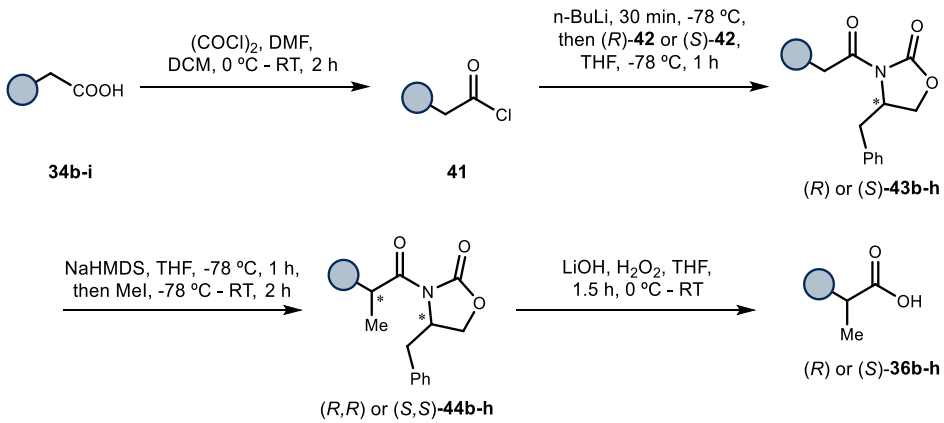

GP1.1 – General procedure for Preparation of Acid Chlorides **41**

Carboxylic acid **34** (1 equiv.) was placed in a dry flask equipped with a stirring bar under Argon atmosphere. Anhydrous CH_2Cl_2 (0.08 M) was added and the mixture was cooled to 0 °C. Oxalyl chloride (1.05 equiv.) was added, followed by a drop of anhydrous DMF. Then, the ice bath was removed and the mixture was stirred until gas evolution ceased (approx. 2 hours). The mixture was concentrated under reduced pressure and the acid chlorides **41** were used without further purification.

GP1.2 – General procedure for the Synthesis of Amides **43**

(R)- or *(S)*-Oxazolidinone **42** (1.05 equiv.) were placed in a dry flask under Argon atmosphere. After addition of anhydrous tetrahydrofuran (THF) (0.3 M) the mixture was cooled to -78 °C and *n*-BuLi (1.05 equiv., 1.6 N in hexanes) was added dropwise and stirred vigorously for 30 minutes. A solution of acid chloride **41** in dry THF was added dropwise and the mixture was stirred for another 60 minutes at -78 °C. The ice bath was removed and the reaction mixture was allowed to warm to RT and then quenched with NH_4Cl (sat., 20 mL). The mixture was extracted with EtOAc (3 x 30 mL), the combined organic layers were dried with $MgSO_4$ and concentrated. Purification by column chromatography (silica gel, EtOAc/hexanes) afforded the clean product **43**.

GP1.3 – General procedure for methylation of amide **43** *– Synthesis of* **44**

Amide (1 equiv.) was placed in a dry flask, dissolved in anhydrous THF (0.1 M) and cooled to -78 °C under Argon atmosphere. Then, a solution of NaHMDS (1.2 equiv., 1 N in THF) was added and the mixture was stirred for 1 h. Then, methyl iodide (5 equiv.) was added and the mixture was stirred for 2 h. The ice bath was removed, the mixture was stirred overnight and then concentrated under reduced pressure. The crude products were purified by column chromatography (SiO_2, hexane:ethyl acetate 8:2) and only pure fractions were isolated to ensure diastereopure products.

Chiral amides **44b-h** were synthesized according to general procedures *GP1.1* to *GP1.3* starting from carboxylic acids **34b-h**.

GP1.4 – General Procedure for Hydrolysis of Amide 44 – Synthesis of **36**

The following modified procedure was adopted from a literature procedure.[73] Amide **44** (1 equiv.) was dissolved in a mixture of THF (5 mL per mmol amide) and water (2 mL per mmol amide) and cooled to 0 ºC. Then, H_2O_2 (30% in water, 4 equiv.) and LiOH • H_2O (1 N in water, 3 equiv.) was added and the mixture was stirred vigorously for 1 h. The ice bath was removed and attired for another 30 minutes. The mixture was quenched with $Na_2S_2O_3$ (1mL, 10% in water) and 5 mL of water was added. The mixture was extracted with ethyl acetate (20 mL, discard layer), the aqueous layer was acidified to pH = 2 with aqueous 1N HCl and extracted with DCM (3x 20 mL). The combined DCM fractions were dried with $MgSO_4$ and purified by flash column chromatography (SiO_2, hexane:EtOAc 1:1) to afford the pure product **36**.

[73] Glunz, P. W., Mueller, L., Cheney, D. L., Ladziata, V., Zou, Y., Wurtz, N. R., Wei, A., Wong, P. C., Wexler, R. R., Priestley, E. S. "Atropisomer Control in Macrocyclic Factor VIIa Inhibitors" *J. Med. Chem.* **2016**, *59*, 4007–4018.

2-(p-Tolyl)propanoic acid (36b)

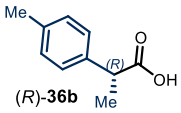

(R)-**36b**: The reaction was performed according to ***GP1.4*** using *(R,R)*-**44b** (743 mg, 2.30 mmol), H_2O_2 (30%, 0.93 mL) and LiOH (1 M, 6.9 mL, 6.9 mmol) to afford 318 mg (84%) of *(R)*-**36b**. **36b** is already described in the literature.[74]

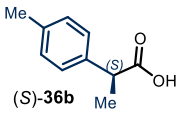

(S)-**36b**: The reaction was performed according to ***GP1.4*** using *(S,S)*-**44b** (1.14 g, 3.51 mmol), H_2O_2 (30%, 1.43 mL) and LiOH (1 M, 10.5 mL, 10.5 mmol) to afford 431 mg (75%) of *(S)*-**36b.**

^{1}H NMR (500 MHz, $CDCl_3$) δ 7.21 (d, *J* = 8.1 Hz, 2H), 7.14 (d, *J* = 8.1 Hz, 2H), 3.71 (q, *J* = 7.2 Hz, 1H), 2.33 (s, 3H), 1.50 (d, *J* = 7.2 Hz, 3H).

$[\alpha]_D^{20}$ (*(S)*-**36b**) = +66.5 (c = 0.11, CH_2Cl_2).

2-(m-Tolyl)propanoic acid (36c)

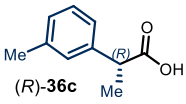

(R)-**36c**: The reaction was performed according to ***GP1.4*** using *(R,R)*-**44c** (137 mg, 0.42 mmol), H_2O_2 (30%, 0.17 mL) and LiOH (1 M, 1.26 mL, 1.26 mmol) to afford 58 mg (84%) of ***(R)***-**36c**. **36c** is already described in the literature.[74]

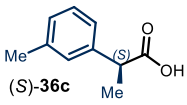

(S)-**36c**: The reaction was performed according to ***GP1.4*** using *(S,S)*-**44c** (159 mg, 0.49 mmol), H_2O_2 (30%, 0.20 mL) and LiOH (1 M, 1.47 mL, 1.47 mmol) to afford 63 mg (78%) of *(S)*-**36c**.

^{1}H NMR (400 MHz, $CDCl_3$): δ 7.22 (td, *J* = 7.4, 1.0 Hz, 1H), 7.15 – 7.05 (m, 3H), 3.71 (q, *J* = 7.2 Hz, 1H), 2.34 (s, 3H), 1.50 (d, *J* = 7.2 Hz, 3H).

$[\alpha]_D^{20}$ (*(S)*-**36c**) = +65.3 (c = 0.5, $CHCl_3$).

2-(o-Tolyl)propanoic acid (36d)

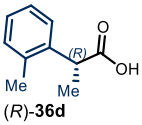

(R)-**36d**: The reaction was performed according to ***GP1.4*** using *(R,R)*-**44d** (361 mg, 1.12 mmol), H_2O_2 (30%, 0.45 mL) and LiOH (1 M, 3.48 mL, 3.48 mmol) to afford 163 mg (89%) of *(R)*-**36d**. **36d** is already described in the literature.[74]

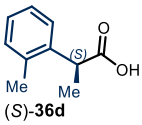

(S)-**36d**: The reaction was performed according to ***GP1.4*** using *(S,S)*-**44d** (439 mg, 1.36 mmol), H_2O_2 (30%, 0.55 mL) and LiOH (1 M, 4.05 mL, 4.05 mmol) to afford 185 mg (83%) of *(S)*-**36d**.

[74] Yao, Y. H., Zou, X. J., Wang, Y., Yang, H. Y., Ren, Z. H., Guan, Z. H. "Palladium-Catalyzed Asymmetric Markovnikov Hydroxycarbonylation and Hydroalkoxycarbonylation of Vinyl Arenes: Synthesis of 2-Arylpropanoic Acids" *Angew. Chem Int. Ed.* **2021**, *60*, 23117–23122.

^{1}H NMR (500 MHz, $CDCl_3$): δ 7.29 (d, *J* = 7.3 Hz, 1H), 7.23 – 7.13 (m, 3H), 3.99 (q, *J* = 7.1 Hz, 1H), 2.38 (s, 3H), 1.50 (d, *J* = 7.1 Hz, 3H).
$[\alpha]_D^{20}$ (***(S)*-36d**) = +83.4 (c = 0.5, $CHCl_3$).

2-(4-Bromophenyl)propanoic acid (36e)

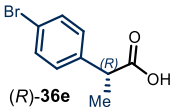

(R)-**36e**: The reaction was performed according to ***GP1.4*** using *(R,R)*-**44e** (404 mg, 1.04 mmol), H_2O_2 (30%, 0.42 mL) and LiOH (1 M, 3.12 mL, 3.12 mmol) to afford 171.2 mg (72%) of *(R)*-**36e**. **36e** is already described in the literature.[74]

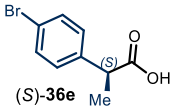

(S)-**36e**: The reaction was performed according to ***GP1.4*** using *(S,S)*-**44e** (426 mg, 1.10 mmol), H_2O_2 (30%, 0.45 mL) and LiOH (1 M, 3.33 mL, 3.33 mmol) to afford 194 mg (77%) of *(S)*-**36e**.

^{1}H NMR (400 MHz, $CDCl_3$): δ 7.46 (d, *J* = 8.5 Hz, 2H), 7.20 (d, *J* = 8.2 Hz, 2H), 3.71 (q, *J* = 7.2 Hz, 1H), 1.50 (d, *J* = 7.2 Hz, 3H).
$[\alpha]_D^{20}$ (***(S)*-36e**) = +43.4 (c = 0.5, $CHCl_3$).

2-(4-Chlorophenyl)propanoic acid (36f)

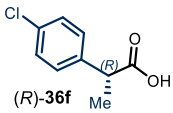

(R)-**36f**: The reaction was performed according to ***GP1.4*** using *(R,R)*-**44f** (324 mg, 0.94 mmol), H_2O_2 (30%, 0.38 mL) and LiOH (1 M, 2.82 mL, 2.82 mmol) to afford 136.9 mg (79%) of *(R)*-**36f**. **36f** is already described in the literature.[74]

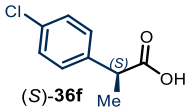

(S)-**36f**: The reaction was performed according to ***GP1.4*** using *(S,S)*-**44f** (384 mg, 1.12 mmol), H_2O_2 (30%, 0.46 mL) and LiOH (1 M, 3.33 mL, 3.33 mmol) to afford 162.3 mg (79%) of *(S)*-**36f**.

^{1}H NMR (400 MHz, $CDCl_3$): δ 7.33 – 7.23 (m, 4H), 3.73 (q, *J* = 7.2 Hz, 1H), 1.51 (d, *J* = 7.2 Hz, 3H). $[\alpha]_D^{20}$ (***(S)*-36f**) = +54.7 (c = 0.5, $CHCl_3$).

2-(4-Fluorophenyl)propanoic acid (36g)

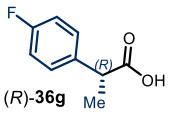

(R)-**36g**: The reaction was performed according to ***GP1.4*** using *(R,R)*-**44g** (250 mg, 0.76 mmol), H_2O_2 (30%, 0.31 mL) and LiOH (1 M, 2.28 mL, 2.28 mmol) to afford 108.9 mg (85%) of *(R)*-**36g**. **36g** is already described in the literature.[74]

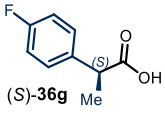

(S)-**36g**: The reaction was performed according to ***GP1.4*** using *(S,S)*-**44g** (239 mg, 0.73 mmol), H_2O_2 (30%, 0.30 mL) and LiOH (1 M, 2.19 mL, 2.19 mmol) to afford 87.8 mg (71%) of *(S)*-**36g**.

^{1}H NMR (400 MHz, $CDCl_3$): δ 7.32 – 7.27 (m, 2H), 7.02 (t, *J* = 8.6 Hz, 2H), 3.74 (q, *J* = 7.2 Hz, 1H), 1.51 (d, *J* = 7.2 Hz, 3H).
$[\alpha]_D^{20}$ (*(S)*-**36g**) = +53.6 (c = 0.5, $CHCl_3$).

2-(4-Methoxyphenyl)propanoic acid (36h)

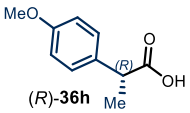

(R)-**36h**: The reaction was performed according to ***GP1.4*** using *(R,R)*-**44h** (142 mg, 0.42 mmol), H_2O_2 (30%, 0.17 mL) and LiOH (1 M, 1.26 mL, 1.26 mmol) to afford 58.8 mg (78%) of *(R)*-**36h**. **36h** is already described in the literature.[74]

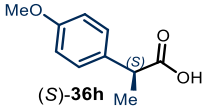

(S)-**36h**: The reaction was performed according to ***GP1.4*** using *(S,S)*-**44h** (146 mg, 0.43 mmol), H_2O_2 (30%, 0.18 mL) and LiOH (1 M, 1.29 mL, 1.29 mmol) to afford 59.5 mg (77%) of *(S)*-**36h**.
^{1}H NMR (500 MHz, $CDCl_3$): δ 7.26 – 7.23 (m, 2H), 6.90 – 6.84 (m, 2H), 3.79 (s, 3H), 3.70 (q, *J* = 7.2 Hz, 1H), 1.50 (d, *J* = 7.2 Hz, 3H). $[\alpha]_D^{20}$ (*(S)*-**36h**) = +56.1 (c = 0.5, $CHCl_3$).

3.6.4.2 GP2 – General Procedure for the Synthesis of Silanes **45** *and* **46**

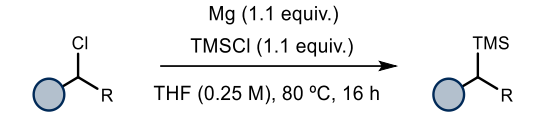

R = H, **47b-h**
R = Me, **48a-h**

R = H, **45b-h**
R = Me, **46a-h**

The general method for the synthesis of silanes **45** and **46** was adapted from a reported procedure.[75] Under argon a round-bottom flask was charged with magnesium tunings (1.1 equiv.), anhydrous THF, and trimethylsilyl chloride (1.1 equiv.). To the resulting suspension, the corresponding benzyl halide **47** or **48** (1 equiv.) in dry THF (0.25 M) was slowly added. The mixture was heated under reflux for 16 h, cooled to room temperature and quenched with saturated aqueous NH_4Cl solution. The solution was extracted with hexane (3 x 25 mL). The combined organic phase was washed with water (1 x 25 mL) and brine (1 x 25mL) and dried over anhydrous $MgSO_4$. The solvent was removed in vacuo and the crude product was purified by flash column chromatography (SiO_2, hexane) to yield silanes **45b-h** and **46a-h**.[31]

[75] Coughlin, D. J.,Salomon, R. G. "New synthetic approach to 4-alkylidenecyclohexenes. reduction-protodesilylation of benzylsilanes" *J. Org. Chem.* **1979**, *44*, 3784–3790.

*Synthesis of (Thiophen-2-ylmethyl)trimethylsilane (**45i**)*

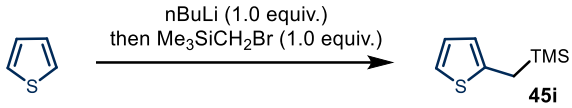

Silane **45i** was prepared according to a reported literature procedure.[76] To a solution of thiophene (400 µL, 5.00 mmol, 1.0 equiv.) in dry THF (7 mL) under argon at -15 ºC *n*-BuLi (2.0 mL, 2.5 N in hexane, 1.0 equiv.) was added dropwise. The solution was stirred for 30 min at -15 ºC. Me_3SiCH_2Br (714 µL, 5.00 mmol, 1.0 equiv.) was added dropwise and the mixture was allowed to warm up slowly to room temperature and stirred for 16 h. The yellowish solution was treated with cold aqueous NH_4Cl (20 mL) and was extracted with Et_2O (2x25mL). The combined organic layers were washed with water and brine and dried over $MgSO_4$. The solvent was removed *in vacuo*. Silane **45i** (604 mg, 3.6 mmol, 71%) was obtained as yellowish liquid. The silane was used without further purification. The characterization of the title compound was consistent with the data available in the literature.[77]

^{1}H NMR (400 MHz, $CDCl_3$) δ 6.97 (dd, *J* = 5.2, 1.2 Hz, 1H), 6.87 (dd, *J* = 5.2, 3.4 Hz, 1H), 6.59 (dq, *J* = 3.3, 1.0 Hz, 1H), 2.29 (s, 2H), 0.04 (s, 9H).

*Synthesis of (1-(4-Bromophenyl)ethyl)trimethylsilane (**46e**)*

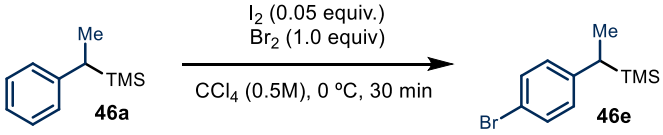

Silane **46e** was prepared according to a reported literature procedure.[78] To a solution of silane **46a** (1.03 mL, 5.00 mmol, 1.0 equiv.) in CCl_4 (10 mL) at 0 ºC, I_2 (63 mg, 0.25 mmol, 0.05 equiv.) was added, followed by the dropwise addition of Br_2 (256 µL, 5.0 mmol, 1.0 equiv.). The reaction was stirred for 30 min and then was quenched with aqueous 20% $Na_2S_2O_3$ solution (20 mL). The mixture was extracted with DCM (2x25 mL). The combined organic layers were washed with water and brine and dried with $MgSO_4$. The solvent was removed *in*

[76] Dembech, P., Seconi, G., Eaborn, C., Rodriguez, J. A., Stamper, J. G. "Cleavage of furan-2-yl, 2-thienyl-, benzo[b]furan-2-yl-, and benzo[b]thiophen-2-yl-methyl(trimethyl)silanes (RCH_2SiMe_3) by methanolic sodium methoxide; acidities of the corresponding RCH3 Species" *J. Chem. Soc. Perkin Trans.* **1986**, *2*, 197–198.

[77] Tamao, K., Kodama, S., Nakajima, I., Kumada, M., Minato, A., Suzuki, K. "Nickel-phosphine complex-catalyzed Grignard coupling-II. Grignard coupling of heterocyclic compounds" *Tetrahedron* **1982**, *38*, 3347–3354.

[78] Das, M. & O'Shea, D. F. "Synthesis and application of benzyl-TMS derivatives as bench stable benzyl anion equivalents" *Tetrahedron*. **2013**, *69*, 6448–6460.

vacuo. The crude product was purified by column flash chromatography (SiO_2, hexanes). Silane **46e** (677 mg, 2.63 mmol, 53%) was obtained as colorless liquid.
^{1}H NMR (400 MHz, $CDCl_3$) δ 7.37 – 7.30 (m, 2H), 6.93 – 6.87 (m, 2H), 2.13 (q, *J* = 7.5 Hz, 1H), 1.33 (d, *J* = 7.5 Hz, 3H), -0.07 (s, 9H).
^{13}C NMR (101 MHz, $CDCl_3$) δ 145.2, 131.1, 128.8, 117.8, 29.5, 14.8, -3.3.

3.6.5 Reference Compounds Synthesis

The reference compounds described in this section were used to determine the response factor for quantifying the enzymatic products through GC-FID analysis. Additionally, they were used as racemic samples for determining the enantiomeric excess through UPC^2 analysis. The samples were prepared using organocatalytic protocols, which typically resulted in mixtures of diastereoisomers.

Synthesis and Characterization of Reference Compounds **35** *and* **37**
GP3 – General Procedure for the Organocatalyzed Synthesis of the Racemic Reference Compounds **35** *and* **37**

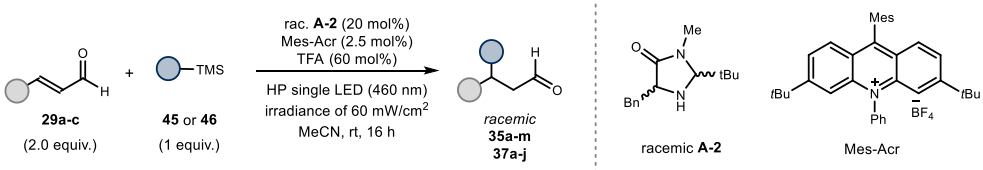

Reference compounds **35** and **37** were synthesized following a reported literature procedure.[79] To a 5 mL argon-purged glass vial, containing a racemic mixture (mixing (*R*,*R*) and (*S*,*S*) in a 1:1 ratio) of the amine catalyst **A-2** (0.04 mmol, 0.2 equiv.), the photocatalyst Mes-Acr (5.0 µmol, 2.5 mol%) and the silane **45** or **46** (0.2 mmol, 1 equiv.), enal **29** (0.4 mmol, 2 equiv.) was added. Then, 400 µL of an argon-sparged 0.3 M acetonitrile solution of TFA (9.2 µL, 0.12 mmol, 60 mol%) was added. The vial was sealed with Parafilm, and then placed into a 3D-printed holder, fitted with a 460 nm high-power single LED. The irradiance was fixed at 60±2 mW/cm^2, as controlled by an external power supply and measured using a photodiode light detector at the start of each reaction. This setup secured a reliable irradiation while keeping a distance of 1 cm between the reaction vessel and the light source. The reaction was stirred at room temperature for 16 h, then the solvent was evaporated and the crude mixture was purified by flash column chromatography on silica gel to furnish the product **35** and **37**.

[79] Le Saux, E., Ma, D., Bonilla, P., Holden, C. M., Lustosa, D., Melchiorre, P. "A General Organocatalytic System for Enantioselective Radical Conjugate Additions to Enals" *Angew. Chem., Int. Ed.* **2021**, *60*, 5357–5362.

3,4-Diphenylbutanal (35a)

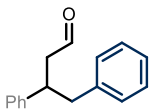

35a

Prepared according to **GP3**, using benzyltrimethylsilane **45a** (38 µL, 0.2 mmol), the racemic amine catalyst **A-2** (9.9 mg, 40 µmol), the photocatalyst Mes-Acr (2.9 mg, 5 µmol, 2.5 mol%) and cinnamaldehyde **29a** (51 µL, 0.4 mmol) in 0.3 M acetonitrile solution of TFA (9.2 µL, 0.12 mmol, 60 mol%). The solution was irradiated for 16h at room temperature. The crude mixture was purified by flash column chromatography (SiO_2, hexane:Et_2O 95:5, two consecutive purifications) to afford racemic product **35a** (31.4 mg, 0.14 mmol, 70% yield) as colorless oil. The enantiomers of the corresponding 2,4-dinitrophenylhydrazone (obtained upon condensation with 2,4-dinitrophenylhydrazine) were separated by UPC^2 analysis on a Daicel Chiralpak ID-3 column: isocratic 100% CO_2 for 1 min; gradient from 100% CO_2 to 60:40 CO_2/*i*-PrOH for 5 min; isocratic 60:40 CO_2/*i*-PrOH for 2 min, gradient from 60:40 CO_2/*i*-PrOH to 100% CO_2 for 1 min, flow rate 2.0 mL/min, λ = 347 nm, **35a**: τ = 6.4 min and τ = 6.6 min. The characterization of the title compound was consistent with the data available in the literature.[52]

^{1}H NMR (400 MHz, $CDCl_3$) δ 9.60 (t, *J* = 2.0 Hz, 1H), 7.32 – 7.26 (m, 2H), 7.26 – 7.15 (m, 6H), 7.10 – 7.04 (m, 2H), 3.51 (p, *J* = 7.7 Hz, 1H), 3.02 – 2.86 (m, 2H), 2.85 – 2.69 (m, 2H).

3-Phenyl-4-(*p*-tolyl)butanal (35b)

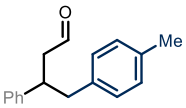

35b

Prepared according to **GP3**, using silane **45b** (41 µL, 0.2 mmol), the racemic amine catalyst **A-2** (9.9 mg, 40 µmol), the photocatalyst Mes-Acr (2.9 mg, 5 µmol, 2.5 mol%) and cinnamaldehyde **29a** (51 µL, 0.4 mmol) in 0.3 M acetonitrile solution of TFA (9.2 µL, 0.12 mmol, 60 mol%). The solution was irradiated for 16h at room temperature. The crude mixture was purified by flash column chromatography (SiO_2, hexane:Et_2O 95:5, two consecutive purifications) to afford racemic product **35b** (29.6 mg, 0.124 mmol, 62% yield) as colorless oil. The enantiomers of the corresponding 2,4-dinitrophenylhydrazone (obtained upon condensation with 2,4-dinitrophenylhydrazine) were separated by UPC^2 analysis on a Daicel Chiralpak ID-3 column: isocratic 100% CO_2 for 1 min; gradient from 100% CO_2 to 60:40 CO_2/*i*-PrOH for 5 min; isocratic 60:40 CO_2/*i*-PrOH for 2 min, gradient from 60:40 CO_2/*i*-PrOH to 100% CO_2 for 1 min, flow rate 2.0 mL/min, λ = 346 nm, **35b**: τ = 6.3 min and τ = 6.5 min. The characterization of the title compound was consistent with the data available in the literature.[52]

^{1}H NMR (500 MHz, $CDCl_3$) δ 9.58 (t, *J* = 2.0 Hz, 1H), 7.32 – 7.25 (m, 2H), 7.23 – 7.14 (m, 3H), 7.05 (d, *J* = 7.8 Hz, 2H), 6.96 (d, *J* = 7.9 Hz, 2H), 3.52 – 3.42 (m, 1H), 2.94 (dd, *J* = 13.6, 6.9 Hz, 1H), 2.83 (dd, *J* = 13.6, 8.1 Hz, 1H), 2.77 – 2.70 (m, 2H), 2.30 (s, 3H).

3-Phenyl-4-(*m*-tolyl)butanal (35c)

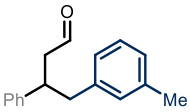

35c

Prepared according to **GP3**, using silane **45c** (36 mg, 0.2 mmol), the racemic amine catalyst **A-2** (9.9 mg, 40 µmol), the photocatalyst Mes-Acr (2.9 mg, 5 µmol, 2.5 mol%) and cinnamaldehyde **29a** (51 µL, 0.4 mmol) in 0.3 M acetonitrile solution of TFA (9.2 µL, 0.12 mmol, 60 mol%). The solution was irradiated for 16h at room temperature. The crude mixture was purified by flash column chromatography (SiO_2, hexane:Et_2O 95:5, two consecutive purifications) to afford racemic product **35c** (18.8 mg, 0.08 mmol, 39% yield) as colorless oil. The enantiomers of the corresponding 2,4-dinitrophenylhydrazone (obtained upon condensation with 2,4-dinitrophenylhydrazine) were separated by UPC^2 analysis on a Daicel Chiralpak ID-3 column: isocratic 100% CO_2 for 1 min; gradient from 100% CO_2 to 60:40 CO_2/*i*-PrOH for 5 min; isocratic 60:40 CO_2/*i*-PrOH for 2 min, gradient from 60:40 CO_2/*i*-PrOH to 100% CO_2 for 1 min, flow rate 2.0 mL/min, λ = 348 nm, **35c**: τ = 6.3 min and τ = 6.4 min.

^{1}H NMR (500 MHz, $CDCl_3$) δ 9.58 (t, *J* = 2.0 Hz, 1H), 7.33 – 7.26 (m, 2H), 7.24 – 7.17 (m, 3H), 7.14 (t, *J* = 7.6 Hz, 1H), 7.01 (ddt, *J* = 7.6, 1.9, 0.9 Hz, 1H), 6.91 (pd, *J* = 1.3, 0.9 Hz, 1H), 6.89 – 6.84 (m, 1H), 3.49 (tt, *J* = 8.3, 6.7 Hz, 1H), 2.95 (dd, *J* = 13.5, 6.7 Hz, 1H), 2.83 (dd, *J* = 13.5, 8.3 Hz, 1H), 2.78 – 2.70 (m, 2H), 2.30 (s, 3H).

^{13}C NMR (126 MHz, $CDCl_3$) δ 201.8, 143.5, 139.3, 138.1, 130.2, 128.7, 128.3, 127.6, 127.2, 126.9, 126.4, 49.0, 43.5, 42.2, 21.5.

HRMS (APCI): calculated for $[M-H]^+$ $[C_{17}H_{17}O]^+$: 237.1274; found: 237.1269.

3-Phenyl-4-(*o*-tolyl)butanal (35d)

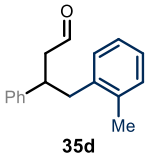

35d

Prepared according to **GP3**, using silane **45d** (40 µL, 0.2 mmol), the racemic amine catalyst **A-2** (9.9 mg, 40 µmol), the photocatalyst Mes-Acr (2.9 mg, 5 µmol, 2.5 mol%) and cinnamaldehyde **29a** (51 µL, 0.4 mmol) in 0.3 M acetonitrile solution of TFA (9.2 µL, 0.12 mmol, 60 mol%). The solution was irradiated for 16h at room temperature. The crude mixture was purified by flash column chromatography (SiO2, hexane:Et_2O 95:5, two consecutive purifications) to afford racemic product **35d** (31.0 mg, 0.13 mmol, 65% yield) as colorless oil. The enantiomers of the corresponding 2,4-dinitrophenylhydrazone (obtained upon condensation with 2,4-dinitrophenylhydrazine) were separated by UPC^2 analysis on a Daicel Chiralpak ID-3 column: isocratic 100% CO_2 for 1 min; gradient from 100% CO_2 to 60:40 CO_2/*i*-PrOH for 5 min; isocratic 60:40 CO_2/*i*-PrOH for 2 min, gradient from 60:40 CO_2/*i*-PrOH to 100% CO_2 for 1 min, flow rate 2.0 mL/min, λ = 348 nm, **35d**: τ = 6.3 min and τ = 6.5 min. The characterization of the title compound was consistent with the data available in the literature.[52]

^{1}H NMR (500 MHz, $CDCl_3$) δ 9.58 (t, *J* = 2.0 Hz, 1H), 7.31 – 7.26 (m, 2H), 7.24 – 7.14 (m, 3H), 7.14 – 7.02 (m, 4H), 6.99 – 6.94 (m, 1H), 3.47 (p, *J* = 7.7 Hz, 1H), 2.97 – 2.86 (m, 2H), 2.86 – 2.73 (m, 1H), 2.26 (s, 3H).

4-(4-Bromophenyl)-3-phenylbutanal (35e)

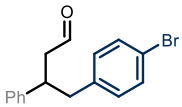

35e

Prepared according to **GP3**, using silane **45e** (40 µL, 0.2 mmol), the racemic amine catalyst **A-2** (9.9 mg, 40 µmol), the photocatalyst Mes-Acr (2.9 mg, 5 µmol, 2.5 mol%) and cinnamaldehyde **29a** (51 µL, 0.4 mmol) in 0.3 M acetonitrile solution of TFA (9.2 µL, 0.12 mmol, 60 mol%). The solution was irradiated for 16h at room temperature. The crude mixture was purified by flash column chromatography (SiO2, two consecutive purifications with hexane:Et_2O 95:5 then toluene) to afford racemic product **35e** (27.0 mg, 0.09 mmol, 44% yield) as white solid. The enantiomers of the corresponding 2,4-dinitrophenylhydrazone (obtained upon condensation with 2,4-dinitrophenylhydrazine) were separated by UPC[2] analysis on a Daicel Chiralpak ID-3 column: isocratic 100% CO_2 for 1 min; gradient from 100% CO_2 to 60:40 CO_2/*i*-PrOH for 5 min; isocratic 60:40 CO_2/*i*-PrOH for 2 min, gradient from 60:40 CO_2/*i*-PrOH to 100% CO_2 for 1 min, flow rate 2.0 mL/min, λ = 347 nm, **35e**: τ = 7.3 min and τ = 7.6 min. The characterization of the title compound was consistent with the data available in the literature.[52]

^{1}H NMR (400 MHz, $CDCl_3$) δ 9.63 (t, *J* = 1.8 Hz, 1H), 7.37 – 7.30 (m, 2H), 7.31 – 7.24 (m, 2H), 7.24 – 7.16 (m, 1H), 7.15 – 7.08 (m, 2H), 6.92 – 6.85 (m, 2H), 3.45 (p, *J* = 7.4 Hz, 1H), 2.88 (dd, *J* = 7.4, 1.4 Hz, 2H), 2.84 – 2.69 (m, 2H).

4-(4-Chlorophenyl)-3-phenylbutanal (35f)

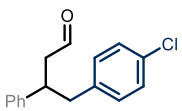

35f

Prepared according to **GP3**, using silane **45f** (40 µL, 0.2 mmol), the racemic amine catalyst **A-2** (9.9 mg, 40 µmol), the photocatalyst Mes-Acr (2.9 mg, 5 µmol, 2.5 mol%) and cinnamaldehyde **29a** (51 µL, 0.4 mmol) in 0.3 M acetonitrile solution of TFA (9.2 µL, 0.12 mmol, 60 mol%). The solution was irradiated for 16h at room temperature. The crude mixture was purified by flash column chromatography (SiO_2, two consecutive purifications with hexane:Et_2O 95:5 then toluene) to afford racemic product **35f** (29.0 mg, 0.11 mmol, 56% yield) as white solid. The enantiomers of the corresponding 2,4-dinitrophenylhydrazone (obtained upon condensation with 2,4-dinitrophenylhydrazine) were separated by UPC[2] analysis on a Daicel Chiralpak ID-3 column: isocratic 100% CO_2 for 1 min; gradient from 100% CO_2 to 60:40 CO_2/*i*-PrOH for 5 min; isocratic 60:40 CO_2/*i*-PrOH for 2 min, gradient from 60:40 CO_2/*i*-PrOH to 100% CO_2 for 1 min, flow rate 2.0 mL/min, λ = 347 nm, **35f**: τ = 6.8 min and τ = 7.1 min. The characterization of the title compound was consistent with the data available in the literature.[80]

^{1}H NMR (500 MHz, $CDCl_3$) δ 9.63 (t, *J* = 1.8 Hz, 1H), 7.30 – 7.24 (m, 2H), 7.24 – 7.14 (m, 3H), 7.14 – 7.08 (m, 2H), 6.96 – 6.90 (m, 2H), 3.45 (p, *J* = 7.4 Hz, 1H), 2.94 – 2.84 (m, 2H), 2.84 – 2.68 (m, 2H).

[80] Chen, Z. M., Hilton, M. J., Sigman, M. S. "Palladium-Catalyzed Enantioselective Redox-Relay Heck Arylation of 1,1-Disubstituted Homoallylic Alcohols" *J. Am. Chem. Soc.* **2016**, *138*, 11461–11464.

4-(4-Fluorophenyl)-3-phenylbutanal (35g)

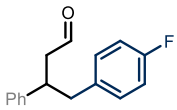

35g

Prepared according to **GP3**, using silane **45g** (36 mg, 0.2 mmol), the racemic amine catalyst **A-2** (9.9 mg, 40 µmol), the photocatalyst Mes-Acr (2.9 mg, 5 µmol, 2.5 mol%) and cinnamaldehyde **29a** (51 µL, 0.4 mmol) in 0.3 M acetonitrile solution of TFA (9.2 µL, 0.12 mmol, 60 mol%). The solution was irradiated for 16h at room temperature. The crude mixture was purified by flash column chromatography (SiO_2, two consecutive purifications with hexane:Et_2O 95:5 then toluene) to afford racemic product **35g** (28.7 mg, 0.12 mmol, 59% yield) as colorless oil. The enantiomers of the corresponding 2,4-dinitrophenylhydrazone (obtained upon condensation with 2,4-dinitrophenylhydrazine) were separated by UPC[2] analysis on a Daicel Chiralpak ID-3 column: isocratic 100% CO_2 for 1 min; gradient from 100% CO_2 to 60:40 CO_2/*i*-PrOH for 5 min; isocratic 60:40 CO_2/*i*-PrOH for 2 min, gradient from 60:40 CO_2/*i*-PrOH to 100% CO_2 for 1 min, flow rate 2.0 mL/min, λ = 347 nm, **35g**: τ = 6.2 min and τ = 6.5 min. The characterization of the title compound was consistent with the data available in the literature.[52]

^{1}H NMR (400 MHz, $CDCl_3$) δ 9.63 (t, *J* = 1.9 Hz, 1H), 7.32 – 7.23 (m, 2H), 7.23 – 7.17 (m, 1H), 7.16 – 7.08 (m, 2H), 7.01 – 6.93 (m, 2H), 6.93 – 6.85 (m, 2H), 3.44 (p, *J* = 7.4 Hz, 1H), 2.89 (d, *J* = 7.4 Hz, 2H), 2.84 – 2.69 (m, 2H).

^{19}F NMR (376 MHz, $CDCl_3$) δ -116.5.

4-(4-Methoxyphenyl)-3-phenylbutanal (35h)

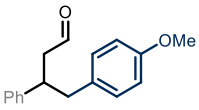

35h

Prepared according to **GP3**, using silane **45h** (39 mg, 0.2 mmol), the racemic amine catalyst **A-2** (9.9 mg, 40 µmol), the photocatalyst Mes-Acr (2.9 mg, 5 µmol, 2.5 mol%) and cinnamaldehyde **29a** (51 µL, 0.4 mmol) in 0.3 M acetonitrile solution of TFA (9.2 µL, 0.12 mmol, 60 mol%). The solution was irradiated for 16h at room temperature. The crude mixture was purified by flash column chromatography (SiO_2, hexane:Et_2O 95:5, two consecutive purifications) afford racemic product **35h** (25.7 mg, 0.10 mmol, 50% yield) as colorless oil. The enantiomers of the corresponding 2,4-dinitrophenylhydrazone (obtained upon condensation with 2,4-dinitrophenylhydrazine) were separated by UPC[2] analysis on a Daicel Chiralpak ID-3 column: isocratic 100% CO_2 for 1 min; gradient from 100% CO_2 to 60:40 CO_2/*i*-PrOH for 5 min; isocratic 60:40 CO_2/*i*-PrOH for 2 min, gradient from 60:40 CO_2/*i*-PrOH to 100% CO_2 for 1 min, flow rate 2.0 mL/min, λ = 349 nm, **35h**: τ = 7.0 min and τ = 7.2 min. The characterization of the title compound was consistent with the data available in the literature.[52]

^{1}H NMR (500 MHz, $CDCl_3$) δ 9.59 (t, *J* = 2.0 Hz, 1H), 7.29 (dd, *J* = 8.1, 6.8 Hz, 2H), 7.24 – 7.18 (m, 1H), 7.18 – 7.14 (m, 2H), 7.00 – 6.95 (m, 2H), 6.80 – 6.77 (m, 2H), 3.77 (s, 3H), 3.46 (p, *J* = 7.4 Hz, 1H), 2.92 (dd, *J* = 13.7, 7.1 Hz, 1H), 2.83 (dd, *J* = 13.7, 7.8 Hz, 1H), 2.75 (dt, *J* = 6.8, 2.1 Hz, 2H).

3-Phenyl-4-(thiophen-2-yl)butanal (35i)

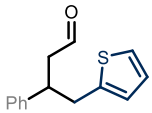

35i

Prepared according to **GP3**, using silane **45i** (34 mg, 0.2 mmol), the racemic amine catalyst **A-2** (9.9 mg, 40 µmol), the photocatalyst Mes-Acr (2.9 mg, 5 µmol, 2.5 mol%) and cinnamaldehyde **29a** (51 µL, 0.4 mmol) in 0.3 M acetonitrile solution of TFA (9.2 µL, 0.12 mmol, 60 mol%). The solution was irradiated for 16h at room temperature. The crude mixture was purified by flash column chromatography (SiO_2, hexane:Et_2O 95:5, two consecutive purifications) to afford racemic product **35i** (26.4 mg, 0.11 mmol, 57% yield) as colorless oil. The enantiomers of the corresponding 2,4-dinitrophenylhydrazone (obtained upon condensation with 2,4-dinitrophenylhydrazine) were separated by UPC^2 analysis on a Daicel Chiralpak ID-3 column: isocratic 100% CO_2 for 1 min; gradient from 100% CO_2 to 60:40 CO_2/*i*-PrOH for 5 min; isocratic 60:40 CO_2/*i*-PrOH for 2 min, gradient from 60:40 CO_2/*i*-PrOH to 100% CO_2 for 1 min, flow rate 2.0 mL/min, λ = 348 nm, **35i**: τ = 6.7 min and τ = 6.9 min.

^{1}H NMR (500 MHz, $CDCl_3$) δ 9.62 (t, *J* = 1.9 Hz, 1H), 7.31 (ddt, *J* = 7.2, 6.6, 0.9 Hz, 2H), 7.25 – 7.18 (m, 3H), 7.10 (dd, *J* = 5.1, 1.2 Hz, 1H), 6.87 (dd, *J* = 5.1, 3.4 Hz, 1H), 6.69 (dq, *J* = 3.4, 0.9 Hz, 1H), 3.52 (p, *J* = 7.4 Hz, 1H), 3.21 – 3.10 (m, 2H), 2.82 – 2.78 (m, 2H).

^{13}C NMR (126 MHz, $CDCl_3$) δ 201.3, 142.9, 141.7, 128.8, 127.7, 127.1, 126.9, 126.0, 124.0, 49.2, 42.4, 37.2.

HRMS (APCI): calculated for $[M+H]^+$ $[C_{14}H_{15}OS]^+$: 231.0838; found: 231.0843.

4-Phenyl-3-(p-tolyl)butanal (35k)

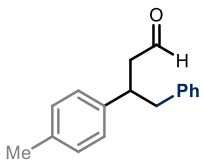

35k

Prepared according to **GP3**, using benzyltrimethylsilane **45a** (38 µL, 0.2 mmol), the racemic amine catalyst **A-2** (9.9 mg, 40 µmol), the photocatalyst Mes-Acr (2.9 mg, 5 µmol, 2.5 mol%) and enal **29b** (58 mg, 0.4 mmol) in 0.3 M acetonitrile solution of TFA (9.2 µL, 0.12 mmol, 60 mol%). The solution was irradiated for 16h at room temperature. The crude mixture was purified by flash column chromatography (SiO_2, hexane:Et_2O 95:5, two consecutive purifications) to afford racemic product **35k** (23.7 mg, 0.10 mmol, 50% yield) as colorless oil. The enantiomers of the corresponding 2,4-dinitrophenylhydrazone (obtained upon condensation with 2,4-dinitrophenylhydrazine) were separated by UPC^2 analysis on a Daicel Chiralpak ID-3 column: isocratic 100% CO_2 for 1 min; gradient from 100% CO_2 to 60:40 CO_2/*i*-PrOH for 5 min; isocratic 60:40 CO_2/*i*-PrOH for 2 min, gradient from 60:40 CO_2/*i*-PrOH to 100% CO_2 for 1 min, flow rate 2.0 mL/min, λ = 347 nm, **35k**: τ = 6.3 min and τ = 6.5 min. The characterization of the title compound was consistent with the data available in the literature.[52]

^{1}H NMR (500 MHz, $CDCl_3$) δ 9.58 (t, *J* = 2.0 Hz, 1H), 7.29 – 7.22 (m, 2H), 7.22 – 7.16 (m, 1H), 7.14 – 6.96 (m, 6H), 3.47 (tt, *J* = 8.1, 6.7 Hz, 1H), 2.96 (dd, *J* = 13.5, 7.0 Hz, 1H), 2.87 (dd, *J* = 13.5, 8.0 Hz, 1H), 2.79 – 2.66 (m, 2H), 2.32 (s, 3H).

3-(4-Methoxyphenyl)-4-phenylbutanal (35l)

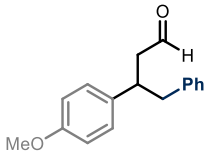

35l

Prepared according to **GP3**, using benzyltrimethylsilane **45a** (38 µL, 0.2 mmol), the racemic amine catalyst **A-2** (9.9 mg, 40 µmol), the photocatalyst Mes-Acr (2.9 mg, 5 µmol, 2.5 mol%) and enal **29c** (65 mg, 0.4 mmol) in 0.3 M acetonitrile solution of TFA (9.2 µL, 0.12 mmol, 60 mol%). The solution was irradiated for 16h at room temperature. The crude mixture was purified by flash column chromatography (SiO_2, hexane:Et_2O 95:5, two consecutive purifications) to afford racemic product **35l** (24.6 mg, 0.10 mmol, 48% yield) as colorless oil. The enantiomers of the corresponding 2,4-dinitrophenylhydrazone (obtained upon condensation with 2,4-dinitrophenylhydrazine) were separated by UPC^2 analysis on a Daicel Chiralpak ID-3 column: isocratic 100% CO_2 for 1 min; gradient from 100% CO_2 to 60:40 CO_2/*i*-PrOH for 5 min; isocratic 60:40 CO_2/*i*-PrOH for 2 min, gradient from 60:40 CO_2/*i*-PrOH to 100% CO_2 for 1 min, flow rate 2.0 mL/min, λ = 347 nm, **35l**: τ = 6.8 min and τ = 7.0 min.

^{1}H NMR (500 MHz, $CDCl_3$) δ 9.58 (t, *J* = 2.0 Hz, 1H), 7.33 – 7.20 (m, 2H), 7.21 – 7.14 (m, 1H), 7.12 – 7.00 (m, 4H), 6.86 – 6.76 (m, 2H), 3.78 (s, 3H), 3.45 (p, *J* = 7.4 Hz, 1H), 2.93 (dd, *J* = 13.5, 7.2 Hz, 1H), 2.86 (dd, *J* = 13.5, 7.8 Hz, 1H), 2.75 – 2.67 (m, 2H).

^{13}C NMR (126 MHz, $CDCl_3$) δ 201.9, 158.4, 139.5, 135.4, 129.4, 128.6, 128.4, 126.4, 114.10, 55.4, 49.3, 43.7, 41.4.

HRMS (ESI): calculated for $[M+MeOH+Na]^+$ $[C_{18}H_{22}NaO_3]^+$: 309.1461; found: 309.1463.

3-(4-Bromophenyl)-4-phenylbutanal (35m)

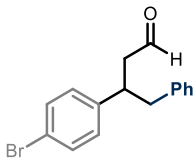

35m

Prepared according to **GP3**, using benzyltrimethylsilane **45a** (38 µL, 0.2 mmol), the racemic amine catalyst **A-2** (9.9 mg, 40 µmol), the photocatalyst Mes-Acr (2.9 mg, 5 µmol, 2.5 mol%) and enal **29d** (84 mg, 0.4 mmol) in 0.3 M acetonitrile solution of TFA (9.2 µL, 0.12 mmol, 60 mol%). The solution was irradiated for 16h at room temperature. The crude mixture was purified by flash column chromatography (SiO_2, two consecutive purifications: hexane:Et_2O 95:5 then toluene) to afford racemic product **35m** (43.3 mg, 0.14 mmol, 71% yield) as colorless crystals. The enantiomers of the corresponding 2,4-dinitrophenylhydrazone (obtained upon condensation with 2,4-dinitrophenylhydrazine) were separated by UPC^2 analysis on a Daicel Chiralpak ID-3 column: isocratic 100% CO_2 for 1 min; gradient from 100% CO_2 to 60:40 CO_2/MeOH for 13 min; isocratic 60:40 CO_2/MeOH for 2 min, gradient from 60:40 CO_2/MeOH to 100% CO_2 for 1 min, flow rate 2.0 mL/min, λ = 350 nm: **35m**: τ = 13.2 min and τ = 13.5 min. The characterization of the title compound was consistent with the data available in the literature.[52]

^{1}H NMR (500 MHz, $CDCl_3$) δ 9.60 (t, *J* = 1.7 Hz, 1H), 7.42 – 7.37 (m, 2H), 7.26 – 7.21 (m, 2H), 7.21 – 7.16 (m, 1H), 7.03 (td, *J* = 6.2, 1.8 Hz, 4H), 3.47 (p, *J* = 7.4 Hz, 1H), 2.89 (d, *J* = 7.5 Hz, 2H), 2.75 (dd, *J* = 7.3, 1.7 Hz, 2H).

^{13}C NMR (126 MHz, $CDCl_3$) δ 201.0, 142.4, 138.9, 131.8, 129.4, 129.3, 128.5, 126.6, 120.6, 49.0, 43.2, 41.4.

3,4-Diphenylpentanal (37a)

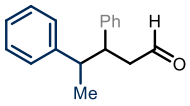

37a

Prepared according to **GP3**, using silane **46a** (41 µL, 0.2 mmol), the racemic amine catalyst **A-2** (9.9 mg, 40 µmol), the photocatalyst Mes-Acr (2.9 mg, 5 µmol, 2.5 mol%) and cinnamaldehyde **29a** (51 µL, 0.4 mmol) in 0.3 M acetonitrile solution of TFA (9.2 µL, 0.12 mmol, 60 mol%). The solution was irradiated for 16h at room temperature. The crude mixture was purified by flash column chromatography (SiO_2, hexane:Et_2O 95:5, two consecutive purifications) to afford the racemic product as an inseparable mixture of two diastereomers *syn*-**37a** and *anti*-**37a** (27.6 mg, 0.12 mmol, 58% yield, 1.2:1 d.r.) as colorless oil. The enantiomers of the corresponding 2,4-dinitrophenylhydrazone (obtained upon condensation with 2,4-dinitrophenylhydrazine) were separated by UPC^2 analysis on a Daicel Chiralpak IE-3 column: isocratic 100% CO_2 for 1 min; gradient from 100% CO_2 to 60:40 CO_2/*i*-PrOH for 15 min; isocratic60:40 CO_2/ *i*-PrOH for 8 min, gradient from 60:40 CO_2/*i*-PrOH to 100% CO_2 for 1 min, flow rate 2.0 mL/min, λ = 345 nm: *syn*-**37a**: τ = 19.3 min and τ = 19.5 min; *anti*-**37a**: τ = 21.2 min and τ = 21.6 min. The characterization of the title compound was consistent with the data available in the literature.[52]

^{1}H NMR (400 MHz, $CDCl_3$, *mixture of diastereoisomers*) δ 9.57 (t, *J* = 2.1 Hz, 1H), 9.35 (dd, *J* = 2.5, 1.6 Hz, 1H), 7.37 – 7.29 (m, 4H), 7.26 – 7.09 (m, 12H), 6.98 (ddd, *J* = 8.0, 3.0, 1.5 Hz, 4H), 3.46 (q, *J* = 7.3 Hz, 1H), 3.30 (td, *J* = 10.2, 4.6 Hz, 1H), 3.07 (p, *J* = 7.0 Hz, 1H), 2.89 (dt, *J* = 11.1, 6.9 Hz, 1H), 2.83 – 2.77 (m, 2H), 2.62 (ddd, *J* = 16.8, 10.0, 2.5 Hz, 1H), 2.47 (ddd, *J* = 16.8, 4.6, 1.6 Hz, 1H), 1.29 (d, *J* = 7.1 Hz, 3H), 1.05 (d, *J* = 6.9 Hz, 3H).

3-Phenyl-4-(*p*-tolyl)pentanal (37b)

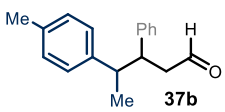

37b

Prepared according to **GP3**, using silane **46b** (38 mg, 0.2 mmol), the racemic amine catalyst **A-2** (9.9 mg, 40 µmol), the photocatalyst Mes-Acr (2.9 mg, 5 µmol, 2.5 mol%) and cinnamaldehyde **29a** (51 µL, 0.4 mmol) in 0.3 M acetonitrile solution of TFA (9.2 µL, 0.12 mmol, 60 mol%). The solution was irradiated for 16h at room temperature. The crude mixture was purified by flash column chromatography (SiO_2, two consecutive purifications with hexane:Et_2O 95:5) to afford racemic product as an inseparable mixture of two diastereomers *syn*-**37b** and *anti*-**35b** (40.0 mg, 0.16 mmol, 79% yield, 1.1:1 d.r.) as yellowish oil. The enantiomers of the corresponding 2,4-dinitrophenylhydrazone (obtained upon condensation with 2,4-dinitrophenylhydrazine) were separated by UPC^2 analysis on a Daicel Chiralpak IA-3 column: isocratic 100% CO_2 for 1 min; gradient from 100% CO_2 to 60:40 CO_2/EtOH for 11 min; isocratic 60:40 CO_2/EtOH for 6 min, gradient from 60:40 CO_2/EtOH to 100% CO_2 for 1 min, flow rate 1.0 mL/min, λ = 352 nm: *syn*-**37b**: τ = 16.1 min and τ = 16.5 min; *anti*-**37b**: τ = 13.8

min and τ = 14.3 min. The characterization of the title compound was consistent with the data available in the literature.[71]

^{1}H NMR (400 MHz, $CDCl_3$, mixture of diastereoisomers) δ 9.58 (t, *J* = 2.1 Hz, 1H), 9.37 (dd, *J* = 2.6, 1.6 Hz, 1H), 7.35 (dd, *J* = 8.1, 6.7 Hz, 2H), 7.28 – 7.20 (m, 6H), 7.16 (d, *J* = 1.5 Hz, 4H), 7.05 – 7.00 (m, 4H), 6.91 (d, *J* = 8.0 Hz, 2H), 3.48 (q, *J* = 7.2 Hz, 1H), 3.29 (td, *J* = 10.2, 4.7 Hz, 1H), 3.07 (p, *J* = 6.9 Hz, 1H), 2.88 (dq, *J* = 10.5, 6.9 Hz, 1H), 2.83 – 2.78 (m, 2H), 2.63 (ddd, *J* = 16.7, 10.0, 2.6 Hz, 1H), 2.50 (ddd, *J* = 16.7, 4.7, 1.6 Hz, 1H), 2.37 (s, 3H), 2.30 (s, 3H), 1.27 (d, *J* = 7.1 Hz, 3H), 1.05 (d, *J* = 6.9 Hz, 3H).

3-Phenyl-4-(*m*-tolyl)pentanal (37c)

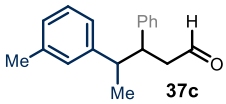

37c

Prepared according to **GP3**, using silane **46c** (38 mg, 0.2 mmol), the racemic amine catalyst **A-2** (9.9 mg, 40 µmol), the photocatalyst Mes-Acr (2.9 mg, 5 µmol, 2.5 mol%) and cinnamaldehyde **29a** (51 µL, 0.4 mmol) in 0.3 M acetonitrile solution of TFA (9.2 µL, 0.12 mmol, 60 mol%). The solution was irradiated for 16h at room temperature. The crude mixture was purified by flash column chromatography (SiO_2, hexane:Et_2O 95:5, two consecutive purifications) to afford the racemic product as an inseparable mixture of two diastereomers *syn*-**37c** and *anti*-**37c** (24.3 mg, 0.10 mmol, 51% yield, 1:1.1 d.r.) as colorless oil. The enantiomers of the corresponding 2,4-dinitrophenylhydrazone (obtained upon condensation with 2,4-dinitrophenylhydrazine) were separated by UPC^2 analysis on a Daicel Chiralpak ID-3 column: isocratic 100% CO_2 for 1 min; gradient from 100% CO_2 to 60:40 CO_2/ EtOH for 13 min; isocratic 60:40 CO_2/EtOH for 2 min, gradient from 60:40 CO_2/EtOH to 100% CO_2 for 1 min, flow rate 2.0 mL/min, λ = 347 nm: *syn*-**37c**: τ = 10.0 min and τ = 10.4 min; *anti*-**37c**: τ = 10.7 min and τ = 11.3 min.

^{1}H NMR (500 MHz, $CDCl_3$, mixture of diastereoisomers) δ 9.57 (t, *J* = 2.1 Hz, 1H), 9.37 (dd, *J* = 2.6, 1.5 Hz, 1H), 7.35 (td, *J* = 7.4, 1.4 Hz, 2H), 7.29 – 7.20 (m, 6H), 7.19 – 7.14 (m, 1H), 7.14 – 7.05 (m, 4H), 7.05 – 6.96 (m, 3H), 6.85 – 6.79 (m, 2H), 3.49 (dt, *J* = 9.0, 6.4 Hz, 1H), 3.31 (td, *J* = 10.2, 4.5 Hz, 1H), 3.06 (p, *J* = 7.0 Hz, 1H), 2.92 – 2.84 (m, 1H), 2.84 – 2.74 (m, 2H), 2.63 (ddd, *J* = 16.8, 10.2, 2.6 Hz, 1H), 2.49 (ddd, *J* = 16.8, 4.5, 1.6 Hz, 1H), 2.39 (s, 3H), 2.29 (s, 3H), 1.28 (d, *J* = 7.1 Hz, 3H), 1.06 (d, *J* = 6.9 Hz, 3H).

^{13}C NMR (126 MHz, $CDCl_3$, mixture of diastereoisomers) δ 202.2, 201.8, 145.2, 143.8, 142.9, 141.6, 138.4, 137.6, 129.0, 128.7, 128.7, 128.7, 128.4, 128.2, 128.1, 128.0, 127.6, 127.1, 126.9, 126.6, 125.2, 124.7, 49.2, 47.6, 46.6, 46.1, 45.9, 45.0, 21.6, 21.5, 20.7, 17.8.

HRMS (ESI): Calculated for $[M+MeOH+Na]^+$ $[C_{19}H_{24}NaO_2]^+$: 307.1669, found: 307.1669.

3-Phenyl-4-(*o*-tolyl)pentanal (37d)

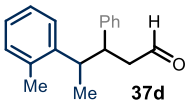

37d

Prepared according to **GP3**, using silane **46d** (38 mg, 0.2 mmol), the racemic amine catalyst **A-2** (9.9 mg, 40 µmol), the photocatalyst Mes-Acr (2.9 mg, 5 µmol, 2.5 mol%) and cinnamaldehyde **29a** (51 µL, 0.4 mmol) in 0.3 M acetonitrile solution of TFA (9.2 µL, 0.12 mmol, 60 mol%). The solution was

irradiated for 16h at room temperature. The crude mixture was purified by flash column chromatography (SiO_2, hexane:Et_2O 95:5, two consecutive purifications) to afford the racemic product as an inseparable mixture of two diastereomers *syn*-**37d** and *anti*-**37d** (37.6 mg, 0.16 mmol, 79% yield, 1:1.1 d.r.) as colorless oil. The enantiomers of the corresponding 2,4-dinitrophenylhydrazone (obtained upon condensation with 2,4-dinitrophenylhydrazine) were separated by UPC^2 analysis on a Daicel Chiralpak ID-3 column: isocratic 100% CO_2 for 1 min; gradient from 100% CO_2 to 60:40 CO_2/ MeOH for 13 min; isocratic 60:40 CO_2/MeOH for 2 min, gradient from 60:40 CO_2/MeOH to 100% CO_2 for 1 min, flow rate 2.0 mL/min, λ = 350 nm: *syn*-**37d**: τ = 9.6 min and τ = 10.0 min; *anti*-**37d**: τ = 10.4 min and τ = 11.2 min.

^{1}H NMR (500 MHz, $CDCl_3$, mixture of diastereoisomers) δ 9.57 (t, *J* = 2.1 Hz, 1H), 9.37 (dd, *J* = 2.6, 1.6 Hz, 1H), 7.35 (td, *J* = 7.4, 1.4 Hz, 2H), 7.31 – 7.20 (m, 6H), 7.19 – 7.14 (m, 1H), 7.14 – 7.04 (m, 4H), 7.04 – 6.97 (m, 3H), 6.86 – 6.79 (m, 2H), 3.49 (dt, *J* = 9.0, 6.4 Hz, 1H), 3.31 (td, *J* = 10.3, 4.5 Hz, 1H), 3.06 (p, *J* = 7.0 Hz, 1H), 2.92 – 2.84 (m, 1H), 2.84 – 2.74 (m, 2H), 2.63 (ddd, *J* = 16.8, 10.1, 2.6 Hz, 1H), 2.49 (ddd, *J* = 16.8, 4.5, 1.6 Hz, 1H), 2.39 (s, 3H), 2.29 (s, 3H), 1.28 (d, *J* = 7.1 Hz, 3H), 1.06 (d, *J* = 6.9 Hz, 3H).

^{13}C NMR (126 MHz, $CDCl_3$, mixture of diastereoisomers) δ 202.2, 201.8, 145.2, 143.8, 142.9, 141.6, 138.4, 137.6, 129.0, 128.7, 128.7, 128.7, 128.4, 128.2, 128.1, 128.0, 127.6, 127.1, 126.9, 126.6, 125.2, 124.7, 49.2, 47.62, 46.6, 46.1, 45.9, 45.0, 21.6, 21.5, 20.7, 17.8.

HRMS (ESI): Calculated for $[M+MeOH+Na]^+$ $[C_{19}H_{24}NaO_2]^+$: 307.1669, found: 307.1682.

4-(4-Bromophenyl)-3-phenylpentanal (37e)

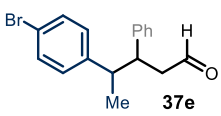

37e

Prepared according to **GP3**, using silane **46e** (51 mg, 0.2 mmol), the racemic amine catalyst **A-2** (9.9 mg, 40 µmol), the photocatalyst Mes-Acr (2.9 mg, 5 µmol, 2.5 mol%) and cinnamaldehyde **29a** (51 µL, 0.4 mmol) in 0.3 M acetonitrile solution of TFA (9.2 µL, 0.12 mmol, 60 mol%). The solution was irradiated for 16 h at room temperature. The crude mixture was purified by flash column chromatography (SiO_2, hexane:Et_2O 95:5, two consecutive purifications) to afford the racemic product as an inseparable mixture of two diastereomers *syn*-**37e** and *anti*-**37e** (29.4 mg, 0.09 mmol, 46% yield, 1:1.1 d.r.) as colorless crystals. The enantiomers of the corresponding 2,4-dinitrophenylhydrazone (obtained upon condensation with 2,4-dinitrophenylhydrazine) were separated by UPC^2 analysis on a Daicel Chiralpak IB-3 column: isocratic 100% CO_2 for 1 min; gradient from 100% CO_2 to 85:15 CO_2/*i*-PrOH for 37 min; isocratic 85:15 CO_2/ *i*-PrOH for 26 min, gradient from 85:15 CO_2/ *i*-PrOH to 100% CO_2 for 1 min, flow rate 1.0 mL/min, λ = 344 nm: *syn*-**37e**: τ = 50.8 min and τ = 54.9 min; *anti*-**37e**: τ = 58.8 min and τ = 60.0 min.

^{1}H NMR (500 MHz, $CDCl_3$, mixture of diastereoisomers) δ 9.59 (t, *J* = 2.0 Hz, 1H), 9.39 (dd, *J* = 2.4, 1.4 Hz, 1H), 7.49 – 7.42 (m, 2H), 7.36 – 7.27 (m, 4H), 7.27 – 7.17 (m, 5H), 7.17 – 7.12 (m, 1H), 7.12 – 7.07 (m, 2H), 6.97 – 6.93 (m, 2H), 6.85 – 6.81 (m, 2H), 3.41 (q, *J* = 7.4 Hz, 1H), 3.28 (td, *J* = 10.1, 4.5 Hz, 1H), 3.02 (p, *J* = 7.1 Hz, 1H), 2.89 (dq, *J* = 10.1, 6.9 Hz,

1H), 2.80 (dd, *J* = 7.5, 2.1 Hz, 2H), 2.64 (ddd, *J* = 16.8, 10.1, 2.4 Hz, 1H), 2.46 (ddd, *J* = 16.9, 4.5, 1.5 Hz, 1H), 1.27 (d, *J* = 7.1 Hz, 3H), 1.03 (d, *J* = 6.9 Hz, 3H).

^{13}C NMR (126 MHz, $CDCl_3$, mixture of diastereoisomers) δ 201.8, 201.4, 144.3, 143.0, 142.2, 141.2, 131.9, 131.2, 129.9, 129.5, 128.8, 128.6, 128.3, 128.2, 127.1, 126.8, 120.5, 120.1, 48.8, 47.3, 46.6, 46.5, 45.5, 44.7, 20.4, 18.7.

HRMS (ESI): Calculated for $[M+Na]^+$ $[C_{17}H_{17}BrNaO]^+$: 339.0355, found: 339.0343.

4-(4-Chlorophenyl)-3-phenylpentanal (37f)

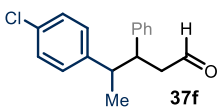

37f

Prepared according to **GP3**, using silane **46f** (43 mg, 0.2 mmol), the racemic amine catalyst **A-2** (9.9 mg, 40 µmol), the photocatalyst Mes-Acr (2.9 mg, 5 µmol, 2.5 mol%) and cinnamaldehyde **29a** (51 µL, 0.4 mmol) in 0.3 M acetonitrile solution of TFA (9.2 µL, 0.12 mmol, 60 mol%). The solution was irradiated for 16h at room temperature. The crude mixture was purified by flash column chromatography (SiO_2 two consecutive purifications: hexane:Et_2O 95:5 then toluene) to afford the racemic product as an inseparable mixture of two diastereomers *syn*-**37f** and *anti*-**37f** (24.3 mg, 0.09 mmol, 45% yield, 1:1.1 d.r.) as white solid The enantiomers of the corresponding 2,4-dinitrophenylhydrazone (obtained upon condensation with 2,4-dinitrophenylhydrazine) were separated by UPC^2 analysis on a Daicel Chiralpak IE-3 column: isocratic 100% CO_2 for 1 min; gradient from 100% CO_2 to 60:40 CO_2/ EtOH for 21 min; isocratic 60:40 CO_2/EtOH for 6 min, gradient from 60:40 CO_2/EtOH to 100% CO_2 for 1 min, flow rate: 1.0 mL/min, λ = 350 nm: *syn*-**37f**: τ = 22.1 min and τ = 22.7 min; *anti*-**37f**: τ = 23.2 min and τ = 23.5 min.

^{1}H NMR (500 MHz, $CDCl_3$, mixture of diastereoisomers) δ 9.59 (t, *J* = 2.0 Hz, 1H), 9.39 (dd, *J* = 2.4, 1.5 Hz, 1H), 7.37 – 7.11 (m, 14H), 6.97 – 6.93 (m, 2H), 6.91 – 6.85 (m, 2H), 3.41 (q, *J* = 7.4 Hz, 1H), 3.27 (td, *J* = 10.1, 4.5 Hz, 1H), 3.03 (p, *J* = 7.1 Hz, 1H), 2.90 (dq, *J* = 10.1, 6.9 Hz, 1H), 2.80 (dd, *J* = 7.5, 2.0 Hz, 2H), 2.64 (ddd, *J* = 16.9, 10.1, 2.4 Hz, 1H), 2.46 (ddd, *J* = 16.9, 4.5, 1.5 Hz, 1H), 1.28 (d, *J* = 7.0 Hz, 3H), 1.03 (d, *J* = 6.9 Hz, 3H).

^{13}C NMR (126 MHz, $CDCl_3$, mixture of diastereoisomers) δ 201.8, 201.4, 143.7, 142.5, 142.3, 141.2, 132.5, 132.1, 129.5, 129.1, 128.9, 128.8, 128.6, 128.3, 128.3, 128.2, 127.1, 126.8, 48.8, 47.4, 46.7, 46.5, 45.4, 44.6, 20.4, 18.7.

HRMS (ESI): Calculated for $[M+MeOH+Na]^+$ $[C_{18}H_{21}ClNaO_2]^+$: 327.1122, found: 327.1132.

4-(4-Fluorophenyl)-3-phenylpentanal (37g)

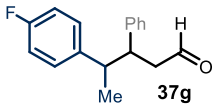

37g

Prepared according to **GP3**, using silane **46g** (39 mg, 0.2 mmol), the racemic amine catalyst **A-2** (9.9 mg, 40 µmol), the photocatalyst Mes-Acr (2.9 mg, 5 µmol, 2.5 mol%) and cinnamaldehyde **29a** (51 µL, 0.4 mmol) in 0.3 M acetonitrile solution of TFA (9.2 µL, 0.12 mmol, 60 mol%). The solution was irradiated for 16h at room temperature. The crude mixture was purified by flash column

chromatography (SiO_2 two consecutive purifications: hexane:Et_2O 95:5 then toluene) to afford the racemic product as an inseparable mixture of two diastereomers *syn*-**37g** and *anti*-**37g** (34.9 mg, 0.14 mmol, 68% yield, 1:1.2 d.r.) as colorless oil. The enantiomers of the corresponding 2,4-dinitrophenylhydrazone (obtained upon condensation with 2,4-dinitrophenylhydrazine) were separated by UPC^2 analysis on a Daicel Chiralpak IE-3 column: isocratic 100% CO_2 for 1 min; gradient from 100% CO_2 to 70:30 CO_2/ EtOH for 9 min; isocratic 70:30 CO_2/EtOH for 4 min, gradient from 70:30 CO_2/EtOH to 100% CO_2 for 1 min, flow rate: 2.0 mL/min, λ = 347 nm: *syn*-**37g**: τ = 10.7 min and τ = 10.7 min; *anti*-**37g**: τ = 11.3 min and τ = 11.5 min.

^{1}H NMR (500 MHz, $CDCl_3$, mixture of diastereoisomers) δ 9.59 (t, *J* = 2.0 Hz, 1H), 9.38 (dd, *J* = 2.4, 1.6 Hz, 1H), 7.36 – 7.29 (m, 2H), 7.27 – 7.10 (m, 8H), 7.07 – 6.98 (m, 2H), 6.96 – 6.83 (m, 6H), 3.41 (q, *J* = 7.4 Hz, 1H), 3.27 (td, *J* = 10.0, 4.6 Hz, 1H), 3.04 (p, *J* = 7.1 Hz, 1H), 2.91 (dq, *J* = 10.1, 6.9 Hz, 1H), 2.85 – 2.77 (m, 2H), 2.63 (ddd, *J* = 16.8, 10.0, 2.4 Hz, 1H), 2.47 (ddd, *J* = 16.8, 4.7, 1.6 Hz, 1H), 1.28 (d, *J* = 7.1 Hz, 3H), 1.03 (d, *J* = 6.9 Hz, 3H).

^{13}C NMR (126 MHz, $CDCl_3$, mixture of diastereoisomers) δ 201.9, 201.5, 162.7, 162.4, 160.8, 160.5, 142.4, 141.4, 140.9, 140.9, 139.6, 139.6, 129.5, 129.5, 129.1, 129.0, 128.8, 128.6, 128.3, 128.2, 115.7, 115.5, 114.9, 114.8, 48.9, 47.6, 46.7, 46.6, 45.3, 44.5, 20.6, 18.8.

^{19}F NMR (471 MHz, $CDCl_3$, mixture of diastereoisomers) δ -116.2, -116.8.

HRMS (ESI): Calculated for $[M+MeOH+Na]^+$ $[C_{18}H_{21}FNaO_2]^+$: 311.1418, found: 311.1422.

4-(4-Methoxyphenyl)-3-phenylpentanal (37h)

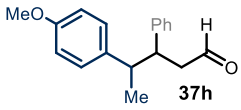

37h

Prepared according to **GP3**, using silane **46h** (42 mg, 0.2 mmol), the racemic amine catalyst **A-2** (9.9 mg, 40 µmol), the photocatalyst Mes-Acr (2.9 mg, 5 µmol, 2.5 mol%) and cinnamaldehyde **29a** (51 µL, 0.4 mmol) in 0.3 M acetonitrile solution of TFA (9.2 µL, 0.12 mmol, 60 mol%). The solution was irradiated for 16h at room temperature. The crude mixture was purified by flash column chromatography (SiO_2, hexane:Et_2O 95:5, two consecutive purifications) to afford the racemic product as an inseparable mixture of two diastereomers *syn*-**37h** and *anti*-**37h** (18.5 mg, 0.07 mmol, 35% yield, 1:1.1 d.r.) as colorless crystals. The enantiomers of the corresponding 2,4-dinitrophenylhydrazone (obtained upon condensation with 2,4-dinitrophenylhydrazine) were separated by UPC^2 analysis on a Daicel Chiralpak ID-3 column: isocratic 100% CO_2 for 1 min; gradient from 100% CO_2 to 70:30 CO_2/ EtOH for 21 min; isocratic 70:30 CO_2/EtOH for 6 min, gradient from 70:30 CO_2/EtOH to 100% CO_2 for 2 min, flow rate 1.0 mL/min, λ = 346 nm: *syn*-**37h**: τ = 20.0 min and τ = 20.6 min; *anti*-**37h**: τ = 21.1 min and τ = 22.1 min.

^{1}H NMR (500 MHz, $CDCl_3$, mixture of diastereoisomers) δ 9.57 (t, *J* = 2.1 Hz, 1H), 9.35 (dd, *J* = 2.5, 1.6 Hz, 1H), 7.38 – 7.28 (m, 2H), 7.25 – 7.17 (m, 6H), 7.17 – 7.12 (m, 3H), 7.01 – 6.94 (m, 2H), 6.92 – 6.84 (m, 3H), 6.76 – 6.72 (m, 2H), 3.81 (s, 3H), 3.76 (s, 3H), 3.43 (q, *J* = 7.3 Hz, 1H), 3.25 (td, *J* = 10.1, 4.7 Hz, 1H), 3.03 (p, *J* = 7.0 Hz, 1H), 2.86 (dq, *J* = 10.3, 6.9

Hz, 1H), 2.78 (dd, *J* = 7.4, 2.0 Hz, 2H), 2.60 (ddd, *J* = 16.7, 9.9, 2.5 Hz, 1H), 2.49 (ddd, *J* = 16.7, 4.7, 1.6 Hz, 1H), 1.25 (d, *J* = 7.1 Hz, 3H), 1.02 (d, *J* = 6.9 Hz, 3H).

^{13}C NMR (126 MHz, $CDCl_3$, mixture of diastereoisomers) δ 202.3, 201.9, 158.5, 158.1, 142.9, 141.6, 137.2, 135.8, 129.1, 128.8, 128.7, 128.6, 128.2, 128.2, 126.9, 126.7, 114.2, 113.5, 55.4, 55.3, 49.2, 47.9, 46.7, 46.3, 45.3, 44.2, 20.8, 18.3.

HRMS (ESI): Calculated for $[M+Na]^+$ $[C_{18}H_{20}NaO_2]^+$: 291.1356, found: 291.1355.

4-Phenyl-3-(*p*-tolyl)pentanal (37i)

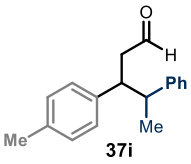

37i

Prepared according to **GP3**, using silane **46a** (41 µL, 0.2 mmol), the racemic amine catalyst **A-2** (9.9 mg, 40 µmol), the photocatalyst Mes-Acr (2.9 mg, 5 µmol, 2.5 mol%) and enal **29b** (58 mg, 0.4 mmol) in 0.3 M acetonitrile solution of TFA (9.2 µL, 0.12 mmol, 60 mol%). The solution was irradiated for 16h at room temperature. The crude mixture was purified by flash column chromatography (SiO_2, hexane:Et_2O 95:5, two consecutive purifications) to afford the racemic product as an inseparable mixture of two diastereomers *syn*-**37i** and *anti*-**37i** (27.2 mg, 0.11 mmol, 54% yield, 1:1.1 d.r.) as colorless oil. The enantiomers of the corresponding 2,4-dinitrophenylhydrazone (obtained upon condensation with 2,4-dinitrophenylhydrazine) were separated by UPC^2 analysis on a Daicel Chiralpak IE-3 column: isocratic 100% CO_2 for 1 min; gradient from 100% CO_2 to 60:40 CO_2/MeOH for 14 min; isocratic 60:40 CO_2/EtOH for 4 min, gradient from 60:40 CO_2/EtOH to 100% CO_2 for 1 min, flow rate 2.0 mL/min, λ = 353 nm: *syn*-**37i**: τ = 13.5 min and τ = 13.7 min; *anti*-**37i**: τ = 14.1 min and τ = 14.4 min.

^{1}H NMR (500 MHz, $CDCl_3$, mixture of diastereoisomers) δ 9.55 (t, *J* = 2.2 Hz, 1H), 9.35 (dd, *J* = 2.6, 1.6 Hz, 1H), 7.36 – 7.30 (m, 2H), 7.27 – 7.18 (m, 6H), 7.18 – 7.13 (m, 4H), 7.03 – 6.98 (m, 4H), 6.90 – 6.85 (m, 2H), 3.44 (dt, *J* = 8.6, 6.7 Hz, 1H), 3.27 (td, *J* = 10.3, 4.6 Hz, 1H), 3.06 (p, *J* = 7.0 Hz, 1H), 2.87 (dq, *J* = 10.5, 6.9 Hz, 1H), 2.82 – 2.71 (m, 2H), 2.59 (ddd, *J* = 16.7, 10.1, 2.6 Hz, 1H), 2.44 (ddd, *J* = 16.7, 4.6, 1.6 Hz, 1H), 2.34 (s, 3H), 2.28 (s, 3H), 1.27 (d, *J* = 7.1 Hz, 3H), 1.05 (d, *J* = 6.9 Hz, 3H).

^{13}C NMR (126 MHz, $CDCl_3$, mixture of diastereoisomers) δ 202.4, 202.0, 145.4, 144.0, 139.6, 138.4, 136.5, 136.2, 129.5, 128.9, 128.8, 128.5, 128.2, 128.1, 128.1, 127.7, 126.8, 126.4, 49.2, 47.3, 46.2, 46.2, 46.1, 45.1, 21.2, 21.1, 20.7, 17.9.

HRMS (ESI): Calculated for $[M+Na]^+$ $[C_{18}H_{20}NaO]^+$: 275.1406, found: 275.1395.

3-(4-Bromophenyl)-4-phenylpentanal (37j)

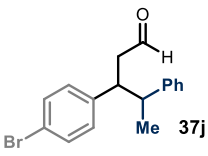

37j

Prepared according to **GP3**, using silane **46a** (41 µL, 0.2 mmol), the racemic amine catalyst **A-2** (9.9 mg, 40 µmol), the photocatalyst Mes-Acr (2.9 mg, 5 µmol, 2.5 mol%) and enal **29d** (84 mg, 0.4 mmol) in 0.3 M acetonitrile solution of TFA (9.2 µL, 0.12 mmol, 60 mol%). The solution was irradiated for 16h at room temperature. The crude mixture

was purified by flash column chromatography (SiO_2 two consecutive purifications: hexane:Et_2O 95:5 then toluene) to afford the racemic product as an inseparable mixture of two diastereomers *syn*-**37j** and *anti*-**37j** (44.8 mg, 0.14 mmol, 71% yield, 1:1.1 d.r.) as colorless oil. The enantiomers of the corresponding 2,4-dinitrophenylhydrazone (obtained upon condensation with 2,4-dinitrophenylhydrazine) were separated by UPC^2 analysis on a Daicel Chiralpak IE-3 column: isocratic 100% CO_2 for 1 min; gradient from 100% CO_2 to 70:30 CO_2/ EtOH for 5 min; isocratic 70:30 CO_2/EtOH for 10 min, gradient from 70:30 CO_2/EtOH to 100% CO_2 for 1 min, flow rate 2.0 mL/min, λ = 348 nm: *syn*-**37j**: τ = 10.7 min and τ = 11.2 min; *anti*-**37j**: τ = 12.0 min and τ = 12.3 min.

^{1}H NMR (400 MHz, $CDCl_3$, mixture of diastereoisomers) δ 9.58 (dd, *J* = 2.3, 1.5 Hz, 1H), 9.36 (dd, *J* = 2.3, 1.3 Hz, 1H), 7.48 – 7.43 (m, 2H), 7.36 – 7.27 (m, 4H), 7.25 – 7.08 (m, 8H), 6.98 – 6.93 (m, 2H), 6.85 – 6.79 (m, 2H), 3.43 (dt, *J* = 9.2, 6.4 Hz, 1H), 3.29 (td, *J* = 10.1, 4.6 Hz, 1H), 3.02 (p, *J* = 7.1 Hz, 1H), 2.91 – 2.82 (m, 1H), 2.82 – 2.70 (m, 2H), 2.60 (ddd, *J* = 17.1, 9.9, 2.3 Hz, 1H), 2.48 (ddd, *J* = 17.1, 4.6, 1.4 Hz, 1H), 1.28 (d, *J* = 7.1 Hz, 3H), 1.04 (d, *J* = 6.9 Hz, 3H).

^{13}C NMR (101 MHz, $CDCl_3$, mixture of diastereoisomers) δ 201.5, 201.1, 144.8, 143.5, 141.9, 140.7, 131.9, 131.3, 130.4, 130.0, 128.9, 128.3, 128.2, 127.7, 127.0, 126.6, 120.7, 120.5, 49.0, 46.9, 46.6, 46.0, 45.9, 45.0, 20.5, 18.5.

HRMS (ESI): Calculated for $[M+MeOH+Na]^+$ $[C_{18}H_{21}NaO_2]^+$: 371.0617, found: 371.0607.

Synthesis of 4-Methyl-4-(5-oxotetrahydrofuran-2-yl)-3-phenylpentanal (39)

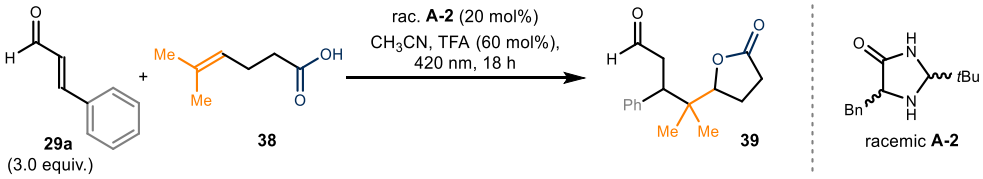

Reference compounds **39** was synthesized following a reported literature procedure.[71] A dry vial was charged with cinnamaldehyde **29a** (75.5 µL, 0.6 mmol, 3.0 equiv.), 5-methylhex-4-enoic acid **38** (25.6 mg, 0.2 mmol, 1.0 equiv.) and racemic amine catalyst **A-2** (9.9 mg, 40 µmol, 20 mol%). The vial was sealed with a septum, flushed with argon, dry acetonitrile (400 µL) and TFA (9.2 µL, 0.12 mmol, 60 mol%) was added and the vial was stirred for 18 h under irradiation with 420 nm (single LED, 120 mW/cm^3) under ambient conditions. The crude mixture was purified by flash column chromatography (SiO_2, hexane:EtOAc 70:30) to afford the lactone product **39** (45.8 mg, 0.18 mmol, 88% yield, 1:1 d.r.) as a mixture of two diastereomers. The corresponding 2,4-dinitrophenylhydrazones (obtained upon condensation with 2,4-dinitrophenylhydrazine) could be separated by preparative TLC and the enantiomers could be separated by UPC^2 analysis on a Daicel Chiralpak ID-3 column: isocratic 100% CO_2

for 1 min; gradient from 100% CO_2 to 70:30 CO_2/EtOH for 5 min; isocratic 70:30 CO_2/EtOH for 9 min, gradient from 70:30 CO_2/EtOH to 100% CO_2 for 1 min, flow rate 2.0 mL/min, λ = 346 nm: **39**: diastereomer 1: τ = 9.6 min and τ = 11.8 min, diastereomer 2: τ = 10.8 min and τ = 11.2 min.

^{1}H NMR (400 MHz, $CDCl_3$, mixture of diastereoisomers) δ 9.51 (dd, *J* = 2.6, 1.2 Hz, 1H), 9.49 (dd, *J* = 2.9, 1.5 Hz, 1H), 7.34 – 7.18 (m, 10H), 4.28 (dd, *J* = 8.8, 7.0 Hz, 1H), 4.09 (dd, *J* = 8.8, 7.3 Hz, 1H), 3.52 (dd, *J* = 10.6, 5.0 Hz, 1H), 3.34 (dd, *J* = 10.9, 4.3 Hz, 1H), 3.04 (ddd, *J* = 17.0, 10.9, 2.6 Hz, 1H), 2.96 – 2.76 (m, 3H), 2.57 – 2.39 (m, 4H), 2.17 – 1.91 (m, 4H), 1.03 (s, 3H), 0.96 (s, 3H), 0.87 (s, 3H), 0.78 (s, 3H).

Synthesis of 2-(4-Methoxy-2-phenylbut-3-en-1-yl)furan (**54**) *for the Determination of Enantiomeric Ratio of* **35j**

3-(Furan-2-yl)-2-phenylpropanal (50)

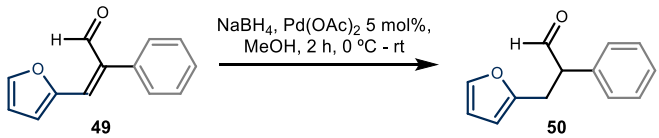

The procedure was adapted from a literature procedure.[81] A dry round bottom flask, equipped with magnet a septum and 3 empty balloons was charged under Argon atmosphere with 3-(2-furyl)-2-phenylpropenal **49** (594 mg, 3.0 mmol, 1.0 equiv.), $NaBH_4$ (113 mg, 3.0 mmol, 1.0 equiv.) and $Pd(OAc)_2$ (33.7 mg, 5 mol%). The flask was cooled to 0 ºC and dry methanol (3 mL) was carefully added dropwise (evolution of hydrogen!). The ice bath was removed and the mixture was stirred for 2 h, filtered over celite and concentrated. The residue was re-dissolved in DCM (50 mL) and washed with brine. The organic layer was dried with $MgSO_4$, filtered and concentrated. Column chromatography (SiO_2, hexane:EtOAc 9:1) afforded aldehyde **50** (40 mg, 0.20 mmol, 7%) as colorless oil (side product).

^{1}H NMR (500 MHz, $CDCl_3$): δ 9.75 (d, *J* = 1.4 Hz, 1H), 7.41 – 7.33 (m, 2H), 7.32 – 7.27 (m, 2H), 7.19 – 7.15 (m, 2H), 6.22 (dd, *J* = 3.2, 1.9 Hz, 1H), 5.91 (dd, *J* = 3.2, 0.8 Hz, 1H), 3.98 (td, *J* = 7.3, 1.4 Hz, 1H), 3.47 (dd, *J* = 15.5, 7.1 Hz, 1H), 3.04 (dd, *J* = 15.4, 7.5 Hz, 1H).

^{13}C NMR (126 MHz, $CDCl_3$): δ 199.5, 152.6, 141.4, 135.5, 129.2, 128.9, 128.0, 110.4, 106.9, 57.8, 28.6.

HRMS (ESI): calculated for $[M+Na]^+$ $[C_{13}H_{12}NaO_2]^+$: 223.0730, found 223.0724.

[81] De Castro, K. A., Oh, S., Yun, J., Lim, J. K., An, G., Kim, D. K.,Rhee, H. "Colloidal palladium nanoparticles with in situ H_2: Reducing system for α,β-unsaturated carbonyl compounds" *Synth. Commun.* **2009**, *39*, 3509–3520.

2-(4-Methoxy-2-phenylbut-3-en-1-yl)furan (51)

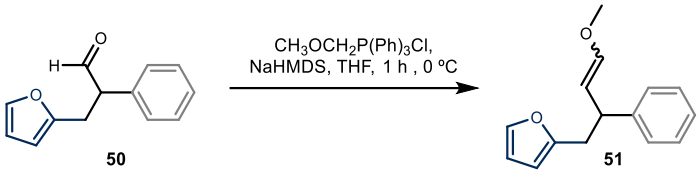

A dry flask was charged with methoxymethyl-triphenylphosphonium chloride (249 mg, 0.729 mmol, 3.9 equiv.) under an argon atmosphere and anhydrous THF (3 mL) was added. After cooling to 0 ºC, NaHMDS (0.73 mL, 0.73 mmol, 3.9 equiv., 1 M in THF) was added and the mixture was stirred for 10 minutes. Then, a solution of aldehyde **50**(40 mg, 0.187 mmol, 1 equiv.) in anhydrous THF (2 mL) was added and the mixture was stirred for 1 h at 0 ºC. The mixture was filtered over a plug of silica gel (after washing with ethylacetate) and concentrate. Column chromatography (SiO_2, hexane:EtOAc 95:5) afforded 2.2 mg (5%) of enol ether **51** (2.2 mg, 9.6 µmol, 5%, 4:1 mixture of double bond isomers). The enantiomers of the corresponding 2,4-dinitrophenylhydrazone (obtained upon condensation with 2,4-dinitrophenylhydrazine) were separated by UPC[2] analysis on a Daicel Chiralpak ID-3 column: isocratic 100% CO_2 for 1 min; gradient from 100% CO_2 to 60:40 CO_2/*i*-PrOH for 5 min; isocratic 60:40 CO_2/*i*-PrOH for 2 min, gradient from 60:40 CO_2/*i*-PrOH to 100% CO_2 for 1 min, flow rate 2.0 mL/min, λ = 347 nm, **35j**: τ = 6.0 min and τ = 6.1 min.

^{1}H NMR (500 MHz, $CDCl_3$, *major isomer*): δ 7.32 – 7.14 (m, 6H), 6.25 (d, *J* = 12.6 Hz, 1H), 6.22 (dd, *J* = 3.2, 1.9 Hz, 1H), 5.87 (dd, *J* = 3.1, 0.7 Hz, 1H), 4.94 (dd, *J* = 12.6, 8.5 Hz, 1H), 3.66 – 3.57 (m, 1H), 3.48 (s, 3H), 3.07 – 2.92 (m, 2H).

^{13}C NMR (126 MHz, $CDCl_3$, *mixture of isomers*): δ 154.6, 154.2, 148.0, 146.4, 144.9, 141.0, 140.9, 128.6, 128.5, 127.4, 127.4, 126.4, 126.2, 110.2, 110.1, 109.7, 106.5, 106.3, 106.1, 59.8, 56.1, 43.9, 39.5, 36.1, 35.6.

HRMS (ESI): calculated for $[M+Na]^+$ $[C_{15}H_{16}NaO_2]^+$: 251.1043, found: 251.1053.

3.6.6 General Procedures and Scope of the Biocatalytic Radical Coupling

3.6.6.1 Experimental Setup

Set-up: The biocatalytic reactions were performed using a purple LED strip as the light source. A commercial 5-meter LED strip was wrapped around a 9 cm crystallizing dish, while a fan was used to cool down the reactor (the reaction temperature was measured to be between 28-33 ºC). The experiments at 405 nm were conducted using a 5 m strip, from Arotelicht, model number: 5M SMD 2835 LED purchased from Amazon.

Analytical scale (Set-up 1): The set up for the analytical scale consisted of a crystallizing dish with a 3D printed support of 10 positions, and a hole of 47 mm in the middle to allow ventilation (Figure 3.37, left). Each of the positions could be used to fit a standard 16 mm diameter vial.

Semipreparative scale (Set-up 2): A 50 mL round bottom flask was placed in the middle of the photoreactor (Figure 3.37, right).

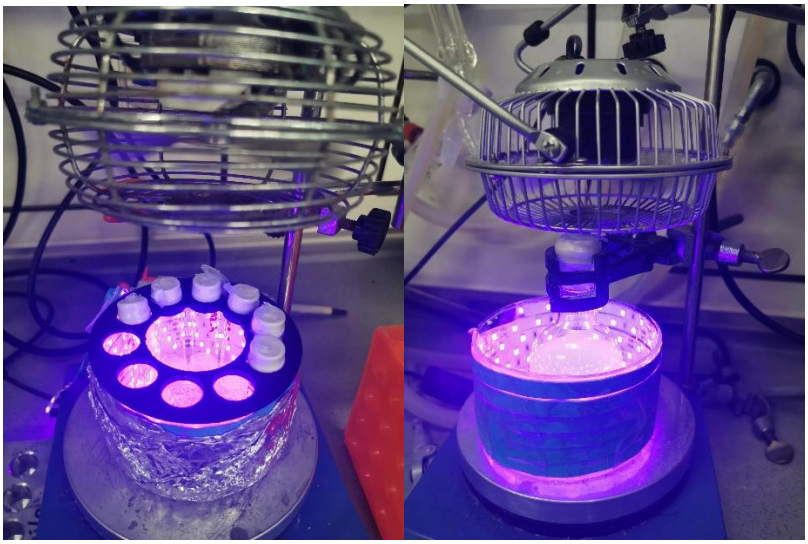

Figure 3.37. Left panel: *Set-up 1* for the analytical scale enzymatic reactions (1.25 µmol scale) right panel: *Set-up 2* for the semi-preparative scale enzymatic reactions (0.075 mmol scale)

3.6.6.2 Analytical Scale Biocatalytic Reactions – Enantioselective Procedure

GP4 – General Procedure for the Analytical Scale Biocatalytic Synthesis of Compounds **39**

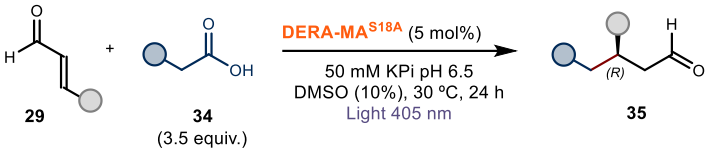

A stock solution of enal **29** (50 mM) and a stock solution of the corresponding acid **34** (175 mM) in DMSO were added to a 5 mL glass vial containing KPi buffer pH 6.5. The headspace of the vial was purged with argon and the purified enzyme DERA-MA^{S18A} (62.5 nmol, 0.05 equiv.) in KPi buffer pH 6.5 was added to reach the final volume of 500 µL. The vial was then placed in the 3D printed support photoreactor (see section I1) and irradiated under stirring

(5 mm x 2 mm, VWR, 360 rpm) for 16 hours. The crude mixture was extracted once with 600 µL ethyl acetate containing 5 mM of the internal standard 1,3,5-trimethoxybenzene. The organic extract was dried over anhydrous $MgSO_4$, filtered and analyzed by GC-FID on HP-5 column. Calibration curves not reported in the present dissertation, were obtained using the previously synthesized reference compounds **35** and 1,3,5-trimethoxybenzene as the internal standard. The GC-FID data for the analytical scale reactions were fit in the equation to determine the analytical yield of the products **35**. The enantiomeric excess was determined by UPC^2 analysis.

(*R*)-3,4-Diphenylbutanal (35a)

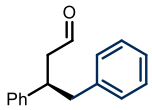

35a

Prepared according to **GP4**, using phenylacetic acid **34a** (25 µL of a 175 mM stock solution in DMSO, 4.4 µmol) and cinnamaldehyde **29a** (25 µL of a 50 mM stock solution in DMSO, 1.25 µmol) as substrates in a 10% v/v DMSO/KPi buffer pH 6.5 mixture. The crude extract was analyzed by GC-FID on HP-5 column. The analytical yield of product **35a** was determined according to the calibration curve (response factor = 2.12) using 1,3,5-trimethoxybenzene as the internal standard and as an average of three runs (57% yield, >99% ee). The enantiomeric excess of the corresponding 2,4-dinitrophenylhydrazone (obtained upon condensation with 2,4-dinitrophenylhydrazine) was determined using UPC^2 on a Daicel Chiralpak ID-3 column: isocratic 100% CO_2 for 1 min; gradient from 100% CO_2 to 60:40 CO_2/*i*-PrOH for 5 min; isocratic 60:40 CO_2/*i*-PrOH for 2 min, gradient from 60:40 CO_2/*i*-PrOH to 100% CO_2 for 1 min, flow rate 2.0 mL/min, λ = 347 nm, **35a**: τ_{major} = 6.4 min and τ_{minor} = 6.5 min. The absolute configuration was assigned by comparison of the enzymatic product with the corresponding product **35a** obtained via the organocatalytic route.

(*R*)-3-Phenyl-4-(p-tolyl)butanal (35b)

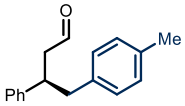

35b

Prepared according to **GP4**, using p-tolylacetic acid **34b** (25 µL of a 175 mM stock solution in DMSO, 4.4 µmol) and cinnamaldehyde **29a** (25 µL of a 50 mM stock solution in DMSO, 1.25 µmol) as substrates in a 10% v/v DMSO/KPi buffer pH 6.5 mixture. The crude extract was analyzed by GC-FID on HP-5 column. The analytical yield of product **35b** was determined according to the calibration curve (response factor = 2.20) given below using 1,3,5-trimethoxybenzene as the internal standard and as an average of three runs (53% yield, >99% ee). The enantiomeric excess of the corresponding 2,4-dinitrophenylhydrazone (obtained upon condensation with 2,4-dinitrophenylhydrazine) was determined using UPC^2 on a Daicel Chiralpak ID-3 column isocratic 100% CO_2 for 1 min; gradient from 100% CO_2 to 60:40 CO_2/i-PrOH for 5 min; isocratic 60:40 CO_2/i-PrOH for 2 min, gradient from 60:40 CO_2/i-PrOH to 100% CO_2, flow rate 2.0 mL/min, λ = 348 nm, **35b**: τ_{major} = 6.3 min and τ_{minor} = 6.5 min.

(*R*)-3-Phenyl-4-(*m*-tolyl)butanal (35c)

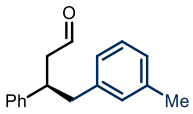

35c

Prepared according to **GP4**, using *m*-tolylacetic acid **34c** (25 µL of a 175 mM stock solution in DMSO, 4.4 µmol) and cinnamaldehyde **29a** (25 µL of a 50 mM stock solution in DMSO, 1.25 µmol) as substrates in a 10% v/v DMSO/KPi buffer pH 6.5 mixture. In this case, parental enzyme DERA-MA (62.5 nmol, 0.05 equiv.) was added. The crude extract was analyzed by GC-FID on HP-5 column. The analytical yield of product **35c** was determined according to the calibration curve (response factor = 2.28) given below using 1,3,5-trimethoxybenzene as the internal standard and as an average of three runs (53% yield, >99% ee). The enantiomeric excess of the corresponding 2,4-dinitrophenylhydrazone (obtained upon condensation with 2,4-dinitrophenylhydrazine) was determined using UPC^2 on a Daicel Chiralpak ID-3 column: isocratic 100% CO_2 for 1 min; gradient from 100% CO_2 to 60:40 CO_2/i-PrOH for 5 min; isocratic 60:40 CO_2/i-PrOH for 2 min, gradient from 60:40 CO_2/i-PrOH to 100% CO_2, flow rate 2.0 mL/min, λ = 348 nm, **35c**: τ_{major} = 6.3 min and τ_{minor} = 6.4 min.

(*R*)-3-Phenyl-4-(*o*-tolyl)butanal (35d)

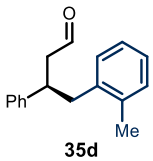

35d

Prepared according to **GP4**, using *o*-tolylacetic acid **34d** (25 µL of a 175 mM stock solution in DMSO, 4.4 µmol) and cinnamaldehyde **29a** (25 µL of a 50 mM stock solution in DMSO, 1.25 µmol) as substrates in a 10% v/v DMSO/KPi buffer pH 6.5 mixture. In this case, parental enzyme DERA-MA (62.5 nmol, 0.05 equiv.) was added. The crude extract was analyzed by GC-FID on HP-5 column. The analytical yield of product **35d** was determined according to the calibration curve (response factor = 2.15) given below using 1,3,5-trimethoxybenzene as the internal standard and as an average of three runs (35% yield, 99% ee). The enantiomeric excess of the corresponding 2,4-dinitrophenylhydrazone (obtained upon condensation with 2,4-dinitrophenylhydrazine) was determined by UPC^2 analysis on a Daicel Chiralpak ID-3 column isocratic 100% CO_2 for 1 min; gradient from 100% CO_2 to 60:40 CO_2/i-PrOH for 5 min; isocratic 60:40 CO_2/i-PrOH for 2 min, gradient from 60:40 CO_2/i-PrOH to 100% CO_2, flow rate 2.0 mL/min, λ = 348 nm, **35d**: τ_{major} = 6.3 min and τ_{minor} = 6.5 min.

(*R*)-4-(4-Bromophenyl)-3-phenylbutanal (35e)

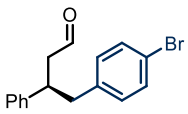

35e

Prepared according to **GP4**, using 4-bromophenylacetic acid **34e** (25 µL of a 175 mM stock solution in DMSO, 4.4 µmol) and cinnamaldehyde **29a** (25 µL of a 50 mM stock solution in DMSO, 1.25 µmol) as substrates in a 10% v/v DMSO/KPi buffer pH 6.5 mixture. The crude extract was analyzed by GC-FID on HP-5 column. The analytical yield of product **35e** was determined according to the calibration curve (response factor = 2.09) given below using 1,3,5-trimethoxybenzene as the internal standard and as an average of three runs (37% yield,

>99% ee). The enantiomeric excess of the corresponding 2,4-dinitrophenylhydrazone (obtained upon condensation with 2,4-dinitrophenylhydrazine) was determined by UPC^2 analysis on a Daicel Chiralpak ID-3 column: isocratic 100% CO_2 for 1 min; gradient from 100% CO_2 to 60:40 CO_2/i-PrOH for 5 min; isocratic 60:40 CO_2/i-PrOH for 2 min, gradient from 60:40 CO_2/i-PrOH to 100% CO_2, flow rate 2.0 mL/min, λ = 347 nm, **35e**: τ_{major} = 7.3 min and τ_{minor} = 7.6 min.

(*R*)-4-(4-Chlorophenyl)-3-phenylbutanal (35f)

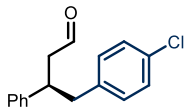

35f

Prepared according to **GP4**, using 4-chlorophenylacetic acid **34f** (25 µL of a 175 mM stock solution in DMSO, 4.4 µmol) and cinnamaldehyde **29a** (25 µL of a 50 mM stock solution in DMSO, 1.25 µmol) as substrates in a 10% v/v DMSO/KPi buffer pH 6.5 mixture. The crude extract was analyzed by GC-FID on HP-5 column. The analytical yield of product **35f** was determined according to the calibration curve (response factor = 2.17) given below using 1,3,5-trimethoxybenzene as the internal standard and as an average of three runs (46% yield, >99% ee). The enantiomeric excess of the corresponding 2,4-dinitrophenylhydrazone (obtained upon condensation with 2,4-dinitrophenylhydrazine) was determined by UPC^2 analysis on a Daicel Chiralpak ID-3 column: isocratic 100% CO_2 for 1 min; gradient from 100% CO_2 to 60:40 CO_2/i-PrOH for 5 min; isocratic 60:40 CO_2/i-PrOH for 2 min, gradient from 60:40 CO_2/i-PrOH to 100% CO_2, flow rate 2.0 mL/min, λ = 347 nm, **35f**: τ_{major} = 6.9 min and τ_{minor} = 7.1 min.

(*R*)-4-(4-Fluorophenyl)-3-phenylbutanal (35g)

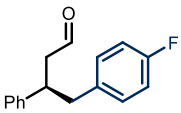

35g

Prepared according to **GP4**, using 4-fluorophenylacetic acid **34g** (25 µL of a 175 mM stock solution in DMSO, 4.4 µmol) and cinnamaldehyde **29a**(25 µL of a 50 mM stock solution in DMSO, 1.25 µmol) as substrates in a 10% v/v DMSO/KPi buffer pH 6.5 mixture. The crude extract was analyzed by GC-FID on HP-5 column. The analytical yield of product **35g** was determined according to the calibration curve (response factor = 2.16) given below using 1,3,5-trimethoxybenzene as the internal standard and as an average of three runs (43% yield, >99% ee). The enantiomeric excess of the corresponding 2,4-dinitrophenylhydrazone (obtained upon condensation with 2,4-dinitrophenylhydrazine) was determined by UPC^2 analysis on a Daicel Chiralpak ID-3 column isocratic 100% CO_2 for 1 min; gradient from 100% CO_2 to 60:40 CO_2/*i*PrOH for 5 min; isocratic 60:40 CO_2/*i*PrOH for 2 min, gradient from 60:40 CO_2/*i*-PrOH to 100% CO_2, flow rate 2.0 mL/min, λ = 347 nm, **35g**: τ_{major} = 6.2 min and τ_{minor} = 6.5 min.

(*R*)-4-(4-Methoxyphenyl)-3-phenylbutanal (35h)

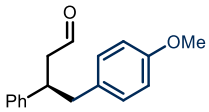

35h

Prepared according to **GP4**, using 4-methoxyphenylacetic acid **34h** (25 µL of a 175 mM stock solution in DMSO, 4.4 µmol) and cinnamaldehyde **29a** (25 µL of a 50 mM stock solution in DMSO, 1.25 µmol) as substrates in a 10% v/v DMSO/KPi buffer pH 6.5 mixture. The crude extract was analyzed by GC-FID on HP-5 column. The analytical yield of product **35h** was determined according to the calibration curve (response factor = 2.13) given below using 1,3,5-trimethoxybenzene as the internal standard and as an average of three runs (61% yield, >99% ee). The enantiomeric excess of the corresponding 2,4-dinitrophenylhydrazone (obtained upon condensation with 2,4-dinitrophenylhydrazine) was determined by UPC^2 analysis on a Daicel Chiralpak ID-3 column: isocratic 100% CO_2 for 1 min; gradient from 100% CO_2 to 60:40 CO_2/*i*PrOH for 5 min; isocratic 60:40 CO_2/*i*PrOH for 2 min, gradient from 60:40 CO_2/*i*PrOH to 100% CO_2, flow rate 2.0 mL/min, λ = 349 nm, **35h**: τ_{major} = 7.0 min and τ_{minor} = 7.2 min.

(*R*)-3-Phenyl-4-(thiophen-2-yl)butanal (35i)

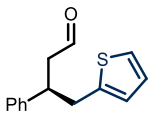

35i

Prepared according to **GP4**, using thiophene-2-acetic acid **34i** (25 µL of a 175 mM stock solution in DMSO, 4.4 µmol) and cinnamaldehyde **29a** (25 µL of a 50 mM stock solution in DMSO, 1.25 µmol) as substrates in a 10% v/v DMSO/KPi buffer pH 6.5 mixture. The crude extract was analyzed by GC-FID on HP-5 column. The analytical yield of product **35i** was determined according to the calibration curve (response factor = 2.05) given below using 1,3,5-trimethoxybenzene as the internal standard and as an average of three runs (46% yield, >99% ee). The enantiomeric excess of the corresponding 2,4-dinitrophenylhydrazone (obtained upon condensation with 2,4-dinitrophenylhydrazine) was determined by UPC^2 analysis on a Daicel Chiralpak ID-3 column: isocratic 100% CO_2 for 1 min; gradient from 100% CO_2 to 60:40 CO_2/*i*PrOH for 5 min; isocratic 60:40 CO_2/*i*PrOH for 2 min, gradient from 60:40 CO_2/*i*PrOH to 100% CO_2, flow rate 2.0 mL/min, λ = 348 nm, **35i**: τ_{major} = 6.7 min and τ_{minor} = 6.9 min.

(*R*)-3-Phenyl-4-(furan-2-yl)butanal (35j)

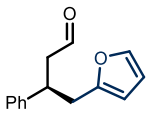

35j

Prepared according to **GP4**, using 2-furanacetic acid **34j** (25 µL of a 175 mM stock solution in DMSO, 4.4 µmol) and cinnamaldehyde **29a** (25 µL of a 50 mM stock solution in DMSO, 1.25 µmol) as substrates in a 10% v/v DMSO/KPi buffer pH 6.5 mixture. The crude extract was analyzed by GC-FID on HP-5 column. The analytical yield of product **35j** was determined according to the calibration curve (response factor = 1.97) given below using 1,3,5-trimethoxybenzene as the internal standard and as an average of three runs (71% yield, >99% ee). The enantiomeric excess of the corresponding 2,4-dinitrophenylhydrazone (obtained upon condensation with

2,4-dinitrophenylhydrazine) was determined by UPC^2 analysis on a Daicel Chiralpak ID-3 column: isocratic 100% CO_2 for 1 min; gradient from 100% CO_2 to 60:40 CO_2/*i*PrOH for 5 min; isocratic 60:40 CO_2/*i*PrOH for 2 min, gradient from 60:40 CO_2/*i*PrOH to 100% CO_2, flow rate 2.0 mL/min, λ = 347 nm, **35j**: τ_{major} = 6.0 min and τ_{minor} = 6.1 min.

(*R*)-4-Phenyl-3-(p-tolyl)butanal (35k)

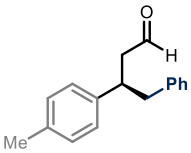

35k

Prepared according to **GP4**, using phenylacetic acid **34a** (25 µL of a 175 mM stock solution in DMSO, 4.4 µmol) and *p*-methylcinnamaldehyde **29b** (25 µL of a 50 mM stock solution in DMSO, 1.25 µmol) as substrates in a 10% v/v DMSO/KPi buffer pH 6.5 mixture. The crude extract was analyzed by GC-FID on HP-5 column. The analytical yield of product **35k** was determined according to the calibration curve (response factor = 2.32) given below using 1,3,5-trimethoxybenzene as the internal standard and as an average of three runs (58% yield, >99% ee). The enantiomeric excess of the corresponding 2,4-dinitrophenylhydrazone (obtained upon condensation with 2,4-dinitrophenylhydrazine) was determined using UPC^2 analysis on a Daicel Chiralpak ID-3 column: isocratic 100% CO_2 for 1 min; gradient from 100% CO_2 to 60:40 CO_2/*i*PrOH for 5 min; isocratic 60:40 CO_2/*i*PrOH for 2 min, gradient from 60:40 CO_2/*i*PrOH to 100% CO_2, flow rate 2.0 mL/min, λ = 347 nm, **35k**: τ_{major} = 6.3 min and τ_{minor} = 6.5 min.

(*R*)-3-(4-Methoxyphenyl)-4-phenylbutanal (35l)

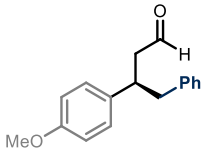

35l

Prepared according to **GP4**, using phenylacetic acid **34a** (25 µL of a 175 mM stock solution in DMSO, 4.4 µmol) and *p*-methoxycinnamaldehyde **29c** (25 µL of a 50 mM stock solution in DMSO, 1.25 µmol) as substrates in a 10% v/v DMSO/KPi buffer pH 6.5 mixture. The crude extract was analyzed by GC-FID on HP-5 column. The analytical yield of product **35l** was determined according to the calibration curve (response factor = 2.11) given below using 1,3,5-trimethoxybenzene as the internal standard and as an average of three runs (29% yield, 96% ee). The enantiomeric excess of the corresponding 2,4-dinitrophenylhydrazone (obtained upon condensation with 2,4-dinitrophenylhydrazine) was determined using UPC^2 analysis on a Daicel Chiralpak ID-3 column: isocratic 100% CO_2 for 1 min; gradient from 100% CO_2 to 60:40 CO_2/*i*PrOH for 5 min; isocratic 60:40 CO_2/*i*PrOH for 2 min, gradient from 60:40 CO_2/*i*PrOH to 100% CO_2, flow rate 2.0 mL/min, λ = 348 nm, **35l**: τ_{major} = 6.8 min and τ_{minor} = 7.0 min.

(*R*)-3-(4-Bromophenyl)-4-phenylbutanal (35m)

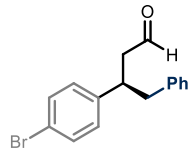

35m

Prepared according to **GP4**, using phenylacetic acid **34a** (25 µL of a 175 mM stock solution in DMSO, 4.4 µmol) and *p*-bromocinnamaldehyde **29d** (25 µL of a 50 mM stock solution in DMSO, 1.25 µmol) as substrates in a 10% v/v DMSO/KPi buffer pH 6.5 mixture. The crude extract was analyzed by GC-FID on HP-5 column. The analytical yield of product **35m** was determined according to the calibration curve (response factor = 2.07) given below using 1,3,5-trimethoxybenzene as the internal standard and as an average of three runs (48% yield, >99% ee). The enantiomeric excess of the corresponding 2,4-dinitrophenylhydrazone (obtained upon condensation with 2,4-dinitrophenylhydrazine) was determined using UPC^2 analysis on a Daicel Chiralpak ID-3 column: isocratic 100% CO_2 for 1 min; gradient from 100% CO_2 to 60:40 CO_2/MeOH for 13 min; isocratic 60:40 CO_2/MeOH for 2 min, gradient from 60:40 CO_2/MeOH to 100% CO_2 for 1 min, flow rate 2.0 mL/min, λ = 350 nm, **35m**: τ_{major} = 13.2 min and τ_{minor} = 13.5 min.

(3*R*)-4-Methyl-4-(5-oxotetrahydrofuran-2-yl)-3-phenylpentanal (39)

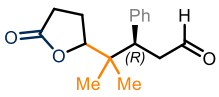

39

Prepared according to **GP4**, using 5-methylhex-4-enoic acid **38** (25 µL of a 175 mM stock solution in DMSO, 4.4 µmol) and cinnamaldehyde **29a** (25 µL of a 50 mM stock solution in DMSO, 1.25 µmol) as substrates in a 10% v/v DMSO/KPi buffer pH 6.5 mixture was added. The crude extract was analyzed by GC-FID on HP-5 column. The analytical yield of product **39** was determined according to the calibration curve (response factor = 1.53) given below using mesitylene as the internal standard and as an average of three runs (19% yield, 3.8:1 d.r., >99% ee). The enantiomeric excess of the corresponding 2,4-dinitrophenylhydrazone (obtained upon condensation with 2,4-dinitrophenylhydrazine) was determined using UPC^2 analysis on a Daicel Chiralpak ID-3 column: isocratic 100% CO_2 for 1 min; gradient from 100% CO_2 to 70:30 CO_2/EtOH for 5 min; isocratic 70:30 CO_2/EtOH for 9 min, gradient from 70:30 CO_2/EtOH to 100% CO_2 for 1 min, flow rate 2.0 mL/min, λ = 346 nm: **39**: diastereomer 1: τ = 9.6 min, diastereomer 2: τ = 10.8 min.

3.6.6.3 Analytical Scale Biocatalytic Reactions – Stereospecific Procedure

GP5 – General Procedure for the Analytical Scale the Stereospecific Biocatalytic Synthesis of Compounds **37**

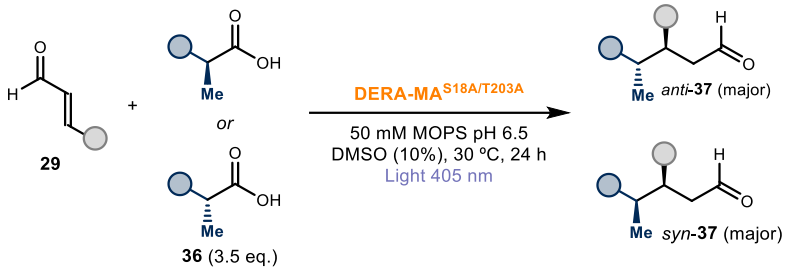

A stock solution of enal **29** (50 mM) and a stock solution of the corresponding (*R*)- or (*S*)-acid **36** (175 mM) in DMSO were added to a 5 mL glass vial containing 50 mM MOPS buffer pH 6.5. The headspace of the vial was purged with argon and the purified enzyme DERA-MA$^{S18A/T203A}$ (62.5 nmol, 1.0 equiv.) in MOPS buffer pH 6.5 was added to reach the final volume of 500 µL. The vial was then placed in the 3D printed support photoreactor and irradiated under stirring for 16 hours. The crude mixture was extracted once with 600 µL ethyl acetate containing 5 mM of the internal standard 1,3,5-trimethoxybenzene or mesitylene. The organic extract was dried over anhydrous $MgSO_4$, filtered and analyzed by GC-FID on HP-5 column. Calibration curves not reported in the present dissertation, were obtained using the previously synthesized reference compounds **37** and internal standard (1,3,5-trimethoxybenzene or mesitylene). The GC-FID data for the analytical scale reactions were fit in the equation to determine the analytical yield and diastereomeric ratio of the products **37**. The enantiomeric excess was determined by UPC^2 analysis on chiral stationary phase columns.

(3*S*)-3,4-Diphenylpentanal (37a)

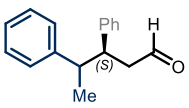

syn- or *anti*-**37a**

Prepared according to **GP5**, using (*R*)- or (*S*)-2-phenylpropionic acid **36a** (25 µL of a 87.5 mM stock solution in DMSO, 2.2 µmol) and cinnamaldehyde **29a** (25 µL of a 25 mM stock solution in DMSO, 0.68 µmol) as substrates in a 10% v/v DMSO/MOPS buffer pH 6.5 mixture. The crude extract was analyzed by GC-FID on HP-5 column. The analytical yield of product **37a** was determined according to the calibration curve (response factor: *syn*-**37a** = 2.13 and *anti*-**37a** = 2.29) using 1,3,5-trimethoxybenzene as the internal standard and as an average of three runs. In case of using (*R*)-**36a** the product *syn*-**37a** (82% yield, 7.5:1 d.r., >99% ee) was obtained, while the diastereomer *anti*-**37a**(47% yield, 15:1 d.r., >99% ee) was obtained when using (*S*)-**36a**. The enantiomeric excess of the corresponding 2,4-dinitrophenylhydrazone (obtained upon condensation with 2,4-dinitrophenylhydrazine) was determined using UPC^2

analysis on a Daicel Chiralpak IE-3 column: isocratic 100% CO_2 for 1 min; gradient from 100% CO_2 to 60:40 CO_2/*i*-PrOH for 15 min; isocratic CO_2/ *i*-PrOH 60:40 for 8 min, gradient from 60:40 CO_2/*i*-PrOH to 100% CO_2 for 1 min, flow rate 2.0 mL/min, λ = 345 nm: *syn*-**37a**: τ = 19.3 min and *anti*-**37a**: τ = 21.2 min. The relative and absolute configurations were assigned by comparison with the crystal structure of **37k** (*Section 3.6.10*)

(3*S*)-3-Phenyl-4-(*p*-tolyl)pentanal (37b)

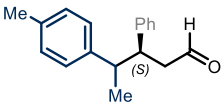

syn- or *anti*-**37b**

Prepared according to **GP5**, using (*R*)- or (*S*)-2-(*p*-tolyl)propanoic acid **36b** (25 µL of a 87.5 mM stock solution in DMSO, 2.2 µmol) and cinnamaldehyde **29a** (25 µL of a 25 mM stock solution in DMSO, 0.68 µmol) as substrates in a 10% v/v DMSO/MOPS buffer pH 6.5 mixture. The crude extract was analyzed by GC-FID on HP-5 column. The analytical yield of product **37b** was determined according to the calibration curve (response factor: *syn*-**37b** = 1.61 and *anti*-**37b** = 1.73) using mesitylene as the internal standard and as an average of three runs. In case of using (*R*)-**36b** the product *syn*-**37b** (79% yield, 5.7:1 d.r., >99% ee) was obtained, while the diastereomer *anti*-**36b** (47% yield, 22:1 d.r., >99% ee) was obtained when using (*S*)-**36b**. The enantiomeric excess of the corresponding 2,4-dinitrophenylhydrazone (obtained upon condensation with 2,4-dinitrophenylhydrazine) was determined using UPC^2 analysis on a Daicel Chiralpak IA-3 column: isocratic 100% CO_2 for 1 min; gradient from 100% CO_2 to 60:40 CO_2/EtOH for 11 min; isocratic 60:40 CO_2/EtOH for 6 min, gradient from 60:40 CO_2/EtOH to 100% CO_2 for 1 min, flow rate 1.0 mL/min, λ = 352 nm: *syn*-**37b**: τ = 16.5 min; *anti*-**37b**: τ = 14.3 min.

(3*S*)-3-Phenyl-4-(*m*-tolyl)pentanal (37c)

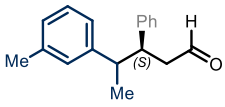

syn- or *anti*-**37c**

Prepared according to **GP5**, using (*R*)- or (*S*)-2-(*m*-tolyl)propanoic acid **36c** (25 µL of a 87.5 mM stock solution in DMSO, 2.2 µmol) and cinnamaldehyde **29a** (25 µL of a 25 mM stock solution in DMSO, 0.68 µmol) as substrates in a 10% v/v DMSO/MOPS buffer pH 6.5 mixture. The crude extract was analyzed by GC-FID on HP-5 column. The analytical yield of product **37c** was determined according to the calibration curve (response factor: *syn*-**37c** = 2.33 and *anti*-**37c** = 2.30) using mesitylene as the internal standard and as an average of three runs. In case of using (*R*)-**36c** the product *syn*-**37c** (46% yield, 6:1 d.r., >99% ee) was obtained, while the diastereomer *anti*-**37c** (47% yield, 12.6:1 d.r., >99% ee) was obtained when using (*S*)-**36c**. The enantiomeric excess of the corresponding 2,4-dinitrophenylhydrazone (obtained upon condensation with 2,4-dinitrophenylhydrazine) was determined using UPC^2 analysis on a Daicel Chiralpak ID-3 column: isocratic 100% CO_2 for 1 min; gradient from 100% CO_2 to 60:40 CO_2/ EtOH for 13 min; isocratic 60:40 CO_2/EtOH for 2 min, gradient from 60:40 CO_2/EtOH to 100% CO_2 for 1 min, flow rate 2.0 mL/min, λ = 347 nm: *syn*-**37c**: τ = 10.0 min and *anti*-**37c**: τ = 10.7 min.

(3*S*)-3-Phenyl-4-(*o*-tolyl)pentanal (37d)

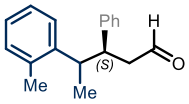

syn- or *anti*-**37d**

Prepared according to **GP5**, using (*R*)- or (*S*)-2-(*o*-tolyl)propanoic acid **36d** (25 µL of a 87.5 mM stock solution in DMSO, 2.2 µmol) and cinnamaldehyde **29a** (25 µL of a 25 mM stock solution in DMSO, 0.68 µmol) as substrates in a 10% v/v DMSO/MOPS buffer pH 6.5 mixture. The crude extract was analyzed by GC-FID on HP-5 column. The analytical yield of product **37d** was determined according to the calibration curve (response factor: *syn*-**37d** = 1.86 and *anti*-**37d** = 1.73) using mesitylene as the internal standard and as an average of three runs. In case of using (*R*)-**36d** the product *syn*-**37d** (38% yield, 4.9:1 d.r., 94% ee) was obtained, while the diastereomer *anti*-**37d** (35% yield, 6.7:1 d.r., 99% ee) was obtained when using (*S*)-**36d**. The enantiomeric excess of the corresponding 2,4-dinitrophenylhydrazone (obtained upon condensation with 2,4-dinitrophenylhydrazine) was determined using UPC^2 analysis on a Daicel Chiralpak ID-3 column: isocratic 100% CO_2 for 1 min; gradient from 100% CO_2 to 60:40 CO_2/ MeOH for 13 min; isocratic 60:40 CO_2/MeOH for 2 min, gradient from 60:40 CO_2/MeOH to 100% CO_2 for 1 min, flow rate 2.0 mL/min, λ = 350 nm: *syn*-**37d**: : τ_{Mayor} = 9.6 min and τ_{Minor} = 10.0 min and *anti*-**37d**: τ = 10.4 min.

(3*S*)-4-(4-Bromophenyl)-3-phenylpentanal (37e)

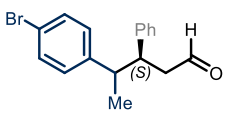

syn- or *anti*-**37e**

Prepared according to **GP5**, using (*R*)- or (*S*)-2-(4-bromophenyl)propionic acid **36e** (25 µL of a 87.5 mM stock solution in DMSO, 2.2 µmol) and cinnamaldehyde **29a** (25 µL of a 25 mM stock solution in DMSO, 0.68 µmol) as substrates in a 10% v/v DMSO/MOPS buffer pH 6.5 mixture. The crude extract was analyzed by GC-FID on HP-5 column. The analytical yield of product **37e** was determined according to the calibration curve (response factor: *syn*-**37e** = 1.79 and *anti*-**37e** = 1.82) using mesitylene as the internal standard and as an average of three runs. In case of using (*R*)-**36e** the product *syn*-**37e** (54% yield, 5.8:1 d.r., 90 % ee) was obtained, while the diastereomer *anti*-**37e** (50% yield, 7.8:1 d.r., 96% ee) was obtained when using (*S*)-**36e**. The enantiomeric excess of the corresponding 2,4-dinitrophenylhydrazone (obtained upon condensation with 2,4-dinitrophenylhydrazine) was determined using UPC^2 analysis on a Daicel Chiralpak IB-3 column: isocratic 100% CO_2 for 1 min; gradient from 100% CO_2 to 85:15 CO_2/*i*-PrOH for 37 min; isocratic 85:15 CO_2/*i*-PrOH for 26 min, gradient from 85:15 CO_2/*i*-PrOH to 100% CO_2 for 1 min, flow rate 1.0 mL/min, λ = 344 nm: *syn*-**37e**: τ = 54.9 min and *anti*-**37e**: τ = 58.8 min.

(3*S*)-4-(4-Chlorophenyl)-3-phenylpentanal (37f)

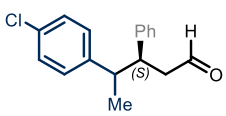

syn- or *anti*-**37f**

Prepared according to **GP5**, using (*R*)- or (*S*)-2-(4-chlorophenyl)propionic acid **36f** (25 µL of a 87.5 mM stock solution in DMSO, 2.2 µmol) and cinnamaldehyde **29a** (25 µL of a 25 mM stock solution in DMSO, 0.68 µmol) as substrates in a 10% v/v DMSO/MOPS buffer pH 6.5 mixture. The crude extract was analyzed by GC-FID on HP-5 column. The analytical yield of product **37f** was determined according to the calibration curve (response factor: *syn*-**37f** = 1.69 and *anti*-**37f** = 1.75) using mesitylene as the internal standard and as an average of three runs. In case of using (*R*)-**36f** the product *syn*-**37f** (55% yield, 6.1:1 d.r., 98% ee) was obtained, while the diastereomer *anti*-**37f** (42% yield, 16:1 d.r., 98% ee) was obtained when using (*S*)-**36f**. The enantiomeric excess of the corresponding 2,4-dinitrophenylhydrazone (obtained upon condensation with 2,4-dinitrophenylhydrazine) was determined using UPC^2 analysis on a Daicel Chiralpak IE-3 column: isocratic 100% CO_2 for 1 min; gradient from 100% CO_2 to 60:40 CO_2/ EtOH for 21 min; isocratic 60:40 CO_2/EtOH for 6 min, gradient from 60:40 CO_2/EtOH to 100% CO_2 for 1 min, flow rate: 1.0 mL/min, λ = 350 nm: *syn*-**37f:** τ = 22.1 min and *anti*-**37f**: τ = 23.2 min.

(3*S*)-4-(4-Fluorophenyl)-3-phenylpentanal (37g)

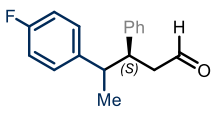

syn- or *anti*-**37g**

Prepared according to **GP5**, using (*R*)- or (*S*)-2-(4-fluorophenyl)propionic acid **36g** (25 µL of a 87.5 mM stock solution in DMSO, 2.2 µmol) and cinnamaldehyde **29a** (25 µL of a 25 mM stock solution in DMSO, 0.68 µmol) as substrates in a 10% v/v DMSO/MOPS buffer pH 6.5 mixture. The crude extract was analyzed by GC-FID on HP-5 column. The analytical yield of product **37g** was determined according to the calibration curve (response factor: *syn*-**37g** = 1.77 and *anti*-**37g** = 1.75) using mesitylene as the internal standard and as an average of three runs. In case of using (*R*)-**36g** the product *syn*-**37g** (54% yield, 6.5:1 d.r., 98% ee) was obtained, while the diastereomer *anti*-**37g** (40% yield, 12.3:1 d.r., 96% ee) was obtained when using (*S*)-**36g**. The enantiomeric excess of the corresponding 2,4-dinitrophenylhydrazone (obtained upon condensation with 2,4-dinitrophenylhydrazine) was determined using UPC^2 analysis on a Daicel Chiralpak IE-3 column: isocratic 100% CO_2 for 1 min; gradient from 100% CO_2 to 70:30 CO_2/ EtOH for 9 min; isocratic70:30 CO_2/EtOH for 4 min, gradient from 70:30 CO_2/EtOH to 100% CO_2 for 1 min, flow rate: 2.0 mL/min, λ = 347 nm: *syn*-**37g**: τ = 10.7 min and *anti*-**37g**: τ = 11.3 min.

(3*S*)-4-(4-Methoxyphenyl)-3-phenylpentanal (37h)

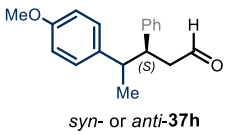

syn- or *anti*-**37h**

Prepared according to **GP5**, using (*R*)- or (*S*)-2-(4-methoxyphenyl)propionic acid **36h** (25 µL of a 87.5 mM stock solution in DMSO, 2.2 µmol) and cinnamaldehyde **29a** (25 µL of a 25 mM stock solution in DMSO, 0.68 µmol) as substrates in a 10% v/v

DMSO/MOPS buffer pH 6.5 mixture. The crude extract was analyzed by GC-FID on HP-5 column. The analytical yield of product **37h** was determined according to the calibration curve (response factor: *syn*-**37h** = 1.73 and *anti*-**37h** = 1.64) using mesitylene as the internal standard and as an average of three runs. In case of using (*R*)-**36h** the product *syn*-**37h** (54% yield, 3.2:1 d.r., >99% ee) was obtained, while the diastereomer *anti*-**37h** (43% yield, 6.7:1 d.r., >99% ee) was obtained when using (*S*)-**36h**. The enantiomeric excess of the corresponding 2,4-dinitrophenylhydrazone (obtained upon condensation with 2,4-dinitrophenylhydrazine) was determined using UPC^2 analysis on a Daicel Chiralpak ID-3 column: isocratic 100% CO_2 for 1 min; gradient from 100% CO_2 to 70:30 CO_2/ EtOH for 21 min; isocratic 70:30 CO_2/EtOH for 6 min, gradient from 70:30 CO_2/EtOH to 100% CO_2 for 2 min, flow rate 1.0 mL/min, λ = 346 nm: *syn*-**37h**: τ = 20.0 min and *anti*-**37h**: τ = 21.1 min.

(3*S*)-4-Phenyl-3-(p-tolyl)pentanal (37i)

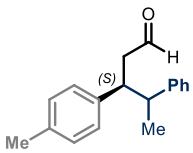

syn- or *anti*-**37i**

Prepared according to **GP5**, using (*R*)- or (*S*)-2-phenylpropionic acid **36a** (25 µL of a 87.5 mM stock solution in DMSO, 2.2 µmol) and enal **29b** (25 µL of a 25 mM stock solution in DMSO, 0.68 µmol) as substrates in a 10% v/v DMSO/MOPS buffer pH 6.5 mixture. The crude extract was analyzed by GC-FID on HP-5 column. The analytical yield of product **37i** was determined according to the calibration curve (response factor: *syn*-**37i** = 1.86 and *anti*-**37i** = 1.83) using mesitylene as the internal standard and as an average of three runs. In case of using (*R*)-**36a** the product *syn*-**37i** (65% yield, 7.7:1 d.r., >99% ee) was obtained, while the diastereomer *anti*-**37i** (37% yield, 13.8:1 d.r., >99% ee) was obtained when using (*S*)-**36a**. The enantiomeric excess of the corresponding 2,4-dinitrophenylhydrazone (obtained upon condensation with 2,4-dinitrophenylhydrazine) was determined using UPC^2 analysis on a Daicel Chiralpak IE-3 column: isocratic 100% CO_2 for 1 min; gradient from 100% CO_2 to 60:40 CO_2/MeOH for 14 min; isocratic 60:40 CO_2/EtOH for 4 min, gradient from 60:40 CO_2/EtOH to 100% CO_2 for 1 min, flow rate 2.0 mL/min, λ = 353 nm: *syn*-**37i**: τ = 13.5 min and *anti*-**37i**: τ = 14.4 min.

(3*S*)-3-(4-Bromophenyl)-4-phenylpentanal (37j)

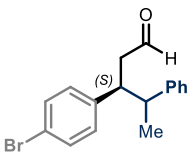

syn- or *anti*-**37j**

Prepared according to **GP5**, using (*R*)- or (*S*)-2-phenylpropionic acid **36a** (25 µL of a 87.5 mM stock solution in DMSO, 2.2 µmol) and enal **29d** (25 µL of a 25 mM stock solution in DMSO, 0.68 µmol) as substrates in a 10% v/v DMSO/MOPS buffer pH 6.5 mixture. The crude extract was analyzed by GC-FID on HP-5 column. The analytical yield of product **37j** was determined according to the calibration curve (response factor: *syn*-**37j** = 2.04 and *anti*-**37j** = 2.14) using mesitylene as the internal standard and as an average of three runs. In case of using (*R*)-**36a** the product *syn*-**37j** (38% yield, 13:87 d.r., >99% ee) was obtained, while the diastereomer *anti*-**37j** (26% yield, 93:7 d.r., >99% ee) was obtained

when using (*S*)-**36a**. The enantiomeric excess of the corresponding 2,4-dinitrophenylhydrazone (obtained upon condensation with 2,4-dinitrophenylhydrazine) was determined using UPC^2 analysis on a Daicel Chiralpak IE-3 column: isocratic 100% CO_2 for 1 min; gradient from 100% CO_2 to 70:30 CO_2/ EtOH for 5 min; isocratic 70:30 CO_2/EtOH for 10 min, gradient from 70:30 CO_2/EtOH to 100% CO_2 for 1 min, flow rate 2.0 mL/min, λ = 348 nm: *syn*-**37j**: τ = 10.7 min and *anti*-**37j**: τ = 12.0 min.

3.6.6.4 Analytical Scale Biocatalytic Reactions – Kinetic Resolution Procedure

GP6 – General Procedure for the Analytical Scale of the Kinetic Resolution of Compounds **37**

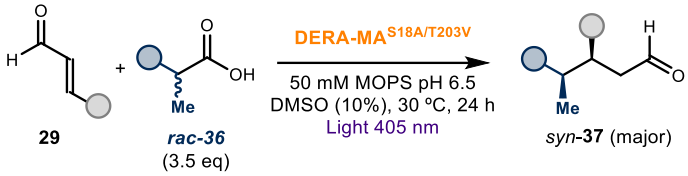

A stock solution of cinnamaldehyde **29** (50 mM) and a stock solution of the corresponding racemic mixture of acid **36** (175 mM) in DMSO were added to a 5 mL glass vial containing 50 mM MOPS buffer pH 6.5. The headspace of the vial was purged with argon and the purified enzyme DERA-MA$^{S18A/T203V}$ (62.5 nmol, 1.0 equiv.) in MOPS buffer pH 6.5 was added to reach the final volume of 500 µL. The vial was then placed in the 3D printed support photoreactor (see *Section 3.6.3.1*) and irradiated under stirring for 16 hours. The crude mixture was extracted once with 600 µL ethyl acetate containing 5 mM of the internal standard 1,3,5-trimethoxybenzene or mesitylene. The organic extract was dried over anhydrous $MgSO_4$, filtered and analyzed by GC-FID on HP-5 column. Calibration curves were obtained using the previously synthesized reference compounds **37** and internal standard (1,3,5-trimethoxybenzene or mesitylene). The GC-FID data for the analytical scale reactions were fit in the equation to determine the analytical yield and diastereomeric ratio of the products **37**. The enantiomeric excess was determined by UPC^2.

(3*S*,4*R*)-3,4-Diphenylpentanal (37a)

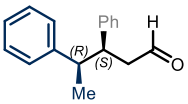

syn-**37a**

Prepared according to **GP6**, using racemic 2-phenylpropionic acid **36a** (25 µL of a 175 mM stock solution in DMSO, 4.4 µmol) and cinnamaldehyde **29a** (25 µL of a 50 mM stock solution in DMSO, 1.25 µmol) as substrates in a 10% v/v DMSO/MOPS buffer pH 6.5 mixture. The crude extract was analyzed by GC-FID on HP-5 column. The analytical yield of product **37a** was determined according to the calibration curve (response factor: *syn*-**37a** = 2.13 and *anti*-**37a** = 2.29) using 1,3,5-trimethoxybenzene as the internal standard and as an average of three runs. The product *syn*-**37a** (67% yield, 5.4:1 d.r., >99% ee) was obtained. The

enantiomeric excess of the corresponding 2,4-dinitrophenylhydrazone (obtained upon condensation with 2,4-dinitrophenylhydrazine) was determined using UPC^2 analysis on a Daicel Chiralpak IE-3 column: isocratic 100% CO_2 for 1 min; gradient from 100% CO_2 to 60:40 CO_2/*i*-PrOH for 15 min; isocratic 60:40 CO_2/ *i*-PrOH for 8 min, gradient from 60:40 CO_2/*i*-PrOH to 100% CO_2 for 1 min, flow rate 2.0 mL/min, λ = 345 nm: *syn*-**37a**: τ = 19.2 min and *anti*-**37a**: τ = 21.1 min.

(3*S*,4*R*)-3-Phenyl-4-(p-tolyl)pentanal (37b)

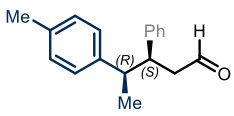

syn-**37b**

Prepared according to **GP6**, using racemic 2-(*p*-tolyl)propanoic acid **36b** (25 µL of a 175 mM stock solution in DMSO, 4.4 µmol) and cinnamaldehyde **29a** (25 µL of a 50 mM stock solution in DMSO, 1.25 µmol) as substrates in a 10% v/v DMSO/MOPS buffer pH 6.5 mixture. The crude extract was analyzed by GC-FID on HP-5 column. The analytical yield of product **37b** was determined according to the calibration curve (response factor: *syn*-**37b** = 1.61 and *anti*-**37b** = 1.73) using mesitylene as the internal standard and as an average of three runs. The product *syn*-**37b** (76% yield, 5.5:1 d.r., >99% ee) was obtained. The enantiomeric excess of the corresponding 2,4-dinitrophenylhydrazone (obtained upon condensation with 2,4-dinitrophenylhydrazine) was determined using UPC^2 analysis on a Daicel Chiralpak IA-3 column: isocratic 100% CO_2 for 1 min; gradient from 100% CO_2 to 60:40 CO_2/EtOH for 11 min; isocratic 60:40 CO_2/EtOH for 6 min, gradient from 60:40 CO_2/EtOH to 100% CO_2 for 1 min, flow rate 1.0 mL/min, λ = 352 nm: *syn*-**37b**: τ = 16.5 min.

(3*S*,4*R*)-3-Phenyl-4-(*m*-tolyl)pentanal (37c)

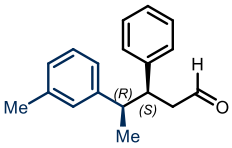

syn-**37c**

Prepared according to **GP6**, using racemic 2-(*m*-tolyl)propanoic acid **36c** (25 µL of a 175 mM stock solution in DMSO, 4.4 µmol) and cinnamaldehyde **29a** (25 µL of a 50 mM stock solution in DMSO, 1.25 µmol) as substrates in a 10% v/v DMSO/MOPS buffer pH 6.5 mixture. The crude extract was analyzed by GC-FID on HP-5 column. The analytical yield of product **37c** was determined according to the calibration curve (response factor: *syn*-**37c** = 2.33 and *anti*-**37c** = 2.30) using mesitylene as the internal standard and as an average of three runs. The product *syn*-**37c** (49% yield, 3.1:1 d.r., 95% ee) was obtained. The enantiomeric excess of the corresponding 2,4-dinitrophenylhydrazone (obtained upon condensation with 2,4-dinitrophenylhydrazine) was determined using UPC^2 analysis on a Daicel Chiralpak ID-3 column: isocratic 100% CO_2 for 1 min; gradient from 100% CO_2 to 60:40 CO_2/ EtOH for 13 min; isocratic CO_2/EtOH 60:40 for 2 min, gradient from 60:40 CO_2/EtOH to 100% CO_2 for 1 min, flow rate 2.0 mL/min, λ = 347 nm: *syn*-**37c**: τ_{major} = 9.89 min and τ_{minor} = 10.30 min; *anti*-**37c**: τ_{major} = 10.7 min and τ_{minor} = 11.2 min.

3.6.6.5 Semi-Preparative Scale Biocatalytic Synthesis

Semi-Preparative Scale Enzymatic Synthesis of (R)-3-Phenyl-4-(furan-2-yl)butanal (**35j**)

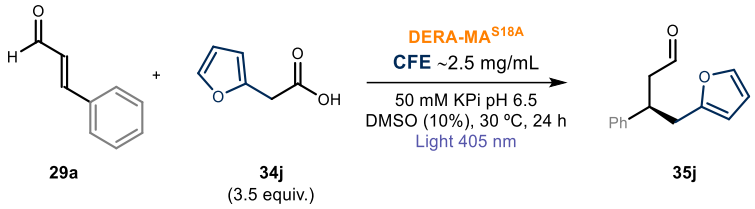

In the DERA-MA^{S18A}-catalyzed biosynthesis of compounds **35j** on a semi-preparative scale, 2.3 g of *E. Coli* cells containing the overexpressed DERA-MA^{S18A} enzyme were resuspended in 27 mL of 50 mM KPi buffer pH 6.5 and sonicated for 20 min. The lysate was cleared by centrifugation for 20 min at 4ºC and the supernatant collected and used without further purification. In a 50 mL round bottom flask a solution of and cinnamaldehyde **29a** (9.4 µL, 75 µmol, 1.0 equiv.) and furan acetic acid **34j** (33.4 mg, 263 µmol, 3.5 equiv.) in DMSO (3mL) was added to the supernatant to reach the final volume of 30 mL (10% v/v DMSO/water buffer). The reaction mixture was irradiated at 30 ºC in the photoreactor (see *chapter 3.6.3.1*) for 24 hours. The crude mixture was extracted with ethyl acetate (2 x 15mL). The combined organic extracts were dried over anhydrous $MgSO_4$, filtered and concentrated under reduced pressure. The crude mixture was purified by flash column chromatography (SiO_2, hexante:Et_2O 9:1) to afford product **35j** (8.6 mg, 37.4 µmol, 50% yield, >99% ee,) as a colorless oil. The enantiomers of the corresponding 2,4-dinitrophenylhydrazone (obtained upon condensation with 2,4-dinitrophenylhydrazine) were separated by UPC^2 analysis on a Daicel Chiralpak ID-3 column: isocratic 100% CO_2 for 1 min; gradient from 100% CO_2 to 60:40 CO_2/*i*-PrOH for 5 min; isocratic 60:40 CO_2/*i*-PrOH for 2 min, gradient from 60:40 CO_2/*i*-PrOH to 100% CO_2 for 1 min, flow rate 2.0 mL/min, λ = 347 nm, **35j**: τ = 6.0 min; $[\alpha]_D^{20}$ = +0.70 (c = 0.275, CH_2Cl_2, >99% ee). The absolute configuration was assigned by comparison with product **35a** (see *chapter 3.6.5.1*).

^{1}H NMR (500 MHz, $CDCl_3$) δ 9.59 (t, *J* = 2.0 Hz, 1H), 7.33 – 7.28 (m, 3H), 7.24 – 7.21 (m, 1H), 7.21 – 7.16 (m, 2H), 6.24 (dd, *J* = 3.2, 1.9 Hz, 1H), 5.92 (dq, *J* = 3.2, 0.8 Hz, 1H), 3.67 – 3.59 (m, 1H), 3.04 – 2.87 (m, 2H), 2.77 (dd, *J* = 7.3, 1.9 Hz, 2H).
^{13}C NMR (126 MHz, $CDCl_3$) δ 201.3, 153.2, 143.2, 141.5, 128.8, 127.4, 127.0, 110.4, 107.2, 49.2, 39.5, 35.4.
HRMS (ESI): Calculated for $[M+Na]^+$ $[C_{14}H_{14}NaO_2]^+$: 237.0886, found: 237.0878.

Semi-Preparative Scale Enzymatic Synthesis of (R)-3-(4-Bromophenyl)-4-phenylbutanal (**35m**)

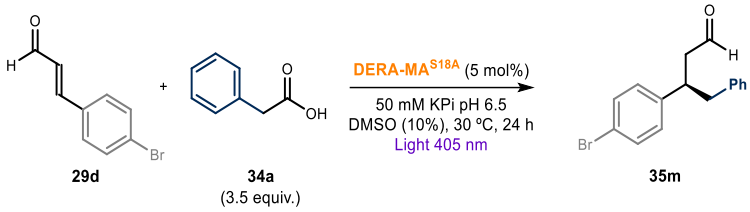

29d **34a** (3.5 equiv.) **35m**

A stock solution of cinnamaldehyde **29d** (0.68 µmol, final concentration of 1.25 mM) and a stock solution of phenylacetic acid **34a** (35.7mg, 263 µmol, 3.5 equiv.) in DMSO (3 mL). were added to a 50 mL round bottom flask containing 50 mM KPi buffer pH 6.5. The purified enzyme DERA-MA^{S18A} (4.2 mL, 900 nM, 5 mol%) in KPi buffer pH 6.5 was added to reach the final volume of 30 mL. The reaction mixture was irradiated at 30 ºC in the photoreactor (see *chapter 3.6.3.1*) for 24 hours. The reaction mixture was extracted with ethyl acetate (2 x 15mL). The combined organic extracts were dried over anhydrous $MgSO_4$, filtered and concentrated under reduced pressure. The crude mixture was purified by flash column chromatography (SiO_2, hexante:Et_2O 9:1) to afford product **35m** (4.7 mg, 22.0 µmol, >99% ee, 29% yield) as a colorless oil. The enantiomers of the corresponding 2,4-dinitrophenylhydrazone (obtained upon condensation with 2,4-dinitrophenylhydrazine) were separated by UPC[2] analysis on a Daicel Chiralpak Chiralpak ID-3 column: isocratic 100% CO_2 for 1 min; gradient from 100% CO_2 to 60:40 CO_2/MeOH for 13 min; isocratic 60:40 CO_2/MeOH for 2 min, gradient from 60:40 CO_2/MeOH to 100% CO_2 for 1 min, flow rate 2.0 mL/min, λ = 350 nm, **35m**: τ = 13.2 min; $[\alpha]_D^{20}$ = +34.9 (c = 0.235, CH_2Cl_2, >99% ee). The absolute configuration was assigned by comparison with product **35a** (see *chapter 3.6.5.1*).
^{1}H NMR (500 MHz, $CDCl_3$) δ 9.60 (t, *J* = 1.7 Hz, 1H), 7.41 – 7.36 (m, 2H), 7.26 – 7.21 (m, 2H), 7.20 – 7.15 (m, 1H), 7.06 – 6.98 (m, 4H), 3.47 (p, *J* = 7.5 Hz, 1H), 2.88 (d, *J* = 7.5 Hz, 2H), 2.75 (dd, *J* = 7.2, 1.8 Hz, 2H).

3.6.7 Computational Studies

The molecular dockings were performed using Autodock Vina as tool incorporated into YASARA. The crystal structure of DERA-MA forming the iminium ion intermediate was used as receptor (PDB: 7P76).[62] In instances where variants of DERA-MA were used, all mutations to the parental enzyme were simulated in silico using the YASARA structure software with the AMBER 03 force field.[82] After the introduction of a mutation or modification, the energy of the system was minimized following a three-step protocol

[80] Oostenbrink, C., Villa, A., Mark, A. E., Van Gunsteren, W. F. "A biomolecular force field based on the free enthalpy of hydration and solvation: The GROMOS force-field parameter sets 53A5 and 53A6." *J. Comput. Chem.* **2004**, *25*, 1656–1676.

deformation. In step one, only the atoms constituting the mutated amino acid residue were subjected to energy minimization. In step two, the process for energy minimization was repeated by including all the atoms of the amino acid residues that are located within 6 Å distance from the mutated residue. In step three, the energy of the overall structure was minimized.

In all dockings, the simulation box was placed 10 Å around the active site of the enzyme. For each simulation, 25 VINA docking runs of each ligand to the receptor were run. Results were sorted by binding energy. More positive energies indicate stronger binding and negative energies mean no binding. All binding poses were inspected visually.

Table 3.9. Dockings performed in this study.

Entry	**Enzyme**	**Substrate**	Docking clusters	*Binding energy (Kcal/mol)*
1	DERA-MA	**34a**	**001**	**000006.0750**
			002	000004.7720
			003	000003.8890
			004	000003.1530
			005	000003.0230
2	DERA-MA^{S18A}	**34a**	**001**	**000005.9100**
			002	000004.5360
			003	-00001.6200
			004	-00021.6400
			005	-00150.4800
3	DERA-MA^{S18A}	(*R*)-**36a**	**001**	**000006.0630**
			002	000004.6130
			003	000001.3530
			004	-00072.6160
4	DERA-MA$^{S18A/T203A}$	(*S*)-**36a**	**001**	**000006.1970**
			002	**000005.0210**
			003	000004.4900
			004	000003.7000
			005	000002.7110
			006	000002.0480
5	DERA-MA$^{S18A/T203A}$	(*R*)-**36a**	001	**000006.2160**
			002	000004.7170
			003	000004.4560
			004	000003.5500

In each case, the docking outcomes guided us to choose the best binding energy as the most compelling option. For example, Figure 3.38 shows that in most cases the second-best binding pose obtained (Table 3.9, entries 1-3 and 5, referred to as **002** in Figure 3.38, substrate in green) are very unlikely to represent a productive binding pose. This is because the substrate binds in a cavity distant from the active site, where the reactive iminium ion is accommodated. We believe that these binding poses are highly unlikely to provide a productive scenario or have any influence on the yield and selectivity of the reactions, simply because the carboxylic acid substrate, being far away from the active site, could not effectively react with the iminium ion.

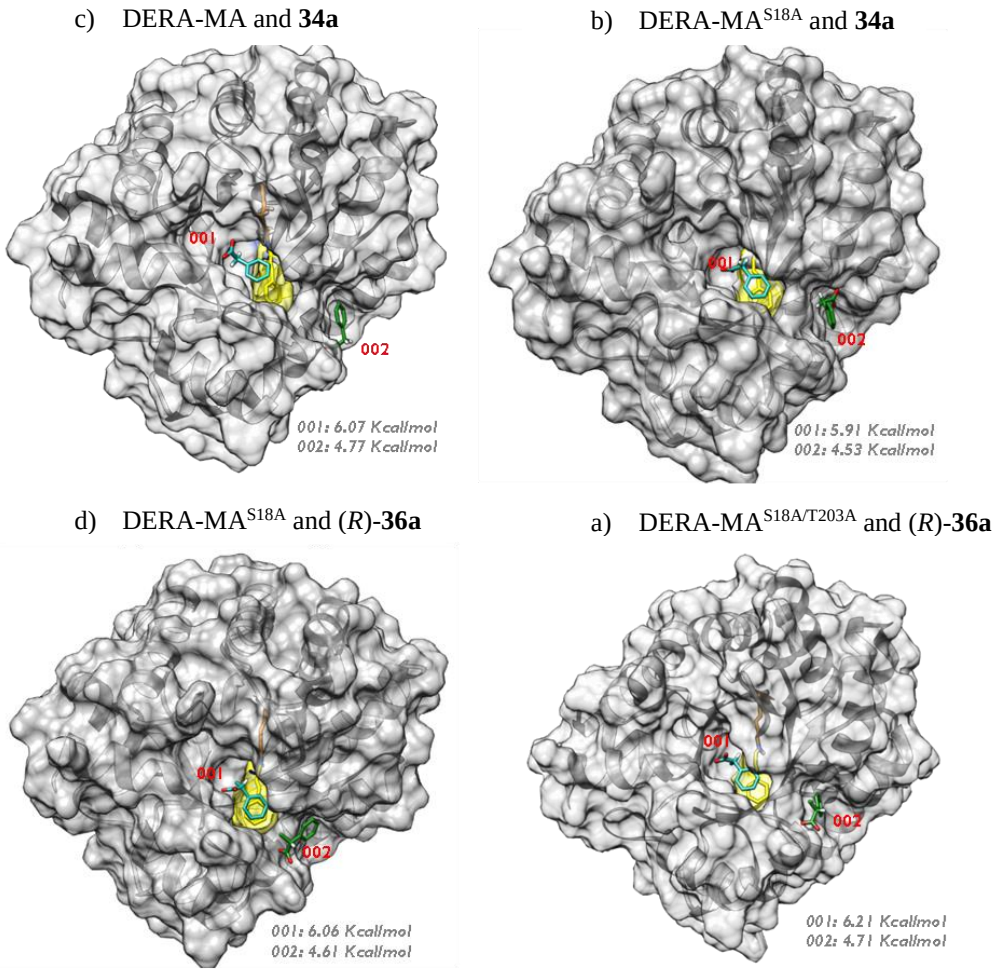

Figure 3.38. Binding poses with the highest binding energies for carboxylic acid **36a** (turquoise or green) into the active site of: a) DERA-MA, b) DERA-MA$^{S18A/T203A}$ and for c) (*R*)-**36a** into the active site of DERA-MA^{S18A} and d) DERA-MA$^{S18A/T203A}$. The iminium ion formed upon condensation of **29a** with K167 is shown in yellow. In all cases the substrate with the highest binding energy (**pose 001**) is shown in turquoise while the one with second-best binding pose (**pose 002**) is shown in green.

3.6.8 Determination of the Stereochemistry of the Products

3.6.8.1 Determination of the Absolute Configuration of Product 39a

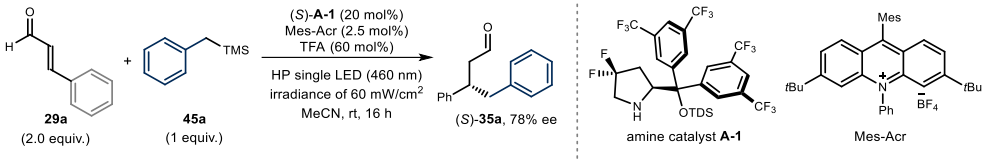

The absolute configuration of product **38a** was inferred by comparison with literature data.[79] Specifically, we replicated the procedure described in the literature using the chiral small organocatalyst **A-1** and compared the optical rotation and UPC^2 spectra of **39a** with the product obtained through the photoenzymatic reaction (Figure 3.39). According to the literature procedure, product (*S*)-**39a** was obtained with an enantiomeric excess of 78%. In contrast, the photoenzymatic reaction yielded the opposite enantiomer with 99% ee. Therefore, the enzymatic product was determined to be (*R*)-**39a**.

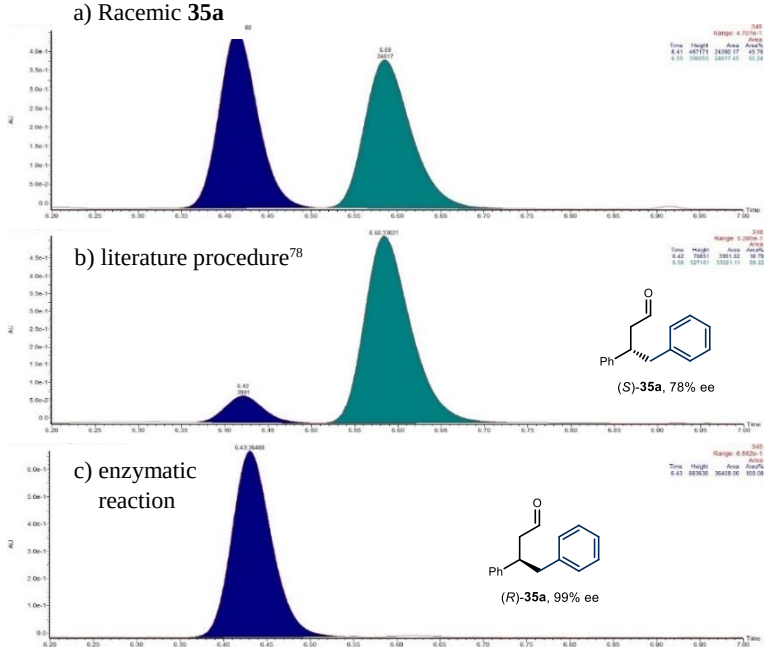

Figure 3.39. UPC^2 traces of **35a** synthesized a) as a racemic mixture, b) using a literature procedure,[79] and c) using our photobiocatalytic protocol with DERA-MA^{S18A}.

3.6.8.2 Determination of the Absolute and Relative Configuration of Products 37

The relative and absolute configuration of product **37k** was inferred by comparison with a reference compound synthesized using a chiral small molecule organocatalyst and crystallized as a single stereoisomer suitable for X-ray crystallographic analysis. The procedure for the synthesis of the reference compound was adapted from the literature[52] and is detailed below.

Synthesis of Reference Compound 3-(4-Chlorophenyl)-4-(p-tolyl)pentanal **37k**

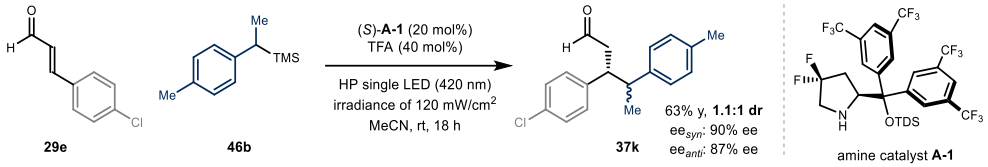

A dry vial was charged with *p*-chloro-cinnamaldehyde **29e** (1.5 equiv., 0.6 mmol, 144.0 mg), trimethyl(1-(p-tolyl)ethyl)silane **46b** (1 equiv., 0.4 mmol, 77.0 mg) and the chiral amino catalyst (*S*)-**A-1** (10 mol%, 0.04 mmol, 28.2 mg). The vial was sealed with a septum, flushed with argon and CH_3CN (0.4 mL) and TFA (20 mol%, 0.08 mmol, 6.1 µL) was added. The heterogeneous mixture was stirred for 18 h under irradiation at 420 nm (single LED, 120 mW/cm^3) at ambient temperature. The mixture was purified by two consecutive column chromatography steps (silica gel, step 1. 20% dichloromethane in hexanes, step 2. 5% EtOAc in hexanes) afforded the desired product **37k** in 63% yield (72.8 mg) as a 1:1.1 mixture of diastereomers.

Preparative TLC (thin layer chromatography, silica gel, 15% EtOAc in hexanes) enabled separation and isolation of the individual *syn* and *anti* diastereoisomers of products **37k**. Crystals from compound *syn*-**37k** were suitable for X-ray analysis, which secured the absolute and relative configuration of the product (see *chapter 3.6.6.1* for details, CCDC 2280852).

***syn-(3R,4S)*-3-(4-Chlorophenyl)-4-(p-tolyl)pentanal (37k)** was obtained in 28.1 mg (24%) as a single diastereomer – the <u>*absolute and relative configuration was unambiguously determined by x-ray crystallographic analysis*</u> (see *chapter 3.6.6.1*). The enantiomeric excess was determined to be 90% *via* analysis of the corresponding 2,4-dinitrophenylhydrazone (obtained upon condensation with 2,4-dinitrophenylhydrazine), which could be separated by UPC^2 analysis on a Daicel Chiralpak ID-3 column: isocratic 100% CO_2 for 1 min; gradient from 100% CO_2 to 70:30 CO_2/*i*PrOH for 5 min; isocratic 70:30 CO_2/*i*PrOH for 9 min, gradient from 70:30 CO_2/*i*PrOH to 100% CO_2 for 1 min, flow rate 2.0 mL/min, λ = 347 nm, *syn*-**37k**: τ_{minor} = 10.8 min and τ_{major} = 11.0 min.

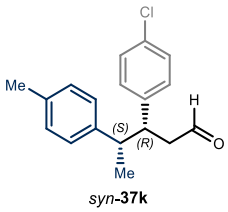

syn-**37k**

^{1}<u>H NMR</u> (500 MHz, $CDCl_3$): δ 9.36 (dd, *J* = 2.3, 1.3 Hz, 1H), 7.30 (d, *J* = 8.4 Hz, 2H), 7.17 (d, *J* = 8.4 Hz, 2H), 7.14 (d, *J* = 8.0 Hz, 2H), 7.10 (d, *J* = 8.1 Hz, 2H), 3.27 (td, *J* = 10.1, 4.6

Hz, 1H), 2.86 – 2.78 (m, 1H), 2.59 (ddd, *J* = 17.0, 9.9, 2.4 Hz, 1H), 2.50 (ddd, *J* = 17.0, 4.6, 1.4 Hz, 1H), 2.34 (s, 3H), 1.02 (d, *J* = 6.9 Hz, 3H).

^{13}C NMR (126 MHz, $CDCl_3$): δ 201.2, 141.8, 141.5, 136.5, 132.6, 129.6, 129.6, 128.9, 127.5, 49.1, 46.9, 45.6, 21.2, 20.6.

HRMS (APCI): calculated for calculated for $C_{18}H_{18}ClO$: 285.1041; found: 285.1036.

anti*-(3R,4R)-3-(4-Chlorophenyl)-4-(p-tolyl)pentanal (37k*) was obtained in 22 % yield (25.3 mg) as a single diastereomer. Enantiomeric excess was determined to be 87% *via* analysis of the corresponding 2,4-dinitrophenylhydrazone (obtained upon condensation with 2,4-dinitrophenylhydrazine), which could be separated by UPC^2 analysis on a Daicel Chiralpak ID-3 column: isocratic 100% CO_2 for 1 min; gradient from 100% CO_2 to 70:30 CO_2/*i*PrOH for 5 min; isocratic 70:30 CO_2/*i*PrOH for 9 min, gradient from 70:30 CO_2/*i*PrOH to 100% CO_2 for 1 min, flow rate 2.0 mL/min, λ = 347 nm, *anti*-**37k**: τ_{minor} = 11.3 min and τ_{major} = 11.8 min.

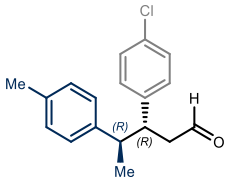

anti-**37k**

^{1}H NMR (500 MHz, $CDCl_3$) δ 9.58 (dd, *J* = 2.3, 1.6 Hz, 1H), 7.15 (d, *J* = 8.6 Hz, 2H), 7.01 (d, *J* = 7.8 Hz, 2H), 6.90 (d, *J* = 8.3 Hz, 2H), 6.85 (d, *J* = 7.9 Hz, 2H), 3.47 – 3.39 (m, 1H), 3.00 (p, *J* = 7.0 Hz, 1H), 2.81 (ddd, *J* = 16.9, 5.7, 1.6 Hz, 1H), 2.74 (ddd, *J* = 16.9, 9.3, 2.3 Hz, 1H), 2.28 (s, 3H), 1.25 (d, *J* = 7.1 Hz, 3H).

^{13}C NMR (126 MHz, $CDCl_3$) δ 201.6, 140.4, 140.2, 136.1, 132.4, 130.0, 128.9, 128.3, 128.0, 46.6, 45.9, 44.5, 21.1, 18.5.

Racemic samples of adduct **37k** were prepared using the organocatalytic procedure described above on a 0.1 mmol scale using the racemic amine catalyst **A-1**. The racemic product **37k** was isolated in 55% yield (16.8 mg) as a 1:1.3 mixture of diastereoisomers. Separation of diastereoisomers by preparative TLC afforded racemic, diastereomerically pure samples of *syn* and *anti* **37k** (Figures 3.40 and 3.41).

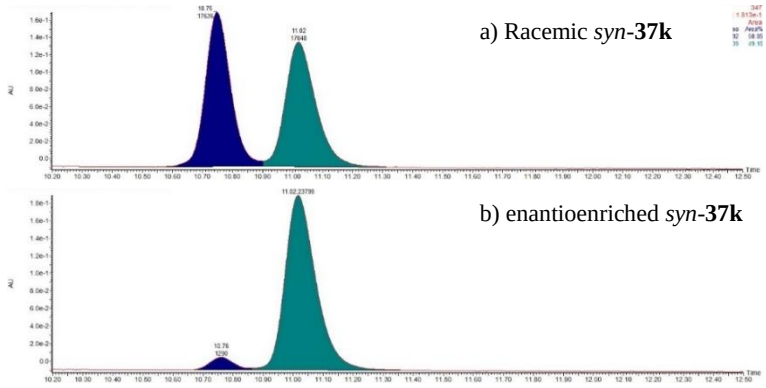

Figure 3.40. UPC^2 analysis of racemic (top) and enantioenriched (bottom) *syn*-**37k**, prepared via the organocatalytic route with catalyst **A-1**

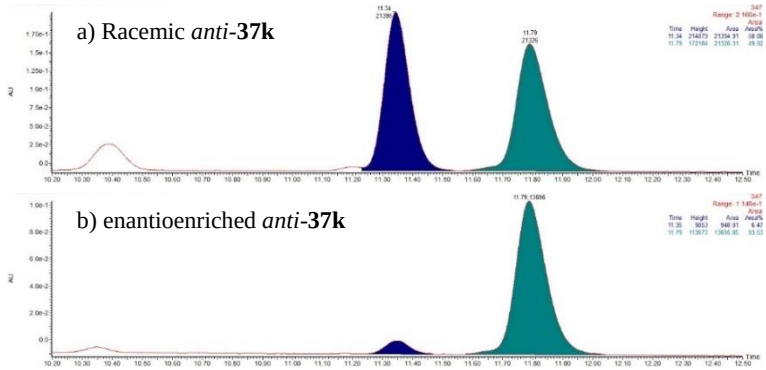

Figure 3.41. UPC² analysis of racemic (top) and enantioenriched (bottom) *anti*-**37k**, prepared via the organocatalytic route with catalyst **A-1**.

Photobiocatalytic Synthesis of Product **37k**

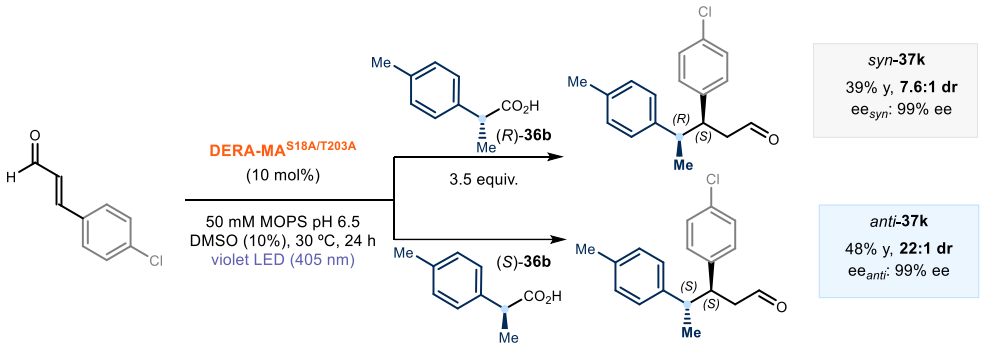

Determination of the Relative Configuration of the Enzymatic Product **37k** *by GC-FID*

The isolated diastereomers *syn*-**37k** and *anti*-**37k**, prepared via the organocatalytic route with catalyst **A-1** mentioned above, were analyzed by GC-FID analysis, which allowed assignment of the individual retention times of both diastereoisomers (Figure 3.42).

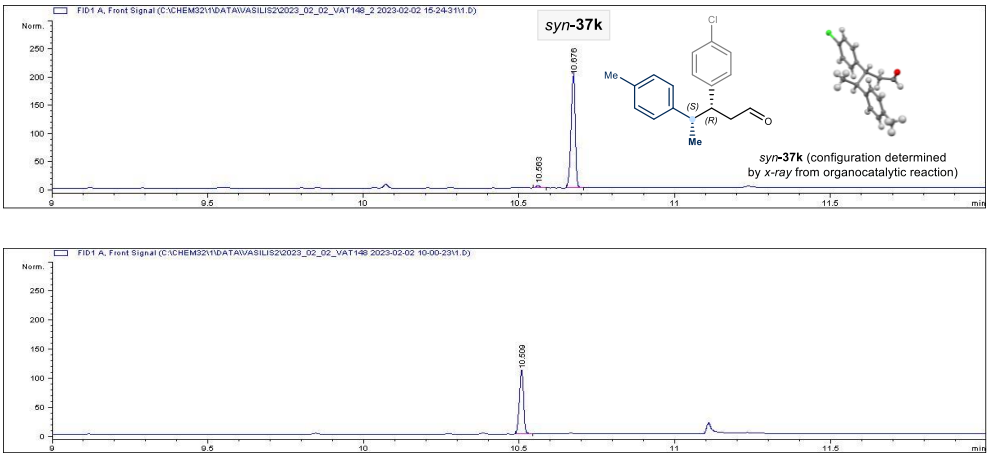

Figure 3.42. GC-FID analysis of *syn*-**37k** (top) and *anti*-**37k** (bottom), prepared via the organocatalytic route with catalyst **A-1.**

These references served to establish the relative configuration of the biocatalytic products **37k**. GC-FID analysis the enzymatic reaction catalyzed by DERA-MA^{S18A} and starting from *(R)*-**36b** showed a retention time consistent with the *syn*-**37k** diastereomer, confirming its identity (shown at the top of Figure 3.45). Conversely, GC-FID analysis of the product of the enzymatic reaction catalyzed by DERA-MA^{S18A} and starting from *(S)*-**36b** matched the retention time of *anti*-**37k** (bottom in Figure 3.43).

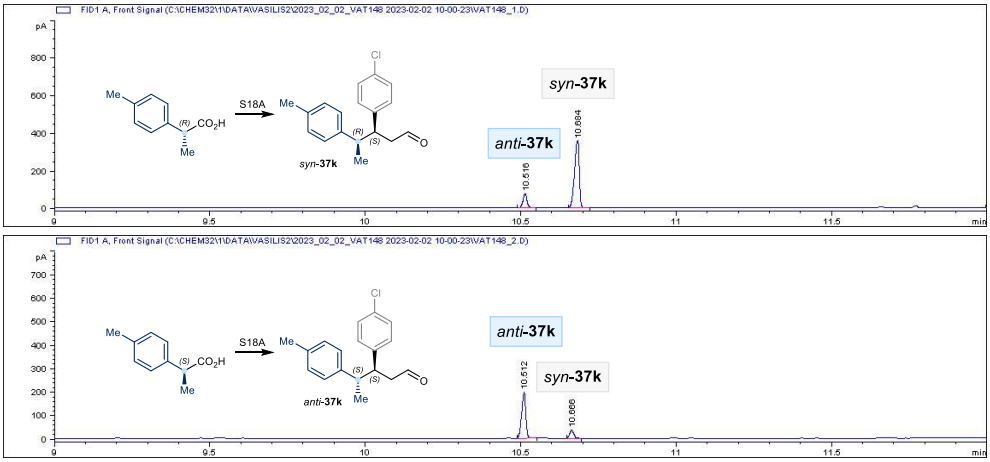

Figure 3.43. GC-FID analysis of the enzymatic reaction catalyzed by DERA^{S18A} using (*R*)-**36b** (top) or (*S*)-**36b** (bottom), affording *syn*-**37k** or *anti*-**37k** respectively.

Determination of the Absolute Configuration of **37k** *by UPC² Analysis*

The absolute configuration of adducts **37k** prepared via the photoenzymatic reaction was established by UPC² analysis and comparison with the reference samples prepared via the organocatalytic route. This comparison further confirmed the relative configuration of the enzymatic products. Specifically, we used the isolated enantioenriched and racemic products of *syn*-**37k** and *anti*-**37k**, prepared via the organocatalytic route with catalyst **A-1**, to assign the individual retention times of all 4 possible stereoisomers.

UPC² analysis of the products of the enzymatic reaction catalyzed by DERA-MA^{S18A} using *(R)*-**36b** confirmed that *syn*-**37k** was preferentially formed (Figure 3.44). Conversely, analysis of the product of the enzymatic reaction catalyzed by DERA-MA^{S18A} and starting from *(S)*-**36b** showed a retention time consistent with the *anti*-**37k** diastereomer.

This analysis also allowed us to unambiguously assign the absolute configuration of the enzymatic products **37k**. X-ray analysis of *syn*-**37k**, prepared via the organocatalytic route using catalyst (*S*)-**A-1**, established an (3*R*,4*S*) absolute configuration. Direct comparison of the UPC traces of *syn*-**37k**, prepared via the enzymatic route, showed that the opposite enantiomer was formed instead, establishing an (3*S*,4*R*) absolute configuration.

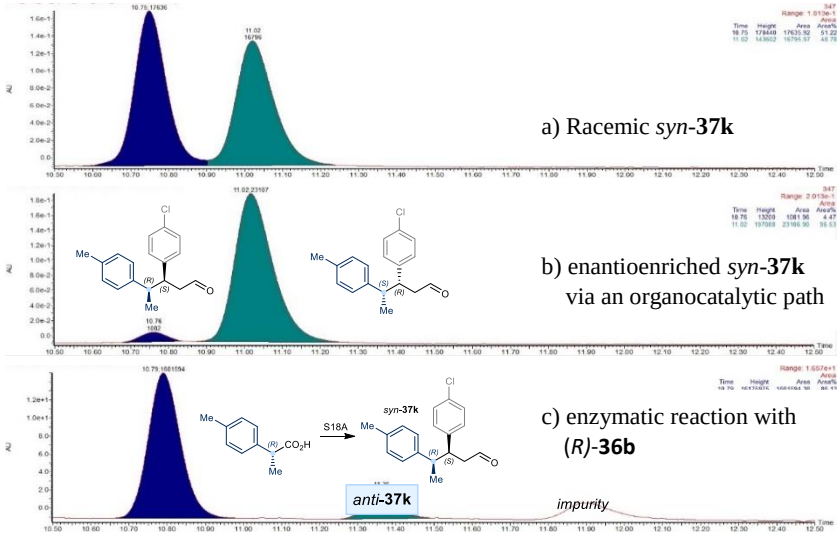

Figure 3.44. UPC analysis of a) racemic *syn*-**37k**, b) enantioenriched *syn*-**37k** prepared via the organocatalytic route with catalyst **A-1**, c) *syn*-**37k** prepared via the enzymatic reactions performed with DERA^{S18A} using (*R*)-**36b**.

We then repeated the same comparison to establish the stereochemistry of the *anti*-**37k** prepared via the enzymatic reaction catalyzed by DERA-MA^{S18A}. First, we confirmed that using the chiral carboxylic acid *(S)*-**36b** the *anti*-**37k** was preferentially formed (Figure 3.45).

The absolute configuration of X-ray analysis of *anti*-**37k**, prepared via the organocatalytic route using catalyst (*S*)-**A-1**, was established to be (3*R*,4*R*). This conclusion is based on the fact that the chiral amine catalyst **A1** has the ability to control only the formation of the stereogenic center at the 3 position. Consequently, the absolute configuration of this stereogenic center remained unchanged in comparison to the *syn*-**37k** adduct (for which we obtained unambiguous evidence of the absolute configuration through X-ray analysis). Direct comparison of the UPC traces of *anti*-**37k**, prepared via the enzymatic route from *(S)*-**36b**, showed that the opposite enantiomer was formed instead, establishing an (3*S*,4*S*) absolute configuration.

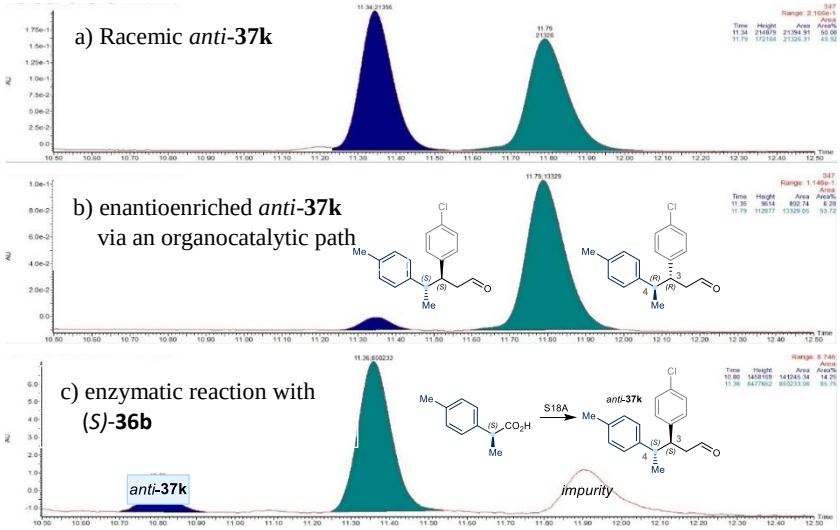

Figure 3.45. UPC analysis of a) racemic *anti*-**37k**, b) enantioenriched *anti*-**37k** prepared via the organocatalytic route with catalyst **A-1**, c) *anti*-**37k** prepared via the enzymatic reactions performed with DERA^{S18A} using (*S*)-**36b**.

Crystallization of a Derivative of the Enzymatically Obtained Product **37e**

To confirm the stereochemical course of the reaction directly from a product obtained from the enzymatic reaction, we conducted the crystallization of a derivative from adduct *syn*-**37e**. This product was obtained from the reaction between (*R*)-**36e** and cinnamaldehyde **29a** using DERA-MA^{S18A}, following the procedure described below.

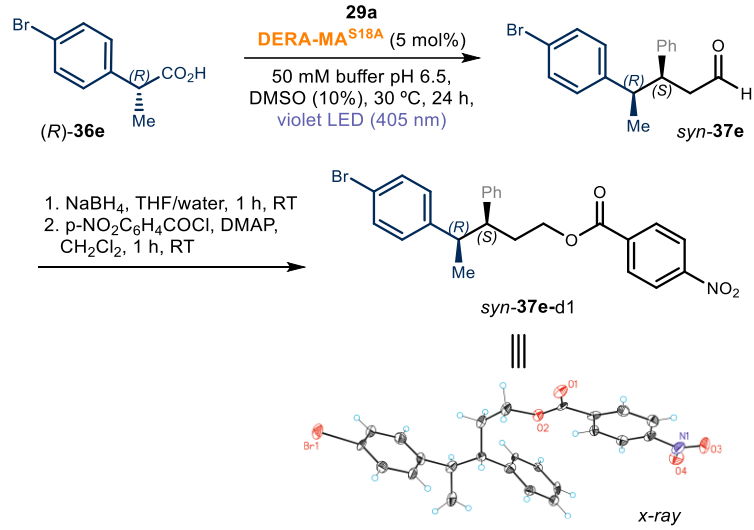

Aldehyde *syn*-**37e** was synthesized using DERA-MA^{S18A} as biocatalyst. Isolation of the ***major*** diastereoisomer by column chromatography (silica gel, 5% EtOAc in hexanes) afforded diastereopure product *syn*-**37e**.

*To facilitate the crystallization process, a reduction and esterification sequence of syn-**37e** was performed as following: a*ldehyde *syn*-**37e** (1 eq., 7.5 mg, 23.0 µmol) was dissolved in THF/water (0.5 mL, 4:1) and cooled to 0 °C using an ice bath. Then, $NaBH_4$ (10 eq., 0.23 mmol, 8.7 mg) was added portion wise, the ice bath was removed and the mixture was stirred for 30 min. After cooling to 0 °C again, excessive reductant was carefully quenched by dropwise addition of 1 N HCl until gas evolution ceased. Water (0.5 mL) was added, and the mixture was extracted with DCM (3x10 mL). The combined organic layers were dried with $MgSO_4$ and concentrated. The crude alcohol was dissolved in CH_2Cl_2 (anhydrous, 0.2 mL) and *p*-$NO_2C_6H_4Cl$ (5 eq, 21.3 mg, 115.0 µmol) and DMAP (3 eq., 8.4 mg, 69.0 µmol) were added. The mixture was stirred for 1 h at RT and directly loaded on prepTLC (30% EtOAc in hexanes), which afforded 8.0 mg of ester derivative *syn*-**37e**-d1. The compound was then directly crystallized by slow evaporation from diethylether/hexane in the refrigerator (5 ºC). The *x-ray* crystallographic analysis confirmed the (3*S*,4*R*) absolute configuration, in analogy to product *syn*-**37k**.

3.6.9 X-Ray Crystallographic Data

3.6.9.1 Crystallographic data for *syn*-37k

Single Crystal X-ray Diffraction Data for Crystals of the compound *syn*-**37k** (prepared using the chiral amine catalyst (*S*)-**A-1**, see *Section 3.6.5.2*) were obtained by slow evaporation of a DCM/hexane solution.

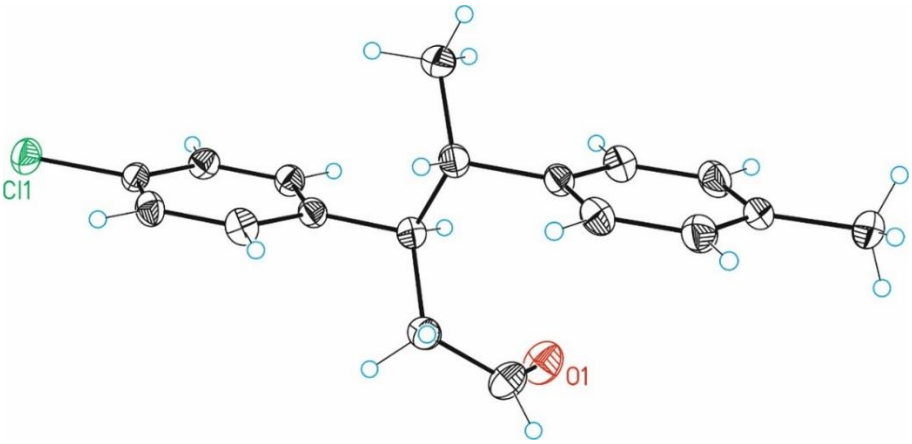

Table 3.10. Crystal data and structure refinement for *syn*-**37k** (*CCDC 2280852*)

Identification code	MBE558F1_a	
Empirical formula	C18 H19 Cl O	
Formula weight	286.78	
Temperature	100(2)K	
Wavelength	0.71073 Å	
Crystal system	orthorhombic	
Space group	P 21 21 21	
Unit cell dimensions	a = 5.7579(5)Å	a= 90°.
	b = 7.4820(6)Å	b = 90°.
	c = 35.275(4)Å	g = 90°.
Volume	1519.7(2) $Å^3$	
Z	4	
Density (calculated)	1.253 Mg/m^3	
Absorption coefficient	0.245 mm^{-1}	

F(000)	608
Crystal size	0.200 x 0.200 x 0.200 mm^3
Theta range for data collection	3.465 to 29.716°.
Index ranges	-7<=h<=8,-9<=k<=10,-43<=l<=48
Reflections collected	22095
Independent reflections	3989[R(int) = 0.0360]
Completeness to theta =29.716°	94.9%
Absorption correction	Multi-scan
Max. and min. transmission	1.00 and 0.80
Refinement method	Full-matrix least-squares on F^2
Data / restraints / parameters	3989/ 0/ 183
Goodness-of-fit on F^2	1.073
Final R indices [I>2sigma(I)]	R1 = 0.0356, wR2 = 0.0932
R indices (all data)	R1 = 0.0379, wR2 = 0.0941
Flack parameter	x =0.038(15)
Largest diff. peak and hole	0.446 and -0.166 e.$Å^{-3}$

3.6.9.2 Crystallographic Data for *syn*-37e-d1

Single Crystal X-ray Diffraction Data for Crystals of the compound *syn*-3**7e-d1** (prepared using DERA-MA^{S18A}, see *Section 3.6.5.2*) were obtained by slow evaporation of a diethyl ether/hexane solution at 5 ºC.

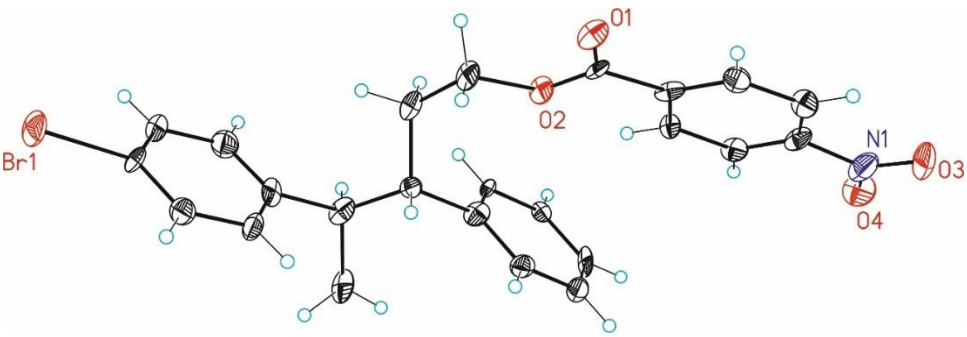

Table 3.11. Crystal data and structure refinement for *syn*-**37e**-d1 (*CCDC 2281644*)

Identification code	MBELKQ3
Empirical formula	C24 H22.50 Br N O4
Formula weight	468.84
Temperature	100(2)K

Wavelength	0.71073 Å
Crystal system	monoclinic
Space group	P 21
Unit cell dimensions	a = 7.5278(3)Å □=
90°.	
	b = 5.7284(2)Å □ =
92.582(4)°.	
	c = 24.2837(8)Å □ =
90°.	
Volume	1046.10(7) $Å^3$
Z	2
Density (calculated)	1.488 Mg/m^3
Absorption coefficient	1.996 mm^{-1}
F(000)	481
Crystal size	0.200 x 0.050 x 0.010 mm^3
Theta range for data collection	2.519 to 29.179°.
Index ranges	-9<=h<=10,-7<=k<=7,-32<=l<=32
Reflections collected	15056
Independent reflections	4872[R(int) = 0.0493]
Completeness to theta =29.179°	91.5%
Absorption correction	Multi-scan
Max. and min. transmission	1.00 and 0.84
Refinement method	Full-matrix least-squares on F^2
Data / restraints / parameters	4872/ 61/ 521
Goodness-of-fit on F^2	1.039
Final R indices [I>2sigma(I)]	R1 = 0.0362, wR2 = 0.0885
R indices (all data)	R1 = 0.0455, wR2 = 0.0934
Flack parameter	x =-0.009(9)
Largest diff. peak and hole	0.708 and -0.499 $e.Å^{-3}$

3.6.10 GC-FID and UPC² Traces

3.6.10.1 Analytical Scale Biocatalytic Reaction Enantioselective Procedure

(*R*)-3,4-Diphenylbutanal (35a)

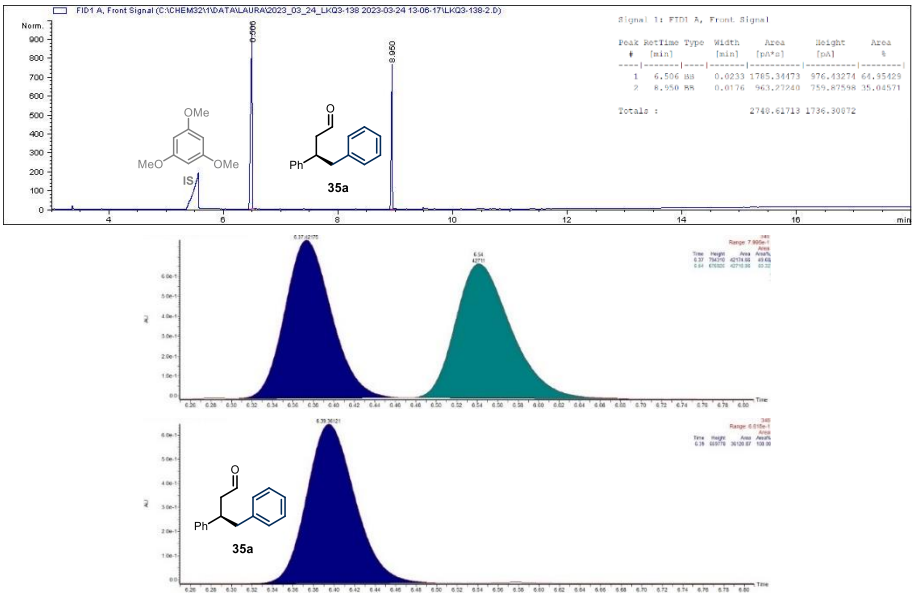

(*R*)-3-Phenyl-4-(p-tolyl)butanal (35b)

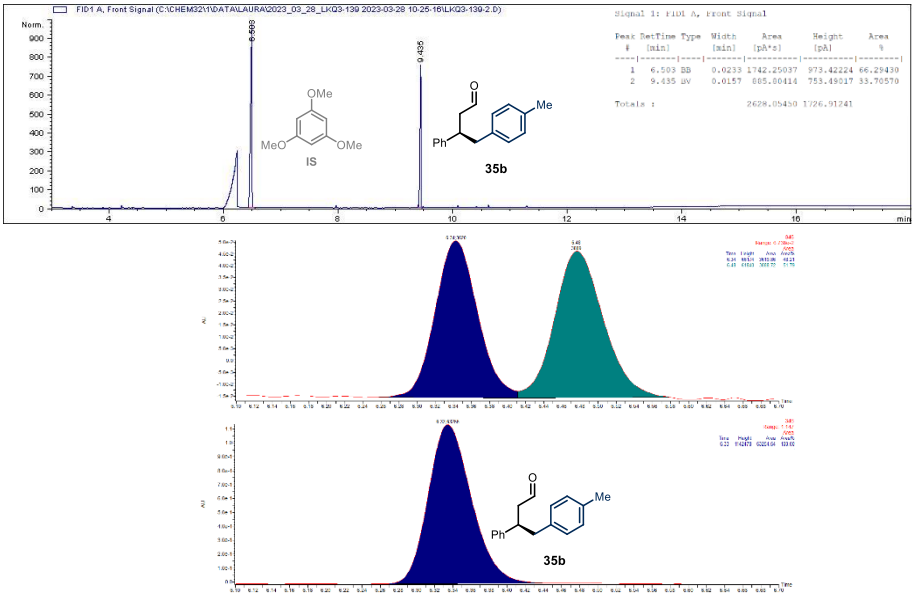

(*R*)-3-Phenyl-4-(*m*-tolyl)butanal (35c)

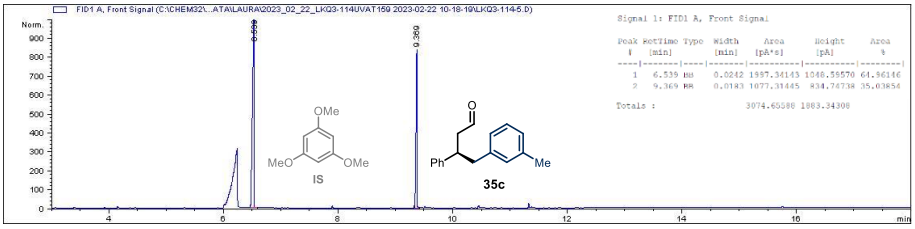

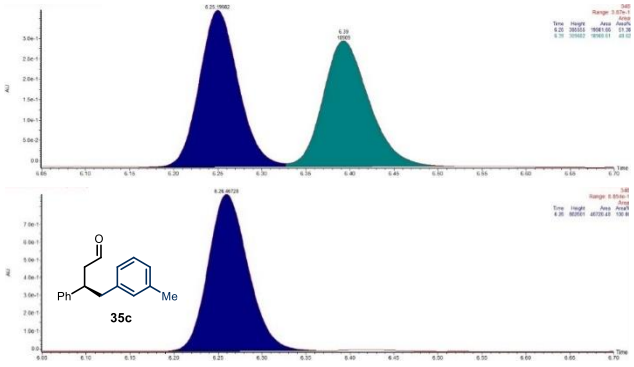

(*R*)-3-Phenyl-4-(*o*-tolyl)butanal (35d)

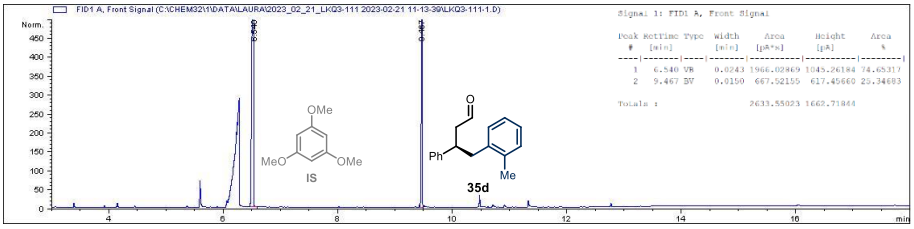

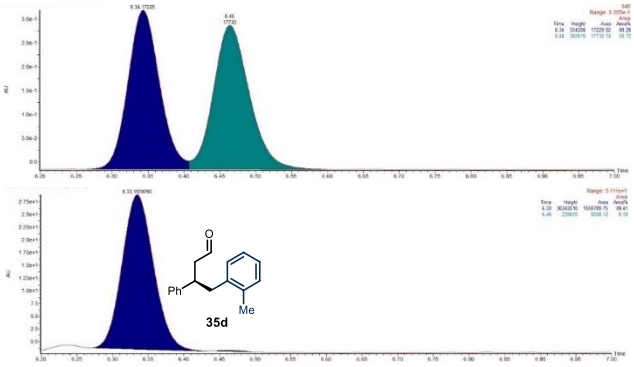

(*R*)-4-(4-Bromophenyl)-3-phenylbutanal (35e)

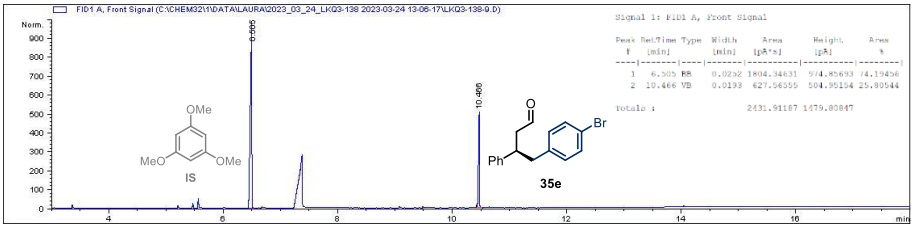

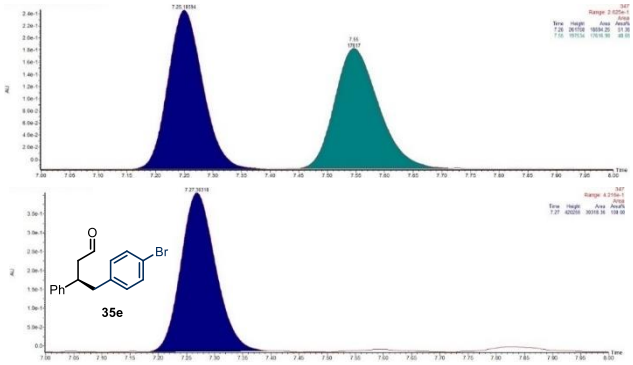

(*R*)-4-(4-Chlorophenyl)-3-phenylbutanal (35f)

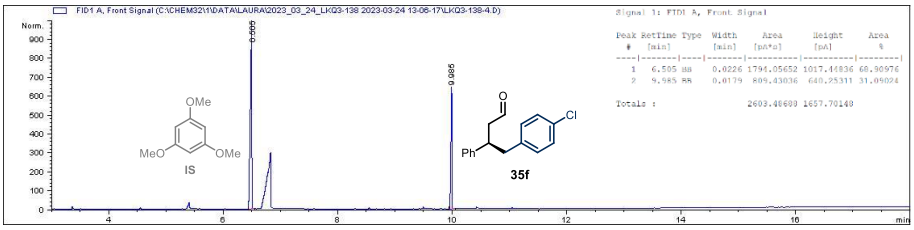

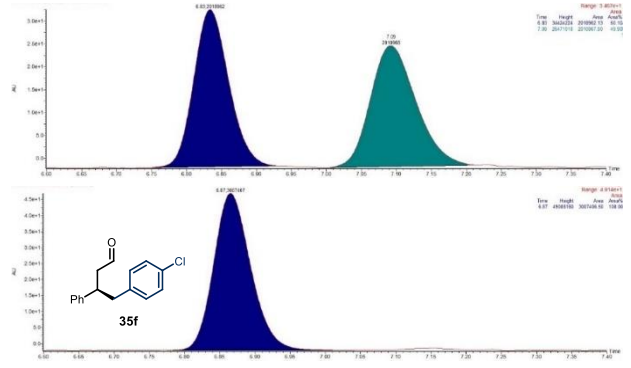

(*R*)-4-(4-Fluorophenyl)-3-phenylbutanal (35g)

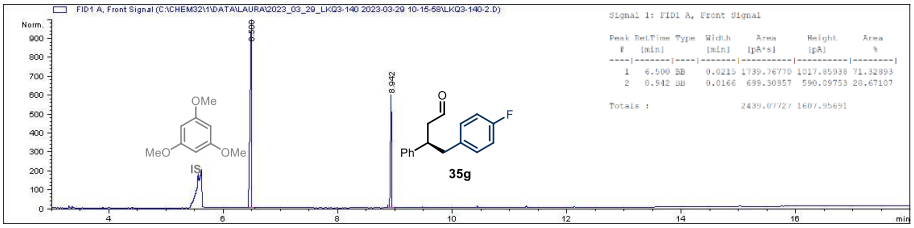

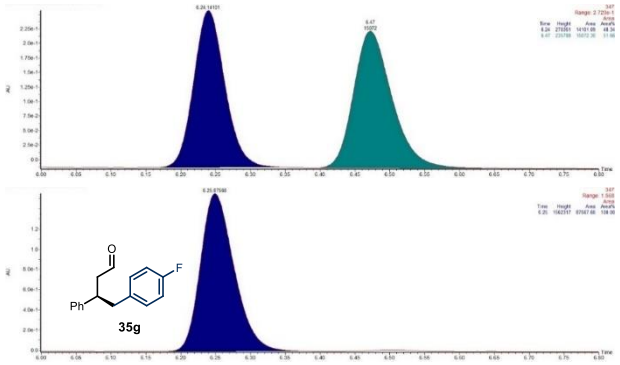

(*R*)-4-(4-Methoxyphenyl)-3-phenylbutanal (35h)

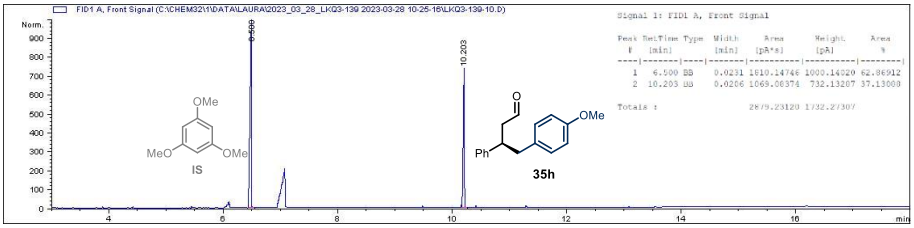

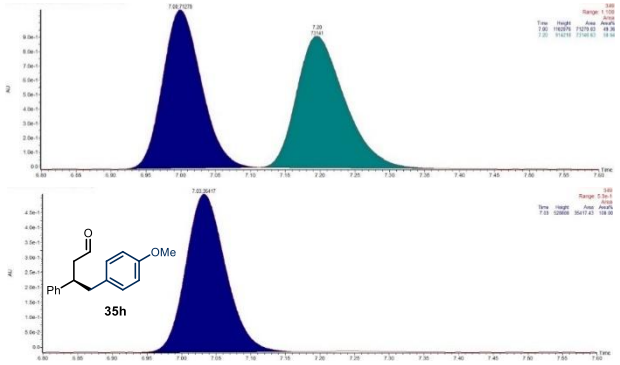

(*R*)-3-Phenyl-4-(thiophen-2-yl)butanal (35i)

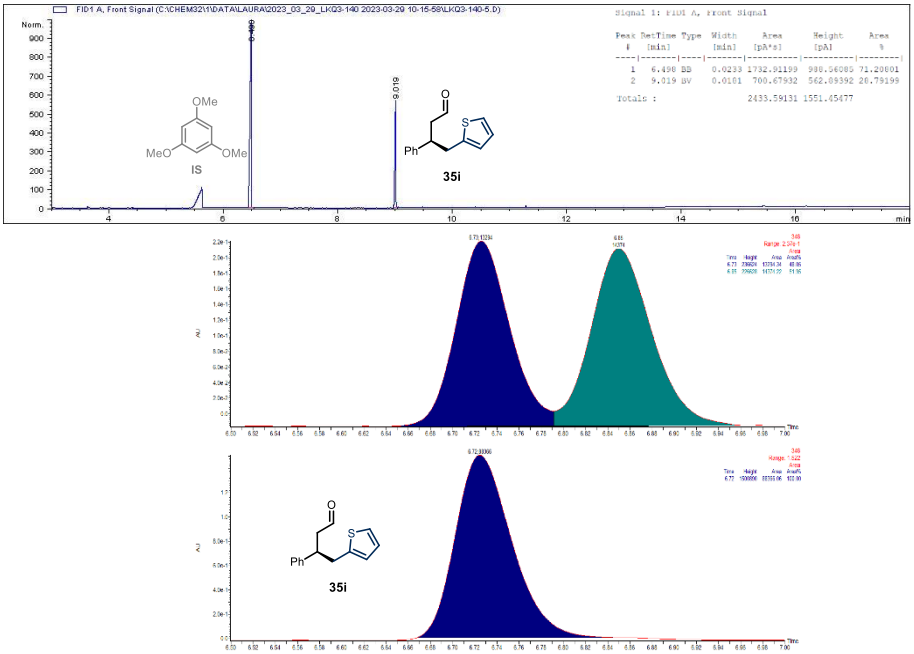

(*R*)-3-Phenyl-4-(furan-2-yl)butanal (35j)

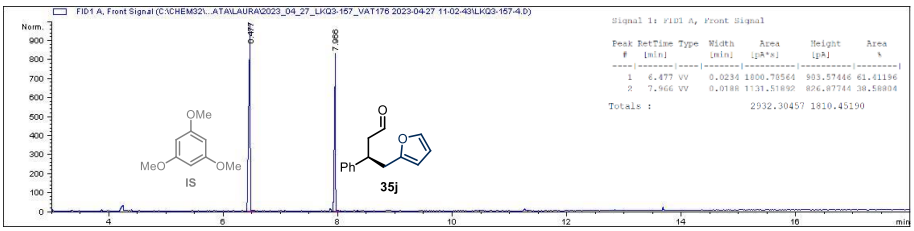

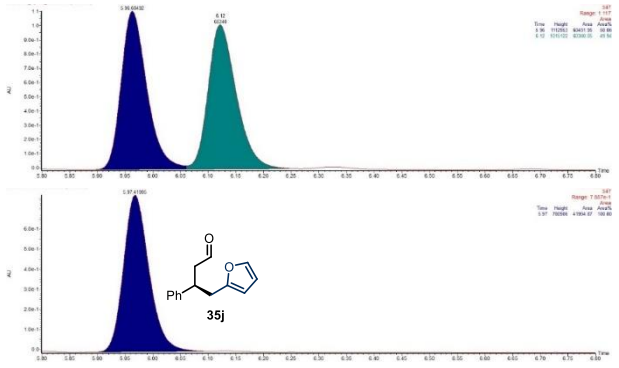

(*R*)-4-Phenyl-3-(p-tolyl)butanal (35k)

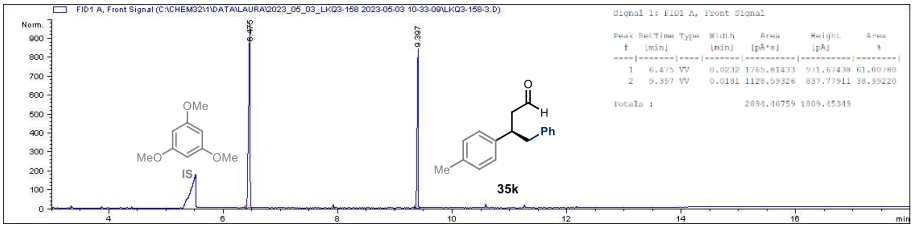

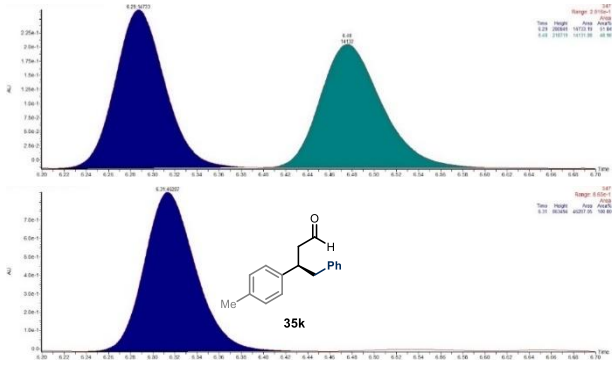

(*R*)-3-(4-Methoxyphenyl)-4-phenylbutanal (35l)

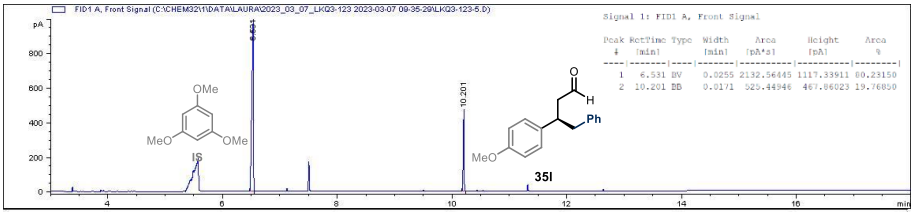

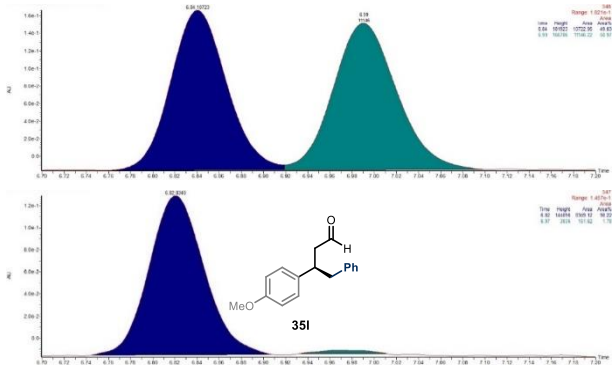

(*R*)-3-(4-Bromophenyl)-4-phenylbutanal (35m)

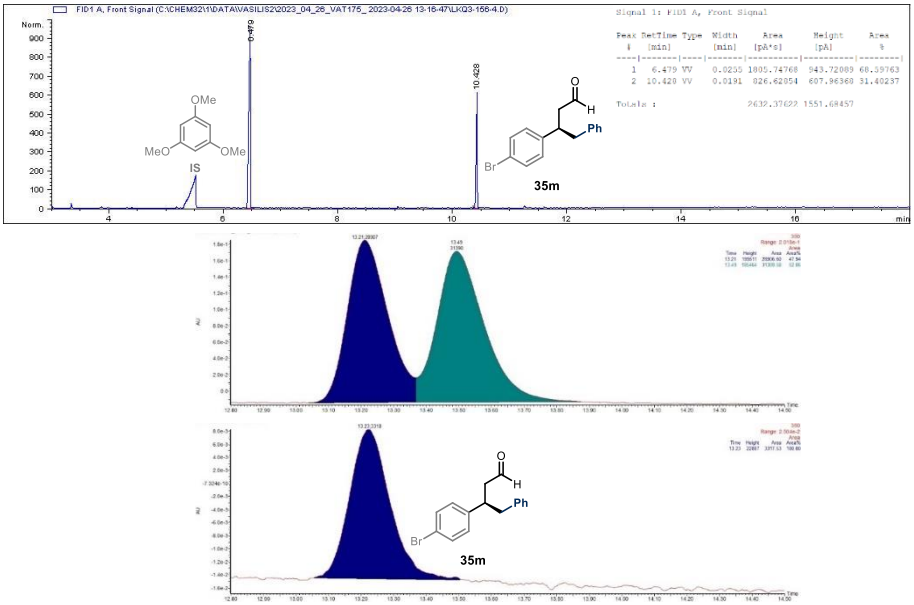

(3*R*)-4-Methyl-4-(5-oxotetrahydrofuran-2-yl)-3-phenylpentanal (39)

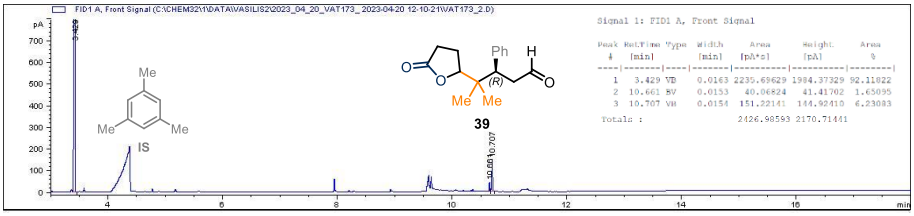

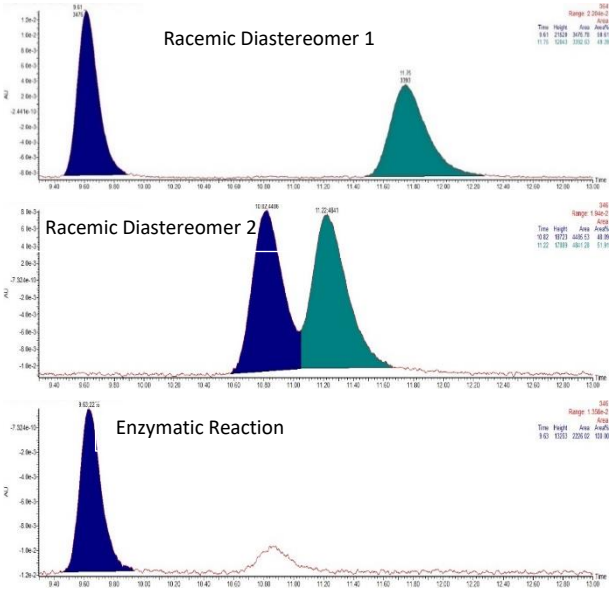

3.6.10.2 Analytical Scale Biocatalytic Reactions – Stereospecific Procedure

(3*S*)-3,4-Diphenylpentanal (37a)

With (*R*)-acid **36a**:

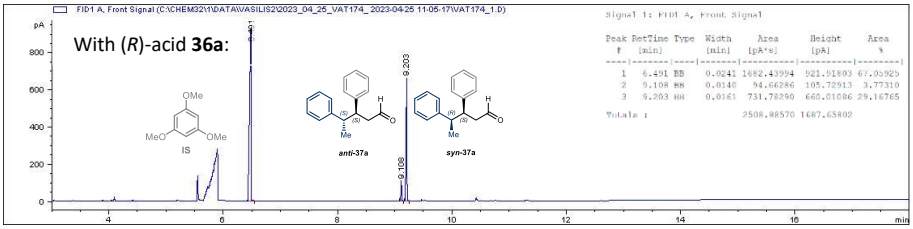

With (*S*)-acid **36a**:

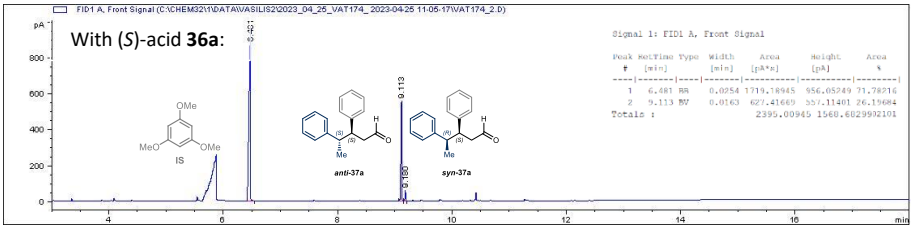

With
(*R*)-Acid **36a**:

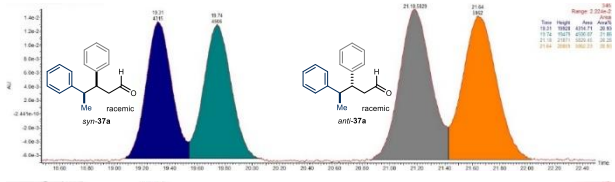

With
(*S*)-Acid **36a**:

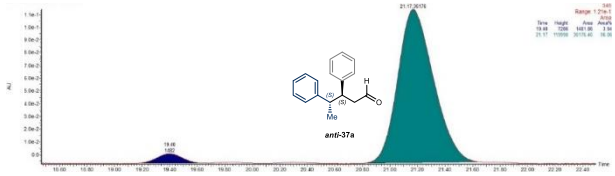

(3*S*)-3-Phenyl-4-(*p*-tolyl)pentanal (37b)

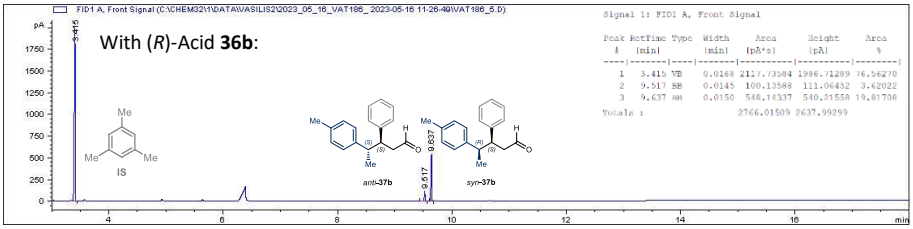

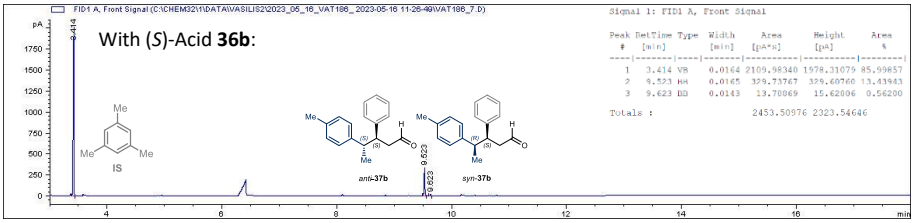

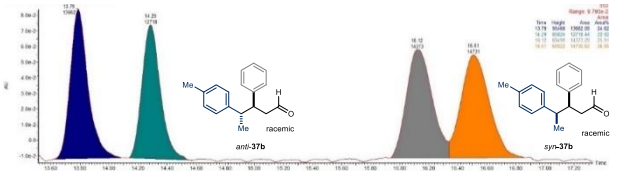

With (*R*)-Acid **36b**:

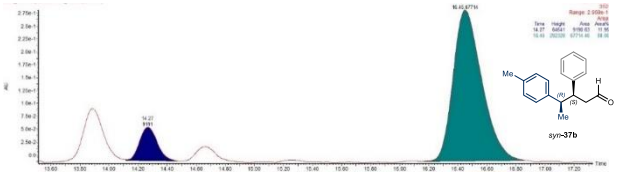

With (*S*)-Acid **36b**:

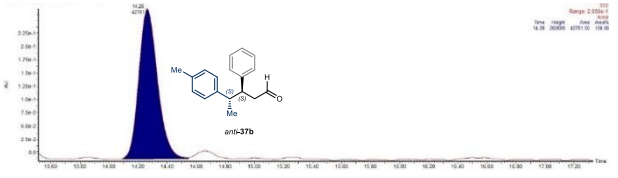

(3*S*)-3-Phenyl-4-(*m*-tolyl)pentanal (37c)

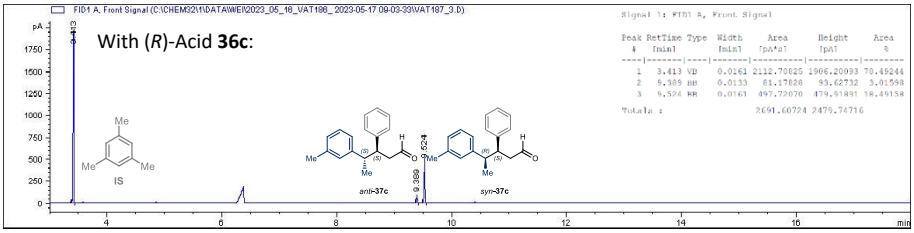

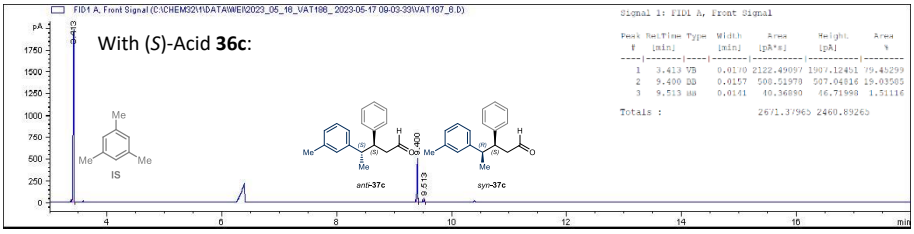

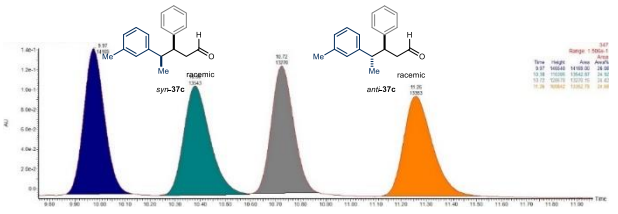

With (*R*)-Acid **36c**:

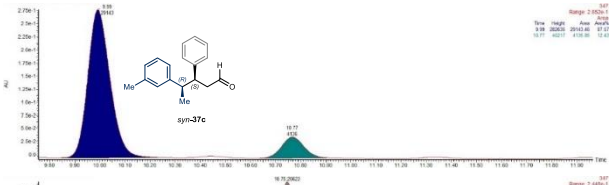

With (*S*)-Acid **36c**:

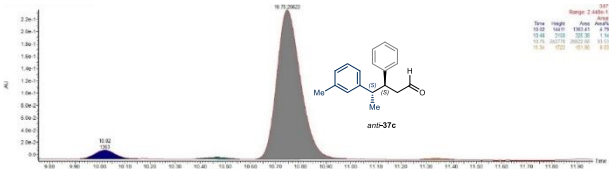

(3*S*)-3-Phenyl-4-(*o*-tolyl)pentanal (37d)

With (*R*)-Acid **36d**:

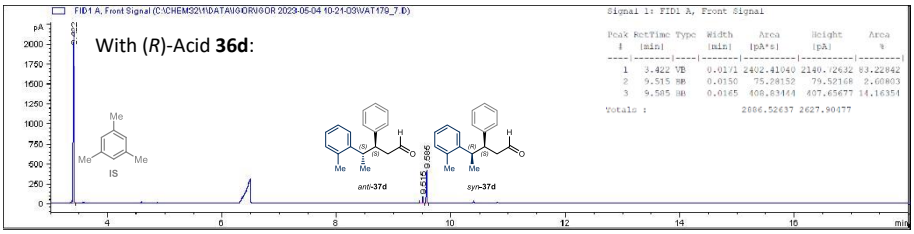

With (*S*)-Acid **36d**:

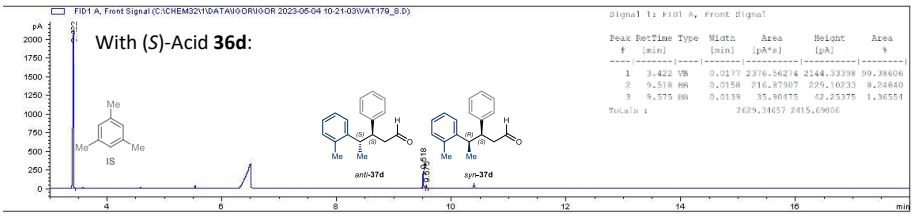

With (*R*)-Acid **36d**:

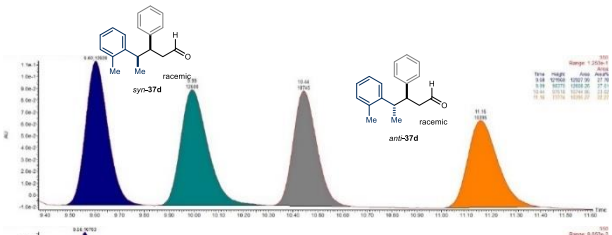

With (*S*)-Acid **36d**:

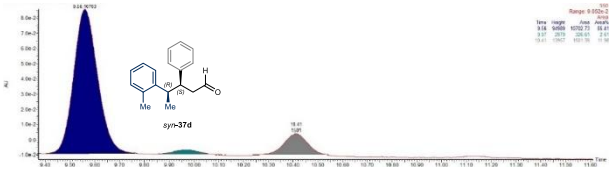

(3*S*)-4-(4-Bromophenyl)-3-phenylpentanal (37e)

With (*R*)-Acid **36e**:

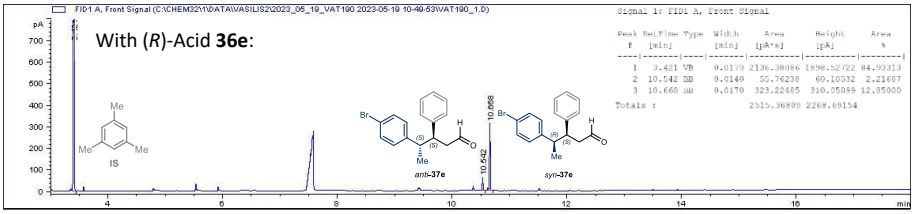

With (*S*)-Acid **36e**:

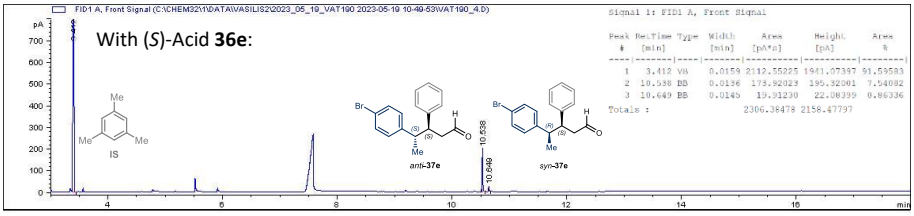

With (*R*)-Acid **36e**:

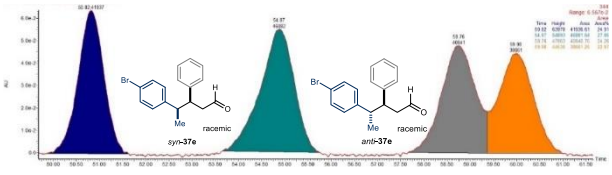

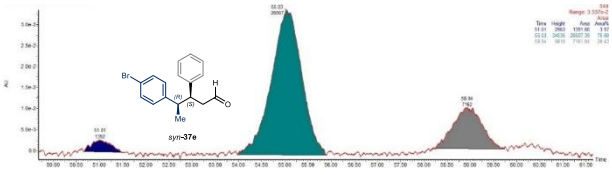

With (*S*)-Acid **36e**:

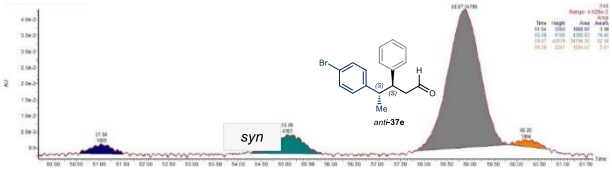

(3*S*)-4-(4-Chlorophenyl)-3-phenylpentanal (37f)

With (*R*)-Acid **36f**:

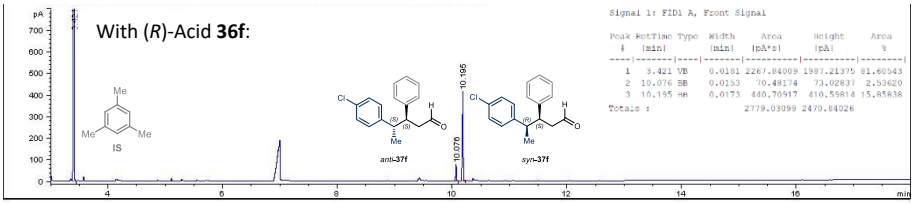

With (*S*)-Acid **36f**:

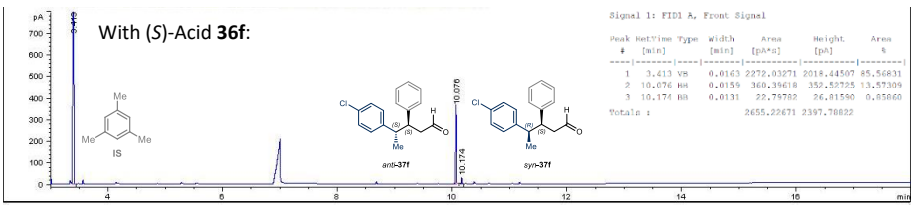

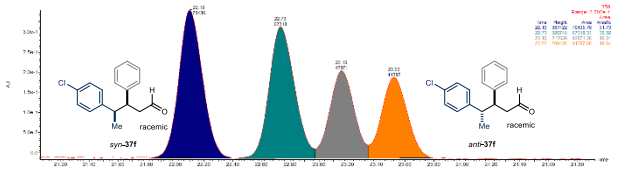

With
(*R*)-Acid **36f**:

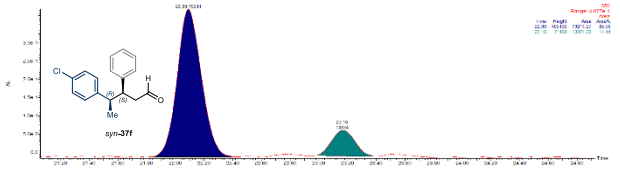

With
(*S*)-Acid **36f**:

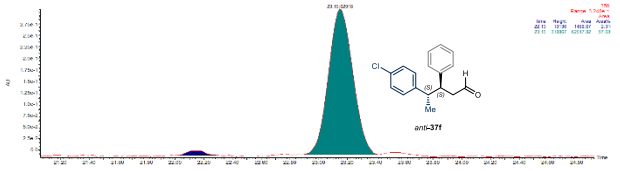

(3*S*)-4-(4-Fluorophenyl)-3-phenylpentanal (37g)

With (*R*)-Acid **36g**:

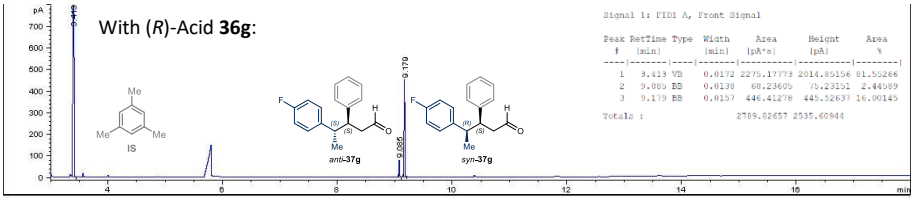

Signal 1: FID1 A, Front Signal

Peak #	RetTime [min]	Type	Width [min]	Area [pA*s]	Height [pA]	Area %
1	3.413	VB	0.0172	2275.17773	2014.85156	81.50266
2	9.089	BB	0.0138	68.23605	75.23101	2.44589
3	9.179	BB	0.0157	446.41278	445.52637	16.00145
Totals :				2789.82657	2535.60944	

With (*S*)-Acid **36g**:

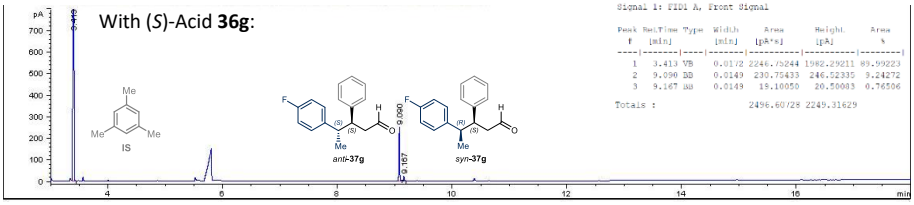

Signal 1: FID1 A, Front Signal

Peak #	RetTime [min]	Type	Width [min]	Area [pA*s]	Height [pA]	Area %
1	3.413	VB	0.0172	2246.75244	1982.29211	89.99223
2	9.090	BB	0.0149	230.75433	246.52335	9.24272
3	9.167	BB	0.0149	18.10050	20.50083	0.76506
Totals :				2496.60728	2249.31629	

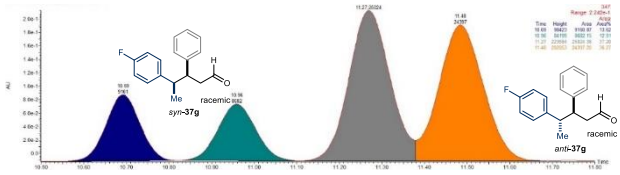

With (*R*)-Acid **36g**:

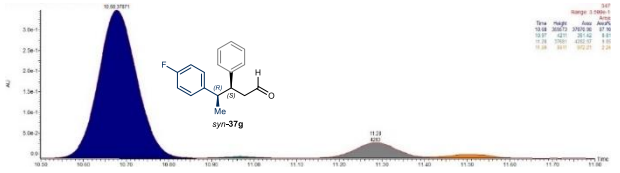

With (*S*)-Acid **36g**:

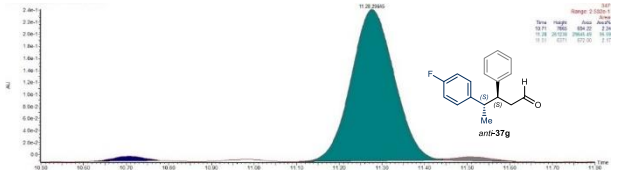

(3*S*)-4-(4-Methoxyphenyl)-3-phenylpentanal (37h)

With (*R*)-Acid **36h**:

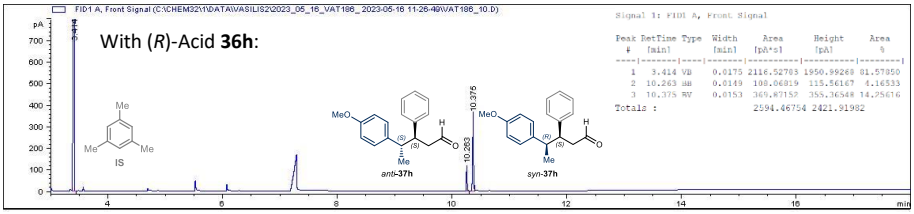

With (*S*)-Acid **36h**:

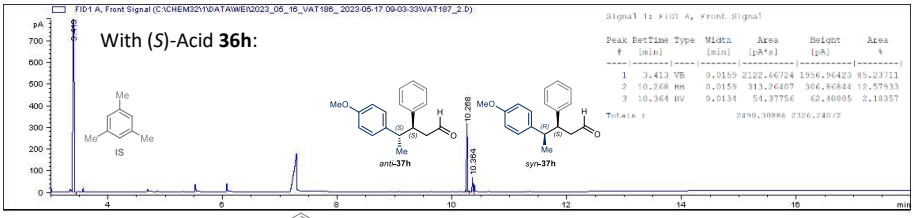

With
(*R*)-Acid **36h**:

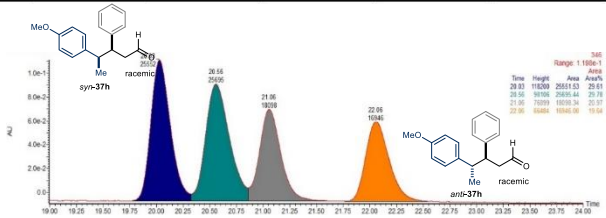

With
(*S*)-Acid **36h**:

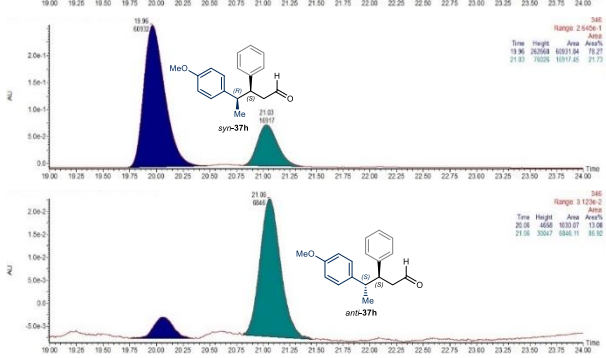

(3*S*)-4-Phenyl-3-(p-tolyl)pentanal (37i)

With (*R*)-Acid **36a**:

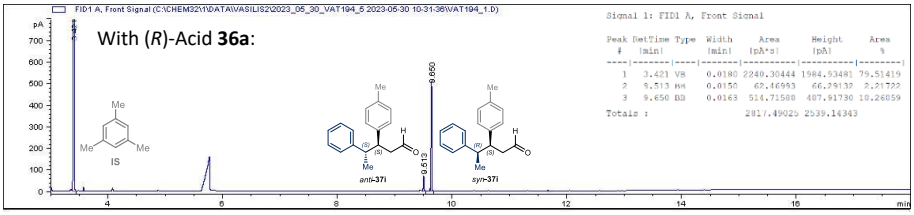

With (*S*)-Acid **36a**:

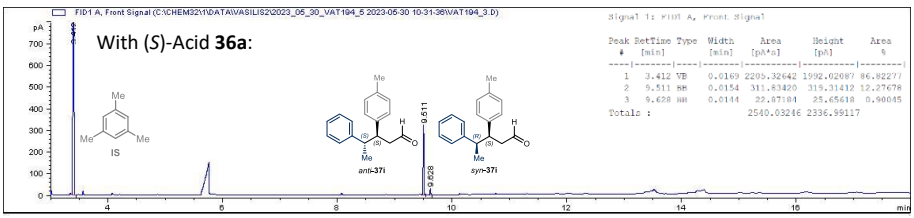

With (*R*)-Acid **36a**:

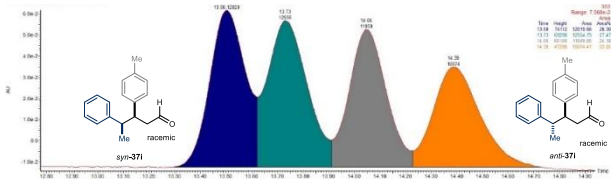

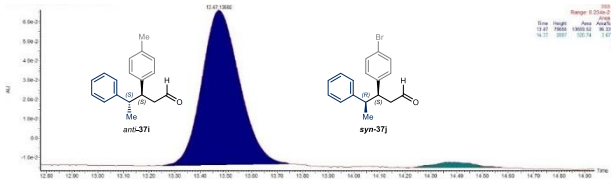

With (*S*)-Acid **36a**:

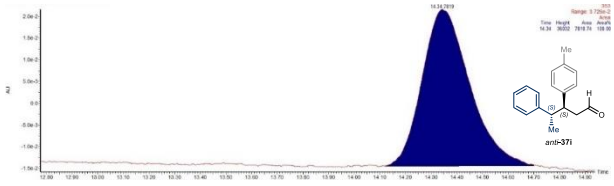

(3*S*)-3-(4-Bromophenyl)-4-phenylpentanal (37j)

With (*R*)-Acid **36a**:

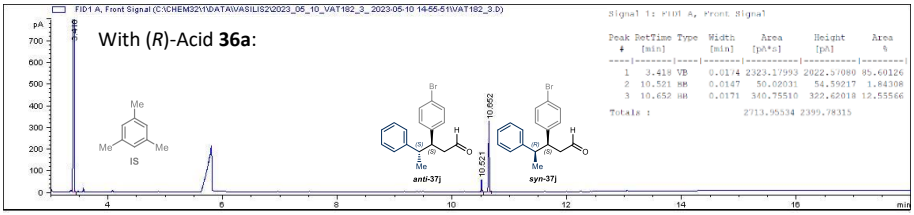

With (*S*)-Acid **36a**:

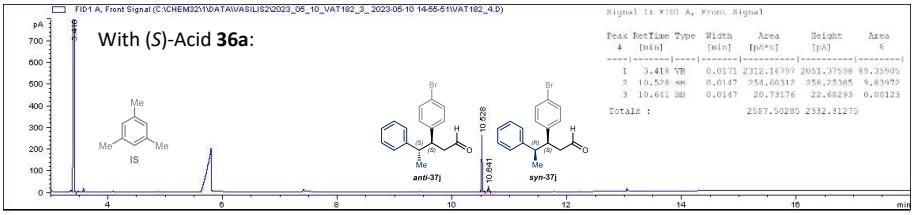

With
(*R*)-Acid **36a**:

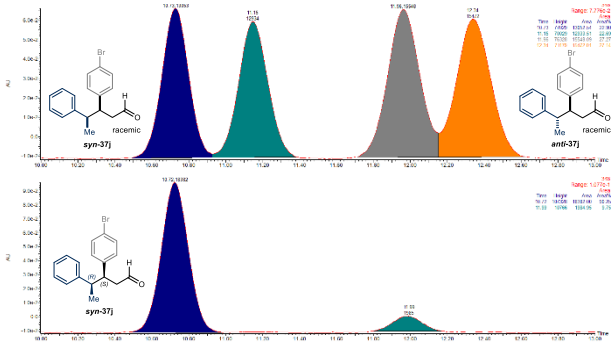

With
(*S*)-Acid **36a**:

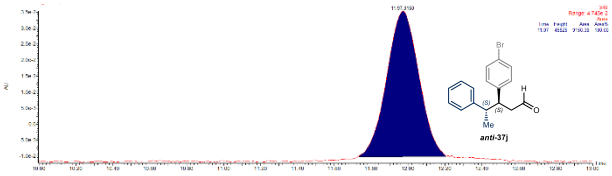

3.6.10.3 Analytical Scale Biocatalytic Reactions – Kinetic Resolution Procedure

(3*S*,4*R*)-3,4-Diphenylpentanal (37a)

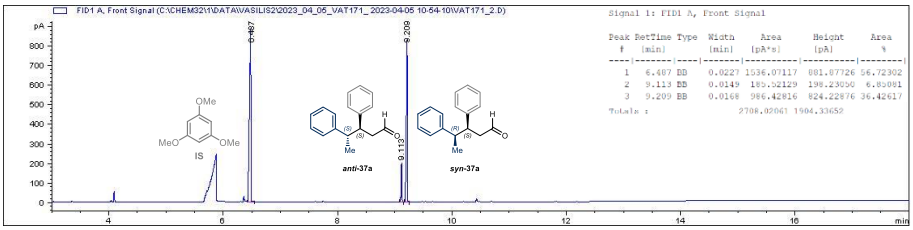

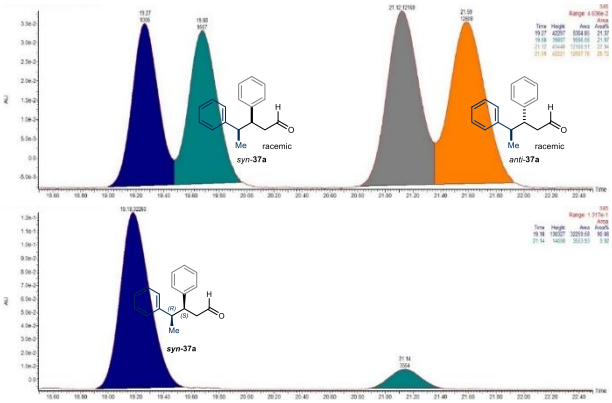

(3*S*,4*R*)-3-Phenyl-4-(p-tolyl)pentanal (37b)

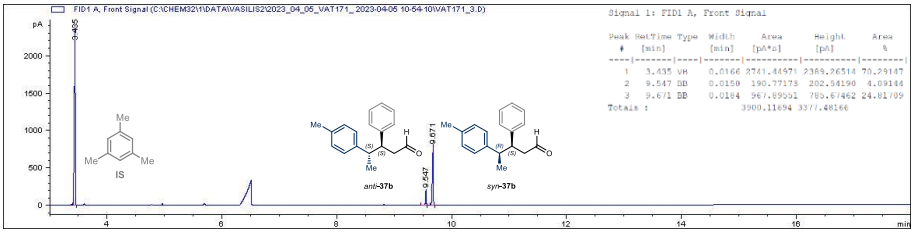

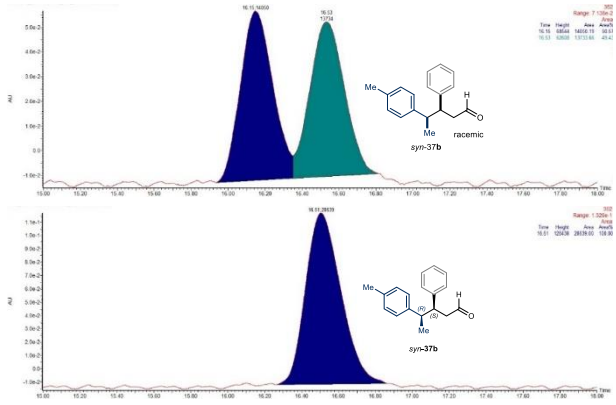

(3*S*,4*R*)-3-Phenyl-4-(*m*-tolyl)pentanal (37c)

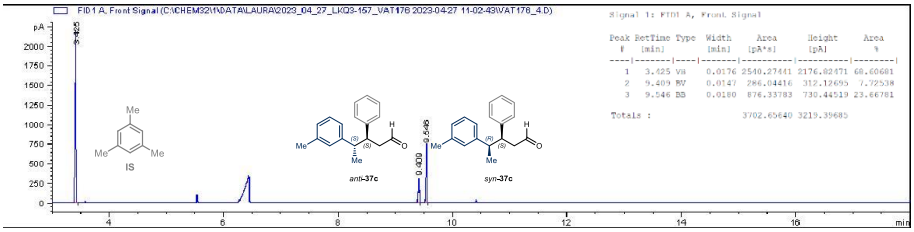

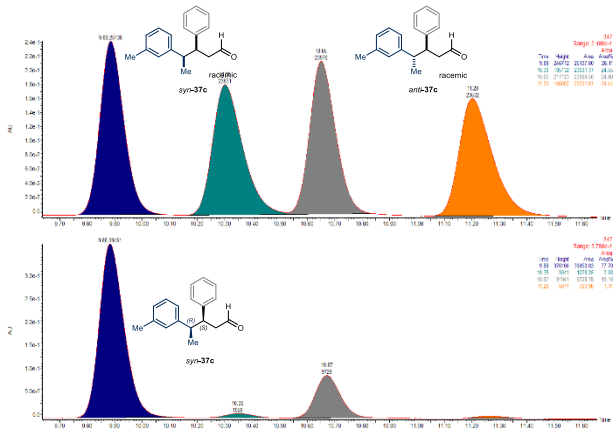

3.6.11 NMR Spectra

^{1}H NMR, 400 MHz, $CDCl_3$

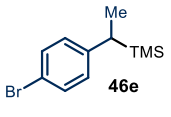

46e

^{13}C NMR, 101 MHz, $CDCl_3$

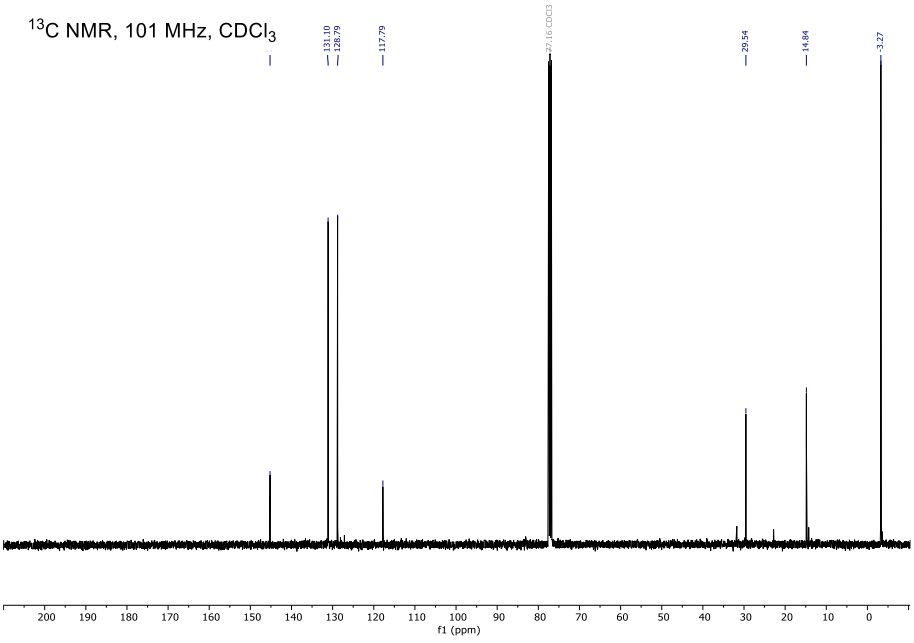

^{1}H NMR, 500 MHz, $CDCl_3$

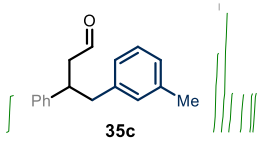

35c

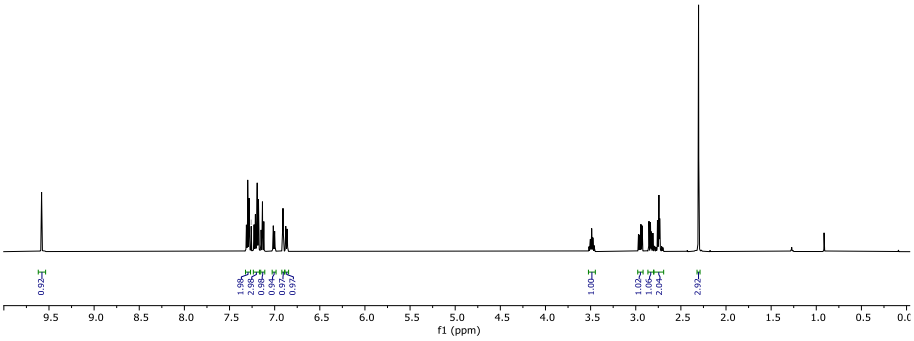

^{13}C NMR, 126 MHz, $CDCl_3$

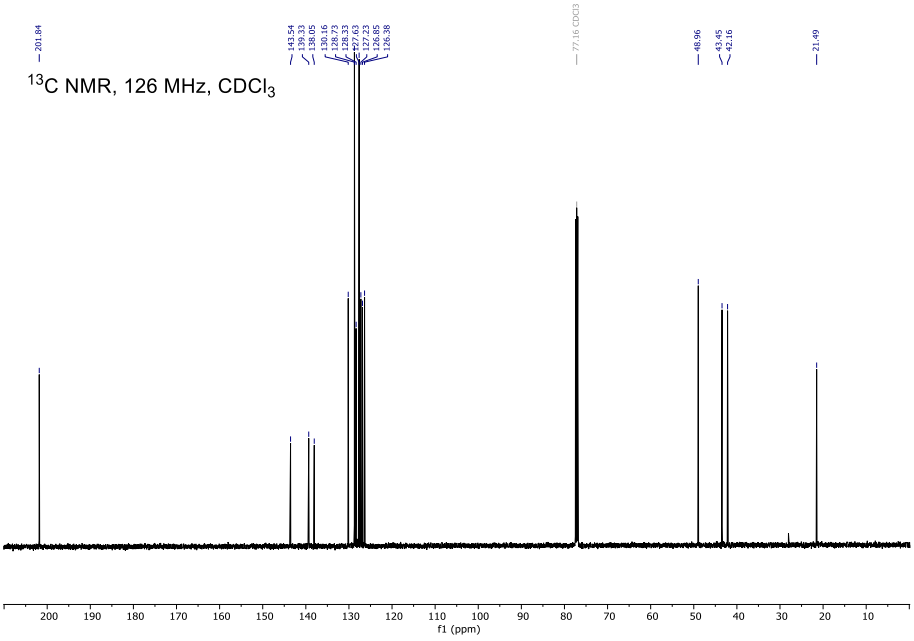

^{1}H NMR, 500 MHz, $CDCl_3$

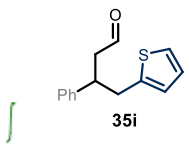

35i

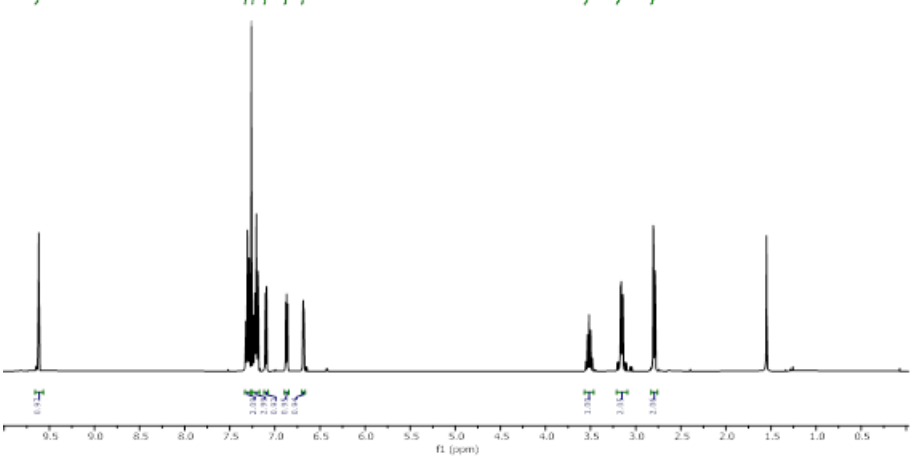

^{13}C NMR, 126 MHz, $CDCl_3$

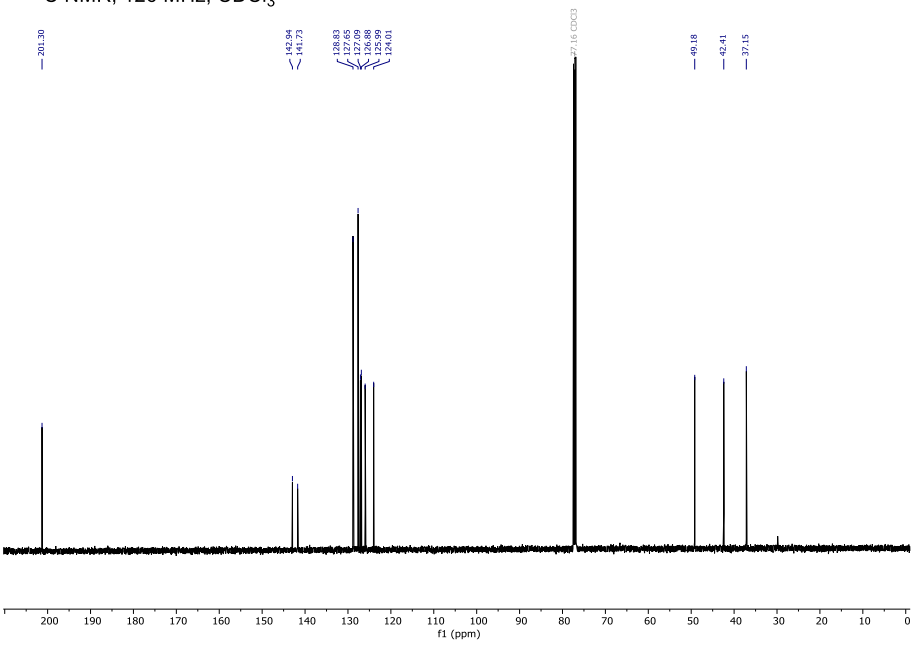

^{1}H NMR, 500 MHz, $CDCl_3$

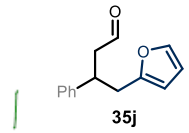

35j

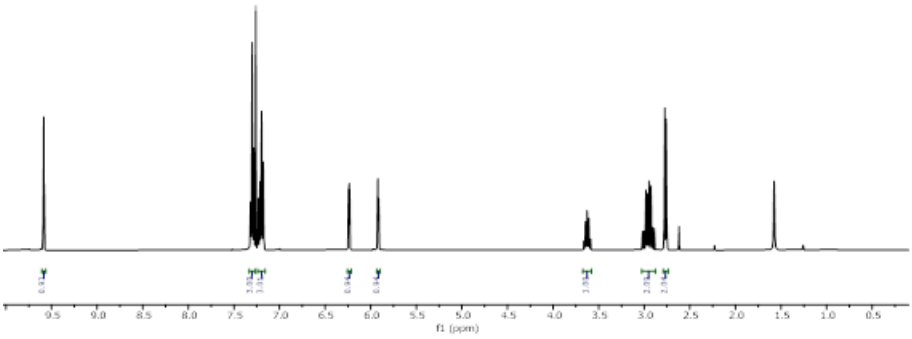

^{13}C NMR, 126 MHz, $CDCl_3$

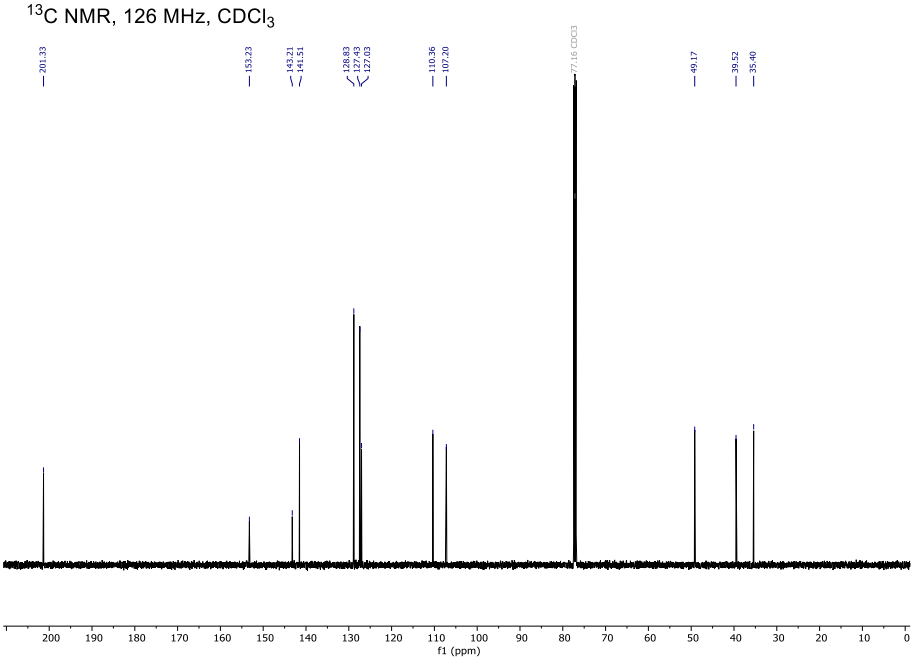

^{1}H NMR, 500 MHz, $CDCl_3$

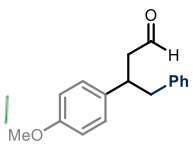

35l

^{13}C NMR, 126 MHz, $CDCl_3$

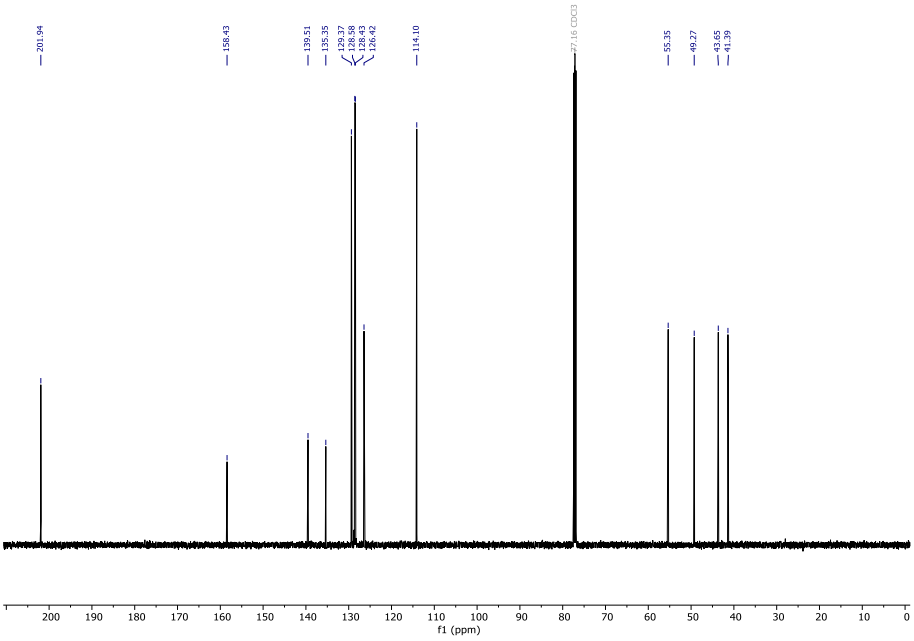

^{1}H NMR, 500 MHz, $CDCl_3$

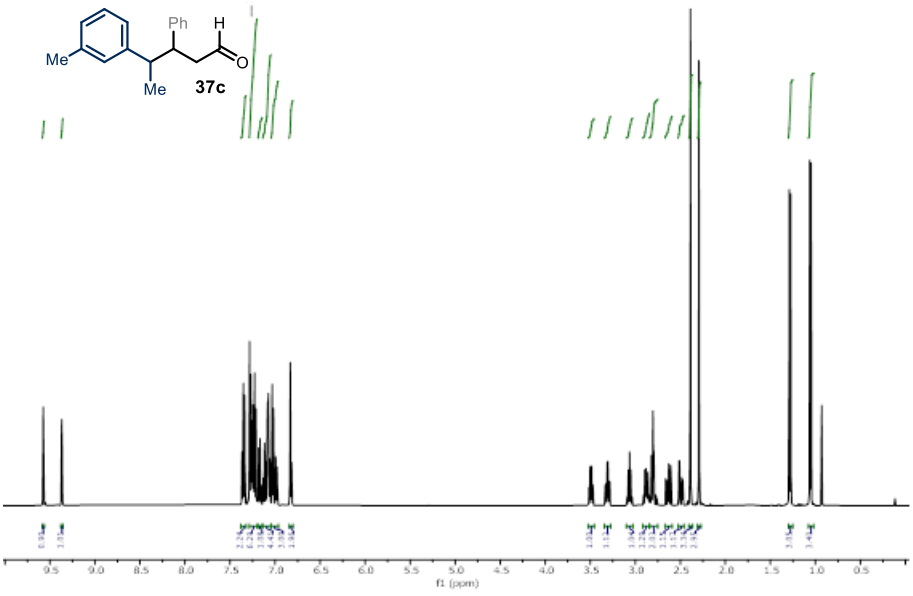

^{13}C NMR, 126 MHz, $CDCl_3$

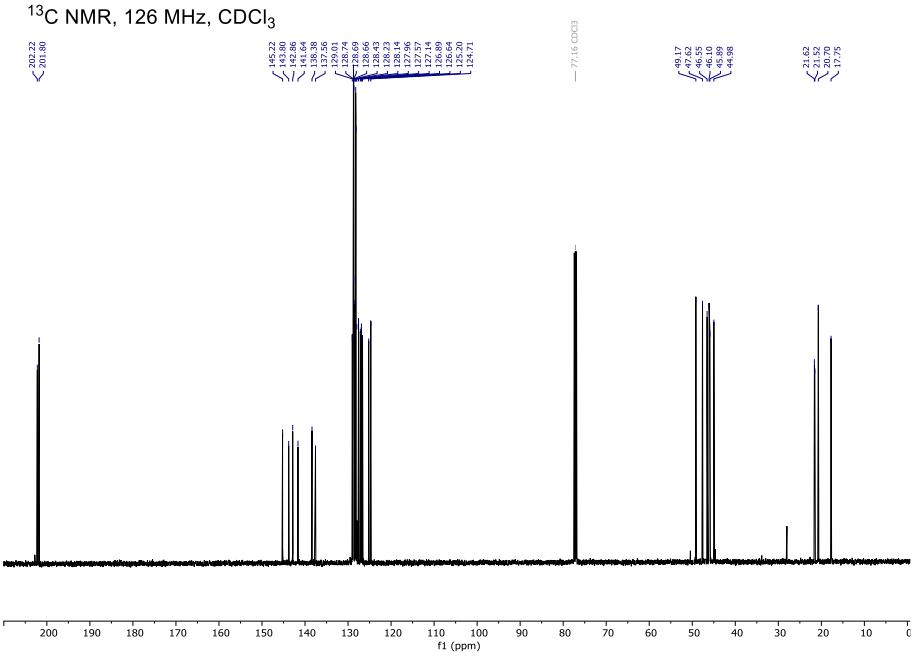

^{1}H NMR, 500 MHz, $CDCl_3$

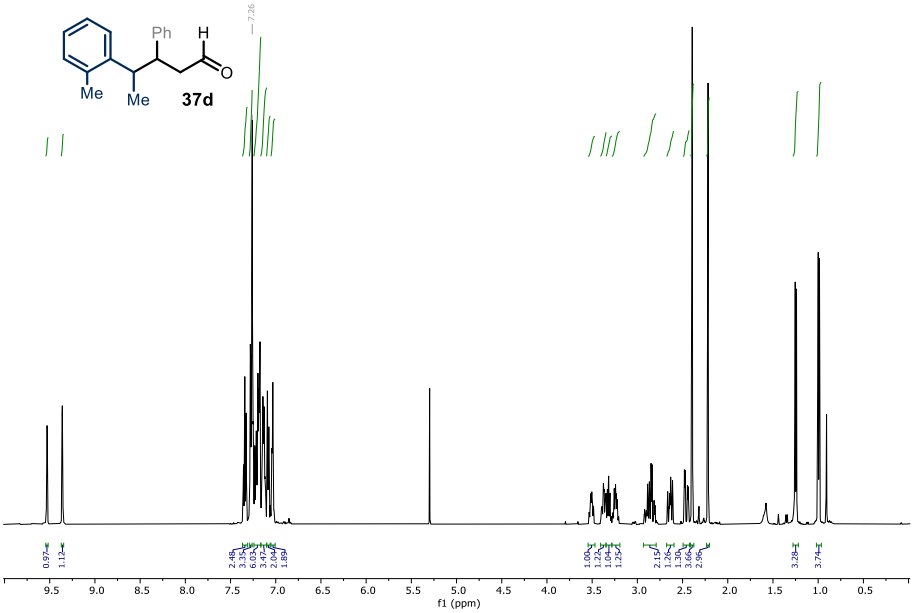

^{13}C NMR, 126 MHz, $CDCl_3$

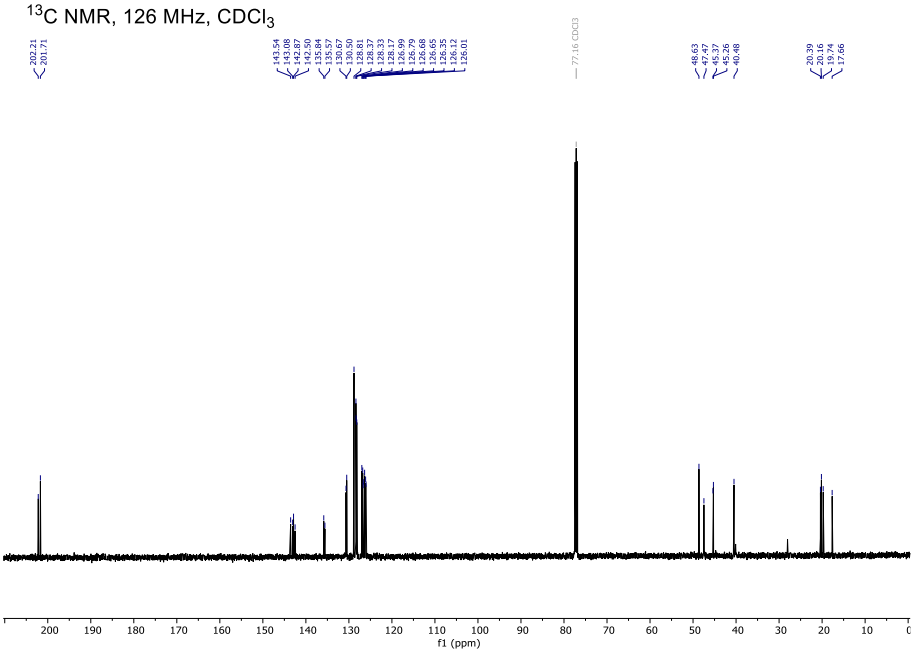

^{1}H NMR, 500 MHz, $CDCl_3$

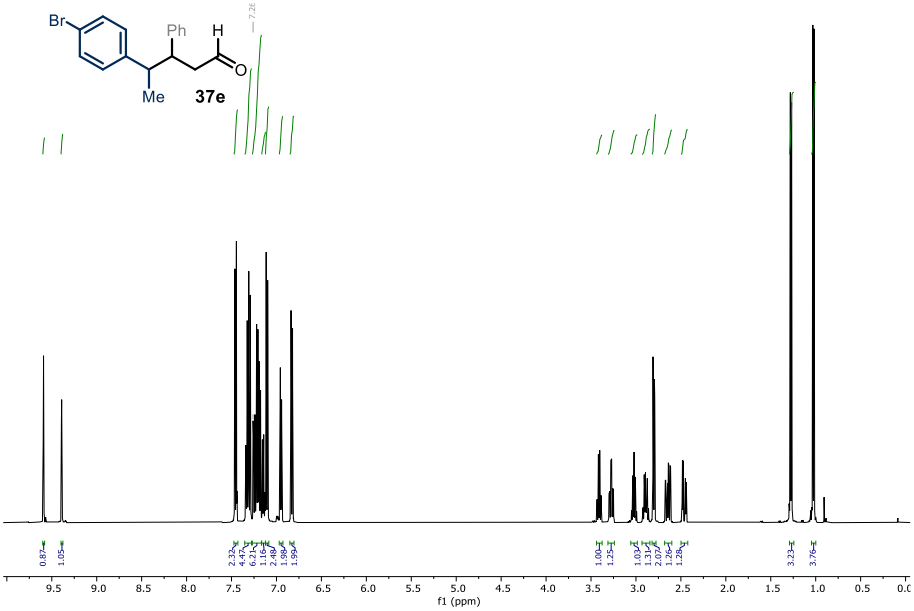

^{13}C NMR, 126 MHz, $CDCl_3$

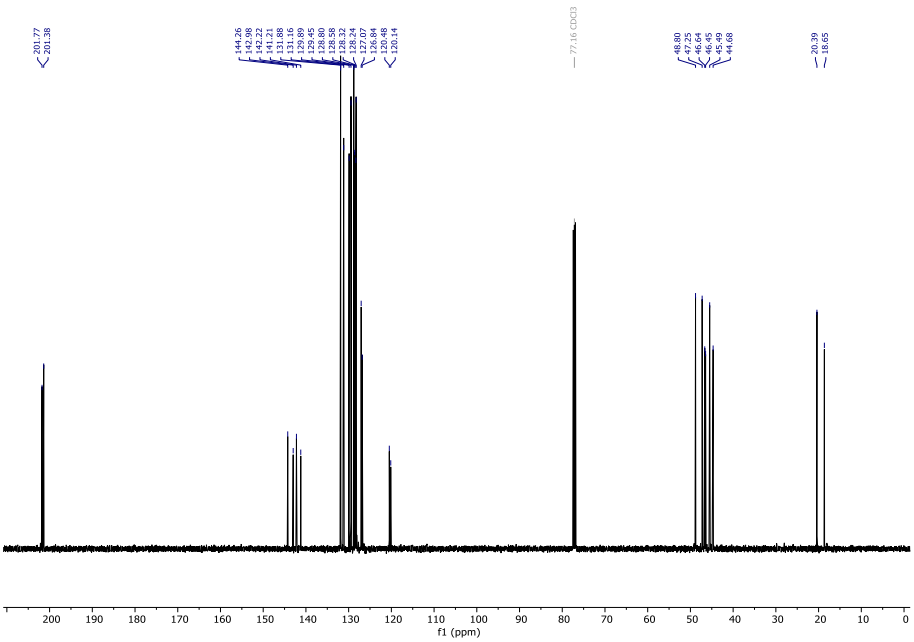

^{1}H NMR, 500 MHz, $CDCl_3$

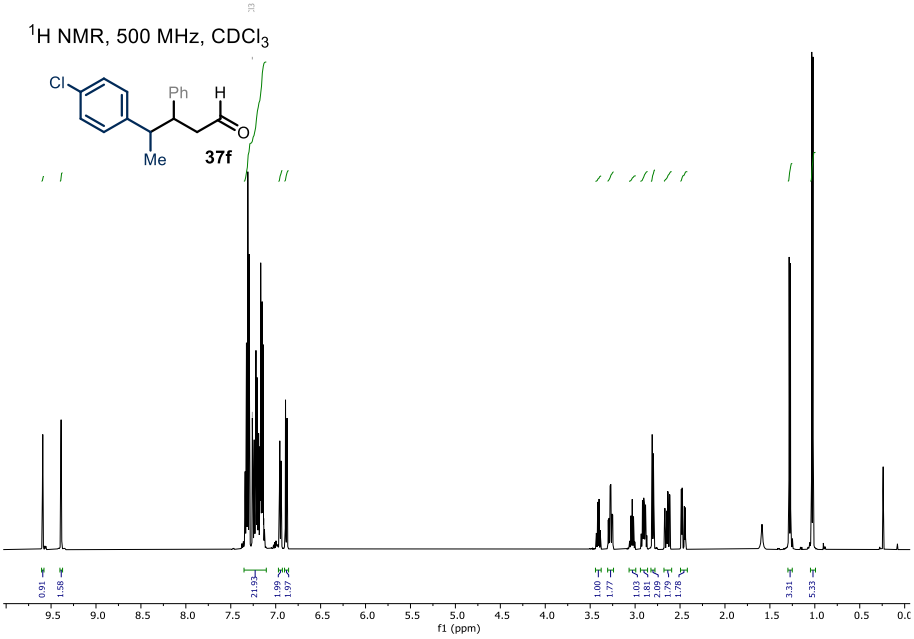

^{13}C NMR, 126 MHz, $CDCl_3$

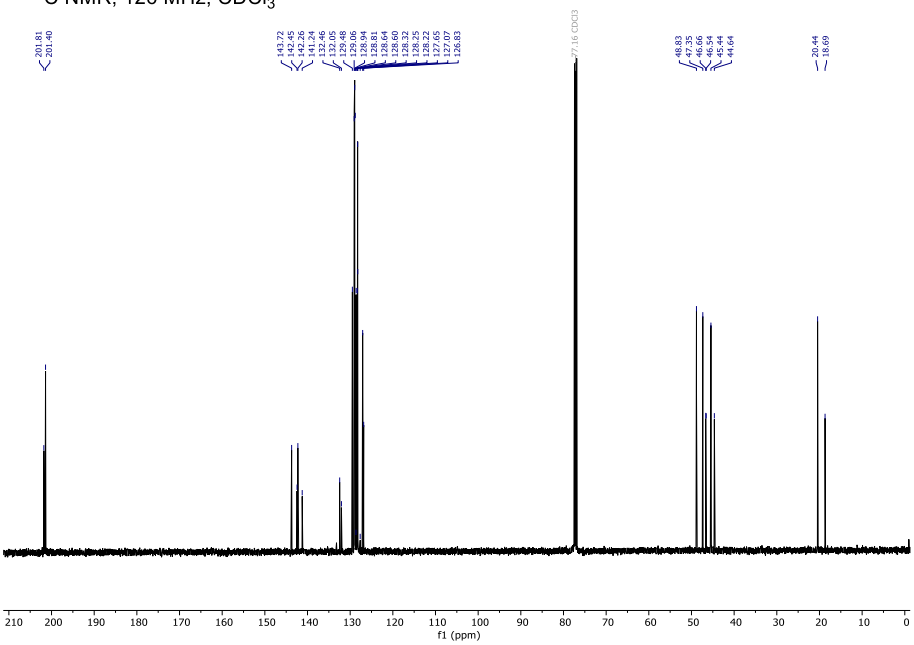

^{1}H NMR, 500 MHz, $CDCl_3$

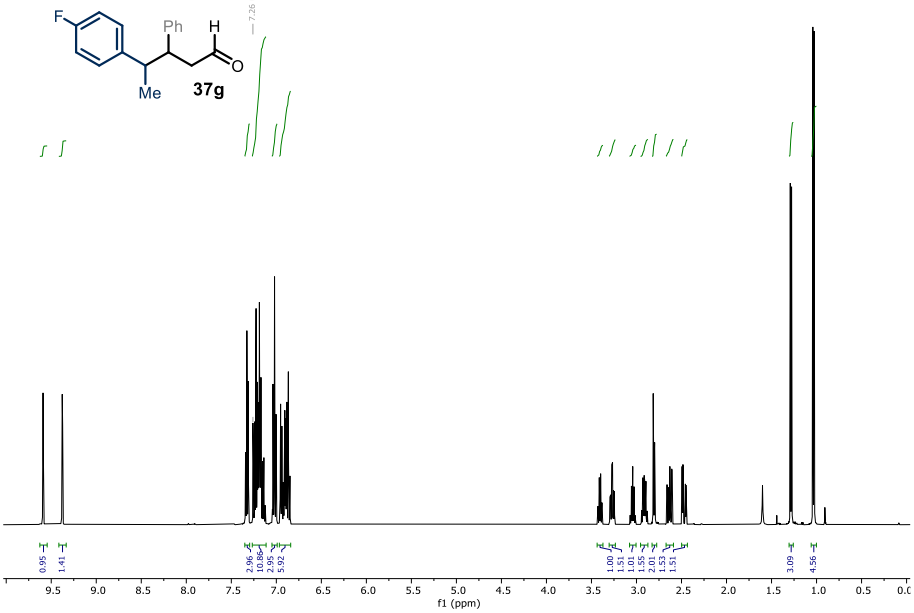

^{13}C NMR, 126 MHz, $CDCl_3$

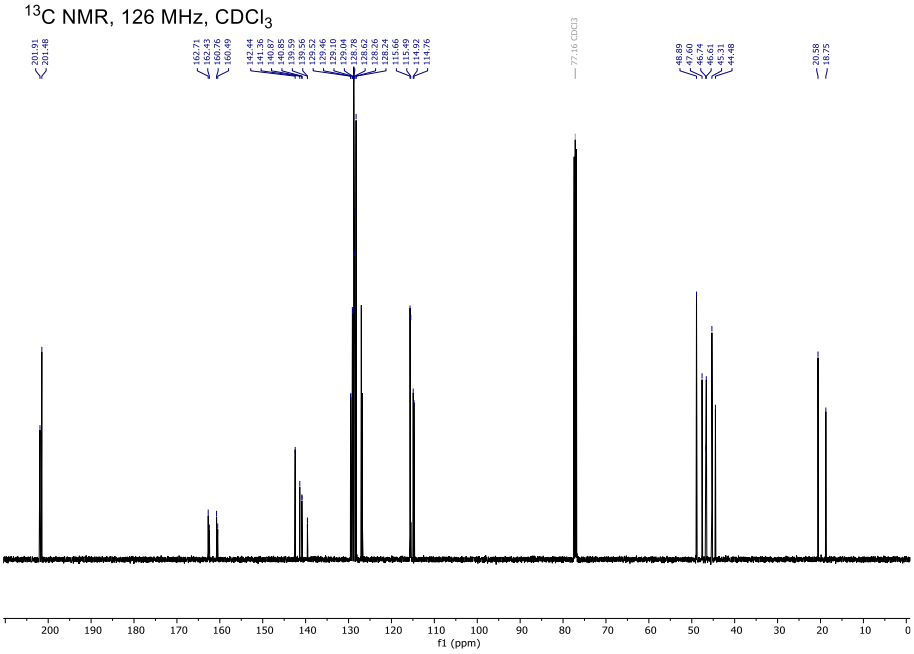

^{1}H NMR, 500 MHz, $CDCl_3$

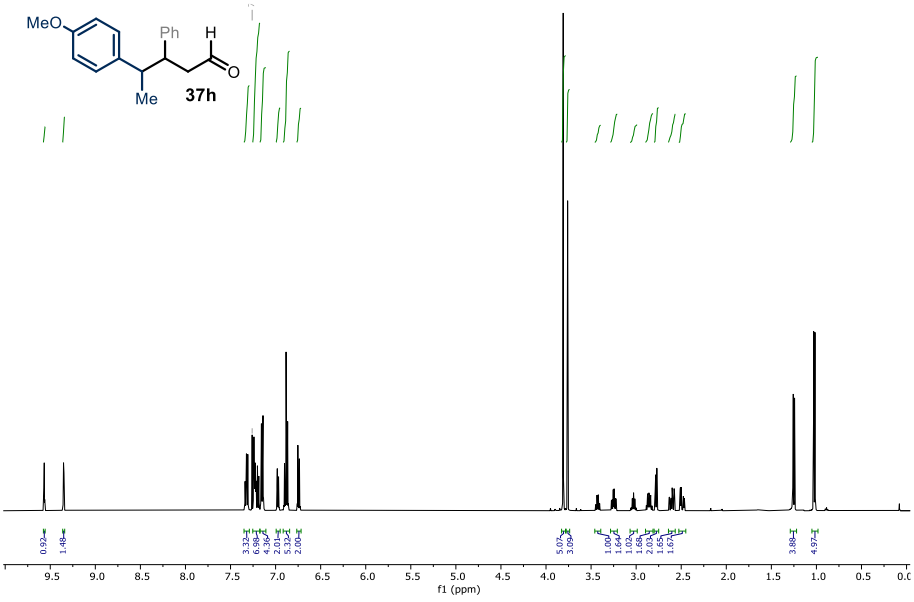

^{13}C NMR, 126 MHz, $CDCl_3$

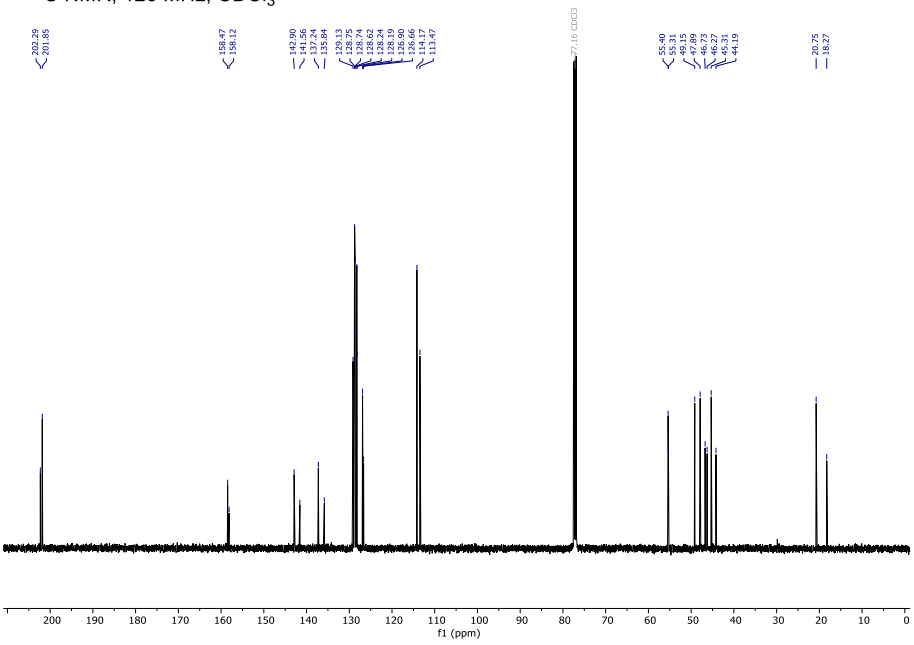

^{1}H NMR, 500 MHz, $CDCl_3$

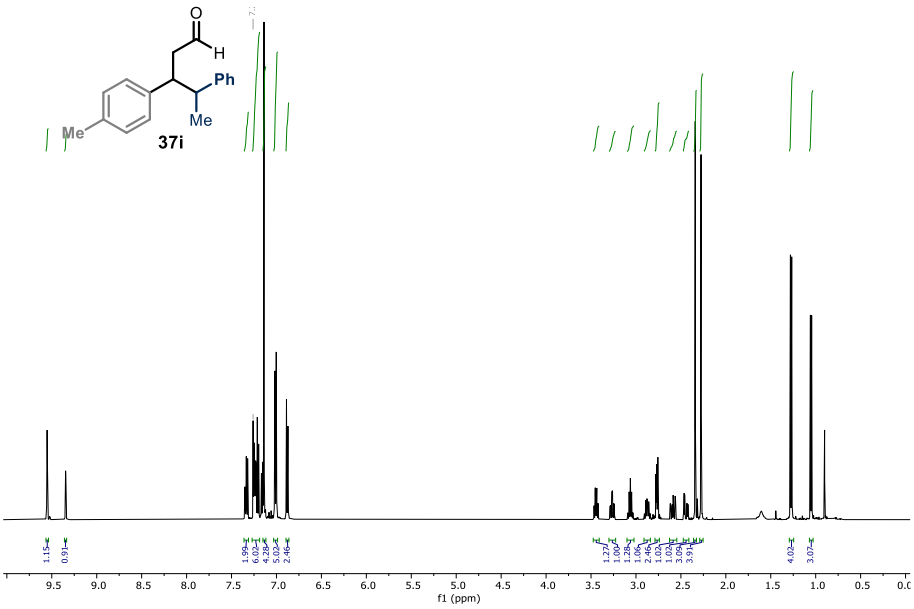

^{13}C NMR, 126 MHz, $CDCl_3$

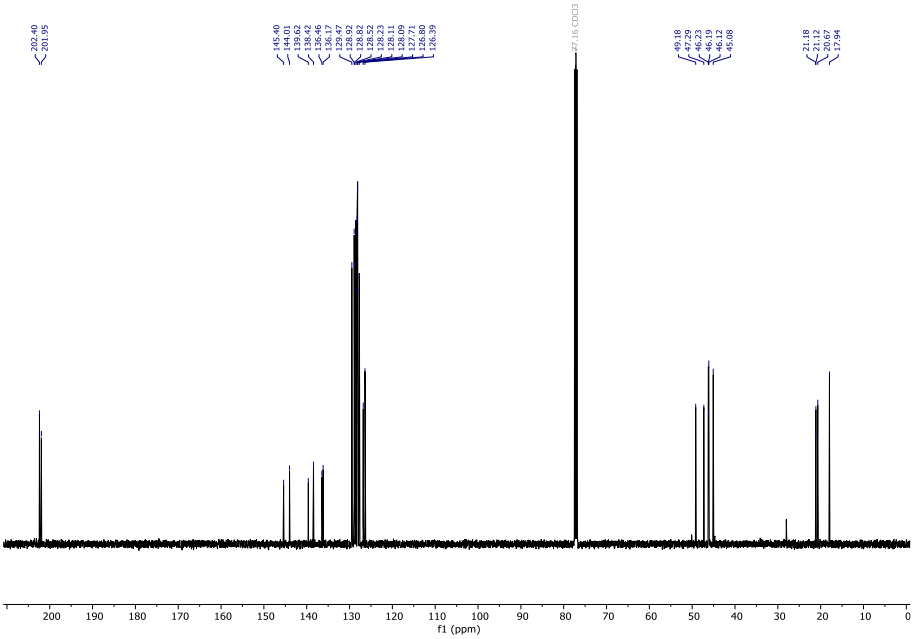

^{1}H NMR, 400 MHz, $CDCl_3$

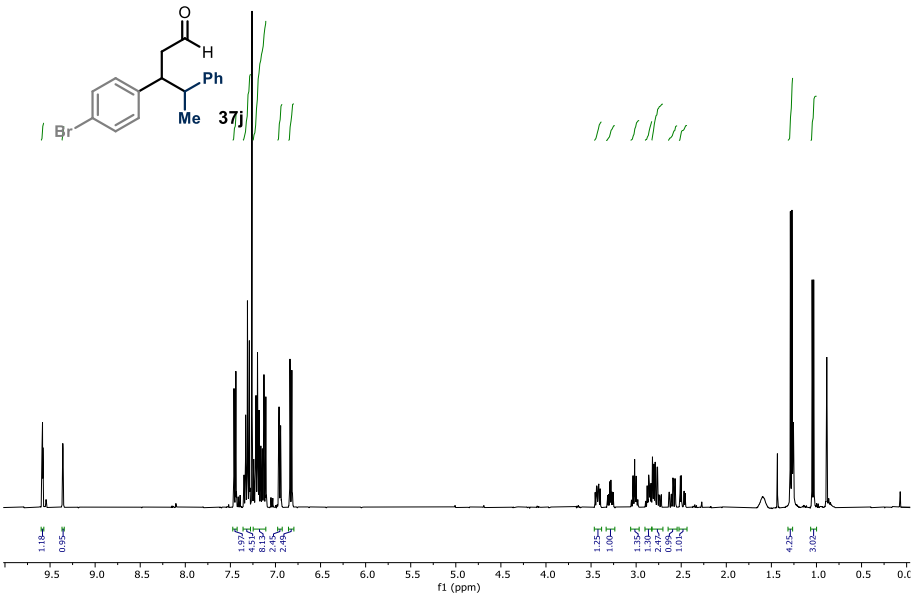

^{13}C NMR, 101 MHz, $CDCl_3$

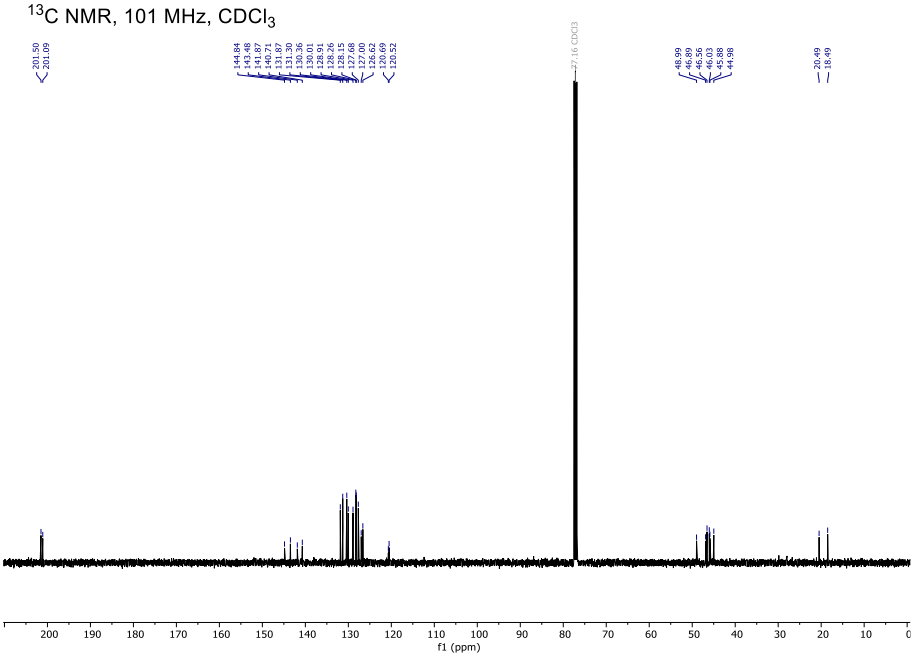

^{1}H NMR, 500 MHz, $CDCl_3$

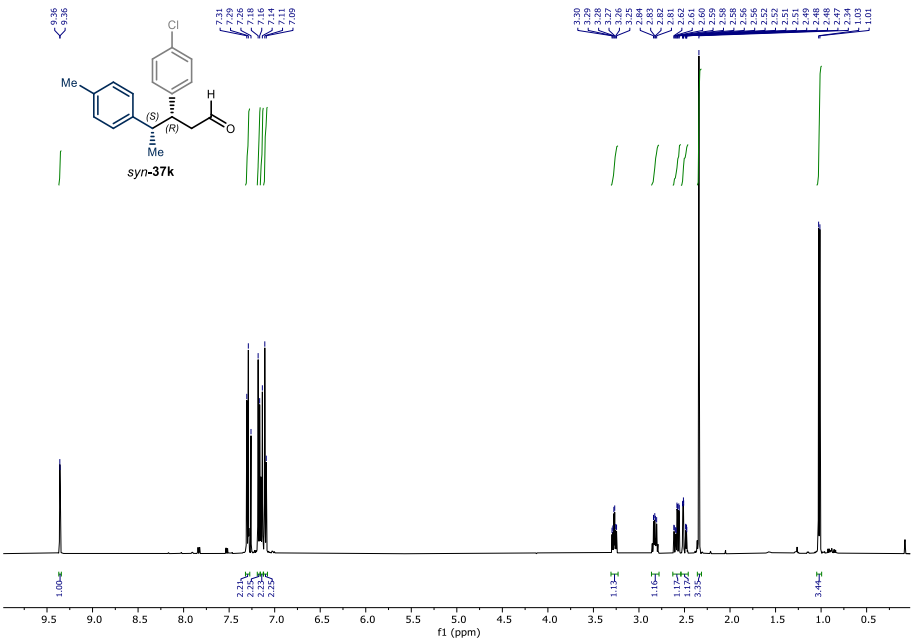

^{13}C NMR, 126 MHz, $CDCl_3$

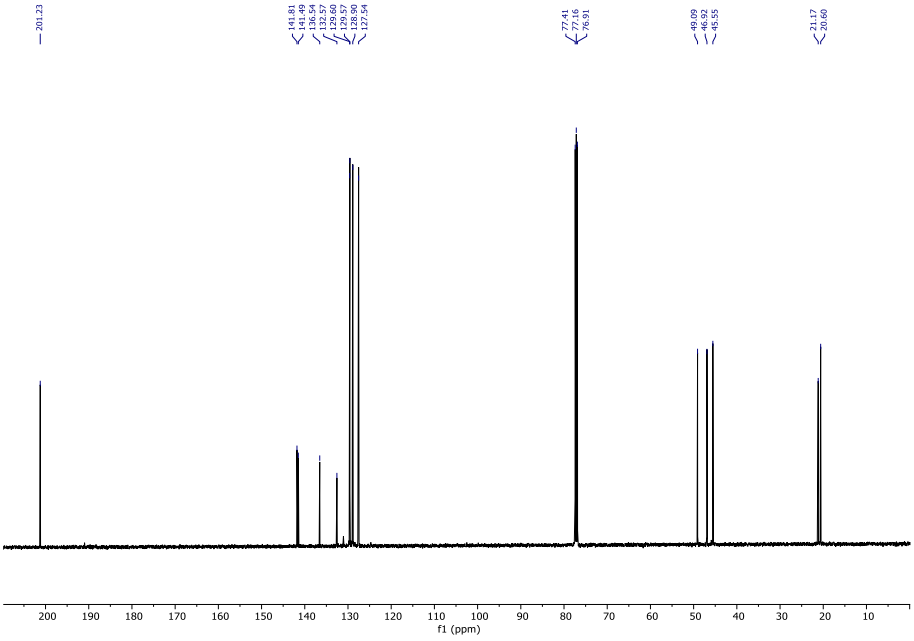

^{1}H NMR, 500 MHz, $CDCl_3$

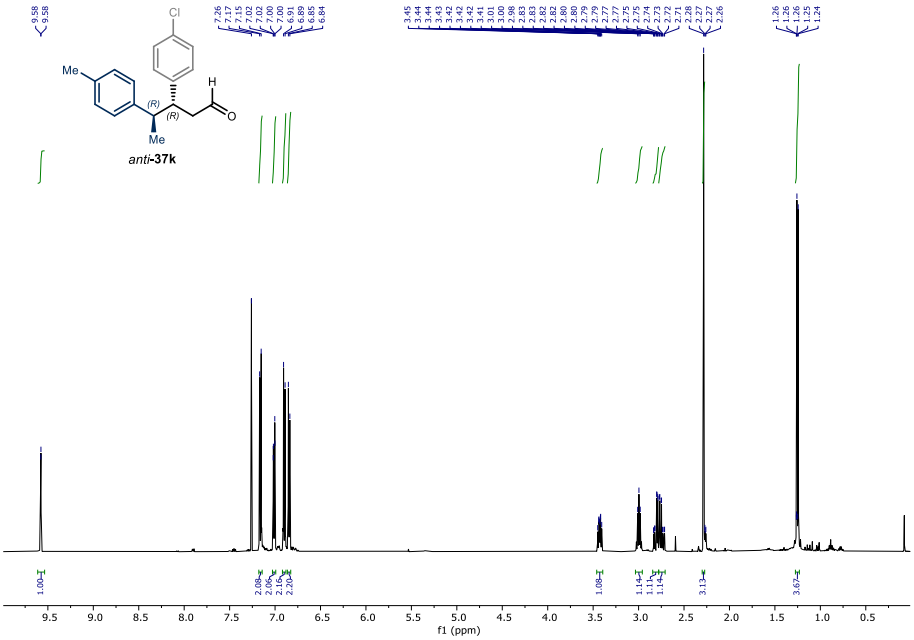

^{13}C NMR, 126 MHz, $CDCl_3$

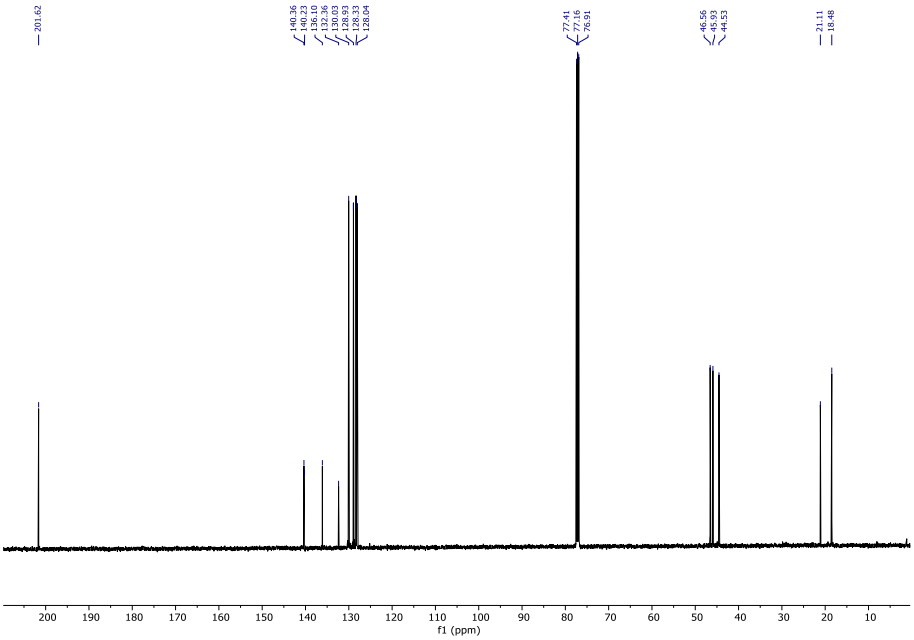

^{1}H NMR, 500 MHz, $CDCl_3$

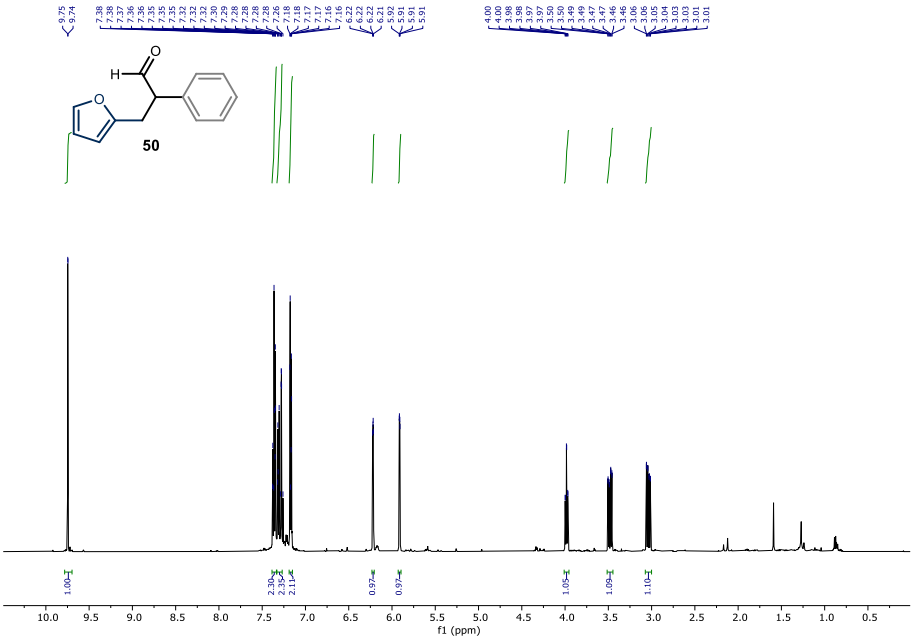

^{13}C NMR, 126 MHz, $CDCl_3$

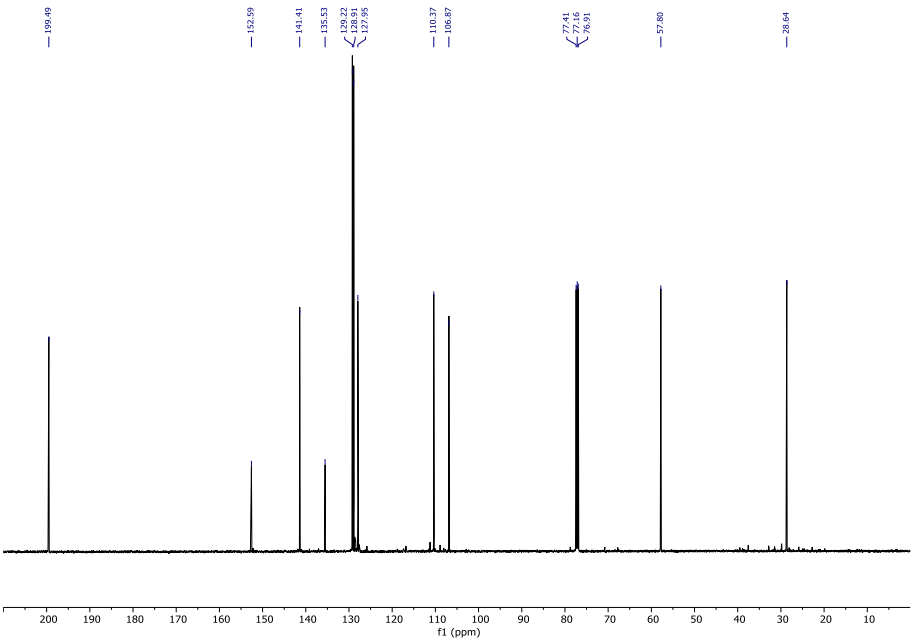

^{1}H NMR, 500 MHz, $CDCl_3$

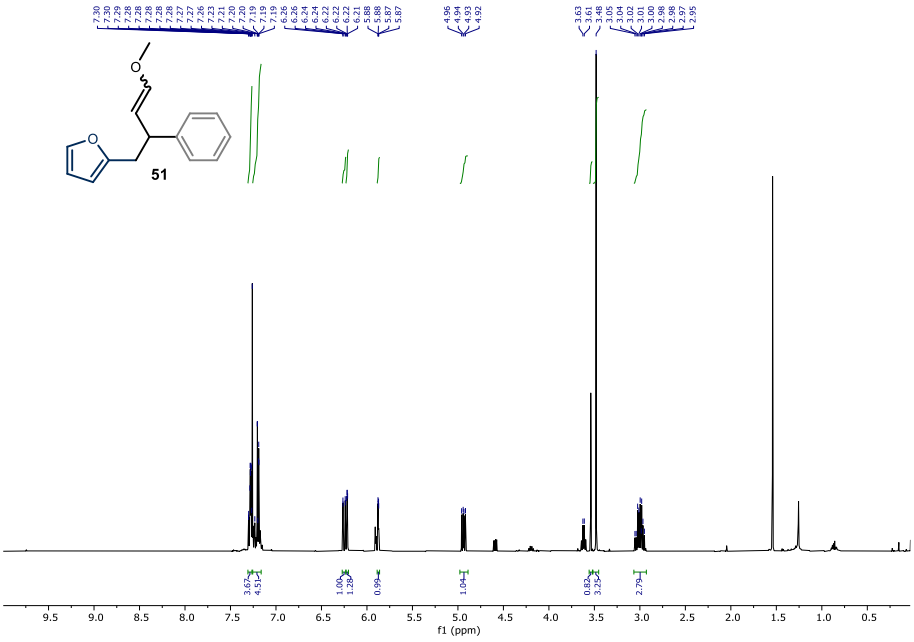

^{13}C NMR, 126 MHz, $CDCl_3$

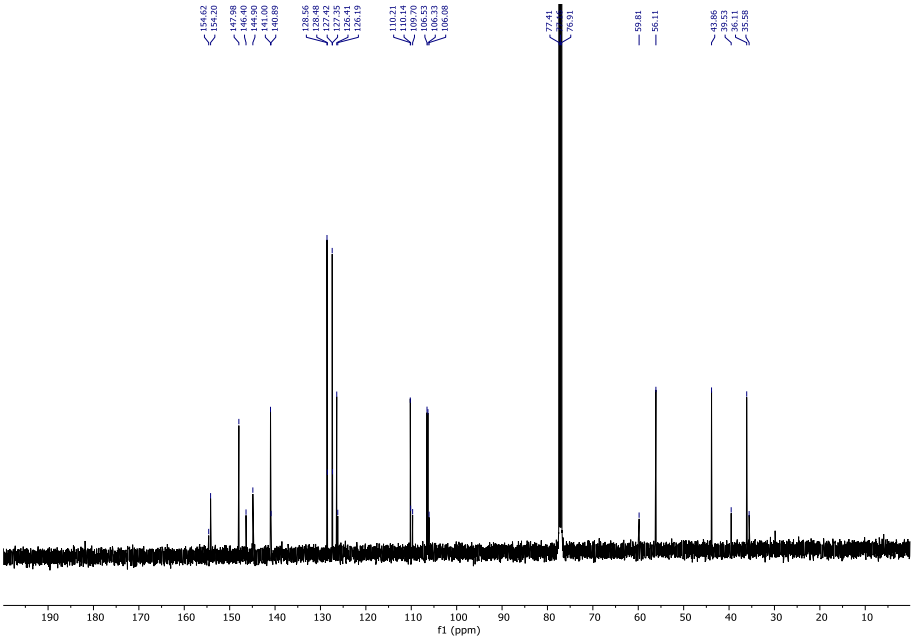

Chapter IV

General Conclusion

My doctoral thesis investigated the repurposing of enzymes to achieve new-to-nature transformations, encompassing both ground-state and excited-state reactivity. We developed enzymes with novel or enhanced reaction capabilities by applying protein engineering to incorporate reactivity principles from organocatalysis. This research harnessed the remarkable selectivity of enzymes. By combining it with organocatalysis and photochemistry, we unlocked entirely new catalytic abilities to create chiral molecules with high stereocontrol.
Chapter II details our investigations onto the structural modifications of 4-OT tautomerase enzymes, previously reported to activate aldehydes and enals via enamine or iminium ion formation, respectively. Using protein-engineering techniques, we identified two novel enzyme variants with the ability to perform both activation modes sequentially in a cascade process. These enzymes functioned as multifunctional biocatalysts, enabling a one-pot synthesis of complex cyclohexene carbaldehydes. The biocascade reactions yielded the desired products with high efficiency, diastereomeric ratios and enantiomeric excesses. Our study demonstrated that biocatalysis, when compared to traditional organocatalytic approaches, could achieve comparable or even improved efficiency and stereoselectivity.
Chapter III introduces a novel strategy for designing a non-natural photodecarboxylase, leveraging the direct excitation of an enzyme-bound iminium ion intermediates by visible light. This approach enabled asymmetric radical coupling through a unique photoactivation mechanism. We used an engineered DERA class I aldolase enzyme to activate chiral enantiopure carboxylic acids via single-electron transfer oxidation. The resulting radicals were intercepted to generate two stereogenic centers with good to excellent diastereomeric control. Importantly, the enzyme preserved the stereochemical information of the sp^3-hybridized radical, enabling stereospecific cross-coupling with absolute and relative stereocontrol. Consequently, this photobiocatalytic system underscored the active site's ability to transfer stereochemical information from the chiral radical precursor into the product, effectively preventing racemization of prochiral radicals. The resulting ‘memory of chirality’ scenario is a rarity in enantioselective radical chemistry.
This research holds potential for novel light-driven radical methodologies based on the photoexcitation of enzyme-bound intermediates. However, enzyme deactivation remains a current limitation that needs to be addressed.

UNIVERSITAT
ROVIRA i VIRGILI

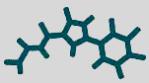

ICIQ
Institut
Català
d'Investigació
Química